Finite 't Hooft coupling corrections and shockwave collisions in AdS/CFT

DISSERTATION ZUR ERLANGUNG DES DOKTORGRADES DER NATURWISSENSCHAFTEN (DR. RER. NAT.) DER FAKULTÄT FÜR PHYSIK DER UNIVERSITÄT REGENSBURG

vorgelegt von

Sebastian Waeber aus
Regensburg

Im Jahr 2019

Promotionsgesuch eingereicht am: 20.5.2019
Diese Arbeit wurde angeleitet von: Prof. Dr. Andreas Schäfer

Abstract

In the first part of this work we compute finite 't Hooft coupling corrections to observables related to charged quantities in a strongly coupled $\mathcal{N} = 4$ supersymmetric Yang-Mills plasma. We correct errors in the literature regarding the finite 't Hooft coupling corrected equations of motion of gauge fields in AdS/CFT. As a consequence the finite 't Hooft coupling corrections to the observables considered, including the conductivity, quasinormal mode frequencies, in and off equilibrium spectral density and photoemission rates, become much smaller, suggesting that infinite coupling results obtained within AdS/CFT are little modified for the real QCD coupling strength.

In addition we study higher derivative corrections to the magnetic black brane geometry, to investigate a quark gluon plasma in a strong magnetic background field at finite coupling. Finite 't Hooft coupling terms to the lowest tensor quasinormal mode in this geometry are determined, shedding light on the equilibration time of a quark gluon plasma in the presence of a magnetic field while including higher derivative terms.

Concluding the analysis of AdS/CFT at finite coupling we present a higher order resummation technique, that suggests that in general observables computed from AdS/CFT are only modestly modified at coupling strengths, which are realistic for hot QCD.

In the second part of this thesis we simulate peripheral heavy ion collisions by computing asymmetric shockwave collisions in maximally supersymmetric Yang-Mills theory via their dual gravitational formulation. We found the post-collision hydrodynamic flow to be well described by appropriate means of the results of symmetric shock collisions. With the universal model for the hydrodynamic flow produced by asymmetric planar collisions one can construct, quantitatively, non-planar, non-central collisions of highly Lorentz contracted projectiles without the need for computing, holographically, collisions of finite size projectiles with very large aspect ratios, given that transverse gradients are small. We confirmed that the hydrodynamization time only negligibly depends on the shock-widths and asymmetry of the shocks. Thus, also for peripheral collisions it merely depends on the energy density per transverse unit area, justifying assumptions made in hydro simulations so far.

Zusammenfassung

Im ersten Teil dieser Arbeit werden endliche 't Hooft Kopplungskorrekturen zu Observablen in einem Super Yang Mills Plasma mit zusätzlicher elektromagnetischer Wechselwirkung berechnet. Dabei korrigieren wir Fehler in der Literatur, welche bei der Herleitung der Bewegungsgleichungen von Eichfeldern in der AdS/CFT mit höheren Ableitungstermen entstanden sind. Die Auswirkungen sind enorm: Die endlichen 't Hooft Kopplungskorrekturen zur Leitfähigkeit des Plasmas, zu Frequenzen von (elektrischen) Quasinormalmoden, zur Spektraldichte und der Photoemissionsrate sind deutlich kleiner als bisher angenommen, was nahelegt, dass Ergebnisse im unendlichen Kopplungslimes sich deutlich moderater von denen bei realistischen Werten für die Kopplungskonstante unterscheiden. Zusätzlich berechnen wir höhere Ableitungskorrekturen zur magnetischen schwarzen Branen Geometrie um ein Quark Gluonen Plasma in einem starken magnetischen Hintergrundfeld bei endlicher 't Hooft Kopplung zu untersuchen. Die Motivation für diese Rechnung ist zum einen, dass starke Magnetfelder für sehr kurze Zeiten während echter Schwerionenstößen am LHC und RHIC entstehen, zum anderen bricht das Hintergrundfeld die Skaleninvarianz der Feldtheorie am Rand des Anti-de Sitter Raumes, was zusammen mit der endlichen Kopplung das Modell deutlich näher an die QCD bringt. Wir analysieren endliche 't Hooft Kopplungskorrekturen zu Tensor-Quasinormalmoden, was es ermöglicht Aussagen über die Equilibrierungszeit eines Quark Gluon Plasmas in einem magnetischen Hintergrundfeld bei endlicher Kopplung zu treffen.

Im zweiten Teil dieser Arbeit simulieren wir periphere Schwerionenstöße durch das Berechnen von asymmetrischen Schockwellenkollisionen in maximal super symmetrischer Yang-Mills Theorie mithilfe ihres gravitationstheoretischen Duals. Wir fanden, dass die Eigenergiedichte nach der Kollision von asymmetrischen Schockwellen durch konkrete Mittel der jeweiligen Größen für symmetrische Kollisionen gegeben ist. Die Fluid-Geschwindigkeit ist auch im asymmetrischen Fall sehr gut durch "boost invariant flow" approximiert. Dies ermöglicht es nicht-planare, nicht-zentrale Kollisionen von hochrelativistischen Projektilen zu modellieren, ohne auf aufwendige Berechnungen nicht planarer Schocks angewiesen zu sein. Die Hydrodynamisierungszeit wurde als unabhängig von Schockdicke und Asymmetrie bestätigt. Sie hängt nur von der transversalen Energiedichte ab. Dies verifiziert Annahmen, welche in so gut wie allen Berechnungen hydrodynamischer Modelle gemacht werden.

Diese Arbeit widme ich meiner Familie.

Underlying papers

Several research works during my PhD studies have been published on *arXiv.org* and the *Journal of High Energy Physics*. This thesis is built on the following list of publications, which are discussed and reviewed in sections 2.1, 2.2, 2.3 and 3.1.

1. S. Waeber, A. Schaefer, A. Vuorinen, L. G. Yaffe, *Finite coupling corrections to holographic predictions for hot QCD*, *J. High Energy Phys.* **1511** (2015) 087, arXiv:1509.02983 [hep-th],

2. S. Waeber and A. Schäfer, *Studying a charged quark gluon plasma via holography and higher derivative corrections*, *J. High Energy Phys.* **1807** (2018) 069, arXiv:1804.01912 [hep-th],

3. S. Waeber *Quasinormal modes of magnetic black branes at finite 't Hooft coupling*, *J. High Energy Phys.* **1908** (2019) 006, arXiv:1811.04040 [hep-th],

4. S. Waeber, A. Rabenstein, A. Schäfer, L. G. Yaffe *Asymmetric shockwave collisions in AdS_5*, *J. High Energy Phys.* **1908** (2019) 005, arXiv:1906.05086 [hep-th]

Contributions of the author

The contributions of the author to works (with potentially multiple authors) listed above are as follows:

1. The underlying idea of this work, most of the calculations and results shown in the paper were produced by the author of this thesis.

2. This paper corrects errors in the literature as well as several papers that built on the original erroneous results. The errors were found and corrected by the author of this thesis, all other calculations and results in this paper were produced by him.

3. This paper is single authored.

4. The author of this thesis is responsible for the results shown in this publication. The used software was written and the data analysis was done by him. The building of the software was strongly guided by L. Yaffe's advice, help and previous works.

Contents

Chapter 1

Introduction: An overview of the AdS/CFT duality and its applications

The duality between gauge theories and theories of gravity has proved to be a very successful instrument to study strongly coupled systems in general. In one of the most prominent and fruitful applications of this duality, one uses the string theoretic dual of $\mathcal{N} = 4$ (maximally) supersymmetric, conformal Yang-Mills theory (SYM) to investigate non-Abelian plasmas of quarks and gluons, formed at high temperatures during heavy ion collisions. The focus of this work is on this specific application of the gauge/gravity duality. In the following introductory chapter we will outline the most important aspects of string theory (section 1.2) and the holographic principle (section 1.3), derive all necessary tools and ingredients of the dictionary between $\mathcal{N} = 4$ SYM and type IIb supergravity in Anti-de Sitter spacetime (AdS/CFT) (section 1.4, 1.5) and discuss how to dynamically model heavy ion collisions using holography (sections 1.6, 1.7). We start with outlining the overall aim this work pursues.

1.1 Objective of this thesis

The central aim of this work is to bring results obtained within the gauge/gravity duality closer to quantum chromodynamics (QCD) without resorting to (bottom-up) modeling. To do so we follow a twofold approach:

By determining higher derivative, or higher α' corrections within string theory to the duality between $\mathcal{N} = 4$ Super Yang Mills theory and type IIb supergravity (SUGRA) we extend the range of validity of the AdS/CFT duality. We correct errors in the literature regarding higher derivative corrections to the equation of motion of gauge fields and quantities derived therefrom including the conductivity, photoemis-

sion rate, in and off equilibrium spectral functions and quasinormal mode spectra. In addition we are going to determine finite coupling corrections to the magnetic black brane metric, which is dual to a quark gluon plasma in a magnetic background field, and consider tensor fluctuations in this geometry. The higher derivative corrections allow us to leave the infinite coupling limit whereas a magnetic background field breaks scale invariance of the dual theory. This is an interesting setting to study, since conformal invariance is incompatible with QCD, which is in general not scale invariant. In addition we are going to introduce and discuss a technique that systematically collects a subset of higher derivative corrections and study the effect this has on finite coupling corrected quantities.

On the other hand we want to investigate properties of the Quark Gluon Plasma (QGP) by numerically simulating dynamical processes. We study asymmetric gravitational shockwave collisions in 5 dimensional Anti- de Sitter space (AdS_5) and analyze the hydrodynamic flow resulting from these collisions. In addition we show in detail how to develop software for this purpose. With the help of these calculations it is possible to model heavy ion collisions as performed at LHC or RHIC holographically and study the early non-hydrodynamic phase.

Although the dual field theory to this holographic setting is only related to QCD, gravitational shockwave collisions are still suited to qualitatively describe the early phase of heavy ion collisions, since for high temperatures both QCD and SYM theories are shown to have similar properties (see e.g. [21, 22]). The holographic approach is the only one that is capable of capturing the non perturbative phase of a highly relativistic heavy ion collision so far, albeit not in the right field theory. Thus, it is of special interest to extend the current models with the aim of bringing the dual field theory as close to QCD as possible and feasible.

In the following we start with introductory chapters outlining the most important aspects of type IIb super string theory and supergravity, the holographic principle, the dictionary of AdS/CFT relating the near boundary geometry of the AdS space with the stress energy tensor of the field theory on the boundary and higher derivative corrections to type IIb SUGRA, respectively finite 't Hooft coupling corrections to the boundary theory observables. The introductory chapter is guided by literature on AdS/CFT and string theory [59] [60] [73].

1.2 (Super) String Theory, (Super) Gravity and higher derivative corrections

The idea behind string theory is that one dimensional strings and not point particles are the fundamental objects, whose excitations give rise to different observable particles and even space time itself. In the same way as particles can be described by a worldline

action, strings are described by an action, which is an integral over their two dimensional worldsheet. The action describing the dynamics of a string in a target space time with coordinates X^m is the Nambu-Goto action given by

$$S = -\frac{1}{2\pi\alpha'}\int d\sigma d\tau \sqrt{-\det((\partial_\alpha X^M)(\partial_\beta X^N)g_{MN})}, \tag{1.2.1}$$

where $l_s = \sqrt{\alpha'}$ is the string length, g_{MN} is the metric of the target space time and σ, τ parametrize the string's worldsheet. With the induced metric $h_{\alpha\beta} = \partial_\alpha X^m \partial_\beta X^N g_{MN}$ the action (1.2.1) can be written as the Polyakov action [3]

$$S_p = -\frac{1}{4\pi\alpha'}\int d\sigma d\tau \sqrt{-h} h^{\alpha\beta}(\partial_\alpha X^M)(\partial_\beta X^N)g_{MN}. \tag{1.2.2}$$

For worldsheets with coordinates X^m the equation of motion derived from (1.2.2) is the relativistic wave equation

$$\partial_\tau^2 X^m - \partial_\sigma^2 X^m = 0. \tag{1.2.3}$$

From the requirement that the boundary term of the action (1.2.2) varied with respect to X^m has to vanish, one concludes that either $\partial_\sigma X^m$ or δX^m is zero on the endpoints of the interval σ lives on. For open strings the former condition is known as the Neumann boundary condition, the latter as the Dirichlet boundary condition. Imposing Dirichlet boundary conditions means fixing the endpoints of the string, which breaks translational invariance and thus momentum conservation. Thus, the hypersurfaces orthogonal to the directions, in which we fixed the endpoints, have to be dynamical objects absorbing the momentum, known as *Dirichlet-* or *D-branes*.

After quantization of the strings it can be shown that the target space for bosonic strings has to be 26 dimensional. This follows from the requirement that the excited string states with lowest mass in fact have to be massless already, due to their transformation behaviour[1]. In addition the spectrum of the lowest massless closed strings contains alongside a symmetric and traceless tensor, which is identified with the graviton, a scalar and an antisymmetric tensor field, known as the dilaton ϕ and the Kalb-Ramond field B_{MN}. The action for closed massless bosonic strings is given by (1.2.2) plus

$$S_{B,\phi} = -\frac{1}{4\pi\alpha'}\int d\sigma d\tau \sqrt{-h}(\epsilon^{\alpha\beta}(\partial_\alpha X^M)(\partial_\beta X^N)B_{MN} + \alpha' R_h \phi), \tag{1.2.4}$$

[1] In four dimensions massive particles can always be boosted into a frame, in which their momentum has only p^0 non-zero, the group of transformations that leaves this 4-vector invariant is $SO(3)$. The 4-vector of massless particles can be brought into the form $(E, 0, 0, E)$ via a suitable transformation. The group of rotations that leaves this vector invariant is $SO(2) \subset ISO(2)$. This pattern can be generalized to arbitrary dimensions D. The lowest excited state in quantized (bosonic) string theory transforms as a vector under $SO(D-2)$. Hence it has to be massless.

where R_h is the Ricci scalar of the induced worldsheet metric $h_{\alpha\beta}$. The requirement that the stress energy tensor derived from this action has to be traceless[2] leads to a set of equations of motion (EoM), which can be derived from the effective target space time action in the string frame

$$S_{eff} = \int dX^D \sqrt{-g} e^{-2\phi} \left(R + 4(\nabla_M \phi)(\nabla_N \phi) g^{MN} - \frac{H_{MNL} H^{MNL}}{12} - \frac{2(D-26)}{3\alpha'} \right), \tag{1.2.5}$$

where D is the dimension of the target space time and H is the field strength of the Kalb-Ramond field. One caveat at this point is that this action reproduces the right EoM only up to the order $\mathcal{O}(\alpha'^0)$.

So far we have only treated bosonic strings. Supersymmetrizing the Polyakov action gives us fermionic fields, whose boundary conditions can be derived from requiring that boundary terms obtained from the variation of the fermionic part of the supersymmetric action vanish. For open strings this leads to two different classes of boundary conditions, which are known as the *Neveu-Schwarz* and the *Ramond* sector. These sectors correspond to the cases that right moving fermionic strings[3] are $+$ or $-$ their left moving counterparts at one of the string endpoints. Once again the lowest excited state, whose mass squared in this case is given by

$$M^2 = \frac{1}{\alpha'} \left(\frac{1}{2} - \frac{D-2}{16} \right) \tag{1.2.6}$$

transforms as a vector in $SO(D-2)$, which means that $M = 0$ and consequently the dimension of the target space time of supersymmetric string theory is 10. For open strings the massless states can be classified according to the representation of $SO(8)$ under which they transform. The lowest closed string states are obtained by two copies of the open ones, such that the different representations of $SO(8) \times SO(8)$ give rise to the different fields present in the low energy limit ($\alpha' \to 0$) of super string theory of massless closed strings. Projecting out tachyonic states leaves several different super string theories, one of which is type IIb super string theory, the theory we are going to focus on in this work. The bosonic part of the low energy effective action of type IIb super string theory, known as type IIb super gravity (SUGRA) can be shown to be

[2] This follows from Weyl invariance that is demanded from the quantized string theory.

[3] Since bosonic strings fulfill a wave equation, their solution can be split into left and right moving parts. The same is true for fermionic strings, obtained from the supersymmetrized action.

given by

$$S_{IIb} = \frac{1}{2\kappa^2}\int d^{10}X\sqrt{-g}\Big(e^{-2\phi}(R + 4(\partial_\mu\phi)(\partial^\mu\phi) - \frac{H_3^2}{2}) - \frac{F_1^2}{2} - \frac{\tilde{F}_3^2}{2} - \frac{\tilde{F}_5^2}{2} - \frac{1}{2}\int C_4 \wedge H_3 \wedge F_3\Big) \tag{1.2.7}$$

where $\kappa^2 = \frac{(2\pi)^7\alpha'^4}{2} = 8\pi G_{10}$, with the ten dimensional Newton constant G_{10}. The differential forms appearing in (1.2.7) fulfill

$$\tilde{F}_5 = dC_4 - \frac{1}{2}C_2 \wedge H_3 + \frac{1}{2}B_2 \wedge F_3 \tag{1.2.8}$$

$$H_3 = dB_2, \quad \tilde{F}_3 = F_3 - C_0 H_3 \quad F_{i+1} = dC_i \ \ \forall i \tag{1.2.9}$$

Typically we are going to be interested in solutions of type IIb SUGRA for which $B_2 = 0$, $F_1 = 0$, $F_3 = 0$ and $\tilde{F}_5 = F_5$, such that the Kaluza-Klein reduction of the action (1.2.7) gives a gravity action whose cosmological constant corresponds to AdS solutions for the geometry (so the electric part of F_5 has to be $-4\epsilon + \dots$ with the volume form ϵ of the internal 5 dimensional manifold. We will discuss this in more detail in the section 1.5). In addition the five form $\tilde{F}_5 = F_5$ is self dual in this order in α'. The self duality condition

$$F_5 = *F_5 \tag{1.2.10}$$

cannot be deduced from an effective action and has to be imposed by hand. The remaining effective action describing the dynamics of the five form F_5 is thus of the form

$$S_{IIb} = \frac{1}{2\kappa^2}\int d^{10}X\sqrt{-g}\Big(R - (\partial_\mu\phi)(\partial^\mu\phi) - \frac{F_5^2}{4\times 5!}\Big), \tag{1.2.11}$$

where we reached the Einstein frame by rescaling the metric with an exponential of the dilaton field times an appropriate constant.

Especially in the context of the holographic principle, which we are going to introduce in the next section, it is interesting to ask which higher derivative correction to the action (1.2.11) effectively describe type IIb super string theory up to the next orders in α'. For type IIb super string theory the corrections to the action (1.2.11) of order α' and α'^2 can be shown to vanish. The corrections of order α'^3 are computed by determining stringy corrections to gravitational scattering amplitudes as done in [55]. The resulting effective action that reproduces these corrections and contains the metric

and the Ramond-Ramond five form can be massaged into the form [4] [4]

$$S_{10}^{\gamma} = \frac{1}{2\kappa_{10}} \int d^{10}x\sqrt{-g}\Big[C^4 + C^3\mathcal{T} + C^2\mathcal{T}^2 + C\mathcal{T}^3 + \mathcal{T}^4\Big]. \tag{1.2.12}$$

The expression for S_{10}^{γ} is schematical and stands for a set of tensor contractions between the Weyl tensor C and $\mathcal{T}$, a 6-tensor that takes care of higher derivative corrections containing the five form. The term in brackets in (1.2.12) is given by [4]

$$\gamma W = \gamma\Big[C^4 + C^3\mathcal{T} + C^2\mathcal{T}^2 + C\mathcal{T}^3 + \mathcal{T}^4\Big] = \frac{\gamma}{86016}\sum_{i=1}^{20} n_i M_i, \tag{1.2.13}$$

where n_i and M_i are explicitly given in Appendix 5.1. The parameter γ is proportional to α'^3. As we will see in the next section, when we apply the holographic principle, it can be linked to the 't Hooft coupling λ of the boundary field theory. Explicitly the relation between γ and λ is

$$\gamma = \frac{\zeta(3)}{8}\lambda^{-\frac{3}{2}}. \tag{1.2.14}$$

Furthermore in equations (1.2.12) and (1.2.13) the tensor $\mathcal{T}$ is given by

$$\mathcal{T}_{abcdef} = i\nabla_a F^{+}_{bcdef} + \frac{1}{16}(F^{+}_{abcmn}F^{+}_{def}{}^{mn} - 3F^{+}_{abfmn}F^{+}_{dec}{}^{mn}), \tag{1.2.15}$$

with two sets of antisymmetrized indices a, b, c and d, e, f. In addition the right hand side of (1.2.15) is symmetrized with respect to the interchange of $(a, b, c) \leftrightarrow (d, e, f)$. Here F^{+} stands for the self dual part $\frac{1}{2}(1+*)F_5$ of the five form. So far it is unknown, whether the terms in (1.2.12) are complete. There are strong indications that this is the case, but since there is no strict mathematical proof we included this cautionary remark. The coupling corrected action finally takes the form

$$S = S_{10} + \gamma S_{10}^{\gamma} + \mathcal{O}(\gamma^{\frac{4}{3}}) \tag{1.2.16}$$

where γ is given in (1.2.14) in terms of the 't Hooft coupling λ, which, via applying the holographic principle, is proportional to $\alpha'^{-\frac{1}{2}}$. This relation between the string theoretic α' and the field theoretic λ is one subject of the discussions in the next section.

1.3 The Holographic Principle

Dualities can be found in almost all disciplines of theoretical physics. From maps between the Ising model and conformal field theories to the gauge/gravity duality linking

[4] This is computed from the results of [55] by closing the sypersymmetric algebra order by order in α'.

theories of gravity, typically (super-) string theories and (supersymmetric) conformal quantum field theories. To motivate the latter we start with considering black hole thermodynamics (BHT). The zeroth law of BHT states that the surface gravity k is constant over the horizon[5]. Comparing this to the zeroth law of regular thermodynamics, which implies the transitivity of 'being in thermal equilibrium', makes it natural to think of k as proportional to the temperature T. This relation can also be shown to be true in a different and more precise way in the context of the gauge/gravity duality. From the first law and with $T = \frac{k}{2\pi}$ for the Hawking temperature of a Schwarzschild black hole Bekenstein could derive the famous relation between the black hole entropy and its surface area A:

$$S_{BH} = \frac{A}{4G}, \tag{1.3.1}$$

where G is the Newton constant. This connection between entropy and area, which at first glance seems very surprising, can be generalized to any space time region: The upper bound of its entropy is given by the surface area of that region. From a geometric point of view a non rotating and uncharged black hole is a mass distribution, whose Schwarzschild radius coincides with its actual radius. With Bekenstein's formula black holes can be understood also from an information theoretic angle: They are subsets of space time, which reach the maximum of information, that can be contained in a region of this size, given by $\frac{1}{4G}$ times the boundary size of this region. The link between the entropy of an n dimensional volume and the size of its $n-1$ dimensional boundary is seen as one of the first hints to the holographic principle.

A more concrete argument for the duality between a conformal field theory and a higher dimensional string theory was motivated by 't Hooft's observation regarding the large N_c limit of Super Yang-Mills Theories (SYMs) with gauge group $SU(N_c)$, while the 't Hooft coupling $\lambda = g_{YM}^2 N_c$ is kept fixed. In this limit only planar diagrams contribute, all other types of diagrams are suppresses as N_c^{2-2g}, where g is the genus of the Riemann surface on which the diagram can be drawn. The Euler characteristic $\chi = 2 - 2g$ of surfaces of genus g appearing as the exponential in a series expansion of a generating functional can also be found in string theory: Let S_p be the Polyakov action, let $g_s = e^{\lambda'}$ be the string coupling and Σ_g be the world sheet of a string with genus g then the generating functional can be written as

$$Z = \sum_{g=0}^{\infty} e^{-\lambda'(2-2g)} \int_{\Sigma_g} \mathcal{D}X^m \mathcal{D}h_{\alpha\beta} e^{-S_p}. \tag{1.3.2}$$

Here λ' is the expectation value of the dilaton field, X^m are the coordinates of the target space time, in which the string is embedded and $h_{\alpha\beta}$ is the metric induced on the world sheet. Identifying the string coupling with $\frac{1}{N_c}$ leaves the expansions of the

[5]The link to thermodynamics is that constant k implies thermal equilibrium.

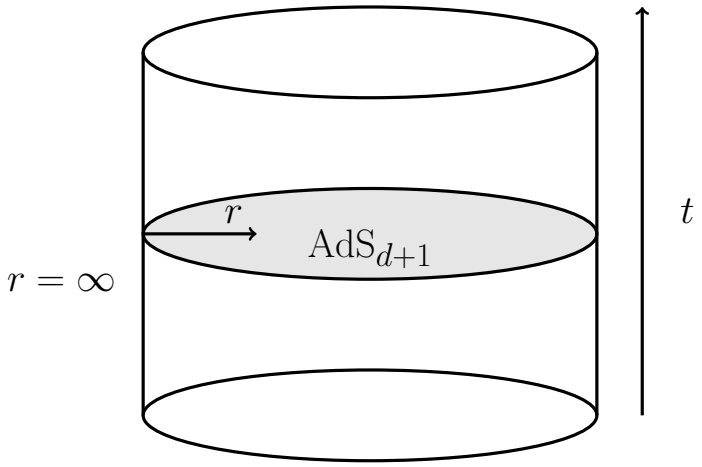

Figure 1.1: Graphic depiction of a $d+1$ dimensional AdS-space. The spatial coordinates of the boundary, on which the d dimensional field theory lives, are wrapped up to a circle, which lies at $r = \infty$. Here r is the radial coordinate of the AdS-space, which can be imagined as a bundle of hyperbolic spaces that are stacked along a temporal axis.

generating functionals of string theory and the SYM in the same form. The large N_c limit links the 'planar' field theory to string theory with vanishing coupling, thus string theory, where higher loop diagrams are ignored.

Aside these rather general motivations for the gauge/gravity duality there is more specific argument for the holographic principle. For this we focus on the most prominent duality between gauge theories and string theories, the AdS/CFT duality, which links $\mathcal{N} = 4$ SYM in 4 dimensions to its dual gravity theory, type IIb superstring theory in $AdS_5 \times S_5$. We start with considering the latter theory in a general 10 dimensional space. If the string coupling g_s is small the part of the action describing the interaction between open and closed strings can be neglected, thus open and closed strings decouple. For low energy excitations the open strings, which begin and end on D-branes, induce a supersymmetric field theory on the worldvolume of the branes they are attached to. In the case of N coinciding $D3$-branes[6] and if we consider α' to be small, the induced field theory becomes $\mathcal{N} = 4$ SYM with coupling constant $g^2_{YM} = 2\pi g_s$. In the low energy limit the closed strings are described by classical supergravity (SUGRA) in $\mathbb{R}^{(9,1)}$.

Instead of the weak coupling perspective we now consider N coinciding massive $D3$ branes in the strong ('t Hooft) coupling limit $1 \ll g_s N$. In this setting $g_s N \propto \frac{L^4}{\alpha'^2}$, where α' can still be small, while $1 \ll L$, in order to have a weak curvature. The N coinciding $D3$ branes are massive and curve space time, such that the geometry deep

[6]This notation implies that the D-brane takes up 3+1 coordinates of the manifold, specifically in this case 3 spatial and the temporal direction.

inside the bulk is not flat anymore. An observer on the boundary searching for low energy closed strings, which are effectively described by SUGRA in this limit, will find two different kinds of those in the bulk, whose energy will seem identically small to him. On the one hand he finds closed strings with low energy propagating close to the boundary, where the geometry is $\mathbb{R}^{(9,1)}$, due to the small curvature. On the other hand he sees strings deep inside the bulk at radial position r, which can reach high energies E_r, but due to the strong curvature close to the stack of $D3$ branes, implying $|g_{00}| \ll 1$ deep in the bulk, the observer measures their energy as

$$E = \sqrt{-g_{00}} E_r \ll 1 \tag{1.3.3}$$

if r is sufficiently small. Near the throat of this space the geometry is $AdS_5 \times S_5$. This gives rise to the duality between type IIb SUGRA in $\mathbb{R}^{(9,1)}$ near the boundary and type IIb SUGRA in $AdS_5 \times S_5$ inside the bulk. The open string/low coupling perspective gave rise to a duality between type IIb SUGRA in $\mathbb{R}^{(9,1)}$ and $\mathcal{N} = 4$ SYM theory, which leads to the conjectured duality between $\mathcal{N} = 4$ SYM theory at large N (small g_s for the strings) and large 't Hooft coupling $\lambda = g_{YM}^2 N$ (small α' for the strings) on the boundary of an Anti-de Sitter space and type IIb SUGRA in the bulk. This version of the holographic principle is known as the weak duality. The argument for the duality between the two theories is enforced by observing that they share the same symmetries. For instance the R-symmetry group of the $\mathcal{N} = 4$ SYM theory $SU(4)_R$ is dual to the symmetry group of the S_5-factor of $AdS_5 \times S_5$, given by $SO(6) \simeq SU(4)$.

The low energy limit was crucial for the open and closed strings to decouple, which lead to the conjectured duality between a classical supergravity ($\alpha' \to 0$) at weak (string) coupling g_s and a conformal field theory at strong ('t Hooft) coupling. However, there are strong indications that the validity of the duality goes even further: Leaving the low energy limit leads to the even bolder conjecture of the duality between $\mathcal{N} = 4$ SYM with finite gauge group rank N_c and finite 't Hooft coupling λ and type IIb super string theory at non zero string coupling and α'. This is know as the strong form of the AdS/CFT conjecture. The conjecture can be generalized to various dimensions and other sectors of string theory. In this work we will mainly focus on the duality derived or motivated above.

Mathematically the AdS/CFT duality can be formulated by equating the generating functionals of the quantum field theory and the string theory in the bulk: Consider a field theory operator $\mathcal{O}$ with (scaling) dimension Δ and source ϕ_0. The generating

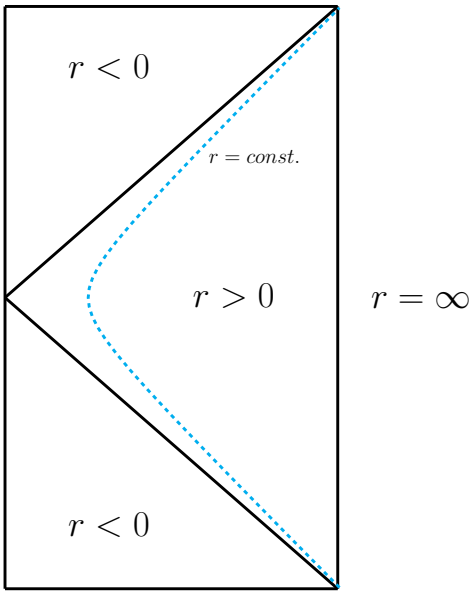

Figure 1.2: After a conformal transformation the AdS space can be depicted in a compact fashion by a *conformal diagram* (here for the example of AdS_2). In this work we are exclusively interested in the $r > 0$-wedge of the shown diagram, the top and bottom of which represent the infinite future $t = \infty$ and infinite past $t = -\infty$ each. The space shown in Fig. 1.1 corresponds to the triangular region, whose edges depict the limits $r = \infty$ and $r = 0$.

functional W for its connected Green's functions is given by

$$Z_{CFT}[\phi_0] = e^{-W[\phi_0]} \tag{1.3.4}$$

$$W[\phi_0] = S - \int d^4x \phi_0 \mathcal{O}, \tag{1.3.5}$$

where S is the action of the CFT. The action governing the dynamics of a field ϕ on the string theory side is still an integral over 10 dimensions. However, the five sphere coordinates can be integrated out. With a Kaluza-Klein reduction we end up with an action describing the dynamics of fields in a 5 dimensional AdS space. Let $z \in [0, 1]$ be the radial coordinate, where the boundary is located at $z = 0$, and let Z_{string} be the generating functional of string theory. The holographic principle now states that

$$Z_{string}[\lim_{z\to 0} \phi z^{\Delta-4} = \phi_0] = Z_{CFT}[\phi_0], \tag{1.3.6}$$

which links the fields on the string theory side to the sources of corresponding operators in the field theory. This duality is valid for gauge invariant (and hence physical) operators only. The equation (1.3.6) allows us to determine n-point functions of said operators by solving the EoM of the dual field ϕ and varying the generating functional

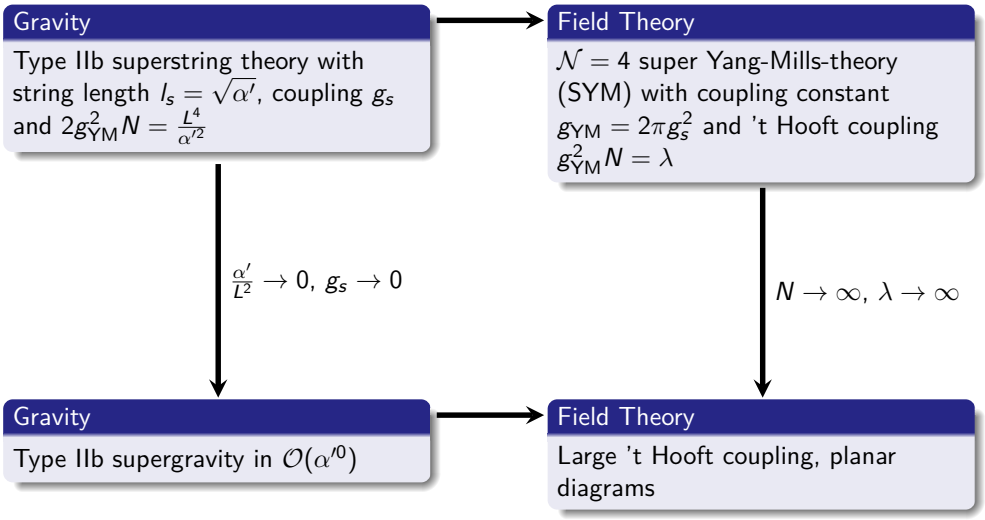

Figure 1.3: A graphic depiction of the strong (top row) and weak (bottom row) gauge/gravity duality between type IIb superstring theory in $AdS_5 \times S_5$ and $\mathcal{N} = 4$ super Yang-Mills theory, known as the AdS/CFT duality.

with respect to ϕ_0. For the weak duality we approximate

$$Z_{string}[\phi] \approx e^{-S_{\text{SUGRA}}[\phi]}. \tag{1.3.7}$$

This gives us all we need to explicitly compute field theoretic observables from gravity using the dictionary, which can be derived from (1.3.6) and (1.3.7). As discussed in section 1.2 we can leave the $N \to \infty$ limit or the $\lambda \to \infty$ limit by computing higher loop corrections or higher α' corrections to gravitational scattering amplitudes and model the effective action accordingly. Let us consider the latter case. In section 1.2 we have seen that the action in (1.3.7) is in this case modified by

$$S_{\text{SUGRA}} \to S_{\text{SUGRA}} + \alpha'^3 S_{10}^{\alpha'^3}, \tag{1.3.8}$$

with $S_{10}^{\alpha'^3}$ taking care of higher α' corrections (1.2.12). This delivers gravitational propagators up to order $\mathcal{O}(\alpha'^3)$, which correspond to field theoretic correlators of order $\mathcal{O}(\lambda^{-3/2})$.

1.4 A glance into the AdS/CFT dictionary

This section is meant to give an overview of the derivation of the standard AdS/CFT recipes and prescriptions, which we are going to apply throughout this work. We are

going to outline how to compute field theoretic quantities and observables e.g. n-point functions, transport coefficients or modes of quasiparticles from gravity. The starting point is relation (1.3.7).

1.4.1 CFT Correlators and graviational propagators

We start with determining the two point function of a scalar operator and the correlator of a $SU(4)_R \supset U(1)$ current in $\mathcal{N} = 4$ SYM in the large N limit from gravity[7].

Let $\mathcal{O}$ be a scalar operator with conformal (scaling) dimension Δ and let ϕ_0 be its source. As its gravitational dual we consider a scalar field ϕ with mass $\Delta(\Delta - 4)$ in AdS space with metric[8]

$$ds^2 = \frac{l^2}{z^2}\Big(dz^2 + \eta_{\mu\nu}dx^\mu dx^\nu\Big), \tag{1.4.1}$$

where l is the AdS radius, which will be set to 1 again with the help of rescaling. In these coordinates the boundary is positioned at $z = 0$. We do not consider backreactions of the field ϕ to the geometry and thus can write its action as

$$S = -c\int dx^4 dz\sqrt{-g}\Big(g^{\mu\nu}(\partial_\mu\phi)(\partial_\nu\phi) + m^2\phi^2\Big). \tag{1.4.2}$$

With the EoM

$$\Box\phi - m^2\phi = 0 \tag{1.4.3}$$

the on shell action induced on $z = \epsilon$ is given by

$$c\int_{z=\epsilon} dx^d\sqrt{-g}g^{zz}\phi\partial_z\phi. \tag{1.4.4}$$

Since the scalar field ϕ with mass $\Delta(\Delta - 4)$ behaves as $z^{4-\Delta}$ at the boundary we set

$$\phi(z,x) = \int \frac{d^4p}{(2\pi)^4}e^{ipx}\Phi(z,p) \tag{1.4.5}$$

$$\Phi(z,p) = \frac{\phi_1(z,p)}{\phi_1(\epsilon,p)}\phi_0(p)\epsilon^{4-\Delta} \tag{1.4.6}$$

[7] The $U(1)$ subgroup of the $SU(4)_R$ symmetry group was chosen, such that two of the Weyl fermions have charges $\pm\frac{1}{2}$ as in [23].

[8] Following the nomenclature often chosen in the literature we denoted the (inverted) radial coordinate of the (pure) AdS-space with z. This should not be confused with the third spatial coordinate, which we call z as well throughout the main part of this thesis. This choice of nomenclature regarding the radial coordinate will be restricted to this introductory chapter.

with appropriate functions ϕ_1 and ϕ_0. With this choice for Φ the field induced on the ϵ-shell is ϕ_0. Inserting Φ and the explicit form of g^{zz} and $\sqrt{-g}$ into the action gives

$$S = \frac{c}{\epsilon^3}\int \frac{d^4p}{(2\pi)^4}\Phi(\epsilon,-p)\partial_z\Phi(z,p)\big|_{z=\epsilon} = \frac{c}{\epsilon^{2\Delta-5}}\int \frac{d^4pd^4q}{(2\pi)^4}\delta^4(p+q)\phi_0(q)\partial_z\frac{\phi_1(z,p)}{\phi_1(\epsilon,p)}\phi_0(p). \tag{1.4.7}$$

The correlator in momentum space of the corresponding scalar operator on the $z=\epsilon$ shell can be written as [51]

$$\langle\mathcal{O}(p)\mathcal{O}(q)\rangle = (2\pi)^8\frac{\delta^2 S}{\delta\phi_0(p)\delta\phi_0(q)} = \frac{(2\pi)^4c\delta^4(p+q)}{\epsilon^{2\Delta-5}}\partial_z\frac{\phi_1(z,p)}{\phi_1(\epsilon,p)}\bigg|_{z=\epsilon}. \tag{1.4.8}$$

In general this result is still divergent and contains contact terms, which have to be removed. After ignoring scheme dependent terms, the remaining logarithmic divergences can be dealt with via counter terms to the action, which allows us to finally take the $\epsilon\to 0$ limit.

For the specific case of a two-point function of an operator $\mathcal{O}$ with conformal weight Δ, where Δ is sufficiently large, we can approximate the correlator using holography as follows [65]

$$\langle\mathcal{O}(t,\vec{x}),\mathcal{O}(t,\vec{x}')\rangle \approx e^{-\Delta L}, \tag{1.4.9}$$

where L is the (bulk) geodesic length between the boundary points $(t,\vec{x})$ and $(t,\vec{x}')$. In this case we regularize by subtracting the vacuum geodesic length L_0, corresponding to the geodesic between the two boundary points in pure AdS. The regularized two-point can thus be approximated

$$\langle\mathcal{O}(t,\vec{x}),\mathcal{O}(t,\vec{x}')\rangle_{reg} \approx e^{-\Delta(L-L_0)}. \tag{1.4.10}$$

Focusing now on gauge fields, the following action can be derived from a specific solution to type IIb SUGRA after integrating out the five sphere coordinates

$$S = \int d^5x\sqrt{-g}\Big(R + 12 + F_{\mu\nu}F^{\mu\nu}\Big), \tag{1.4.11}$$

where $F = dA$ and $A = A_\mu dx^\mu$ is a (co-)vector field in AdS_5. The EoM for A_μ are the standard Maxwell equations in curved space

$$\partial_\mu(\sqrt{-g}g^{\mu\alpha}g^{\nu\beta}F_{\alpha\beta}) = 0. \tag{1.4.12}$$

Let us now consider the AdS_5 Schwarzschild black hole solution to the gravity part of (1.4.11), meaning that we do not consider backreactions of the Maxwell-field A_μ to the geometry. Writing $u = \frac{r_h^2}{r^2}$ with the horizon of the black hole at $r = r_h$ and the boundary of the AdS space at $r=\infty$ this metric is given by the AdS part of (1.5.12).

After Fourier transforming A_μ, the (on shell) action for the $U(1)$-vector field induced on the boundary becomes

$$S \sim \int_{u=0} \frac{dqd\omega}{(2\pi)^2}\Big(A_t\partial_u A_t - f(u)\mathbf{A}\partial_u\mathbf{A}\Big), \tag{1.4.13}$$

with $\mathbf{A} = \{A_x, A_y, A_z\}$. From (1.4.13) we can derive the gravitational propagator of the gauge invariant combinations $E_\perp = \omega A_{x,y}$ and $E_{||} = \omega A_z + qA_t$. After removing contact terms we obtain the propagators in an analogous fashion as before [23]

$$\Pi_{||} = -\frac{N_c^2T^2}{8}\lim_{u\to 0}\frac{\partial_u E_{||}}{E_{||}},\ \Pi_\perp = -\frac{N_c^2T^2}{8}\lim_{u\to 0}\frac{\partial_u E_\perp}{E_\perp} \tag{1.4.14}$$

by using the correct normalization factor $\frac{N_c^2T^2}{16}$ of the action. Here $\Pi_{||}$ and $\Pi_\perp$ are linked to the QFT current-current correlator

$$C_{\mu\nu}(x-y) = -i\theta(x^0-y^0)\langle|J_\mu(x)J_\nu(y)|\rangle \tag{1.4.15}$$

$$C_{\mu\nu}(q) = \int \frac{d^4q}{(2\pi)^4}e^{-iqx}C_{\mu\nu}(x) \tag{1.4.16}$$

in the following way: The Ward identity responsible for current conservation $q_\mu C^{\mu\nu} = 0$ suggests that one building block of $C_{\mu\nu}$ has to be the projector

$$P_{\mu\nu} = \eta_{\mu\nu} - \frac{q_\mu q_\nu}{q^2}, \tag{1.4.17}$$

which can be split up into a transverse $P^T_{ij} = \eta_{ij} - \frac{q_iq_j}{q^2}$ and a longitudinal $P^L_{\mu\nu} = P_{\mu\nu} - P^T_{\mu\nu}$ component. The retarded Greens function for the current thus has the form

$$C_{\mu\nu}(q) = P^T_{\mu\nu}\Pi^T(q) + P^L_{\mu\nu}\Pi^L(q). \tag{1.4.18}$$

The AdS dictionary now identifies Π^T and Π^L in (1.4.18) with the corresponding quantities in (1.4.14).

1.4.2 Quasinormal Modes

With the help of the holographic principle it is possible to describe a $\mathcal{N} = 4$ SYM plasma at strong coupling and far from thermal equilibrium. For increasing temperatures $T > T_c$ hot QCD and $\mathcal{N} = 4$ SYM with large gauge group rank become more similar. One reason for this is that QCD approximates a conformal theory for extremely high energies [21]. This makes it an interesting system to study, even if this field theory is not the one nature has chosen. The equilibration of such a plasma can be analyzed by considering tiny fluctuation around the AdS solution that corresponds to thermal equilibrium. Similarly to gravitational waves in standard general relativity (GR) we

make the ansatz

$$g_{\mu\nu} \to g_{\mu\nu} + h_{\mu\nu} \tag{1.4.19}$$

and linearize the EoM for the metric in $h_{\mu\nu}$. The transformation behaviour under the spatial $SO(3)$ symmetry group allows us to split the perturbations $h_{\mu\nu}$ into spin$= 0, 1, 2$ types [9]. Typically the symmetry of the setting we are studying allows us to decouple the EoM of the different types of perturbations or at least one of them from the rest (see sections 2.1.3.1 and 2.2). We call these fluctuations around the equilibrium state *quasinormal modes* (QNMs). Unlike e.g. eigenmodes of hermitian operators their frequency ω has a non vanishing imaginary part, which damps their amplitude over time. Any out-of-equilibrium plasma eventually enters a phase in which its equilibration can be described by a superposition of QNMs, such that their damping factor obtained from the imaginary part of the QNM frequencies plays a crucial role regarding the equilibration time. Since we have

$$h_{\mu\nu} \sim e^{-i\omega t}, \tag{1.4.20}$$

the QNM, whose corresponding frequency has the smallest absolute imaginary part, dominates the time the system takes to reach thermal equilibrium.

The real parts of the QNM frequencies are proportional to their energies, which allows us to read off thermalization patterns from the distribution of the discrete frequency spectrum on the complex plane: We say a thermalization of a system is *top-down*, if modes with the highest real part of the frequencies thermalize the fastest and *bottom-up* if the contrary is true.

There is a myriad of ways to compute QNMs and their frequencies, which generally can be obtained from the poles of the propagators of the corresponding fluctuation. In sections 2.1.3.1, 2.2 and 2.3 we follow several of them to find finite coupling corrected QNM spectra in different settings and geometries.

1.4.3 Temperature and the black hole radius

Finite temperature field theories are obtained by compactifying the (Euclidean) time coordinate, which has to have a periodicity of $\frac{1}{T}$, where we set $k_b = 1$. This relation is obtained from the requirement that the thermal average of an operator $\mathcal{O}$ coincides with its quantum field theoretic expectation value:

$$\int D\Psi \langle \Psi(t)|\mathcal{O}|\Psi(t)\rangle = \int D\Psi \langle \Psi(t)|\mathcal{O}e^{H/T}|\Psi(t)\rangle = \int D\Psi \langle \Psi(t)|\mathcal{O}|\Psi(t+\frac{i}{T})\rangle. \tag{1.4.21}$$

Rotating to complex time $t = it_E$ implies that t_E has to have periodicity $\frac{1}{T}$. The gauge/gravity duality now requires the (Euclidean version of the) geometry on the gravity side to have the same periodicity. We consider the following metric ansatz for

a static black hole in AdS space

$$ds^2 = T(r)dt_E^2 + \frac{dr^2}{R(r)} + g_{ij}(r)dx^i dx^j, \tag{1.4.22}$$

while we assume this geometry to have a horizon at $r = r_h$, meaning that $T(r_h) = R(r_h) = 0$. With a compact time coordinate $t_E \in [0, \frac{1}{T}]$ we are now at risk of getting a conical singularity at $r = r_h$, if we do not choose the relation between the period length of t and the horizon radius r_h carefully. For small $\rho = r - r_h$ we obtain

$$ds^2 = \frac{1}{R'(r_h)\rho}\left(\rho^2 T'(r_h)R'(r_h)dt_E^2 + d\rho^2\right) + \dots. \tag{1.4.23}$$

The term inside the brackets resembles the line element of a flat two dimensional space in spherical coordinates with angle coordinate t_E. Defining the new radial coordinate u as

$$du^2 = \frac{d\rho^2}{R'(r_h)\rho} \tag{1.4.24}$$

gives

$$ds^2 = \frac{u^2}{4}T'(r_h)R'(r_h)dt_E^2 + du^2 + \dots. \tag{1.4.25}$$

Also shifting the angle coordinate t_E to

$$\phi = \frac{1}{2}\sqrt{T'(r_h)R'(r_h)}t_E \tag{1.4.26}$$

leaves the first two term of the metric in the form

$$u^2 d\phi^2 + du^2. \tag{1.4.27}$$

In order to avoid a defect angle in (1.4.27), the periodicity of the ϕ coordinate has to be 2π, which means

$$\frac{1}{2T}\sqrt{T'(r_h)R'(r_h)} = 2\pi. \tag{1.4.28}$$

Solving this equation for r_h gives us the horizon radius in terms of the temperature of the boundary field theory. We would have obtained the same result if we demanded that the temperature of the boundary field theory has to match the Hawking (surface) temperature of the AdS black hole in (1.4.22).

1.4.4 Entanglement Entropy

The entanglement entropy (EE), which is a natural extension to the von-Neumann-entropy, has several applications in quantum field theory and quantum information theory. Most importantly it may be used to describe phases of matter, that can not be classified with the help of standard order parameters. The EE gives a measure for the

entanglement between a subsystem A and a subsystem B of a Hilbert space H.

For a general system composed of states $|\Psi_n\rangle$ in a Hilbert space H with probability p_n, the density matrix ρ, projecting onto the states with the corresponding probabilities, is defined as

$$\rho = \sum_n p_n |\Psi_n\rangle\langle\Psi_n| \tag{1.4.29}$$

With the help of this, we can define a quantum mechanical version of the thermodynamic entropy, which is given by the von-Neumann-entropy

$$S = -\mathrm{Tr}(\rho \ln(\rho)). \tag{1.4.30}$$

If the Hilbert space factorizes in the form $H = H_A \times H_B$, where each $H_{A,B}$ is the Hilbert space of a subsystem labeled A, B, then we define the entanglement entropy of A with the help of the reduced density matrix

$$\rho_A = \mathrm{Tr}_B(\rho), \tag{1.4.31}$$

where we traced out all states in B, as follows

$$S_A = -\mathrm{Tr}_A(\rho_A \ln \rho_A). \tag{1.4.32}$$

Holographically the EE of a region A on the boundary of the AdS space, where the field theory lives, can be computed from the minimal surface Σ_A that extends into the bulk of the AdS space, and whose boundary is ∂A, the boundary of the region A. Explicitly this means for a five dimensional AdS space

$$S_A = \frac{\mathrm{vol}(\Sigma_A)}{4G_5}, \tag{1.4.33}$$

where G_5 is the Newton constant in five dimensions and $\mathrm{vol}(\Sigma_A)$ is the volume of Σ_A. Since $\mathrm{vol}(\Sigma_A)$ diverges, due to contributions coming from segments close to the boundary, we have to regularize it by an UV cutoff, similarly to the procedure in section 1.4.1. Choosing the cutoff by considering the radial coordinate z of the AdS space to lie in the interval $[\epsilon, 1]$, gives a leading term of

$$S_A \propto \frac{1}{\epsilon^2} + \dots. \tag{1.4.34}$$

In section 3.2.1 we will see this procedure at work in more detail. The regularization there is built on the regularization of geodesic lengths in Anti- de Sitter space.

1.4.5 Transport coefficients and linear response

Consider a quantum field theoretic system described by the action

$$S + \int d^4x \mathcal{O}(x)\phi_0(x), \tag{1.4.35}$$

in which we coupled a source field ϕ_0 to an operator $\mathcal{O}$. We think of the field ϕ_0 as a tiny perturbation of the system and search for the one-point function $\langle\mathcal{O}\rangle_{\phi_0}$, encoding the response to this perturbation. If we assume $\langle\mathcal{O}\rangle_{\phi_0=0} = 0$, which can be achieved by subtracting the vacuum expectation value at zero ϕ_0, we get

$$\langle\mathcal{O}\rangle_{\phi_0} = -\int d^4y \langle\mathcal{O}(x)\mathcal{O}(y)\rangle_{\phi_0=0}\phi_0(y) + \mathcal{O}(\phi_0^2). \tag{1.4.36}$$

In momentum space this implies

$$\langle\mathcal{O}\rangle_{\phi_0} = G_R(\omega, k)\phi_0(\omega, k). \tag{1.4.37}$$

Hydrodynamic modes evolve slower than any other mode in the system, such that in the hydrodynamic limit these modes can be integrated out and only slowly varying fields survive. In this limit (i.e. $k \to 0$ and $\omega \to 0$) the formula for the response of $\langle\mathcal{O}\rangle_{\phi_0}$ to a time dependent source field ϕ_0 is

$$\langle\mathcal{O}\rangle_{\phi_0} = -\beta\partial_t\phi_0, \tag{1.4.38}$$

where we call β a *transport coefficient*. Transforming (1.4.38) also to momentum space and comparing it with (1.4.37) gives a variant of the *Kubo formula*

$$\beta = -\lim_{\omega\to 0}\frac{1}{\omega}G_R(\omega, k = 0). \tag{1.4.39}$$

With the help from the prescription to compute QFT correlators from gravity, we now have all the tools needed to compute (1.4.39) from holography.

1.4.6 Spectral functions and photoemission rate

Let us remain in the setting of the previous subsection. For a given retarded Green's function $G_R(\omega, k)$ in momentum space we define the *spectral function* $\chi(\omega, k)$ to fulfill

$$G_R(\omega, k) = \lim_{\epsilon\to 0^+}\int\frac{d\omega'}{2\pi}\frac{\chi(\omega', k)}{\omega' - \omega + i\epsilon}. \tag{1.4.40}$$

We can solve this equation for the spectral function χ by

$$-2\mathrm{Im}G_R(\omega,k) = i(G_R(\omega,k) - G_R(\omega,k)^*) = i\lim_{\epsilon\to 0^+}\int\frac{d\omega'}{2\pi}\frac{\chi(\omega',k)}{\omega'-\omega+i\epsilon}$$
$$-i\lim_{\epsilon\to 0^+}\int\frac{d\omega'}{2\pi}\frac{\chi(\omega',k)}{\omega'-\omega-i\epsilon} = \chi(\omega,k). \tag{1.4.41}$$

In the case of a retarded current-current correlator

$$G_R(\omega,k)_{\mu\nu} = -i\int d^4x e^{-ikx}\theta(t)\langle[J^{\mathrm{em}}_\mu(x), J^{\mathrm{em}}_\nu(0)]\rangle, \tag{1.4.42}$$

we call the trace $\chi = \eta^{\mu\nu}\chi(\omega',k)_{\mu\nu}$ the *spectral density*. With the definition of P^T and P^L used in (1.4.18) one receives for the respective transverse and longitudinal components

$$\eta^{\mu\nu}\chi(\omega',k)_{\mu\nu} = \eta^{\mu\nu}P^L_{\mu\nu}\chi_{||}(\omega',k) + \eta^{\mu\nu}P^T_{\mu\nu}\chi_\perp(\omega',k) = -2\mathrm{Im}\Pi^L - 4\mathrm{Im}\Pi^T. \tag{1.4.43}$$

Considering (1.4.39), we can obtain the transport coefficient in this channel, which is the *conductivity*, from a low frequency expansion of $\chi(\vec{k}=0)$.

In thermal quantum field theory The Wightman fuction

$$C^<_{\mu\nu}(k) = \int d^4x e^{-ikx}\langle J^{\mathrm{em}}_\mu(0), J^{\mathrm{em}}_\nu(x)\rangle \tag{1.4.44}$$

links the spectral function $\chi_{\mu\nu}$ to the differential photoemission rate $d\Gamma_\gamma$. Let $n_b(k^0)$ be the Bose Einstein distribution function

$$n_b(k^0) = \frac{1}{e^{k^0/T}-1}, \tag{1.4.45}$$

then we have on shell

$$dk^3\eta^{\mu\nu}n_b(k^0)\chi_{\mu\nu}(k) = dk^3\eta^{\mu\nu}C^<_{\mu\nu}(k) = d\Gamma_\gamma\frac{\pi}{\alpha_{em}|k|}. \tag{1.4.46}$$

This result allows us to determine the photoemission rate from gravity, by using the relation (1.4.14).

1.5 The AdS-Schwarzschild black hole with coupling corrections

We are going to apply the higher derivative corrected AdS-Schwarzschild black hole solution multiple times throughout this thesis. Here we derive this geometry, first found in [5], as an exercise from action (1.3.8), respectively (1.2.16). The field theoretic dual of this solution is a quark gluon plasma in equilibrium with finite coupling.

The free fields, with respect to which we have to vary (1.3.8) in order to find the

relevant EoMs are the four form C_4, while the Ramond-Ramond five form is its exterior derivative $dC_4 = F_5$, the dilaton field ϕ, whose EoM decouples from the rest, such that it can be ignored here and the metric itself. The five form enters (1.2.11) as

$$\cdots - \sqrt{-g}\frac{F_5^2}{4 \times 5!}. \tag{1.5.1}$$

For a specific choice of indices $\{a, b, c, d\}$ labeling coordinates of the 10 dimensional manifold let $\{efghij\}$ be the indices of the remaining 6 coordinates, then

$$\begin{aligned}\frac{\delta S_{10}}{\delta (C_4)_{abcd}} &= \frac{1}{4 \times 5!}\partial_\mu \Big(\sqrt{-g}\frac{(dC_4)_{\alpha\beta\gamma\delta\epsilon} g^{\alpha\alpha'} g^{\beta\beta'} g^{\gamma\gamma'} g^{\delta\delta'} g^{\epsilon\epsilon'} (dC_4)_{\alpha'\beta'\gamma'\delta'\epsilon'}}{\partial_\mu (C_4)_{abcd}} \\ &= \frac{1}{2}\partial_\mu \sqrt{-g} g^{\mu\mu'} g^{aa'} g^{bb'} g^{cc'} g^{dd'} (dC_4)_{\mu' a' b' c' d'} \Big).\end{aligned} \tag{1.5.2}$$

Comparing this with $\frac{1}{2}(d * F_5)_{efghij}$, which is proportional to

$$\partial_\mu \Big(\sqrt{-g} g^{\mu\mu'} g^{aa'} g^{bb'} g^{cc'} g^{dd'} (F_5)_{\mu' a' b' c' d'} \Big) \tag{1.5.3}$$

shows that

$$\frac{\delta S_{10}}{\delta (C_4)_{abcd}} = 0 \tag{1.5.4}$$

for all $\{a, b, c, d\}$ is equivalent to

$$d * F_5 = 0, \tag{1.5.5}$$

This together with $dF_5 = ddC_4 = 0$ are the EoMs for the Ramond-Ramond five form to the lowest order in α'. Before we address higher derivative corrections it is advisable to look in detail at the following prescription of SUGRA to obtain an effective action solely for the metric once we have found a solution for F_5:

> "Take the solution of the 5−form, plug it back into the action and only consider the magnetic part of F_5 and double its contribution, then vary with respect to the metric." (1.5.6)

In the case, where we do not consider α'-corrections or gauge fields A_μ, the solution for the five form of (1.5.5) we are going to work with can be written as

$$F_5 = (1 + *)F_5^{el} \tag{1.5.7}$$

$$F_5^{el} = -4\epsilon_{AdS} = -4\sqrt{-g_{AdS}} dt \wedge du \wedge dx \wedge dy \wedge dz, \tag{1.5.8}$$

where ϵ_{AdS} is the volume form of the AdS-part of our manifold and el labels the electric

part of F_5 [9]. If we want to derive the EoM for general metric components from the type IIb action we, of course, are not allowed to impose a dependence of the five form on $g^{\mu\nu}$ on the level of the action. Instead we have to vary the five form part of the action as follows

$$\delta \int d^{10}x\sqrt{-g}\Big[-\frac{1}{4\cdot 5!}F_5^2\Big] = -\frac{1}{4}\delta \int d^{10}x\sqrt{-g}\Big[g^{tt}g^{uu}g^{xx}g^{yy}g^{zz}(F_5^{el})^2_{tuxyz}+$$
$$g^{y_1y_1}g^{y_2y_2}g^{y_3y_3}g^{y_4y_4}g^{y_5y_5}(F_5^{mag})^2_{y_1y_2y_3y_4y_5}\Big] = -\frac{1}{4}\delta \int d^{10}x\Big[-\sqrt{\frac{g_{y_1y_1}g_{y_2y_2}g_{y_3y_3}g_{y_4y_4}g_{y_5y_5}}{g_{tt}g_{uu}g_{xx}g_{yy}g_{zz}}}$$
$$(F_5^{el})^2_{tuxyz} + \sqrt{\frac{g_{tt}g_{uu}g_{xx}g_{yy}g_{zz}}{g_{y_1y_1}g_{y_2y_2}g_{y_3y_3}g_{y_4y_4}g_{y_5y_5}}}(F_5^{mag})^2_{y_1y_2y_3y_4y_5}\Big], \tag{1.5.9}$$

which leads to a contribution to the EoM for $g^{\mu\nu}$ of the form

$$4\Big((-1)^{1+\sum_{i=1}^5\delta_{\mu y_i}}\frac{\sqrt{-g}}{2}g^{\mu\nu} - (-1)^{\sum_{i=1}^5\delta_{\mu y_i}}\frac{\sqrt{-g}}{2}g^{\mu\nu}\Big). \tag{1.5.10}$$

The same result is obtained from plugging the solution of the five form back into the action, only considering the contribution of the magnetic part times 2. [10]

After applying the prescription (1.5.6) the effective action for the metric reads

$$S = \int d^{10}x\sqrt{-g}\Big(R-8\Big). \tag{1.5.11}$$

We write the solution to the Einstein equations corresponding to an AdS-Scharzschild black hole times a five sphere in the form

$$ds^2 = -r_h^2\frac{dt^2}{u}(1-u^2) + \frac{du^2}{4u^2(1-u^2)} + \frac{r_h^2}{u}(dx^2+dy^2+dz^2) + d\Omega_5^2, \tag{1.5.12}$$

where r_h is the radial position of the black hole's horizon and $u = \frac{r^2}{r_h^2} \in [0,1]$ labels the radial coordinate of the AdS space with the boundary positioned at $u=0$ and the horizon at $u=1$. It is convenient to work with the following S_5-coordinates, for which we define μ_i with $i \in \{1,2,3\}$ to be the direction cosines

$$\mu_1 = \sin(y_1), \qquad \mu_2 = \sin(y_2)\cos(y_1), \qquad \mu_3 = \cos(y_1)\cos(y_2), \tag{1.5.13}$$

[9] Since we haven't solved for the geometry so far, it might be inappropriate to talk about an "AdS-part of the manifold". It is convenient to label the metric used in (1.5.8) as the AdS metric for later use. Strictly speaking F_5 should be proportional to the volume form of a five dimensional internal manifold, whose metric is still to be determined.

[10] The recipe (1.5.6), which is nothing but a calculational tool, is equivalent to the more intuitive but also more tedious approach of treating every metric component and every 4-form component as an independent field on the level of the action, varying with respect to all of them and solving the resulting system of EoM. One important lesson to learn here is that the justification for this prescription requires a self dual five form. This is a subtle point, since self duality is violated in some cases when we include higher derivative corrections [4].

and set the angles

$$\phi_1 = y_3, \qquad \phi_2 = y_4, \qquad \phi_3 = y_5, \tag{1.5.14}$$

such that the metric of the 5−sphere is given as

$$\begin{aligned} d\Omega_5^2 = &\sum_{i=1}^{3}\left(d\mu_i^2 + \mu_i^2 d\phi_i^2\right) = dy_1^2 + \cos(y_1)^2 dy_2^2 + \sin(y_1)^2 dy_3^2 + \\ &\cos(y_1)^2\sin(y_2)^2 dy_4^2 + \cos(y_1)^2\cos(y_2)^2 dy_5^2. \end{aligned} \tag{1.5.15}$$

After this lengthy but necessary preparation let us finally include higher derivative corrections. The ansatz for the metric we make is of the form

$$ds_{10}^2 = -r_h^2 U(u)dt^2 + \tilde{U}(u)du^2 + e^{2V(u)} r_h^2 (dx^2 + dy^2 + dz^2) + L(u)^2 d\Omega_5^2, \tag{1.5.16}$$

where we are forced to give up the product structure of our manifold and admit a u-dependent warping factor $L(u)$ in front of the 5-sphere line element. The EoMs for our 4-form components still have the form (1.5.5) simply because the $\mathcal{T}$-tensor defined in (1.2.15) vanishes on the unperturbed background. Thus, we also have

$$\frac{\delta S_{10}^{\gamma}}{\delta F_5} = 0 \tag{1.5.17}$$

in this case. The solution for the 5-form in order $\mathcal{O}(\gamma^1)$ and without gauge fields is

$$F_5 = (1 + *)F_5^{el} \tag{1.5.18}$$

$$F_5^{el} = \frac{-4}{L(u)^5}\epsilon_{AdS}^{\gamma}, \tag{1.5.19}$$

where ϵ_{AdS}^{γ} is the volume form of the γ-corrected AdS-part of our manifold. The five form is still self dual, such that we are allowed to plug the solution for the five form back into the action, only considering its magnetic part and doubling its contribution, which gives

$$\frac{1}{2\kappa_{10}}\int d^{10}x\sqrt{-\det(g_{10})}\left[R_{10} - \frac{8}{L(u)^{10}} + \gamma W\right]. \tag{1.5.20}$$

The EoM for the metric components from this action can be solved by an expansion in

the variable u^2

$$U(u) = \frac{(1-u^2)}{u}\Big(1 + \frac{5u^2\gamma}{8}(-130 - 130u^2 + 67u^4)\Big) \tag{1.5.21}$$

$$\tilde{U}(u) = \frac{1}{4u^2(1-u^2)}\Big(1 + \gamma\Big(\frac{325}{4}u^2 + \frac{1075}{16}u^4 - \frac{4835}{16}u^6\Big)\Big) \tag{1.5.22}$$

$$V(u) = -\frac{1}{2}\log(u) \tag{1.5.23}$$

$$L(u) = 1 + \frac{15\gamma}{32}(1+u^2)u^4. \tag{1.5.24}$$

This equips us with higher curvature corrected geometry of a non rotating and uncharged black hole in AdS space. Combining the results of this section with section 1.4.3 allows us to compute the temperature of a thermalized quark gluon plasma at finite coupling, given by

$$T = \frac{r_h}{\pi}\Big(1 + \frac{265}{16}\gamma\Big). \tag{1.5.25}$$

1.6 The AdS/CFT prescription for the boundary stress energy tensor

A crucial ingredient, which helps to make sense out of holographic calculations, is the link between the near boundary behaviour of the bulk metric and the stress energy tensor of the field theory living on the boundary. The conjectured AdS/CFT duality links the latter to the (renormalized and regularized) stress energy tensor induced on the boundary by the dual gravitational theory. We are going to present the following derivation in a way that is equivalent to but slightly different from the approach found in the literature [6], [15]. Our aim is to prove this relation in a manner that can be more easily extended to the higher derivative corrected case.

The starting point is the standard gravitational action, which can be written as

$$S = \frac{1}{k}\int d^{d+1}x\sqrt{-g}\Big(R + \frac{d(d-1)}{l^2}\Big) - \frac{2}{k}\int_\partial d^dx\sqrt{-\gamma}K, \tag{1.6.1}$$

where K is the extrinsic curvature of the boundary

$$K^{ab} = \nabla^a n^b \tag{1.6.2}$$

$$K = K^{ab}\gamma_{ab} \tag{1.6.3}$$

γ is the metric induced on the boundary, n^b is its (outward pointing) normal vector (tangent to a geodesic normal to ∂) and k is $\frac{1}{16\pi G}$. Again we will set $l = 1$ in this section. The additional boundary term (Gibbons-Hawking-York term) in (1.6.1) is needed to

cope with terms of the form

$$\ldots_{ab}\, \delta\partial_r g^{\alpha\beta}\Big|_\partial \tag{1.6.4}$$

when varying the action. Here r is the radial coordinate of the AdS-space. In general the boundary term in (1.6.1) can be constructed by requiring that the variation of the gravitational action plus some (regularization) boundary term doesn't produce terms as (1.6.4), thus fulfilling

$$S^{reg} = \int_\partial d^d x \mathcal{L}^{reg} \tag{1.6.5}$$

$$\mathcal{L}^{grav} = \sqrt{-g}\Big(R + d(d-1)\Big) \tag{1.6.6}$$

$$0 = \frac{\partial}{\partial\delta\partial_r\gamma^{ab}}\left(\frac{\partial\mathcal{L}^{grav}}{\partial\partial_r^2 g^{\mu\nu}}\delta\partial_r g^{\mu\nu}\Big|_\partial + \delta S^{reg}\right) \tag{1.6.7}$$

for all indices a, b of the metric induced on the boundary. For the standard gravitational action

$$S^{grav} = \int d^{d+1}x\mathcal{L}^{grav} \tag{1.6.8}$$

this is fulfilled by the term in (1.6.1). We haven't renormalized the action so far. We are still missing a term S^{ct}, such that with this counter term

$$S = S^{grav} + S^{reg} + S^{ct} \tag{1.6.9}$$

doesn't diverge at the boundary. This additional action ensures that the stress energy tensor

$$T^{ab}[\gamma] = \frac{2}{\sqrt{-\gamma}}\frac{\delta S^{\text{on shell}}}{\delta\gamma_{ab}} \tag{1.6.10}$$

is regular. We can invert this logic (see [15]) and search for S^{ct}, a covariant action of the metric induced on the boundary, such that (1.6.10) is regular at the boundary. In the following we work with the general metric ansatz [6]

$$ds^2 = \frac{d\rho^2}{4\rho^2} + \frac{1}{\rho}g^B_{ij}dx^i dx^j, \tag{1.6.11}$$

where ρ corresponds to the radial direction of the AdS-space. Instead of integrating the Lagrange density from $\rho = 0$ to ∞, one could instead consider a non-divergent integral from ϵ to ∞, construct the correct counterterm depending on this quantity, and take the (now finite) $\epsilon \to 0$ limit afterwards. Let γ denote the metric induced on a $\rho = \epsilon$-slice, so $\gamma^{ij} = \frac{g^{ij}}{\epsilon}$, and let $\int_\partial$ be the integral over this submanifold. The variation of the (on shell) action S^{grav} can be computed as follows, where we make use of the sum convention regarding the ($\epsilon-$)boundary indices i, j and primes $'$ denote derivatives

with respect to ρ

$$\begin{aligned}
&\delta\int d^{d+1}x\mathcal{L}^{grav} = \int d^{d+1}x\frac{\partial\mathcal{L}^{grav}}{\partial g_{\mu\nu}}\delta g_{\mu\nu} + \frac{\partial\mathcal{L}^{grav}}{\partial g'_{\mu\nu}}\delta g'_{\mu\nu} + \frac{\partial\mathcal{L}^{grav}}{\partial\partial_i g'_{\mu\nu}}\delta\partial_i g'_{\mu\nu}\\
&+\frac{\partial\mathcal{L}^{grav}}{\partial g''_{\mu\nu}}\delta g''_{\mu\nu} + \frac{\partial\mathcal{L}^{grav}}{\partial\partial_i\partial_j g_{\mu\nu}}\delta\partial_i\partial_j g_{\mu\nu} = -\int_\partial d^dx\frac{\partial\mathcal{L}^{grav}}{\partial g''_{\mu\nu}}\delta g'_{\mu\nu} +\\
&\int d^{d+1}x\Big(\Big(\frac{\partial\mathcal{L}^{grav}}{\partial g'_{\mu\nu}} - \partial_i\frac{\partial\mathcal{L}^{grav}}{\partial\partial_i g'_{\mu\nu}} - \partial_\rho^2\frac{\partial\mathcal{L}^{grav}}{\partial g''_{\mu\nu}}\Big)\delta g_{\mu\nu}\Big)'\\
&= -\int_\partial d^dx\frac{\partial\mathcal{L}^{grav}}{\partial g''_{\mu\nu}}\delta g'_{\mu\nu} - \pi^{\mu\nu}\delta g_{\mu\nu}
\end{aligned} \tag{1.6.12}$$

with

$$\pi^{\mu\nu} = \frac{\partial\mathcal{L}^{grav}}{\partial g'_{\mu\nu}} - \partial_i\frac{\partial\mathcal{L}^{grav}}{\partial\partial_i g'_{\mu\nu}} - \partial_\rho^2\frac{\partial\mathcal{L}^{grav}}{\partial g''_{\mu\nu}}. \tag{1.6.13}$$

Since the standard gravitational action is a two-derivative action one gets from (1.6.7)

$$\mathcal{L}^{reg} = \frac{\partial\mathcal{L}^{grav}}{\partial g''_{\mu\nu}}g'_{\mu\nu}, \tag{1.6.14}$$

such that

$$-\delta\Big(\int d^{d+1}x\mathcal{L}^{grav} + \int_\partial d^dx\mathcal{L}^{reg}\Big) = \int_\partial d^dx\pi^{\mu\nu}\delta g_{\mu\nu} - \int_\partial d^dx\Big(\delta\frac{\partial\mathcal{L}^{grav}}{\partial g''_{\mu\nu}}\Big)g'_{\mu\nu}. \tag{1.6.15}$$

Since S^{grav} doesn't contain second derivatives in ρ-direction of the radial component of the metric, this implies

$$-\frac{\sqrt{-\gamma}}{2}T^{ab}[\gamma] = \pi^{ab}\Big|_\partial - \Big(\frac{\delta}{\delta g_{ab}}\frac{\partial\mathcal{L}^{grav}}{\partial g''_{ij}}\Big|_\partial\Big)\gamma'_{ij} + \frac{\delta\mathcal{L}^{ct}}{\delta\gamma_{ab}}. \tag{1.6.16}$$

The boundary stress energy tensor $T^{ab}[g^B]$, that we are after, is given by

$$T^{ab}[g^B] = \lim_{\epsilon\to 0}\frac{T^{ab}[\gamma]}{\epsilon}. \tag{1.6.17}$$

Thus the ansatz for $\mathcal{L}^{ct}$ can be set to [15]

$$\mathcal{L}^{ct} = \sqrt{-\gamma}\Big(c_1 + c_2R[\gamma]\Big), \tag{1.6.18}$$

while the coefficients c_1 and c_2 have to be chosen, such that $T^{ab}[\gamma] = \mathcal{O}(\epsilon)$. Inserting the metric ansatz given in (1.6.11) into (1.6.16) and requiring (1.6.17) to be finite gives for $d = 4$

$$c_1 = -6,\ c_2 = \frac{1}{2}. \tag{1.6.19}$$

In this step we have to make use of the EoM for $g_{\mu\nu}$ again. For a flat boundary geometry $(g^B)^{\mu\nu}\Big|_{\rho=0} = \eta^{\mu\nu}$ one obtains

$$T_{ab} = 4(g^B_{(2)})_{ab}, \tag{1.6.20}$$

where

$$g^B_{ab} = \eta_{ab} + \rho^2 (g^B_{(2)})_{ab} + \dots . \tag{1.6.21}$$

Our next aim will be to generalize this to theories that include higher derivative corrections.

1.6.1 Including Gauss-Bonnet terms

In order to prepare the computation of the relation between the near boundary geometry of the bulk metric with the (gravitational-) boundary stress energy tensor and hence the stress energy tensor of the dual field theory at finite 't Hooft coupling λ, we are going to have a look at the analogous calculation including Gauss-Bonnet terms. The resulting theory is a curvature squared theory, while the actual α'^3 corrections to SUGRA are of order $\mathcal{R}^4$. The action including the Gauss-Bonnet coupling λ_{GB} is given by

$$S = \frac{1}{k}\int d^5x\sqrt{-g}\Big(R - 2\Lambda + \frac{\lambda_{GB}}{4} l^2 (R^2 - 4R_{\mu\nu}R^{\mu\nu} + R_{\mu\nu\alpha\beta}R^{\mu\nu\alpha\beta})\Big) \tag{1.6.22}$$

where $\Lambda = -6/l^2$. The calculation will be done perturbatively in λ_{GB} and the metric ansatz, which we will consider after the variation, is of the form

$$ds^2_{GB} = \frac{1 + \lambda_{GB} g(\rho)}{4\rho^2} d\rho^2 + \frac{1}{\rho}\Big((g^0)_{\mu\nu} + \lambda_{GB}(g^1)_{\mu\nu}\Big)dx^\mu dx^\nu. \tag{1.6.23}$$

As in [14] we set $l = 1 + 2\lambda_{GB}$, in order to make sure that $g(\rho)$ is at least of order $\mathcal{O}(\rho^1)$. At first one has to find a Gauss-Bonnet coupling corrected version of the Gibbons-Hawking-York term, i.e. relation (1.6.7) has to be fulfilled, where we replace the Lagrangian $\mathcal{L}^{grav}$ with its coupling corrected analogon. This task is still independent from the choice of l.

The first naive proposal for S^{reg} could be of the form

$$\frac{\partial \mathcal{L}^{grav}_{GB}}{\partial g''_{\mu\nu}} g'_{\mu\nu}, \tag{1.6.24}$$

since this already worked in the case $\lambda_{GB} = 0$. However (1.6.24) contains terms of the form $g'_{00}g'^2_{ij}, \dots$, which clearly cause trouble. Since (1.6.24) doesn't contain double derivatives we can translate the problem of finding the right S^{reg} to finding a potential

$\Phi_{GB}(g'_{\mu\nu}, g_{\mu\nu})$ of the 1−form

$$\frac{\partial \mathcal{L}^{grav}_{GB}}{\partial g''_{\mu\nu}} d(g'_{\mu\nu}) = d\Phi_{GB} \tag{1.6.25}$$

on a 16−dimensional[11] manifold, with coordinates $\{g'_{\mu\nu}\}_{\mu\nu\in\partial}$. Where the notation $\mu\nu \in \partial$ means indices corresponding to coordinates which describe submanifold $\rho = const.$ The metric components without derivatives $g_{\mu\nu}$ should be understood as constants in (1.6.25). With this the stress energy tensor is given by

$$-\frac{\sqrt{-\gamma}}{2} T^{ab}[\gamma] = \pi^{ab}_{GB}\Big|_\partial - \frac{\partial \mathcal{L}^{grav}_{GB}}{\partial g''_{ij}}\Big|_\partial \frac{\delta \gamma'_{ij}}{\delta \gamma_{ab}} + \frac{\delta \Phi_{GB}|_\partial}{\delta \gamma_{ab}} + \frac{\delta \mathcal{L}^{ct}}{\delta \gamma_{ab}} \tag{1.6.26}$$

where π_{GB} is defined analogously to π in (1.6.13), with $\mathcal{L}^{grav} \to \mathcal{L}^{grav}_{GB}$. Notice that with Φ_{GB} chosen to fulfill (1.6.25) the term

$$-\frac{\partial \mathcal{L}^{grav}_{GB}}{\partial g''_{ij}}\Big|_\partial \frac{\delta \gamma'_{ij}}{\delta \gamma_{ab}} + \frac{\delta \Phi_{GB}|_\partial}{\delta \gamma_{ab}} \tag{1.6.27}$$

is well defined. The ansatz for the counter term is the same as in the case of a vanishing Gauss-Bonnet coupling, just that c_1 and c_2 will depend on λ_{GB} now

$$c_1 = -6 + \lambda_{GB} c_1^1 + \mathcal{O}(\lambda^2_{GB}) \tag{1.6.28}$$

$$c_2 = \frac{1}{2} + \lambda_{GB} c_2^1 + \mathcal{O}(\lambda^2_{GB}). \tag{1.6.29}$$

In the next step we explicitly derive the EoM for $g_{\mu\nu}$ in order to find the λ_{GB}−corrected constants c_1 and c_2. If we demand the boundary geometry to be $\eta_{\mu\nu}$, the ansatz for the bulk metric takes the form[12]

$$g_{\rho\rho} = \frac{1 + \lambda_{GB}\rho^3 U(\rho)}{4\rho^2} + \mathcal{O}(\lambda^2_{GB}) \tag{1.6.30}$$

$$g_{ij} = \frac{g^0_{ij} + \lambda_{GB}\rho^3 g^1_{ij}(\rho, x^k)}{\rho} + \mathcal{O}(\lambda^2_{GB}). \tag{1.6.31}$$

If we would treat a general boundary metric $g^0_{ij}|_\partial$ we would need to choose both c_1^1 and c_2^1 to be of a certain value, in order to make sure that (1.6.26) is regular. However, it turns out that with our special choice of $g^0_{ij}|_\partial = \eta_{ij}$ the only constant to fix is c_1, for which one obtains

$$c_1 = -6 + 2\lambda_{GB} + \mathcal{O}(\lambda^2_{GB}). \tag{1.6.32}$$

[11] The action doesn't contain double derivatives of the radial components of the metric, thus 16 and not 25 dimensions.

[12] In this step we explicitly use $l = 1 + 2\lambda_{GB}$.

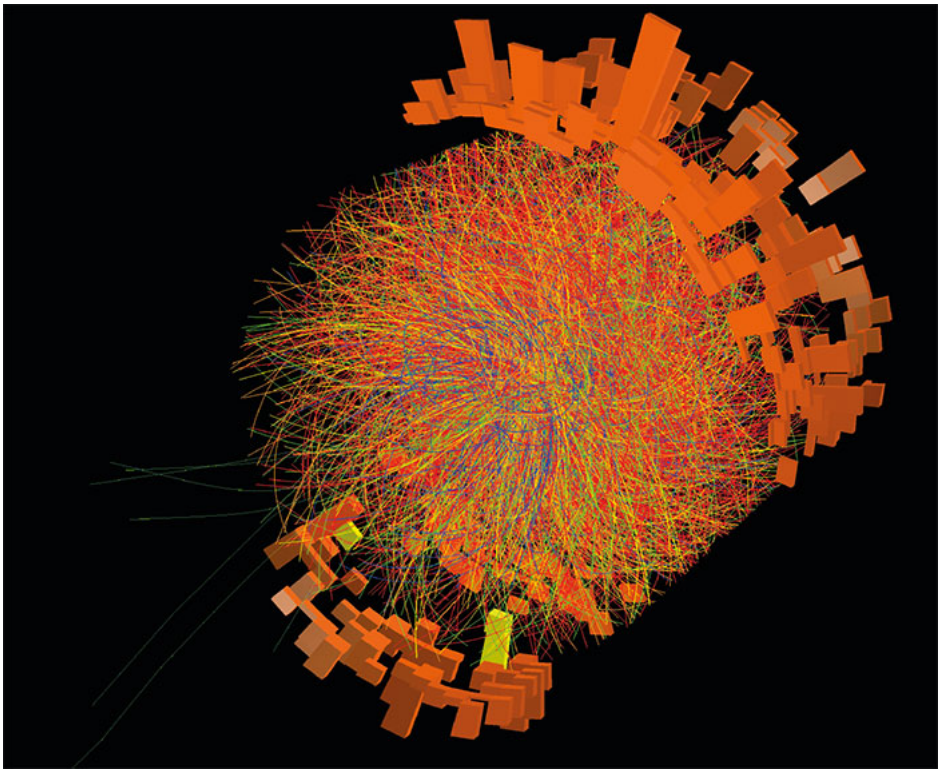

Figure 1.4: The display of tracks of emitted particles during lead-ion collisions at the LHC. The tedious analysis of a myriad of data about distributions and properties of emitted particles provides us with information about the QGP, the high temperature phase during heavy ion collisions above the confinement phase transition and subsequent hadronization. Throughout this thesis we investigate several properties of this phase and simulate its formation during heavy ion collisions via holography.

1.7 Heavy ion collisions and holography

During the collisions of highly relativistic heavy ions at LHC and RHIC, where particles are shot onto each other in two opposing beam lines with energies of about 2.7 TeV for the ALICE experiment at LHC and about 8.9 GeV for RHIC, the constituents of those heavy ions, that hit another particle, enter a phase of high temperature, called the Quark Gluon Plasma (QGP), that resembles the extremely high temperature phase of the early universe, when quarks and gluons where not confined. This phase is not accessible via perturbative calculations nor by lattice simulations, which fail to describe dynamical processes due to the sign problem. Recently it was shown that the onset of validity of relativistic hydrodynamics happens unexpectedly early [67]. Nevertheless the only known model that is both capable of qualitatively describing the far from equilibrium QGP at the time of the collision and is numerical accessible is the holographic simulation of two colliding (gravitational) shockwaves, whose field theoretic

dual is the collisions of two particles each of them described by a certain stress energy tensor.

Einstein's field equations, which are differential equations of second order, require two boundary conditions. If we want to model the geometry encoding the dynamics of a particle described by the stress energy $\langle T^{ab} \rangle$ moving in a manifold with metric $g^{ab}_{(0)}$, then the boundary conditions of the bulk Einstein equations are that the metric induced on the boundary is $g^{ab}_{(0)}$ and that the regularized and renormalized stress energy tensor induced on the boundary is $\langle T^{ab} \rangle$. As seen from e.g. the result (1.6.20), this gives a condition for those near boundary expansion coefficients of the bulk metric, which are not determined by the Einstein equations themselves.

During highly relativistic heavy ion collisions, where particles are accelerated to reach 99.9999% of the speed of light at ALICE/LHC and 99.995% of the speed of light at RHIC, the length contraction becomes so extreme, that the colliding, now lens shaped particles can be approximated by planar shockwaves, where we neglect the fringes of the particle and assume an homogeneous energy distribution. More specifically, the high velocities allow us to split this lens into small pixels, which are causally disconnected throughout the considered time interval. The dynamics of such two colliding subregions can then be modeled by shockwave collisions, where we assume an isotropic energy density along the transverse axes.

To describe one of the colliding particles we use lightcone coordinates $x_- = t - z$ and $x_+ = t + z$ and express the $_{x_-x_-}$-component or short $_{--}$-component of the stress energy tensor as

$$T_{--} = \mu h(x_-), \tag{1.7.1}$$

where μ is the energy scale and h is a function describing the energy per unit area distribution. The Einstein equations for a metric that is conformally equivalent to the Minkowski metric on the boundary and results in (1.7.1) for the boundary field theory, can be solved analytically. In Fefferman-Graham (FG) coordinates this metric reads

$$ds^2 = \frac{d\rho^2}{\rho^2} + \frac{1}{\rho^2}\Big(dx_- dx_+ + dx_\perp^2 + dx_-^2 \rho^4 \mu h(x_-)\Big). \tag{1.7.2}$$

The task is now to solve the bulk geometry of two colliding shockwaves, which, at sufficient spatial separation of the two shocks, is given by the sum of the single shockwave solutions.[13] This statement is, of course, not true for shocks that have approached each other and are starting to overlap. The sum of two single shocks, with sufficient spatial separation, serves as an initial condition for the Einstein equations, that ought to be solved in a coordinate system that allows a convenient foliation of space time, such that we can solve the geometry slice by slice. In section 3.1.4 we will discuss how

[13] At least outside the horizon, which is what we are interested in.

to perform the coordinate transformation from FG coordinates to (infalling) Eddington Finkelstein (EF) coordinates, in which we can formulate the Einstein equations as nested systems of differential equations on null-slices, that can be solved sequentially [68] [34]. This allows us to determine the geometry numerically time step for time step, while only dealing with radial and spatial derivatives on each time slice.

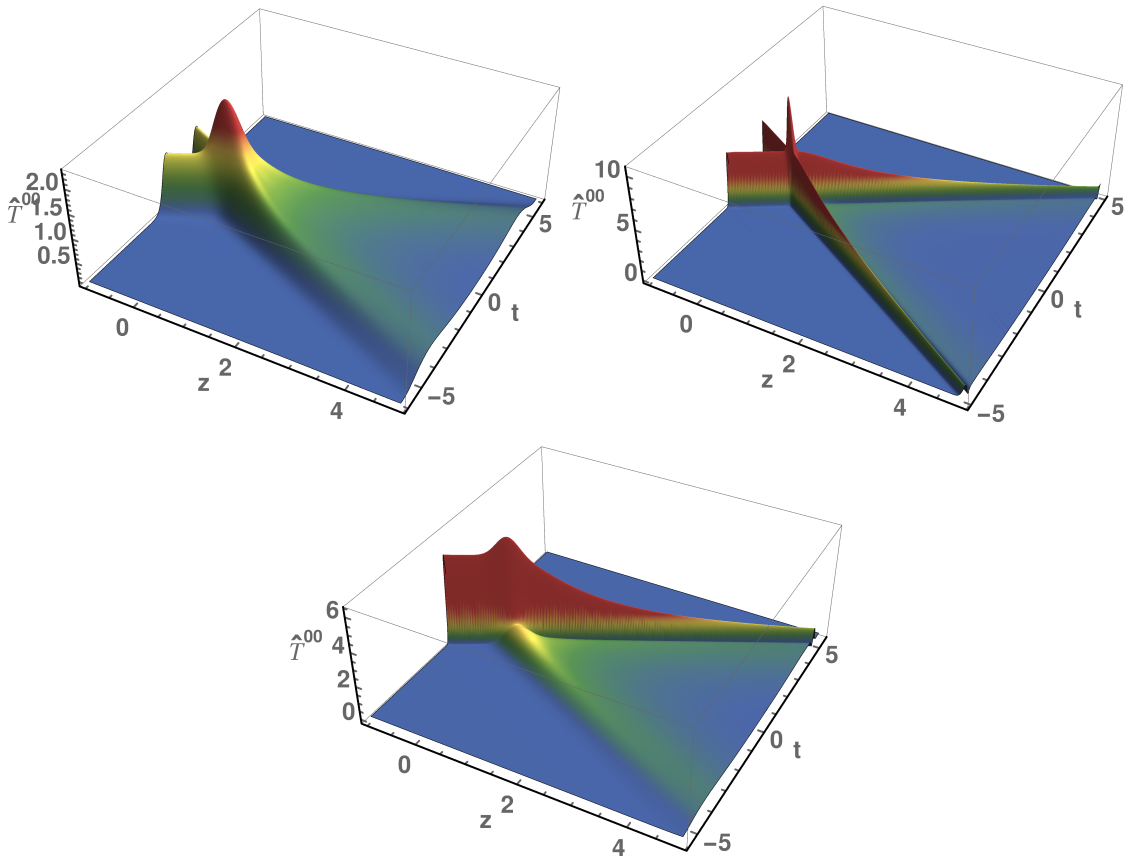

Figure 1.5: The 00-component of the rescaled stress energy tensor $\hat{T}^{\mu\nu} = \frac{2\pi^2}{N^2} T^{\mu\nu}$ plotted for various planar shockwave collisions, computed with a software, whose construction is in detail explained in 3.1.4. The plots show the collision of broad (upper left), narrow (upper right) and asymmetric (bottom) energy density distributions. The explicit parameters, that will be introduced in (3.1.28), are $(w_+ = 0.35, w_- = 0.35)$, $(w_+ = 0.075, w_- = 0.075)$ and $(w_+ = 0.075, w_- = 0.35)$ respectively.

1.7.1 The characteristic formulation of general relativity

The characteristic formulation of GR, discovered by Bondi [48] and Sachs [49], is based on a null slicing of the geometry. The Bondi-Sachs coordinates $(X) = (t = x^0, r, x^i)$ result from the idea of foliating spacetime by outgoing null-hypersurfaces $t = const$, meaning that the normal vector $k_A = -\partial_A t$ satisfies $g^{AB} k_A k_B = 0$. Thus, the tt component of the metric with upper indices vanishes. The covector k^A is tangent

to the null rays, whereas the spatial coordinates x^i are constant along outgoing null geodesics, meaning

$$k^A \partial_A x^i = g^{0i} = 0. \tag{1.7.3}$$

From this one can easily construct the general metric ansatz in Bondi-Sachs form. However, we are interested in a slightly modified version of this formalism, which was pioneered by L. Yaffe and P. Chesler: They provide us with a generalized Bondi-Sachs formalism for asymptotical AdS spacetimes [34] which we will review in this section in more detail.

The form of the coordinates stays the same as before, with the difference that r now takes the role of the radial coordinate in AdS space and the 3 spatial coordinates replace the angular coordinates from before. For the covariant metric component we have $g_{rr} = g_{ri} = 0$. Finally we end up with a generalized infalling Eddington-Finkelstein metric which reads

$$ds^2 = 2dt \left[\beta dr - A dt - F_i dx^i\right] + \Sigma^2 \hat{g}_{ij} dx^i dx^j \tag{1.7.4}$$

where β, A, F_i, Σ and $\hat{g}_{ij}$ are functions of all coordinates and $\det(\hat{g}_{ij}) = 1$. In addition we have the freedom to set $\beta = 1$. It is easy to see that the form of the metric (1.7.4) is invariant under arbitrary radial shifts

$$r \to r + \delta\lambda(x) \ , \tag{1.7.5}$$

the function A, F and G_{ij} transform under this shift as follows

$$\begin{aligned} A(x,r) &\to A(x,r) + \partial_t \delta\lambda(x) \ , \\ F_i(x,r) &\to F_i(x,r) + \partial_i \delta\lambda(x) \ , \\ G_{ij}(x,r) &\to G_{ij}(x, r + \delta\lambda(x)) \ . \end{aligned} \tag{1.7.6}$$

Thus the functions A and F_i transform as components of a gauge field corresponding to this symmetry. In the next step we write the Einsteins equations in a manner which is manifestly covariant under spatial and radial shifts. To do so we replace temporal derivatives by

$$d_+ = \partial_t + A(X)\partial_r \tag{1.7.7}$$

and spatial ones by

$$d_i = \partial_i + F_i(X)\partial_r \quad . \tag{1.7.8}$$

The Einstein equations

$$R^{AB} - \frac{1}{2} R\, g^{AB} - \Lambda\, g^{AB} = 0 \tag{1.7.9}$$

together with the metric ansatz (1.7.4) and the replaced temporal and spatial derivatives take the following nested form

$$\left(\partial_r^2 + Q_\Sigma[\hat{g}]\right) \Sigma = 0 \quad , \tag{1.7.10}$$

$$\left(\delta^i_j \partial_r^2 + P_F[\hat{g}, \Sigma]^j_i \partial_r + Q_F[\hat{g}, \Sigma]^j_i\right) F_j = S_F[\hat{g}, \Sigma]_i \quad , \tag{1.7.11}$$

$$\left(\partial_r + Q_{d_+\Sigma}[\Sigma]\right) d_+\Sigma = S_{d_+\Sigma}[\hat{g}, \Sigma, F] \quad , \tag{1.7.12}$$

$$\left(\delta^k_{(i}\delta^l_{j)} \partial_r + Q_{d_+\hat{g}}[\hat{g}, \Sigma]^{kl}_{ij}\right) d_+\hat{g}_{kl} = S_{d_+\hat{g}}[\hat{g}, \Sigma, F, d_+\Sigma]_{ij} \quad , \tag{1.7.13}$$

$$\partial_r^2 A = S_A[\hat{g}, \Sigma, F, d_+\Sigma, d_+\hat{g}] \quad , \tag{1.7.14}$$

$$\left(\delta^j_i \partial_r + Q_{d_+F}[\hat{g}, \Sigma]^j_i\right) d_+F_j = S_{d_+F}[\hat{g}, \Sigma, F, d_+\Sigma, d_+\hat{g}, A]_i \quad , \tag{1.7.15}$$

$$d_+ \left(d_+\Sigma\right) = S_{d_+^2\Sigma}[\hat{g}, \Sigma, F, d_+\Sigma, d_+\hat{g}, A] \quad . \tag{1.7.16}$$

The full forms for planar shocks can be found in appendix 5.10. All of these equations are ordinary differential equations in radial direction, that can be solved one after another at constant t, if we know the spatial part of the metric $\hat{g}_{ij}$ on that time slice and if we impose further boundary conditions given in (1.7.22), encoding physics in the dual gauge theory.

In the spirit of relation (1.6.20) let us derive the near boundary expansion of the metric from equations (1.7.10)-(1.7.16):

$$A = \frac{1}{2}(r+\lambda)^2 - \partial_t\lambda + a^{(4)} r^{-2} + \mathcal{O}\left(r^{-3}\right) \quad , \quad F_i = -\partial_i\lambda + f_i^{(4)} r^{-2} + \mathcal{O}\left(r^{-3}\right) \quad , \tag{1.7.17}$$

$$\Sigma = r + \lambda + \mathcal{O}\left(r^{-7}\right) \quad , \quad \hat{g}_{ij} = \delta_{ij} + \hat{g}^{(4)}_{ij} r^{-4} + \mathcal{O}\left(r^{-5}\right) \quad , \tag{1.7.18}$$

$$d_+\Sigma = \frac{1}{2}(r+\lambda)^2 + a^{(4)} r^{-2} + \mathcal{O}\left(r^{-3}\right) \quad , \quad d_+\hat{g}_{ij} = -2\hat{g}^{(4)} r^{-3} + \mathcal{O}\left(r^{-4}\right) \quad . \tag{1.7.19}$$

Using (1.6.20), the near-boundary coefficients in FG coordinates can be mapped to the stress-energy tensor of the dual field theory. For EF coordinates this relation is given by

$$\frac{2\pi^2}{N_c^2} \langle T_{\mu\nu} \rangle \equiv \left\langle \hat{T}_{\mu\nu} \right\rangle = g^{(4)}_{\mu\nu} + \frac{1}{4} g^{(4)}_{00} \eta_{\mu\nu} \tag{1.7.20}$$

where N_c is the number of colors in the dual field theory. The metric $g_{\mu\nu}$ in this equation is related to parametrization (1.7.4) via

$$g_{00} = -\frac{2}{r^2}A \quad , \quad g_{0i} = -\frac{1}{r^2}F_i \quad , \quad g_{ij} = \frac{1}{r^2}\Sigma^2\hat{g}_{ij} \quad . \tag{1.7.21}$$

Inserting the near-boundary expansion of the metric we arrive at

$$\left\langle \hat{T}_{00} \right\rangle = -\frac{3}{2}a^{(4)} \quad , \quad \left\langle \hat{T}_{0i} \right\rangle = -f_i^{(4)} \quad , \quad \left\langle \hat{T}_{ij} \right\rangle = \hat{g}_{ij}^{(4)} - \frac{1}{2}a^{(4)} \quad . \tag{1.7.22}$$

The radial shift parameter $\lambda = \lambda(x)$ is undetermined in expansion (1.7.17-1.7.19) and can be chosen arbitrarily. Next we want to use this freedom to fix the horizon on a given time slice $t = conts$ to a constant radial position

$$r_h(x) = r_h, \tag{1.7.23}$$

to give a rectangular shape to the domain of integration. We can find the horizon by considering the outgoing null (geodesic) congruence, restricted to a $t = const$ slice, which should have vanishing expansion rate at r_h. A general geodesic congruence k orthogonal to a hypersurface can be written as

$$k_A = \mu\partial_A\Phi(X), \tag{1.7.24}$$

where k_A is orthogonal to the hypersurface defined by $\Phi(X) = c$, with c constant. Since we require the congruence to be null, we have

$$k_A k^A = 0. \tag{1.7.25}$$

As a geodesic congruence k_A additionally fulfills

$$k^A\nabla_A k^B = 0. \tag{1.7.26}$$

The congruence k^A, as a vector field that is tangential to outgoing geodesics, can be restricted to the spacelike hypersurface $t = const$. Our task is now to determine the derivatives orthogonal to this hypersurface $\partial_t\mu$ and $\partial_t\Phi$ [14], the latter of which can be fixed by equation (1.7.25) giving

$$\partial_t\Phi = K_\Phi(\partial_i\Phi, \mu, g), \tag{1.7.27}$$

[14]It is important to do this before using $\Phi(X) = r = c$, which fixes the horizon to a constant radial position on a given time slice. This equation for Φ is only valid on a specific time slice $t = const$ without further fixing the radial shift invariance.

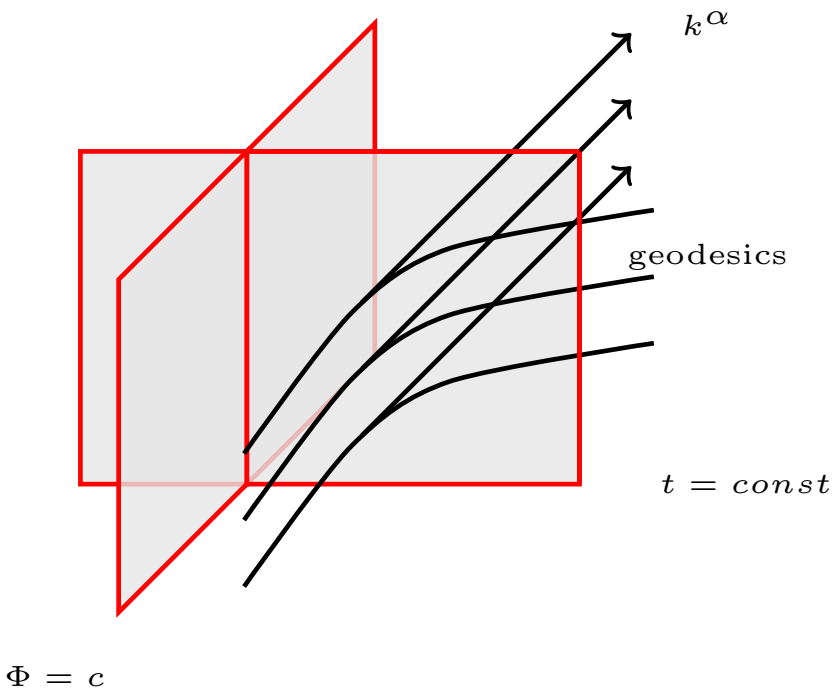

Figure 1.6: The vector field k^α is tangent to the outgoing geodesics, whereas k_α is orthogonal to the hypersurface $\Phi = c$. Fixing the horizon position to be constant on a given timeslice is achieved by setting $\Phi = r$ in the end. Demanding the expansion rate of the geodesic null congruence to vanish at the horizon allows us to write down the condition for the shift λ as the differential equation (1.7.31). Regarding the depiction of outgoing null geodesics above, we showed geodesic rays that still can escape the apparent horizon. Since k_α is normal to the hypersurface $\Phi = c$, k^α is tangential to it and thus this hypersurface is spanned by null geodesics, known as *null generators* [32].

whereas equation (1.7.26) fixes $\partial_t \mu$:

$$\partial_t \mu = K_\mu(\partial_i \Phi, \partial_i^2 \Phi, \mu, \partial_i \mu, g, \partial g). \tag{1.7.28}$$

For $F = 0$ it is easy to guess the outgoing geodesic null congruence modulo the factor μ:

$$k = \mu(X)(-A, 1, 0, 0, 0) \tag{1.7.29}$$

If $F \neq 0$ we can follow the recipe above and get

$$k = \mu(X)\Big(- \frac{e^{2B}F^2 + 2A\Sigma^2}{2\Sigma^2}, 1, 0, 0, 0\Big) \tag{1.7.30}$$

Demanding the expansion rate $\nabla \cdot k$ to vanish at the apparent horizon and exploiting

the relations for $\partial_t \Phi$ and $\partial_t \mu$ gives

$$d_+ \Sigma|_{r_h} = -\frac{1}{2}\partial_r \Sigma F^2 - \frac{1}{3}\Sigma \nabla \cdot F \quad , \tag{1.7.31}$$

where ∇ in (1.7.31) denotes the covariant derivative corresponding to the spatial part of the metric. Fixing the horizon position at all times requires

$$\partial_t d_+ \Sigma|_{r_h} = \partial_t \left(-\frac{1}{2}\partial_r \Sigma F^2 - \frac{1}{3}\Sigma \nabla \cdot F \right) |_{r_h} \quad . \tag{1.7.32}$$

The full form of equations (1.7.31) and (1.7.32) with expanded covariant derivative for planar shockwaves can be found in appendix 5.10.

1.7.2 Comparison with relativistic hydrodynamics

Having computed the collision of two planar shocks, one central aspect to study is the relation of our calculation to relativistic hydrodynamics. The time it takes until the system can be described hydrodynamically is typically very small [67]. However, it still remains to study this for collisions with asymmetric parameters, which can tell us about the hydrodynamization time of certain parts of the QGP during a peripheral heavy ion collision. We will discuss this in depth in section 3.1.5. Here we prepare these calculations by introducing several necessary ingredients.

Two central variables of relativistic hydrodynamics are the fluid velocity u^μ and the proper energy density ϵ. At every spacetime event inside the forward lightcone of a collision, the timelike ($u^\mu u_\mu = -1$) Eigenvector and corresponding eigenvalue of the holographically computed stress-energy tensor determine the fluid 4-velocity u^μ and proper energy density ϵ,[15]

$$\widehat{T}^\mu{}_\nu \, u^\nu = -\epsilon \, u^\mu \, , \tag{1.7.33}$$

with $u^0 > 0$. The tensor $\hat{T}^{\mu\nu}$ denotes the rescaled boundary stress energy tensor $\hat{T}^{\mu\nu} = 2\pi^2/N^2 T^{\mu\nu}$. Using the first order (in gradients) hydrodynamic constitutive relation allows us to construct an hydrodynamic approximation to the stress-energy tensor

$$\widehat{T}^{\mu\nu}_{\text{hydro}} = p \, g^{\mu\nu} + (\epsilon + p) \, u^\mu u^\nu + \Pi^{\mu\nu} \, , \tag{1.7.34}$$

where the viscous stress (also to first order in gradients) is given by

$$\Pi_{\mu\nu} = -\eta \left[\partial_{(\mu} u_{\nu)} + u_{(\mu} u^\rho \partial_\rho u_{\nu)} - \tfrac{1}{3} \, \partial_\alpha u^\alpha (\eta_{\mu\nu} + u_\mu u_\nu) \right] + \mathcal{O}(\partial^2) \, . \tag{1.7.35}$$

[15] A real timelike eigenvector (1.7.33) can fail to exist in spacetime regions where hydrodynamics is not applicable [34]. Since we are interested in behavior within the hydrodynamic region, this is not a concern.

For the conformal fluid of $\mathcal{N}=4$ Yang-Mills theory, the pressure is given by $p = \epsilon/3$ and the shear viscosity $\eta = (\epsilon/3)^{3/4}/\sqrt{2}$. This value for η has been rescaled by the same factor of $2\pi^2/N_c^2$ used in the definition of the rescaled stress-energy tensor (3.1.3).

Thus we can compute a hydrodynamic approximation to any stress energy tensor using this recipe and compare how close (1.7.34) comes to the original tensor.

1.8 Detailed Outline

This work consists of two main parts. The first one will treat higher derivative or higher α' corrections to the AdS/CFT duality, especially to solutions of SUGRA that involve gauge fields and gauge perturbation to the geometry and the five form. We are going to fix errors in the literature [10][11][12][53] regarding the higher derivative corrected EoM of gauge perturbations and thus the finite λ current-current correlator on the field theory side and related quantities, such as the photoemission rate, the conductivity and quasinormal mode spectra. For this we will follow a twofold approach: On the one hand we follow strictly the variation principle and exactly solve the large system of differential equations governing the dynamics of the higher derivative corrected and gauge field perturbed five form components as well as the EoM of the coupling corrected gauge field itself. On the other hand we will introduce a prescription to treat the higher derivative corrected five form, such that one obtains an effective action describing the dynamics of the coupling corrected gauge perturbation and thus simplifying the system of equations tremendously. The coupling corrected physical quantities in equilibrium computed from those two approaches (i.e. quasinormal mode spectra, photoemission rate, conductivity and the spectral function) are identical. This part of the thesis will be built on the author's paper [18].

We proceed with proving the validity of the found prescription in the special case of a magnetic background field. With the help of this mathematically justified simplification of the treatment of the higher derivative corrected five form in the presence of gauge fields we compute coupling corrections to the magnetic black brane geometry, whose $\lambda \to \infty$ solution was found in [13], and determine finite λ corrections to (tensor) quasinormal modes (QNMs) in this geometry. The aim of this calculation is on the one hand to study the influence of a strong magnetic background field[16] on the equilibration of a quark gluon plasma at finite 't Hooft coupling. On the other hand this is part of our endeavour to study holographic settings, where the dual field theory comes as close to QCD as possible: The higher derivative corrections allow us to leave the $\lambda \to \infty$ limit, whereas the magnetic background field simultaneously breaks symmetries, that QCD simply lacks, such as scale invariance. This reviews the author's paper [69].

Finally we are going to consider partial resummations of coupling corrections to

[16] As produced during actual heavy ion collisions for a very short time.

various quantities and observables and study the convergence properties of the coupling constant resummed QNM spectra in different channels, the conductivity and the shear viscosity. We compare the resummed conductivity to results of hot lattice QCD and discuss the strengths and weaknesses of the resummation approach. We conclude this discussion with quantifying the λ-value of breakdown of the resummation technique. This will be built on the author's paper [19].

In the second part we are going to focus on dynamical processes within AdS/CFT. We give a detailed recipe on how to structure code that numerically computes shockwave collisions in AdS_5. Going beyond the current literature we calculate shockwave collisions with asymmetric widths to study subsections of off-center heavy ion collisions holographically. Our focus will be on the hydrodynamization time during such collisions as well as on the generalization of the universal description of the rapidity distribution of the proper energy density to the case of asymmetric collisions. We will show that also in the asymmetric case we come remarkably close to boost invariant flow. We generalize the model describing the post collision flow [33] to the asymmetric case, providing a formula from which hydro initial data to simulate peripheral heavy ion collisions with large aspect ratios can be derived. This chapter is built on the author's paper [70]. Supplementing this discussion, we conclude with studying the entanglement entropy and correlation functions in an asymmetric shockwave collision geometry, generalizing the results of [61]. Finally we are going to prepare calculations of localized shockwave collisions.

Chapter 2

Higher derivative corrections to the AdS/CFT duality

The strongly coupled QGP produced during heavy ion collisions lies somewhere in between the two extreme limits of infinitely strong coupling with 't Hooft coupling $\lambda = \infty$ and weak coupling, which allows a perturbative description. The former limit is accessible via the AdS/CFT duality at infinite 't Hooft coupling and infinite gauge group rank N, the latter via perturbative quantum field theory. Our aim will be to use higher derivative corrected type II SUGRA to compute finite coupling corrections to the AdS/CFT duality and approach the real world by leaving the $\lambda = \infty$ limit. We consider additional contributions of order $\mathcal{O}(\alpha'^3)$ to the dual gravity theory, to determine finite 't Hooft coupling corrected correlators, emission rates and transport coefficients on the field theory side.

2.1 Investigating a charged quark gluon plasma with holography at finite t' Hooft coupling

In the last ten years an even deeper quantitative understanding of holography at finite t' Hooft coupling was reached with direct impact on our understanding of the quark gluon plasma. One important step was the computation of leading coupling corrections to the equations of motion of gauge fields in a strongly-coupled $\mathcal{N} = 4$ SYM plasma by considering $\mathcal{O}(\alpha'^3)$ corrections to the type IIB supergravity action [10, 11]. These α'-corrected equations of motion were then used to study the conductivity and the photoemmission rate, which give important information about the structure of the plasma. Determining α' corrections in general is of great interest, especially since they allow cautious comparisons and interpolations between the spectra of strongly coupled and weakly coupled plasmas [11]. However, the authors of [10, 11] committed

several errors[17] during the derivation of the fundamental coupling corrected EoM of gauge fields in AdS/CFT. Our first aim is to give a corrected derivation of the higher derivative corrected EoM for gauge fields in type IIb SUGRA. After that we revisit the computation of several observables, whose α'^3-corrections so far have been calculated with the EoM form [10, 11]. In general we find that the actual higher derivative corrections to all quantities studied in this work turn out to be substantially smaller than the values found in the literature so far. For instance in [10] the correction factor to the conductivity was given as $(1 + \frac{14993}{9}\gamma)$, whereas we obtained $(1 + 125\gamma)$. A comparison with the transport coefficient of the spin 2 channel is given in table 2.1. In contrast to previous works we find that the behaviour of the photoemission rate and spectral density at finite coupling agree with expectations from weak coupling calculations in both the small and the large energy limit [23]. In [23] the authors derived that in the weak coupling limit decreasing coupling means increasing photoemission rate at small momenta and decreasing photoemission rate at large momenta. The signs of the correction factors we found coincide with these expectations. We start from the higher derivative corrected type IIb action and compute finite coupling corrected QNM spectra, spectral density, photoemission rate and conductivity of the plasma. Before we come to finite coupling corrections we give a detailed description how to derive the $\lambda \to \infty$ setting to which we wish to compute higher derivative corrections. We introduce gauge fields in type IIb SUGRA by twisting the five sphere along specific angles.

2.1.1 Einstein-Maxwell-Gravity from type IIb SUGRA

The aim of this section is to give an overview of how to introduce charge and gauge fields in AdS/CFT starting from the type IIb SUGRA action (1.2.11). In the following calculations we set the constant l, which measures the size of S_5, to 1. We can get rid of it by rescaling. We will perform the calculations in this section in order $\mathcal{O}(\alpha'^0)$ and include coupling corrections in the following subsections.

Maxwell-terms $F_{\mu\nu}F^{\mu\nu}$ in the reduced 5−dimensional theory are obtained from SUGRA by a Kaluza-Klein reduction starting from a metric ansatz in $10D$ that includes a twist of the five sphere S_5 along its fibers in a maximally symmetric manner. The ansatz for the metric in this case has the form

$$ds_{10}^2 = ds_{\text{AdS}}^2 + \sum_{i=1}^{3} (d\mu_i^2 + \mu_i^2(d\phi_i + \frac{2}{\sqrt{3}}A_\mu dx^\mu)^2), \tag{2.1.1}$$

[17] These consisted of the following: A 5-form was used that didn't solve its higher derivative corrected EoM. In addition, unlike stated in these papers, the calculation was done in Euclidean signature, but the five form wasn't transformed appropriately. More specifically, we can reproduce their results, if we leave out an actually needed factor i in front of the five form components of the form $dt \wedge \ldots$ after the transformation to Euclidean signature. Also several terms contributing to the Hodge duals got lost.

with

$$ds^2_{AdS} = -r_h^2 \frac{1-u^2}{u} dt^2 + \frac{1}{4u^2(1-u^2)} du^2 + \frac{r_h^2}{u}(dx^2+dy^2+dz^2), \tag{2.1.2}$$

where the unperturbed metric is just the AdS Schwarzschild black hole solution times S_5 with horizon radius r_h, which we already discussed in (1.5.12). The direction cosines and angles μ_i and ϕ_i are given in (1.5.13,1.5.14). It is straightforward to check that with this metric ansatz we obtain

$$R_{10} = R_{10}^{A_\mu \to 0} - \frac{1}{3} F_{\mu\nu} F^{\mu\nu}, \tag{2.1.3}$$

with $F = dA$. The dilaton part of the action can be ignored again, since its EoM does not couple with those of A_μ and the solution of its EoM in this order in α' is simply zero. Let us, however, focus in detail on the role of the five form part of the action (1.2.11) in this calculation. In the following we will derive the form of the ansatz for F_5:

The five form solution for vanishing gauge field and without higher derivative corrections can be read from (1.5.8, 1.5.7). The factor -4 there ensures that in the dimensionally reduced action we have

$$\frac{\mathrm{vol}(S_5)}{2\kappa_{10}} \int d^5x \sqrt{-\det(g_{AdS})} \Big[R_5 - 8 + R_{S_5} \Big] = \frac{\mathrm{vol}(S_5)}{2\kappa_{10}} \int d^5x \sqrt{-\det(g_{AdS})} \Big[R_5 + 12 \Big]. \tag{2.1.4}$$

Now we want to find a solution for $dF_5 = 0$ and $d * F_5 = 0$ with the metric (2.1.1). In order to see that $F_5^{\mathrm{el}} = -4\epsilon_{\mathrm{AdS}}$ is no longer the correct ansatz for the electric part of the five form we focus at the $tuyzy_1y_3$-direction of the 6-form $d * F_5$. In the following we only consider transverse fields, which means that only A_x is non-vanishing and $A_x = A_x(u,t,z)$. The deduction for longitudinal fields is analogous. Remember that we are interested in linearized differential equations for A_μ, which we consider as tiny fluctuations of our background geometry. This means that terms of order $A_\mu A_\nu$ or higher can be discarded, such that there are only 6 non-diagonal elements in the matrix representation of the metric tensor $g^{\mu\nu}$, namely $g^{xy_3}, g^{xy_4}, g^{xy_5}$ and their symmetric counterparts $x \leftrightarrow y_i$. From our solution in the $A_\mu = 0$ case we already know that we will at least have one non vanishing term in the $tuyzy_3$-direction of the 5-form $*F_5$, which is proportional to

$$\sqrt{-g} g^{y_1y_1} g^{y_2y_2} g^{y_3x} g^{y_4y_4} g^{y_5y_5} (F_5^{A_\mu \to 0})_{y_1y_2y_3y_4y_5}. \tag{2.1.5}$$

Note that we are not making use of the sum-convention here and henceforth in this section unless we stress otherwise explicitly. The expression (2.1.5) is proportional to

A_μ without any derivatives and has a non trivial y_1-dependence, such that we have

$$0 \neq (d * F_5)_{tuyzy_1y_3} = \partial_{y_1}(\sqrt{-g} g^{y_1y_1} g^{y_2y_2} g^{y_3x} g^{y_4y_4} g^{y_5y_5} (F_5^{A_\mu \to 0})_{y_1y_2y_3y_4y_5}) + \dots \quad (2.1.6)$$

without further directions of F_5 being non zero. This term can't be canceled by the EoM for A_μ, since it would give a mass to our gauge field. Consequently there have to be more components of the solution for F_5, which give non-zero contributions, such that these mass terms cancel. The symmetries of this problem should dictate, which directions of the five form vanish and which don't. We instead use a different approach. We start from the fact, that our final ansatz for the C_4 can only depend on the coordinates u, t, z, y_1, y_2, i.e. the coordinates the metric and its fluctuations A_μ depend on. Any other dependence would lead to non-vanishing components of $d * dC_4$. This means the only possible components of C_4 proportional to A_μ that could give a contribution to the $tuyzy_1y_3$-component of $d * dC_4$ are $(C_4)_{xy_1y_4y_5}, (C_4)_{xy_2y_4y_5}, (C_4)_{xzy_4y_5}, (C_4)_{txy_4y_5}, (C_4)_{uxy_4y_5}$ modulo permutations of their 4 indices. In the following, when we address properties of certain directions of forms, e.g. for $(C_4)_{abcd}$ the $abcd$-direction of C_4, it is implied that these properties apply to all permutations of the indices $abcd$ with the correct signs.

Graphically we can depict all relevant contributions of these 4-form components to the differential equations shortly written as $d * dC_4 = 0$ as shown in figure 2.1. Note that this diagram is closed in the sense that together with the contribution in (2.1.6) all terms contributing to the $tuyzy_1y_3$, $uyzy_1y_2y_3$, $tuyzy_2y_3$, $tyzy_1y_2y_3$ and $tuyy_1y_2y_3$-directions of $d * F_5$ are depicted and $(C_4)_{xy_1y_4y_5}$, $(C_4)_{xy_2y_4y_5}$, $(C_4)_{xzy_4y_5}$, $(C_4)_{txy_4y_5}$, $(C_4)_{uxy_4y_5}$ do not contribute to any other directions of $d * F_5$. The next important observation is that $(d * F_5)_{uyzy_1y_2y_3}$, $(d * F_5)_{tyzy_1y_2y_3}$ and $(d * F_5)_{tuyy_1y_2y_3}$ cannot be set to 0 by imposing the EoM of A_x, because they contain odd derivatives in the t and z direction $\partial_z A_x, \partial_t A_x$ or $\partial_z^3 A_x, \partial_t^3 A_x$, if we have only even derivatives in $(d * F_5)_{tuyzy_1y_3}$. From the requirement that there are no mass terms in the EoM for A_x we can deduce from (2.1.6) and the form of $F_5^{A_\mu \to 0}$ that $(*F_5)_{tuyzy_3}$ is proportional to $\sin(y_1)^2$ and has no y_2-dependence. Therefore, $(C_4)_{xy_1y_4y_5}$ doesn't contribute to $(d * F_5)_{tuyzy_1y_3}$ and $(C_4)_{xy_2y_4y_5}$ doesn't contribute to $(d * F_5)_{tuyzy_2y_3}$. Thus, it is possible to choose $(C_4)_{xy_1y_4y_5} = 0$. This leads to the beautiful result that in diagram 2.1 the contributions of $(C_4)_{xzy_4y_5}$, $(C_4)_{txy_4y_5}$, $(C_4)_{uxy_4y_5}$ to $(d * F_5)_{tuyzy_1y_3}$ have the same form as those of $(C_4)_{xy_2y_4y_5}$ and are indistinguishable in the final EoM $(d * F_5)_{tuyzy_2y_3} = 0$, which means it is a legitimate ansatz to set them to 0 and solve $(d * F_5)_{tuyzy_2y_3} = 0$ for $(C_4)_{xy_2y_4y_5}$. This process has to be repeated for two further cases (remember that we only considered the off diagonal element g^{xy_3} so far), which together with the self

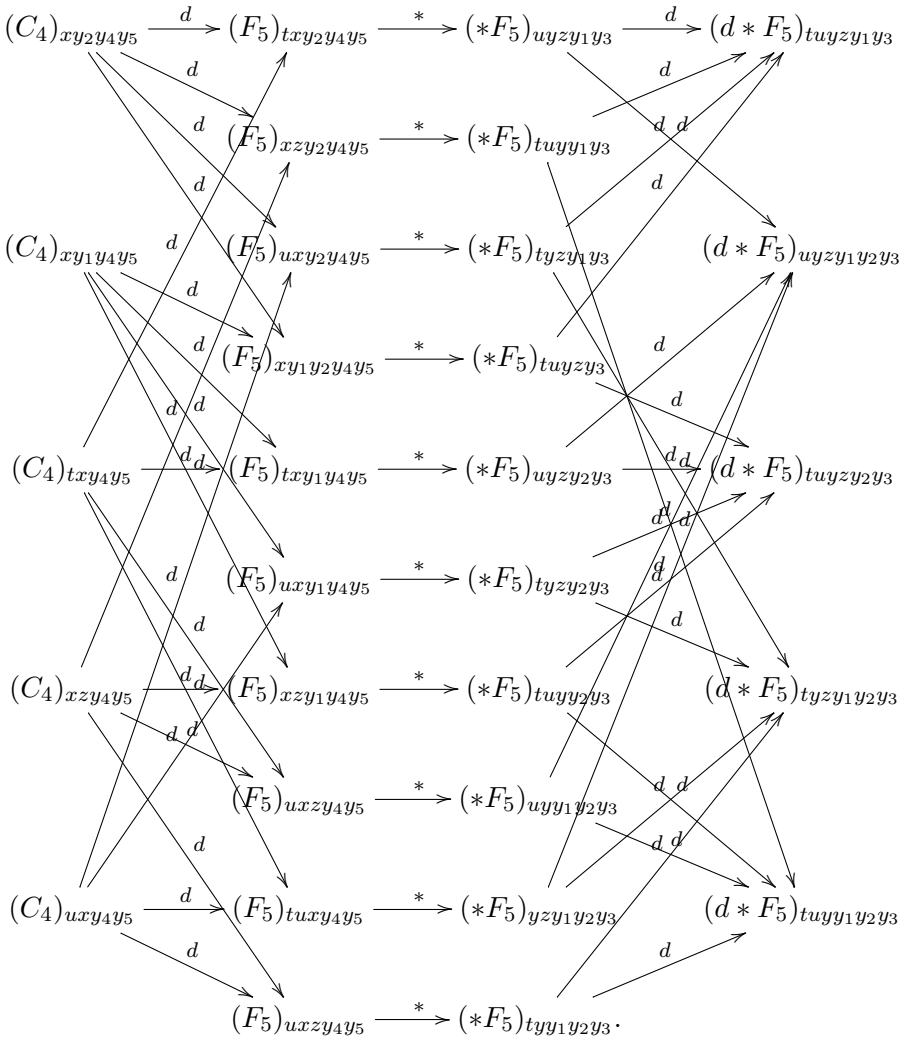

Figure 2.1: Graphic depiction of the "closed" system of differential equations around the $xy_2y_4y_5$-direction of C_4. In this order in α' the right hand side should give zero.

duality of the 5-form leads to the result

$$(F_5^0)^{el} = -4\epsilon_{AdS}, \qquad (F_5^1)^{el} = \frac{1}{\sqrt{3}} \sum_{i=1}^{3} d(\mu_i^2) \wedge d\phi_i \wedge \bar{*}F_2, \tag{2.1.7}$$

and

$$F_5 = (1 + *)((F_5^0)^{el} + (F_5^1)^{el}), \tag{2.1.8}$$

with $F_2 = dA$. In (2.1.7) $\bar{*}$ is the Hodge dual with respect to the inernal five dimensional AdS-manifold. Notice that the result (2.1.8) is proportional to $\mathcal{J} \wedge \bar{*} dA$, with the Kähler-

form of the five sphere $\mathcal{J}$ [18]. The EoM for A_μ can be obtained both by varying the action with respect to A_μ and from the $tuyzy_1y_3$, $tuyzy_2y_4$, $tuyzy_2y_5$, $tuyzy_1y_5$ and $tuyzy_1y_4$-directions of $d*dC_4=0$. Varying the action with respect to A_μ leads to the following well known EoM for transverse fields in order $\mathcal{O}(\gamma^0)$

$$\partial_u^2 A_x - \frac{2u}{1-u^2}\partial_u A_x + \frac{\hat{\omega}^2 - \hat{q}^2(1-u^2)}{u(1-u^2)^2}A_x = 0 \tag{2.1.9}$$

with $\hat{X} = \frac{X}{2r_h} = \frac{X}{2\pi T}$ for $X \in \{q, \omega\}$ and the horizon radius r_h.

2.1.2 Finite 't Hooft coupling corrections to the EoMs of gauge fields

Let us start to consider higher derivative corrections to our theory, meaning that we will continue to work with the $\mathcal{O}(\alpha'^3)$ corrected action (1.2.16), where S_{10}^{γ} is given in (1.2.12). As in section 1.2 we set $\gamma = \frac{\zeta(3)}{8}\lambda^{-\frac{3}{2}}$, with the 't Hooft coupling λ, which is proportional to $\alpha'^{-\frac{1}{2}}$.

The solution of F_5 in order $\mathcal{O}(\gamma^0)$ is self dual and in order $\mathcal{O}(\gamma^1)$ the $\mathcal{O}(\gamma^0)$ part of F_5 is the only contribution of F_5, which enters the higher derivative part of the action (1.2.12). Due to the term proportional to F_5^2 in the action (1.2.11) we still have to determine the coupling corrected EoMs of the 4-form components, meaning that we still have to vary the action with respect to C_4 and thus it makes a difference whether $F_5 = dC_4$ or F^+ enters γW. Let us now introduce gauge fields to our finite λ-corrected solution found in (1.5.16) and (1.5.21-1.5.24). In order to get the correct results in the limits $A_\mu \to 0$ and $\gamma \to 0$ we choose the ansatz again corresponding to a twist of the five sphere along the y_3, y_4, y_5 angles

$$\begin{aligned} ds_{10}^2 =& -r_h^2 U(u)dt^2 + \tilde{U}(u)du^2 + e^{2V(u)}r_h^2(dx^2+dy^2+dz^2) + L(u)^2\frac{4A_x(u,t,z)^2}{3}dx^2 \\ &+ L(u)^2\frac{4A_x(u,t,z)}{\sqrt{3}}dx(dy_3\sin(y_1)^2 + dy_4\cos(y_1)^2\sin(y_2)^2 + dy_5\cos(y_1)^2 \\ &\cos(y_2)^2) + L(u)^2(dy_1^2 + \cos(y_1)^2dy_2^2 + \sin(y_1)^2dy_3^2 + \cos(y_1)^2\sin(y_2)^2dy_4 \\ &+ \cos(y_1)^2\cos(y_2)^2dy_5^2), \end{aligned} \tag{2.1.10}$$

The functions U, $\tilde{U}$, L, V are the ones given in (1.5.21-1.5.24) and correspond to a finite 't Hooft coupling corrected Schwarzschild black hole. We justify the ansatz made above in (2.1.10) in the following. The EoM for A_μ will be obtained by varying the coupling corrected type IIb SUGRA action with respect to the 4-form components and A_μ. Let us convince ourselves that this is equivalent to varying with respect to the

[18] There are more and easier ways to deduce this five form solution. Since we will have little choice but to work with similar brute force in the $\mathcal{O}(\alpha'^3)$-case, due to the complexity of the higher derivative correction terms to the type IIb action, it is a good exercise to already do this in the lowest order in α'.

metric components and the four form components and linearizing the resulting system of differential equations in A_μ: Apparently the xx-component $e^{2V(u)} + L(u)^2 \frac{4A_x(u,t,z)^2}{3}$ of our metric ansatz seems to cause a problem with respect to the equivalence of the aforementioned procedures. Varying the action with respect to e.g. the xy_3-component of the metric and linearizing in A_μ results in an EoM that can at first (and too hasty) glance not be fulfilled by a solution to the differential equation obtained by varying the action with respect to A_μ. This is because after linearizing in A_μ the A_μ^2-term of the xx-component of the metric won't contribute to the former case, but will give a contribution to the latter. In fact, varying the $\sqrt{-g}R_{10}$, $\sqrt{-g}\frac{1}{4*5!}F_5^2$ and $\sqrt{-g}\gamma W$-terms in the action with respect to the xy_3-component of the metric separately and inserting the ansatz (2.1.10) gives mass terms. However, adding everything up leads to the same EoM for A_μ (of course, still depending on some unknown F_5-directions) as varying with respect to A_μ, while the mass terms cancel identically. The same is true for any other off diagonal direction of the metric tensor, such that we can proceed with our calculation.

From now on we will work with $r_h = 1$, which also applies to the Appendix 5.3, and reintroduce r_h wherever needed after having obtained the EoMs. We know that we will end up with differential equations, where r_h only appears in the rescaled frequency $\frac{\omega}{2r_h}$ and momentum $\frac{q}{2r_h}$. Also setting $r_h = 1$ simply corresponds to rescaling t the spatial coordinates and A_x by a constant factor. Changing $\frac{\omega}{2}$ to $\frac{\omega}{2r_h}$ in the end corresponds to scaling back to the form of the metric given in (2.1.10).

Now we are prepared to determine the $\mathcal{O}(\gamma)$ corrected differential equations for gauge fields, the five-form and, less important, the dilaton field. Since its EoM decouple, we will ignore it henceforth. Let us start with the five-form. The system obtained by varying the action with respect to the 4-form components (with $dC_4 = F_5$) can be written in a concise way:

$$d\left(* F_5 - * \frac{2\gamma}{\sqrt{-g}} \frac{\delta \mathcal{W}}{\delta F_5} \right) = 0, \tag{2.1.11}$$

where $\mathcal{W}$ is defined by

$$\mathcal{W} := 2\kappa_{10} S_{10}^{\gamma}. \tag{2.1.12}$$

It is easy to obtain this by observing that for a p-form C with $F = dC$ and an action

$$S = \int d^D x L(F, \nabla F) \tag{2.1.13}$$

for C the variation $\frac{\delta S}{\delta C} = 0$ leads to an equivalent set of differential equations as

$$d\left(* \frac{1}{\sqrt{-g}} \frac{\delta S}{\delta F} \right) = 0. \tag{2.1.14}$$

Indeed we already saw this for an explicit case in the introductory chapter, specifically in form of the derivation (1.5.2)-(1.5.5).

Let us shortly address how to compute $\frac{\delta \mathcal{W}}{\delta F_5}$ in an efficient way. To begin with, one interesting observation is that

$$\frac{\delta \mathcal{W}}{\delta F_5} = \frac{1}{2}\Big(1 - *\Big)\frac{\delta \mathcal{W}}{\delta F_5^+}, \tag{2.1.15}$$

where $F_5^+ = (1+*)F_5$, since only the self dual part of F_5 is entering $\gamma\mathcal{W}$ [19]. This relation could be used to test the result, once we have it, since it means that whatever we will obtain for $\frac{\delta \mathcal{W}}{\delta F_5}$ has to be anti-self dual. In order to vary $\mathcal{W}$ or more specifically

$$\int dx^{10}\sqrt{-g}\gamma W \tag{2.1.16}$$

we think of W as a map

$$W : \Omega^5(\mathcal{M}) \to C^\infty(\mathcal{M}) \tag{2.1.17}$$

from the set of the 5-forms on the manifold $\mathcal{M}$, which denotes the pseudo-Riemannian manifold with metric (2.1.10), to $C^\infty(\mathcal{M})$. In order to compute the component $\frac{\delta \mathcal{W}}{\delta F_5}^{\mu_1,\dots,\mu_5}$ we take the limit

$$\lim_{\alpha\to 0}\frac{1}{\alpha}\int dx^{10}\sqrt{-g}\gamma\Big(W[F_5 + \alpha F(u,t,z,y_1,y_2)dx^{\mu_1}\wedge\cdots\wedge dx^{\mu_5}] - W[F_5]\Big), \tag{2.1.18}$$

where we can already insert the $\mathcal{O}(\gamma^0)$-solution of F_5. We can interpret (2.1.18) as a variation of the functional

$$\begin{aligned}\mathcal{S} :& C^\infty(\mathcal{M}) \to \mathbb{R}\\ & F \mapsto \int dx^{10}\sqrt{-g}\gamma W[F_5 + F dx^{\mu_1}\wedge\cdots\wedge dx^{\mu_5}].\end{aligned} \tag{2.1.19}$$

The argument, why we are allowed to assume that F only depends on u,t,z,y_1,y_2 is the same is in the case $\mathcal{O}(\gamma^0)$, alternatively one easily verifies that

$$\partial_\mu \frac{\partial \mathcal{S}}{\partial \partial_\mu F} = 0, \quad \partial_\mu^2 \frac{\partial \mathcal{S}}{\partial \partial_\mu^2 F} = 0 \tag{2.1.20}$$

for $\mu \in \{x, y, y_3, y_4, y_5\}$. This makes the computation of any component of $\frac{\delta \mathcal{W}}{\delta F_5}$ as easy as determining the variation with respect to a normal function plus we get the directions, which only differ by a permutation of the indices for free.

Clearly (2.1.11) implies that self duality of the five form is broken if $d*\frac{1}{\sqrt{-g}}\frac{\delta \mathcal{W}}{\delta F_5} \neq 0$,

[19] We also checked the relation (2.1.15) explicitly

which is the case if $A_\mu \neq 0$. If F_5 would still be self dual, we had $(1-*)F_5 = 0$, but together with $dF_5 = 0$ (2.1.11) would then lead to a contradiction. This means that we cannot treat the F_5^2-term of the action as in the simple $\mathcal{O}(\gamma^0)$-case. In the following let us focus on the variation of this term with respect to A_μ.

Only being interested in those terms of the final EoM, which are linear in A_μ, allows us to ignore terms of order $\mathcal{O}(A^i)$, $i > 1$ of the metric in F_5^2. In fact, terms of second order coming from the metric could contribute to $\mathcal{O}(A^1)$ EoMs, however, contributions of this form cancel identically, as they have to, since otherwise we would get mass terms. This means that the number of F_5-directions, which actually contribute to

$$\frac{\delta\sqrt{-g}F_5^2}{\delta A_\mu} \tag{2.1.21}$$

is very restricted. As in section one, we only consider transverse fields $A_x(u,t,z)$, with $A_y = A_z = 0$. This implies that the only metric components depending on A_μ, neglecting terms of order $\mathcal{O}(A^2)$, are again $g^{xy_3}, g^{xy_4}, g^{xy_5}, g^{y_3x}, g^{y_4x}, g^{y_5x}$. Therefore, the only directions of F_5, which contribute to (2.1.21) in order $\mathcal{O}(\gamma^1)$, are

$$\begin{aligned}&(F_5)_{y_1y_2y_3y_4y_5}, (F_5)_{tuxyz}, (F_5)_{tuyzy_3}, (F_5)_{tuyzy_4}, (F_5)_{tuyzy_5}, (F_5)_{xy_1y_2y_4y_5}, (F_5)_{xy_1y_2y_3y_5},\\ &(F_5)_{xy_1y_2y_3y_4}.\end{aligned} \tag{2.1.22}$$

We already derived how $(F_5)_{y_1y_2y_3y_4y_5}$ and $(F_5)_{tuxyz}$ look like in order $\mathcal{O}(\gamma^1)$ for $A_\mu = 0$ (1.5.18, 1.5.19) and how these directions are modified in order $\mathcal{O}(\gamma^0)$ for $A_\mu \neq 0$ (2.1.7, 2.1.8). Metric components $g^{xy_3}, g^{xy_4}, g^{xy_5}, g^{y_3x}, g^{y_4x}, g^{y_5x}$ couple them to $(F_5)_{tuyzy_3}$, $(F_5)_{tuyzy_4}$, $(F_5)_{tuyzy_5}$, $(F_5)_{xy_1y_2y_4y_5}$, $(F_5)_{xy_1y_2y_3y_5}$, which are zero for vanishing A_μ. This means in order $\mathcal{O}(A^1)$ and $\mathcal{O}(\gamma^1)$ only the $\mathcal{O}(A^0)$ parts of the coupling corrected solutions of $(F_5)_{y_1y_2y_3y_4y_5}$ and $(F_5)_{tuxyz}$ contribute. Thus, we only have to compute $(F_5)_{tuyzy_3}$, $(F_5)_{tuyzy_4}$, $(F_5)_{tuyzy_5}$, $(F_5)_{xy_1y_2y_4y_5}$, $(F_5)_{xy_1y_2y_3y_5}$, $(F_5)_{xy_1y_2y_3y_4}$ up to first order in γ from (2.1.11). We will return to this later, at first we finish the variation of the rest of the action with respect to the gauge fields.

With our metric (2.1.10) we obtain

$$R_{10} = \left(R_{10}\big|_{A_\mu\to 0}\right) - \frac{L(u)^2}{3}F_{\mu\nu}F^{\mu\nu} \tag{2.1.23}$$

for the Ricci scalar. Varying this part with respect to A_μ is straightforward. The final part

$$\frac{\delta\gamma\sqrt{-g}\mathcal{W}}{\delta A_\mu} \tag{2.1.24}$$

already contains a γ-factor. Therefore, only $\mathcal{O}(\gamma^0)$-parts of the metric and F_5 enter it in order $\mathcal{O}(\gamma^1)$. Knowing already the solutions for F_5 with gauge fields in zeroth order

in γ allows us to compute this term immediately. However, there is a potential trap hidden in the subtlety that only the self dual part of F_5 enters here. Of course, we know already, that after having solved all EoM, we have $(1-*)F_5 = 0$ in order $\mathcal{O}(\gamma^0)$, which might make it tempting to set $F_5 = F_5^+$ from the beginning. But since on the action level the 4-form components and the gauge perturbation of the metric are independent fields, meaning that $\frac{\delta F_5}{\delta A_\mu} = 0$, we have in general that

$$\frac{\delta f(\frac{1}{2}(1+*)F_5)}{\delta A_\mu} \neq \frac{\delta f(F_5)}{\delta A_\mu} \tag{2.1.25}$$

for a functional f, even if $\frac{1}{2}(1+*)F_5 = F_5$ after inserting all solutions of the resulting EoM. This is because A_μ can enter through to the Hodge dual

$$\frac{\delta(*F_5)_{abcdef}}{\delta A_\mu} \neq 0 = \frac{\delta(F_5)_{abcdef}}{\delta A_\mu} \tag{2.1.26}$$

for some directions $abcdef$.

Having avoided this pitfall we can finally tackle the involved variations. Let us split the work up and concentrate on the C^4-part of the higher derivative corrections first. After varying it with respect to A_x, introducing

$$(A_x)_k(u,q,\omega) = \frac{1}{2\pi}\int dtdz e^{iqz}e^{-iwt}A_x(u,z,t) \tag{2.1.27}$$

and exploiting that

$$\gamma(\partial_u^2 A_x - \frac{2u}{1-u^2}\partial_u A_x + \frac{\hat{\omega}^2 - \hat{q}^2(1-u^2)}{u(1-u^2)^2}A_x) = \mathcal{O}(\gamma^2) \tag{2.1.28}$$

we obtain

$$\frac{64u^3\gamma}{3}((A_x)_k(24\hat{q}^4u + \hat{q}^2(162-235u^2) - 60\hat{w}^2) - (u^2-1)(120\hat{q}^2u - 135u^2 + 112)(A_x)_k') + \mathcal{O}(\gamma^2) \tag{2.1.29}$$

as a contribution to the differential equations, rescaled in such a way that the $\mathcal{O}(\gamma^0)$-part has the form $\frac{8(1-u^2)}{3}$ times (2.1.9). We can ignore terms of the form $C\mathcal{T}^3$, $\mathcal{T}^4$. This is because $\mathcal{T} = 0$ on a fluctuation free static metric, thus both $C\mathcal{T}^3$ and $\mathcal{T}^4$ only contribute terms of order $\mathcal{O}(A^2)$ to the EoM. In the chapter (2.2) we will tackle the rather problem of strong background fields, which will force us to also consider these classes of corrections. Since $\frac{\delta\mathcal{T}}{\delta A_\mu} \neq 0$ in the considered orders of A_μ and γ, we still have to determine

$$\frac{\delta\gamma\sqrt{-g}C^2\mathcal{T}^2}{\delta A_x} \quad \text{and} \quad \frac{\delta\gamma\sqrt{-g}C^3\mathcal{T}}{\delta A_x}. \tag{2.1.30}$$

Our strategy to compute the terms above will be to insert the solutions for F_5 in lowest order in γ slightly modified by replacing A_μ by a new independent function $\bar{A}_\mu$ into (2.1.30)

$$F_5\Big|_{A_\mu \to \bar{A}_\mu} \tag{2.1.31}$$

and let $\bar{A}_\mu$ go to A_μ after the variation, since we are not allowed to vary with respect to A_μ appearing in F_5 after inserting the $\mathcal{O}(\gamma^0)$ solution. For this purpose we display this solution explicitly in Appendix 5.2. The complete solution of the five form F_5 in order $\mathcal{O}(\gamma^0)$ is then

$$F_5 = (F_5^{mag})^1 + (F_5^{mag})^0 + (F_5^{el})^1 + (F_5^{el})^0. \tag{2.1.32}$$

The forms $(F_5^{mag})^1$, $(F_5^{mag})^0$, $(F_5^{el})^1$, $(F_5^{el})^0$ are given in Appendix 5.2. We can test this five form solution by computing F_5^2, which turns out to be zero. This is good news, since the Hodge star operator $*$ in a $2p$ dimensional manifold fulfills for any p form F:

$$F \wedge *F = F^2 \tilde{\omega}, \tag{2.1.33}$$

where in our case $\tilde{\omega}$ is the 10 form

$$\tilde{\omega} = dt \wedge du \wedge dx \wedge dy \wedge dz \wedge dy_1 \wedge dy_2 \wedge dy_3 \wedge dy_4 \wedge dy_5. \tag{2.1.34}$$

Since F_5 is self dual in this order in α', we thus have to get[20] $F_5^2 = 0$. Now let us think about which directions of $*F_5$ can actually enter (2.1.30). The only ways A_μ can enter $C^3\mathcal{T}$ and $C^2\mathcal{T}^2$ is through

- the fact that
$$\frac{\partial * (F_5|_{A_\mu \to \bar{A}_\mu})}{\partial A_\mu}\Big|_{\bar{A}\mu \to A_\mu} \neq 0, \tag{2.1.36}$$
- A_μ-dependent terms entering directly via the metric components present in the contractions of C and $\mathcal{T}$,
- the Weyl tensor itself
- and the covariant derivative in (1.2.15).

[20] It should be noted that this, of course, does not hold on the action level, even in the lowest order in α', since

$$\left(\frac{\delta}{\delta A_\mu}\int d^{10}\sqrt{-g}(F_5|_{A_\mu \to \bar{A}_\mu})^2\right)_{\bar{A}_\mu \to A_\mu} \tag{2.1.35}$$

does not have to vanish even if $F_5^2 = 0$ after inserting its solution.

We claim and prove in the following that all we have to care about, regarding

$$F_5|_{A_\mu \to \bar{A}_\mu}) \tag{2.1.37}$$

in (2.1.36) is

$$F_5|_{A_\mu \to \bar{A}_\mu} + \frac{*(F_5^{el})^0 - ((F_5^{mag})^0|_{A_\mu \to \bar{A}_\mu})}{2} + \frac{*((F_5^{mag})^0|_{A_\mu \to \bar{A}_\mu}) - (*(F_5^{mag})^0|_{A_\mu \to \bar{A}_\mu})}{2}. \tag{2.1.38}$$

We also checked this explicitly by computing the not simplified contribution of (2.1.37) and explain in the following why relation (2.1.38) holds.

It is easy to see that this is true for the first term in (2.1.30). There, the argument that $\mathcal{T} = 0$ for $\gamma = 0$ and $A_\mu = 0$ forces all contribution of order $\mathcal{O}(A^2)$, $\mathcal{O}(A\bar{A})$ or $\mathcal{O}(A\partial\bar{A})$ from $*(F_5|_{A_\mu \to \bar{A}_\mu})$ to $C^2\mathcal{T}^2$ to be negligible. But what about potential terms of order $\mathcal{O}(A\partial\bar{A})$ in $*(F_5|_{A_\mu \to \bar{A}_\mu})$ entering $C^3\mathcal{T}$? In fact, since the perturbation of the metric by A_μ was chosen in such a maximally symmetric way, in order to avoid coupling to scalars in order $\mathcal{O}(\gamma^0)$, it is rather straightforward to check that the terms of order $\mathcal{O}(A\partial\bar{A})$ from $*((F_5^{mag})^1|_{A_\mu \to \bar{A}_\mu})$ cancel identically. Considering the definition of the tensor $\mathcal{T}$ one sees that the terms $*((F_5^{el})^1|_{A_\mu \to \bar{A}_\mu})$ of order $\mathcal{O}(A\partial\bar{A})$ only enter those components $\mathcal{T}_{abcdef}$, where at least one of a, b, c, d, e is in $\{y_1, \dots, y_5\}$. The parts of $\mathcal{T}$ coming from $*((F_5^{el})^1|_{A_\mu \to \bar{A}_\mu})$ in order $\mathcal{O}(A\partial\bar{A})$, have to be contracted with the Weyl-tensor part of (2.1.30) computed from the $\gamma = 0$-$A_\mu = 0$-metric. In this case the Weyl tensor splits up block-diagonally into an AdS-part and a S_5-part, the latter of which is zero since the 5-sphere is Weyl flat. Summing up the contributions of both terms in (2.1.30) to the EoM obtained by variation with respect to A_μ one gets

$$\frac{16}{9}u^3\left(349\hat{q}^2(A_x)_k - 1111\left(u^2-1\right)\partial_u(A_x)_k\right) + \mathcal{O}(\gamma^2). \tag{2.1.39}$$

This term is rescaled in the same way as (2.1.29).

Now we have to solve (2.1.11) for the last 6 elements of (2.1.22). We follow the same strategy as in the case $\gamma = 0$ and search for closed diagrams such as figure 2.1, for which

$$(F_5)_{tuyzy_3}, (F_5)_{tuyzy_4}, (F_5)_{tuyzy_5}, (F_5)_{xy_1y_2y_4y_5}, (F_5)_{xy_1y_2y_3y_5}, (F_5)_{xy_1y_2y_4y_4} \tag{2.1.40}$$

contribute to all considered directions of $d * F_5$ on the right side of the diagram and no more. After this task one has to find all directions of C_4 that contribute to these components of $d * F_5$ and make sure that the directions of C_4 on the left side of the diagram don't contribute to another direction of $d * F_5$, otherwise expand the diagram and repeat. Let's assume we thereby collect a set of directions $\{a_ib_ic_id_ie_if_i\}_{i\in I}$ for

which $(d*F_5)_{a_ib_ic_id_ie_if_i}$ with $i \in I$ appears on the right side of one of the diagrams[21]. This means that we have to compute the components

$$\left\{\left(d*\frac{2\gamma}{\sqrt{-g}}\frac{\delta\mathcal{W}}{\delta F_5}\right)_{a_ib_ic_id_ie_if_i}\right\}_{i\in I} \tag{2.1.41}$$

in order to be able to solve for all needed directions of (2.1.11). Since diagram 2.1 was found without using that we are in order $\mathcal{O}(\gamma^0)$, we can simply reuse it now. Its dual diagram is given by figure 2.2. Here the unlabeled arrows in the diagram on the left and right depict derivatives. Due to (2.1.11) the nonzero directions of $d*\frac{2\gamma}{\sqrt{-g}}\frac{\delta\mathcal{W}}{\delta F_5}$ determine the y_1, y_2-dependence of the components of C_4 proportional to γ on the left hand side of the diagram. The form of the solution of the five form in order $\mathcal{O}(\gamma^0)$, which gives the y_1, y_2-dependence of $d*\frac{2\gamma}{\sqrt{-g}}\frac{\delta\mathcal{W}}{\delta F_5}+\mathcal{O}(\gamma^2)$ already illustrates, what becomes more apparent once one calculated the

$$uxy_1y_2y_4y_5, txy_1y_2y_4y_5,\ uxzy_1y_4y_5,\ tuxy_2y_4y_5,\ tuxy_1y_4y_5,\ txzy_2y_4y_5,$$
$$txzy_1y_4y_5,\ uxzy_1y_4y_5,\ xzy_1y_2y_4y_5,\ tuxzy_4y_5-$$

directions of $d*\frac{2\gamma}{\sqrt{-g}}\frac{\delta\mathcal{W}}{\delta F_5}+\mathcal{O}(\gamma^2)$, namely that all directions of C_4 on the left hand side, which contain a y_2 and all directions of $d*F_5$ on the right hand side, which contain a y_1 and no y_2 can be ignored, since all are trivially zero in order $\mathcal{O}(\gamma^1)$. More specifically we have

$$\left(d*\frac{2\gamma}{\sqrt{-g}}\frac{\delta\mathcal{W}}{\delta F_5}\right)_{abcy_1y_4y_5}=\mathcal{O}(\gamma^2) \tag{2.1.42}$$

for all $a, b, c \in \{t, u, x, y, z, y_1, y_3, \ldots, y_5\}$. The results for all directions of $\frac{\delta\mathcal{W}}{\delta F_5}$ needed to compute the EoM obtained by evaluating (2.1.11) for the components corresponding to the right hand side of diagram 2.1 and 2.2 in order $\mathcal{O}(\gamma)$ can be found in the Appendix 5.3. It should be mentioned that due to the anti-self-duality of $\frac{\delta\mathcal{W}}{\delta F_5}$ the components given in the Appendix section 5.3 are all you need to compute diagrams 2.1, 2.2. The other directions can be computed from those or vanish, since we only consider EoMs, which are linearized in A_x.

Now let us sketch how to solve this large set of differential equations. One important observation is that the $xy_2y_3y_4$-direction of C_4 plays a crucial role. Considering which components of $\frac{\delta\mathcal{W}}{\delta F_5}$ are zero and which actually give contributions to (2.1.11) shows that the argument we applied in the first section, when discussing diagram 2.1, for why the $xy_2y_3y_4$-direction of C_4 is the only non-zero one on the left hand side of diagram 2.1, doesn't change if we include α'-corrections. Thus, diagram 2.1 simplifies drastically

[21] Since the five form is no longer self dual in this order in α' we cannot simply skip one half of the diagrams and determine the remaining directions of F_5 with the help of the duality argument, as done in order $\mathcal{O}(\gamma^0)$.

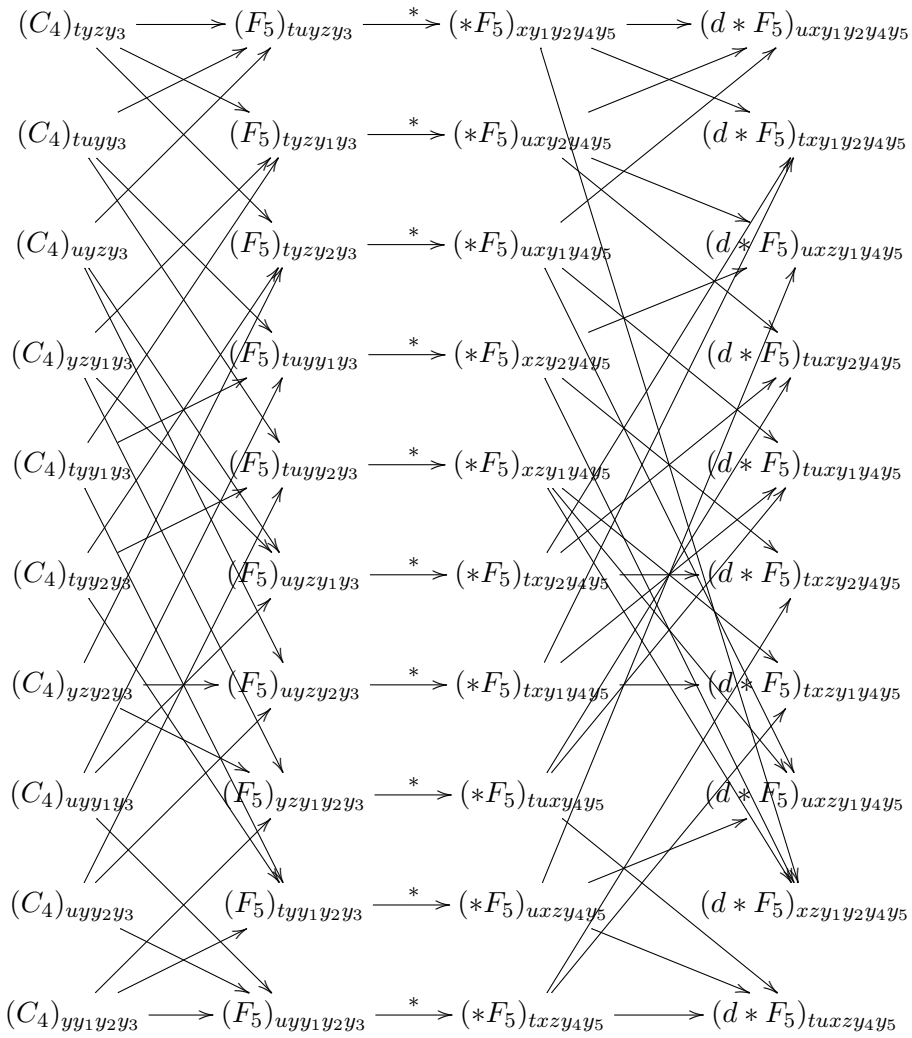

Figure 2.2: Depiction of the system of differential equations, dual to those of diagram 2.1. Contributions of off-diagonal elements of the metric tensor to the Hodge duals were left out for simplicity in this figure. Of course, they are included in the calculation. The right hand side of the diagram has to be equal to the corresponding directions of $d(*\frac{2\gamma}{\sqrt{-g}}\frac{\delta\mathcal{W}}{\delta F_5})$. We omitted the d-labels in the first and third row to keep the diagram readable.

also in order $\mathcal{O}(\alpha'^3)$ and is given in (2.1.44). Our ansatz for $(C_4)_{xy_2y_4y_5}$ will be of the form

$$(C_4)_{xy_2y_4y_5} = \cos(y_1)^4 \sin(2y_2)\frac{A_x + \gamma C(u,q,\omega)}{\sqrt{3}}. \tag{2.1.43}$$

The y_1, y_2-dependence is dictated by the form of the components of $\frac{\delta\mathcal{W}}{\delta F_5}$ listed in section 5.3 and the requirement that $\partial_{y_i} A = 0$. It is possible to find a similar simplification for its dual diagram again obtained by analyzing the y_1, y_2-dependence of the relevant directions of $\frac{\delta\mathcal{W}}{\delta F_5}$. This has to be repeated for the remaining diagrams in order to solve

the EoM for the relevant directions of F_5, obtained by varying the action with respect to A_μ. However, this very tedious calculation can be abbreviated by an elegant shortcut, which we present in the following. We made the effort to calculate the EoMs using both methods to test our results.

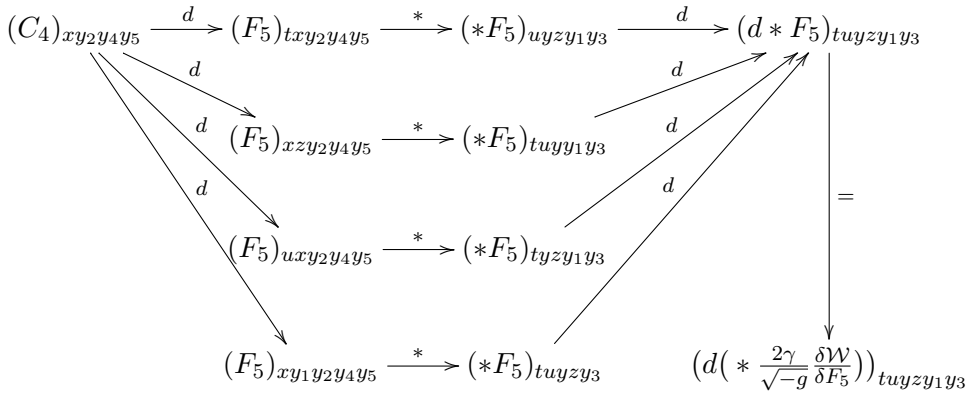

(2.1.44)

There is also a slightly different approach to solve (2.1.11), which relies on the observation that for every solution F_5 also

$$F_5 + \gamma\tilde{F} \tag{2.1.45}$$

with

$$d\tilde{F} = 0,\ d(1-*)\tilde{F} = 0, \tag{2.1.46}$$

solves (2.1.11) and fulfills that there is a four form C_4 with $dC_4 = F_5 + \gamma\tilde{F}$. Let $\tilde{F}_5$ be a solution of (2.1.11) with $d\tilde{F}_5 = 0$. Considering the de Rham-cohomology of our manifold shows that the EoM for the five form can be written as

$$\left(-\tilde{F}_5 + *\tilde{F}_5 - *\frac{2\gamma}{\sqrt{-g}}\frac{\delta\mathcal{W}}{\delta F_5}\right) = \gamma dH_4, \tag{2.1.47}$$

for some 4-form H_4. Since $\frac{\delta\mathcal{W}}{\delta F_5}$ is anti-self dual, also dH_4 has to be anti-self dual. So

$$d(1-*)dH_4 = 2ddH_4 = 0, \tag{2.1.48}$$

such that we can choose $\tilde{F} = -\frac{dH_4}{2}$, set

$$\tilde{F}_5 = F_5 + \gamma\tilde{F} \tag{2.1.49}$$

for another closed solution F_5 of (2.1.11) and thus get

$$F_5 = *\left(F_5 - \frac{2\gamma}{\sqrt{-g}}\frac{\delta \mathcal{W}}{\delta F_5}\right). \tag{2.1.50}$$

To further strengthen the arguments made before, why diagram 2.1 simplifies to (2.1.44), we note that the differential equation depicted in diagram (2.1.44) can be deduced from the $tuyzy_3$, $uxy_2y_4y_5$, $txy_2y_4y_5$ and $zxy_2y_4y_5$-direction of (2.1.50). In addition it helps us to express the $tuyzy_3$-direction of F_5 by its $xy_1y_2y_4y_5$-component and the corresponding direction of $\frac{\mathcal{W}}{\delta F_5}$. Analogously the pairs $(xy_1y_2y_3y_5, tuyzy_4)$ and $(xy_1y_2y_3y_4, tuyzy_5)$, are linked via equation (2.1.50), where it turns out that up to a different y_1, y_2-dependence the directions $tuyzy_i$ with $i \in \{3,4,5\}$ of F_5 are identical, the same is valid for their dual partners. This is great news, since now we can reduce the entire coupled set of EoMs for the 4-form components and the gauge field A_μ to a rather simple system of two coupled differential equations for A_μ and the $xy_2y_4y_5$-component of C_4. Exploiting these relations between the directions $tuyzy_i$ with $i \in \{3,4,5\}$ of the five form and the analogous ones for their dual partner gives after a tedious calculation

$$-\frac{1}{4\cdot 5!}\frac{\partial\sqrt{-g}F_5^2}{\partial A_x} = \frac{16\gamma C(u,q,w)}{3u^2} + \frac{4(F_5)_{tuyzy_3}}{\sqrt{3}\sin(y_1)^2}. \tag{2.1.51}$$

Explicitly the aforementioned relation between $(F_5)_{tuyzy_3}$ and its dual partner derived from (2.1.50) gives

$$(F_5)_{tuyzy_3} = \sqrt{-g}g^{xx}g^{y_1y_1}g^{y_2y_2}g^{y_4y_4}g^{y_5y_5}\Bigg(4\sin(y_1)\cos(y_1)^3\sin(2y_2)\frac{\gamma C(u,q,\omega)}{\sqrt{3}} - \frac{2\gamma}{\sqrt{-g}}\left(\frac{\mathcal{W}}{\delta F_5}\right)_{xy_1y_2y_4y_5}\Bigg). \tag{2.1.52}$$

Adding up and combining everything (2.1.52, 2.1.51, 2.1.44, 2.1.43, 2.1.39, 2.1.29 and Appendix 5.3) we can finally write down the differential equation governing the dynamics of A_x. For this purpose let us define

$$A_x(u,z,t) = A_x^0(u,z,t) + \gamma A_x^1(u,z,t) \tag{2.1.53}$$

$$A_x^j(u,z,t) = \int \frac{d^4k}{(2\pi)^4}\tilde{A^j}_x(u,q,w)e^{-i\omega t+iqz} \tag{2.1.54}$$

with $\tilde{A}_x(u,q,w) =: (A_x)_k$, $k=(w,q)$. The EoM for $(A_x^1)_k$ is given by

$$\partial_u^2(A_x^1)_k + \frac{2u}{-1+u^2}\partial_u(A_x^1)_k + \frac{(\tilde{q}^2(-1+u^2)+\tilde{\omega}^2)}{u(-1+u^2)^2}(A_x^1)_k + \frac{1}{(48u^2(-1+u^2)^2)}(u^3$$
$$(-9216\tilde{q}^4u^3(-1+u^2)+\tilde{q}^2(-3900+73507u^2-145342u^4+75735u^6)+15(520$$
$$-1061u^2+435u^4)\tilde{w}^2)(A_x^0)_k - 2(-1+u^2)(96C(u,q,\omega)+u^3(-1+u^2)(3900-$$
$$23846u^2-23040\tilde{q}^2u^3+675u^4)\partial_u(A_x^0)_k)) = 0. \tag{2.1.55}$$

where $\tilde{\omega} = \frac{\omega}{2r_h}$, $\tilde{q} = \frac{q}{2r_h}$. The coupling corrected relation between horizon radius r_h and temperature T is given by $r_h = \pi T(1-\frac{265}{16}\gamma+\mathcal{O}(\gamma^2))$ (see sections 1.4.3 & 1.5), which can be computed from relation (1.4.28) and (1.5.21)-(1.5.24). If we introduce in (2.1.55) rescaled variables $\hat{\omega} = \frac{\tilde{\omega}}{2\pi T}$ and $\hat{q} = \frac{\tilde{q}}{2\pi T}$ we obtain a differential equation whose characteristic exponents simplify to $\pm\frac{i\hat{\omega}}{2}$ also in order $\mathcal{O}(\gamma)$. From diagram (2.1.44) or the $tuyzy_3$, $uxy_2y_4y_5$, $txy_2y_4y_5$ and $zxy_2y_4y_5$-components of (2.1.50) we obtain the differential equation

$$\partial_u^2(A_x^1)_k + \frac{2u}{-1+u^2}\partial_u(A_x^1)_k + \frac{\tilde{q}^2(-1+u^2)+\tilde{w}^2}{u(-1+u^2)^2}(A_x^1)_k + \frac{1}{48u^2(-1+u^2)^2}(u^3(-9216\tilde{q}^4$$
$$u^3(-1+u^2)+\tilde{q}^2(-3900+116931u^2-260414u^4+147383u^6)+3(2600-10969u^2+$$
$$7839u^4)\tilde{w}^2)(A_x^0)_k + 2(24(-2+2u^2+\tilde{q}^2u(-1+u^2)+u\tilde{w}^2)C(u,q,\omega)-u^2(-1+u^2)$$
$$(u(-1+u^2)(3900-36702u^2-32480\tilde{q}^2u^3+20895u^4)\partial_u(A_x^0)_k - 24(2u\partial_uC(u,q,\omega)+$$
$$(-1+u^2)\partial_u^2C(u,q,\omega))))) = 0. \tag{2.1.56}$$

The boundary conditions of these EoMs are that A_x and C, respectively the $xy_1y_2y_4y_5$-component of the five form, have to be infalling at the horizon. The zeroth expansion coefficient of the near horizon expansion of $A_x/(1-u)^{-\frac{i\hat{\omega}}{2}}$ can be set to 1, since it doesn't affect any physical observables on the boundary due to the form of (2.1.59). The missing condition is that $C(u,q,\omega)$ has to vanish on the boundary, which is a regular singular point of our small system of EoMs. More explicitly this can be obtained from the two different possible boundary behaviours of $C(u,q,\omega)$ given by

$$C(u,q,\omega) = \frac{C_{-2}}{u^2} + \mathcal{O}(u^{-1}) \quad \text{and} \quad C(u,q,\omega) = u^3C_3 + \mathcal{O}(u^4), \tag{2.1.57}$$

extracted from the near boundary analysis of the differential equation obtained by subtracting (2.1.56) from (2.1.55). Equation (2.1.55) shows that the former choice would lead to a gauge field A_x, which diverges at the boundary. This means our missing boundary condition is that

$$C_{-2} = 0, \tag{2.1.58}$$

which in this case implies that $C_{-1} = \dots C_2 = 0$, such that $C(u, q, \omega) = u^3 C_3 + \mathcal{O}(u^4)$. This concludes the derivation of higher derivative corrected equations of motion for gauge fields (with transverse polarization).

2.1.3 Higher derivative corrections to observables in a charged quark gluon plasma

In this chapter we are going to pick several low hanging fruits regarding the determination of α'-corrections to quantities and observables in a charged QGP using the differential equations (2.1.55) and (2.1.56) derived in the previous chapter. We compute finite λ corrections to the conductivity, photoemission rates, quasinormal mode spectra as well as in and off-equilibrium spectral densities. These were first computed in [53], using, however, the results and EoMs of [10–12], which we argue now to be incorrect. Consequently also the results for observables, which can be found in the literature, computed with the γ-corrected EoM for gauge fields change. The differences are quite substantial and are caused by several disagreements: most importantly a missing factor i in front of some components of the five form, when working in Euclidean signature, several missing terms, when computing the Hodge duals, coming from the off-diagonal elements of the metric tensor, and the fact that the five form used by the authors of the papers [10–12] did not solve its α'-corrected EoM. Note that in Euclidean signature there is no self duality, since the Hodge star operator squares to -1 there, such that self dual five forms transform to imaginary anti-self-dual forms $*F_5^{\mathrm{E}} = -iF_5^{\mathrm{E}}$. Continuing to work with $(1 + *)F_5^{el}$ implies that the five form doesn't square to zero anymore, which means it doesn't even solve its EoM in the lowest order in α'. Also the Lorentz-signature version of the coupling corrected five form given in [10–12] is not a solution of (2.1.11).

2.1.3.1 Quasinormal modes and their coupling corrections

Quasinormal modes (QNM) describe the response of the system to small perturbations as explained in more detail in the introduction 1.4.2. In our case these perturbations correspond to tiny twists of the S_5-part, from which we deduced the α'-corrected differential equations (2.1.55) and (2.1.56) for gauge fluctuations. The position of the complex QNM-frequencies ω corresponds to the discrete spectrum of frequencies, at which the propagator of A_x has poles. The negative inverse of the imaginary part of ω gives the thermalization time τ, such that one can expect that increasing γ or decreasing the 't Hooft coupling will decrease the absolute value of the imaginary part of each QNM frequency ω. Applying (1.4.14) one can calculate the retarded propagator for transverse fields Π^T with the help of the prescription

$$\Pi^T = -\frac{N^2 T^2}{8} \lim_{u \to 0} \frac{(A_x)'_k}{(A_x)_k}, \tag{2.1.59}$$

where Π^T corresponds to the transverse part of the retarded current current correlator

$$C^{ret}_{\mu\nu} = -i \int d^4x e^{ikx} \theta(t) \langle [J^{\text{em}}_\mu(x), J^{\text{em}}_\mu(0)] \rangle, \tag{2.1.60}$$

which can be split up into longitudinal and transverse components as done in (1.4.18). In the following we will present several techniques with which we can extract the α'-corrected spectra for different values of q using (2.1.55) and (2.1.56). Independent from the approach used the first information about the solutions we have to exploit is their near horizon behaviour

$$A^0_x(u,\hat{q},\hat{\omega}) = (1-u)^{-\frac{i\hat{\omega}}{2}} \Phi^0(u,\hat{q},\hat{\omega}) \tag{2.1.61}$$

$$A^1_x(u,\hat{q},\hat{\omega}) = (1-u)^{-\frac{i\hat{\omega}}{2}} \Phi^1(u,\hat{q},\hat{\omega}) \tag{2.1.62}$$

$$C(u,\hat{q},\hat{\omega}) = (1-u)^{-\frac{i\hat{\omega}}{2}} \Phi^2(u,\hat{q},\hat{\omega}), \tag{2.1.63}$$

where Φ^0, Φ^1 and Φ^2 are regular at the horizon. Let us start with an easy method to solve (2.1.55) and (2.1.56) with this ansatz. This method, however, is also the numerically most inefficient. For this we simply expand the resulting differential equations around the horizon and require them to hold order by order in $(1-u)$. By determining sufficiently large orders and demanding that[22]

$$\Phi^0(0,\hat{q},\hat{\omega}) + \gamma \Phi^1(0,\hat{q},\hat{\omega}) = 0, \tag{2.1.64}$$

we can extract the α'-corrected spectra for arbitrary values of q.

Alternatively, we can apply spectral methods to reduce our system of differential equations to a generalized eigenvalue problem. For this purpose we use the same notation as in (2.1.63) and subtract (2.1.55) from (2.1.56) to end up with a differential equation only containing Φ^0 and Φ^2. We set $\Phi^2 = u\tilde{\Phi}^2$ as well as

$$A_x(u,\hat{q},\hat{\omega}) = (1-u)^{-\frac{i\hat{\omega}}{2}} \Phi(u,\hat{q},\hat{\omega}) \tag{2.1.65}$$

and obtain after an expansion in γ

$$\Big(\partial_u^2\tilde{\Phi}^2 + \frac{2+iu\hat{w}+iu^2(4i+\hat{w})}{u-u^3}\partial_u\tilde{\Phi}^2 + \frac{1}{4u^2(-1+u)(1+u)^2}(24+u^2(8+4\hat{q}^2-10i\hat{w}$$
$$-3\hat{w}^2)+4u(6+\hat{q}^2-i\hat{w}-\hat{w}^2)-u^3(-8+6i\hat{w}+\hat{w}^2))\tilde{\Phi}^2 + \frac{u^2}{12(-1+u^2)}\big(-i((3214+$$
$$3214u-5055u^2-5055u^3+4248i\hat{w})\hat{w}+8\hat{q}^2(-1357i+295u\hat{w}+u^2(2239i+295\hat{w})))\Phi$$
$$-2(-1+u^2)(-3214-2360\hat{q}^2u+5055u^2)\partial_u\Phi)\Big)\gamma = \mathcal{O}(\gamma^2) \tag{2.1.66}$$

[22] Which follows from the requirement that (2.1.59) has a pole at the QNM frequencies.

and

$$\partial_u^2\Phi - \frac{i(\hat{w}+u(2i+\hat{w}))}{-1+u^2}\partial_u\Phi + \frac{4\hat{q}^2(1+u)-\hat{w}(4\hat{w}+u^2(2i+\hat{w})+u(2i+3\hat{w}))}{(4(-1+u)u(1+u)^2)}\Phi +$$
$$\frac{\gamma}{48u(-1+u^2)}((-9216\hat{q}^4u^5+i(3900u^3-23846u^5+675u^6+675u^7+30u^2(130+313i\hat{w})$$
$$+u^4(-23846-6525i\hat{w})+1590i\hat{w})\hat{w}+\hat{q}^2(1590+3900u^2-69607u^4+45u^6(1683-$$
$$512i\hat{w})-23040iu^5\hat{w}))\Phi-2(96\tilde{\Phi}^2+u^2(-1+u^2)(3900-23846u^2-23040\hat{q}^2u^3+$$
$$675u^4)\partial_u\Phi))=\mathcal{O}(\gamma^2). \tag{2.1.67}$$

From the EoM in order $\mathcal{O}(\gamma^0)$ (2.1.9) we can solve Φ^0 for a given value of $\hat{\omega}$ at a certain $\hat{q}$ using spectral methods almost up to arbitrary numerical precision, due to the simplicity of this differential equation. It would even be possible to find analytic solutions in the lowest order in γ, but for our purposes an approximation by Chebyshev-cardinal functions is sufficient, if we choose the order sufficiently high or the Gauss-Lobatto grid sufficiently dense. We also approximate Φ and $\tilde{\Phi}^2$ in the following by a truncated expansion in cardinal functions on a Gauss-Lobatto grid

$$\{-\cos(\frac{\pi n}{M})\}_{n\in\{0,\dots,M\}} \tag{2.1.68}$$

on the interval $[-1,1]$ for $2u-1$, $u\in[0,1]$, respectively with a grid

$$\left\{\frac{1-\cos(\frac{\pi n}{M})}{2}\right\}_{n\in\{0,\dots,M\}} \tag{2.1.69}$$

on the interval $[0,1]$. More explicitly we set for a certain value of $\hat{q}$

$$\Psi(u,\hat{\omega})=\sum_{i=0}^{M}a_i^{\Psi}(\hat{\omega})c(i,2u-1), \tag{2.1.70}$$

with $c(i,x)$, $x\in[-1,1]$ being the i-th cardinal function for the grid (2.1.68) and $\Psi\in\{\Phi\ ,\ \tilde{\Phi}^2\}$. Now we can bring (2.1.66) and (2.1.67) into the form of a generalized eigenvalue problem for $\hat{\omega}$, if we truncate the differential equations after the first order in γ. This works as follows:

With the help of pseudo spectral methods, explained in more detail in the Appendix 5.9, we replace functions Ψ by vectors of their expansion coefficients (a_i^{Ψ}) corresponding to the projection of Ψ on a finite dimensional Hilbert space spanned by $M+1$ Chebyshev cardinal functions. In this spirit differentiations become matrix multiplications allowing us to write (2.1.66) and (2.1.66) as linear systems for the coefficients

$$\{a_i^{\Psi}\}_{i\in\{0,\dots,M\},\Psi\in\{\Phi\ ,\ \tilde{\Phi}^2\}}, \tag{2.1.71}$$

$\hat{q}=0$	$\gamma=0$	$\mathcal{O}(\gamma^1)$-correction
1. QNM	$1-i$	$\gamma(646.132-207.258i)$
2. QNM	$2-2i$	$\gamma(4896+495.5i)$

$\hat{q}=1$	$\gamma=0$	$\mathcal{O}(\gamma^1)$-correction
1. QNM	$1.54719-0.84972i$	$\gamma(298.289+208.678i)$
2. QNM	$2.39890-1.87434i$	$\gamma(2357+1916i)$

Figure 2.3: The first two QNM frequencies at $q = 2\pi T$ (right) and $q = 0$ (left) normalized by $2\pi T$ and their $\mathcal{O}(\gamma)$-corrections, which turn out to be more than one order of magnitude smaller then found in [53], which was based on the EoM derived in [10–12].

that still depends on $\hat{\omega}$ and γ. For a fixed value of γ the truncated differential equations lead to linear equations of the form

$$\left(A_0+\hat{\omega}A_1+\hat{\omega}^2A_2\right)\begin{pmatrix}a^{\Phi}\\ a^{\tilde{\Phi}^2}\end{pmatrix}=0 \tag{2.1.72}$$

with appropriate matrices A_0, A_1 and A_2. With $v=(a^{\Phi},a^{\tilde{\Phi}^2})$ this is equivalent to the $4(M+1)$ dimensional generalized Eigenvalue problem

$$\begin{pmatrix}A_0 & A_1\\ 0 & 1\end{pmatrix}\begin{pmatrix}v\\ \hat{\omega}v\end{pmatrix}=\hat{\omega}\begin{pmatrix}0 & -A_2\\ 1 & 0\end{pmatrix}\begin{pmatrix}v\\ \hat{\omega}v\end{pmatrix}, \tag{2.1.73}$$

which is easy to solve numerically and has good convergence properties.

In the next step we also consider γ to be on an appropriate Gauss-Lobatto grid and solve the generalized eigenvalue problem for each grid point. At $\gamma=0$ the slopes of the resulting curves of partially resummed poles for different values of γ in the complex plane gives us the $\mathcal{O}(\gamma^1)$-coefficient to the corresponding $\lambda=\infty$-modes. For the first modes these curves are depicted in Figure 2.12. By going to sufficiently dense grids we obtain identical values as with the simpler Frobenius-method discussed above. We find the α'^3-corrections to the QNM spectrum to be one order of magnitude smaller than those found in [53], which used the EoMs of [10–12].

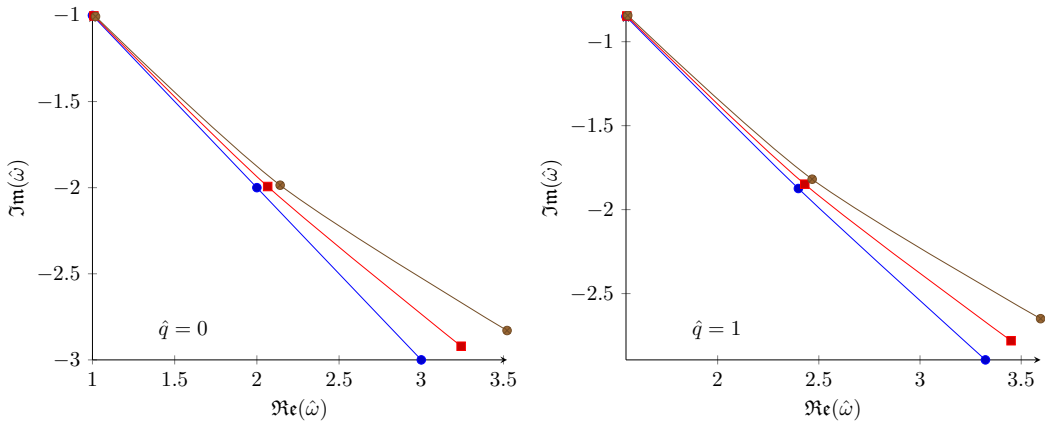

Figure 2.4: The first QNM frequencies at $q = 2\pi T$ (right) and $q = 0$ (left) normalized by $2\pi T$ for $\lambda = \infty$ (blue) and their $\mathcal{O}(\gamma)$-corrections for $\lambda = 500$ (red) and $\lambda = 300$ (brown).

2.1.3.2 Finite coupling corrections to the plasma conductivity and photoemission rate

As shown in section 1.4.6 we simply have to determine the retarded current-current correlator from gravity, or more precisely its imaginary part, in order to compute the spectral density respectively the photoemission rate and its finite coupling corrections from our transverse field A_x[23]

$$\chi_\perp = -4\mathrm{Im}(\Pi^T). \tag{2.1.74}$$

From the low energy regime respectively the first order expansion coefficient of (2.1.74) in $\hat{q}$ with lightlike momentum ($q = \omega$) we can immediately read off the correction to the conductivity[24]. The correction factor to the differential photon production rate can be computed via the relation between the trace of the spectral function χ and the Wightman function as shown in section (1.4.6). To obtain the low energy limit of (2.1.74), more specifically the finite coupling correction to the conductivity, we only have to solve (2.1.55) and (2.1.56) to order $\mathcal{O}(\gamma)$ and $\mathcal{O}(\hat{\omega})$. In this case the solution for $C(u, \hat{q}, \hat{\omega})$ is simply

$$C(u, \hat{q}, \hat{\omega}) = \left(\frac{95u^3}{8} - \frac{959u^5}{24} + \frac{337u^7}{12}\right)\partial_u A_x^0 + \mathcal{O}(\hat{\omega}^2), \tag{2.1.75}$$

[23]This relation is an application of equation (1.4.43), where χ is the trace of the spectral function.
[24]For this consider equation (1.4.39) and (1.4.43)

which means that our EoM for A_x simplifies drastically to

$$\partial_u^2 A_x + \frac{u}{8(-1+u^2)}(16\partial_u A_x + \gamma(920 - 7970u^2 + 7275u^4 - 225u^6)\partial_u A_x) = \mathcal{O}(\gamma^2, \hat{\omega}^2) \tag{2.1.76}$$

Here it suffices to apply Frobenius methods, since after only a couple of orders in $(1-u)$, we obtain stable results. We expand the functions A_x at the horizon

$$A_x = (1-u)^{-\frac{i\hat{\omega}}{2}} \sum_{i=1}^{K} (a_i(1-u)^i + \gamma b_i(1-u)^i), \tag{2.1.77}$$

with K sufficiently large[25]. Inserting this ansatz into (2.1.76) and solving the resulting equations order by order in $(1-u)$ as well as order by order in γ and only up to order $\mathcal{O}(\hat{\omega})$ gives us a low energy approximation of the solution of A_x near the horizon. We continue this computation until we have reached a K for which the numerical results for the conductivity and its γ correction stabilize. We checked our findings by calculating A_x from (2.1.55) and (2.1.56) with the help of spectral methods and took the low energy limit of (2.1.74). For the spectral density in the low energy regime and lightlike momenta we find

$$\chi_\perp^{\omega=q} = \frac{N^2T^2}{2}\Big((1+125\gamma)\hat{q} + \mathcal{O}(\hat{q}^2)\Big) + \mathcal{O}(\gamma^2). \tag{2.1.78}$$

This means that the conductivity σ gets a γ-correction factor of $(1+125\gamma)$. This is identical to the finite coupling correction factor for the photoemission rate at $1 \gg \omega$, which coincides with the expectations of [23] for the low frequency limit, which predicted a growing behaviour for decreasing 't Hooft coupling in this regime.

Let us now turn to the large ω calculation. This is interesting, since originally the authors of [23] expected the high frequency photoemission rate to decrease with decreasing λ. However, the authors in [10–12] found a correction factor of $(1+5\gamma)$, which would indicate the contrary behaviour. Thus we want to see if this behaviour still holds, when using the correct EoM. We choose to determine the functions Φ^0, Φ^1, Φ^2 as an approximation in cardinal functions and compute the large ω limit numerically in the zero-virtuality case $\omega = q$. By using sufficiently large Gauss-Lobatto grids we find the following large-q behaviour

$$\chi_\perp^{\omega=q,q\gg1} = \frac{N^2T^2}{4}\frac{3^{5/6}\Gamma(\frac{2}{3})}{\Gamma(\frac{1}{3})}\Big((1-80.39\gamma)\hat{q}^{2/3} + \dots\Big) + \mathcal{O}(\gamma^2), \tag{2.1.79}$$

[25] For this specific problem the choice $K \approx 20$ delivered stable results, in the sense that including higher orders $K > 20$ only changed the final result negligibly.

where dots stand for terms of order $\hat{q}^\alpha$ with $\alpha < \frac{2}{3}$. In the same way as before we can read off the correction factor to the photoemission rate from this result.

We now want to compare our small and large ω limits with the analogous ones for the spectral density in the spin-2 channel. A quite similar calculation there (as obtained in [52]) gives for $1 \gg \omega$ a correction factor $(1 + 135\gamma)$ to the transport coefficient in this channel, the shear viscosity, which is thus given by

$$\frac{\eta}{s} = \frac{1}{4\pi}\left(1 + 120\gamma + \mathcal{O}(\gamma^{4/3})\right) \tag{2.1.80}$$

in units of the entropy density. In the limit $\lambda \to \infty$ this gives the famous result $\eta/s = 1/4\pi$ [71].

We performed a numerical large ω analysis of the spectral density[26] in the lightlike case also in this channel and obtained a correction factor of $(1 - \frac{290}{3}\gamma)$ there. To sum up we find a quite similar behaviour of the γ-corrected spectral density and photoemission rates in the spin 1 and spin 2 channel, whose sign of the correction factors coincide in both limits with the intuitive expectations, respectively the expectations of [23].

2.1.3.3 Finite coupling corrections to the off-equilibrium spectral density

Let us conclude this series of sections in which we analyze and make use of our differential equations (2.1.55, 2.1.56) and finally turn to determining the γ-corrected on-shell photoemission spectrum in the off-equilibrium case. For this purpose we consider the simplified setting of a collapsing shell of null dust in the coupling corrected geometry that slowly falls towards its Schwarzschild radius. It is assumed that the shell is collapsing so slowly that its radial motion can be neglected. This holographic model describes a QGP that is off-equilibrium, as long as the shell hasn't fallen all the way in. Let us start with the $\gamma = 0$ case. The motivation for the form of the metric we use is given by Birkhoff's theorem, stating that outside of the shell the solution for the Einstein equations is the AdS-Schwarzschild metric, whereas inside of the shell we have a pure AdS-space. In order $\mathcal{O}(\gamma^0)$ this implies

$$ds^2 = \frac{r_h^2}{u^2}\left(f(u)dt^2 + dx^2 + dy^2 + dz^2\right) + \frac{1}{4u^2 f(u)}du^2 \tag{2.1.81}$$

with

$$f(u) = \begin{cases} f_-(u) = 1 & \text{if } u > u_s \\ f_+(u) = 1 - u^2 & \text{if } u_s > u. \end{cases} \tag{2.1.82}$$

[26] We only considered the part of the spectral function that arises from the xy-xy-component of the stress energy correlator, similar to the calculation above (2.1.74), where we restricted our analysis to the transverse components.

and $u_s = \frac{r_h^2}{r_s^2}$, where r_s is the radial position of the shell. Requiring that the metric, solutions for fluctuations etc. are continuous at the position of the shell will give us junction or matching conditions[27]. In order $\mathcal{O}(\gamma)$ the metric outside of the shell will be (1.5.16). From this we can immediately read off the matching condition for the frequency

$$\hat{\omega}_+ = \hat{\omega}_- \sqrt{U(u_s)u_s}, \tag{2.1.83}$$

by comparing the prefactors of dt^2 in the line elements inside and outside of the shell. From now on subindices $_+$ denote quantities outside of the shell and subindices $_-$ inside of the shell. Analogously to the temporal component of the line element continuity at the shell also implies that $dx_+ = dx_-$ and the same for y and z. The calculation we perform in the following is identical to the one, where we require the continuity of the gauge invariant combination ωA_x. Instead of A_x we could have analogously worked with $E = \omega A_x$. In fact one can think of A[28] in the following also as $A = \omega A_x$ and every equation in this section still works. Since we have $t_- = \sqrt{U(u_s)u_s}t_+$ and since we require A to be continuous at the shell position, we obtain

$$A_+(u,z,t)\big|_{u=u_s} = A_-(u,z,t\sqrt{U(u_s)u_s})\big|_{u=u_s}, \tag{2.1.84}$$

thus using equation (2.1.84)

$$\begin{aligned}\bar{A}_+(u,q,\omega_+)\big|_{u=u_s} &= \int dt e^{-i\omega_+ t}\tilde{A}_+(u,q,t)\big|_{u=u_s} = \int \frac{dt}{\sqrt{U(u_s)u_s}} e^{-i\omega_- t}\tilde{A}_-(u,q,t)\big|_{u=u_s} \\ &= \frac{\bar{A}_-(u,q,\omega_-)}{\sqrt{U(u_s)u_s}}\bigg|_{u=u_s},\end{aligned} \tag{2.1.85}$$

where functions with tilde $\tilde{A}_\pm$ and the barred function $\bar{A}_\pm$ stand for the Fourier transformed ones in the former case both in (z,t) and in the latter case only in z. In the following we will write simply A for $\bar{A}$ and $\tilde{A}$ and indicate to which functional space A belongs by the variables it depends on.

For derivatives in t-direction things are similarly easy. Again using relation (2.1.84) gives us

$$\partial_{t_-} A_-(u_s,z,t_-) = \frac{1}{\sqrt{U(u_s)u_s}}\partial_{t_+} A_-(u_s,z,t_+\sqrt{U(u_s)u_s}) = \frac{1}{\sqrt{U(u_s)u_s}}\partial_{t_+} A_+(u_s,z,t_+). \tag{2.1.86}$$

[27] In general the *Israel junction condition* [80] require that the metric induced on the shell from inside and outside is the same and that the difference of extrinsic curvatures inside and outside the shell is proportional to the energy momentum content of the shell.

[28] Which is the notation for the transverse gauge fields we use in the following.

For derivatives in u-direction the junction condition turns out to be slightly more difficult to derive[29]. Inside of the shell the EoM for A_- is given by

$$\partial_u^2 A_-(u,\hat{q},\hat{\omega}) + \left(1+\frac{265}{8}\gamma\right)\frac{\hat{\omega}^2-\hat{q}^2}{u}A_-(u,\hat{q},\hat{\omega}) = 0, \tag{2.1.87}$$

where the γ-correction merely arises due to the modified relation between r_h and T. Outside of the shell the $\mathcal{O}(\gamma^0)$ part of A is a solution to (2.1.9), the $\mathcal{O}(\gamma^1)$ part is a solution to (2.1.55), (2.1.56) together with the coupling corrected solution for the $xy_2y_4y_5$-component of the four form C_4. From the continuity requirement of $C(u,q,\omega)$, or the $xy_2y_4y_5$-component of C_4, we can derive a relation for $(C_4)_{xy_2y_4y_5}$ analogous to (2.1.85). Inside of the shell we have

$$((C_4)_{xy_2y_4y_5})_- = \cos(y_1)^4\sin(2y_2)\frac{A_-}{\sqrt{3}}, \tag{2.1.88}$$

such that at $u=u_s$

$$((C_4)_{xy_2y_4y_5})_+ = \cos(y_1)^4\sin(2y_2)\frac{A_+}{\sqrt{3}}\bigg|_{u=u_s}, \tag{2.1.89}$$

which means

$$C(u,q,\omega_+)_+|_{u=u_s} = C(u,q,\omega_-)_-|_{u=u_s} = 0 \tag{2.1.90}$$

and thus, the contributions of C_4 to (2.1.55) vanish on the surface of the shell. Therefore, at $u=u_s$ we can write the EoM for A_+ as

$$0 = \partial_u^2 A_+(u,\hat{q},\hat{\omega}_+)\big|_{u_s} + f_+^1(u_s,\hat{q},\hat{\omega}_+,\gamma)\partial_u A_+(u,\hat{q},\hat{\omega}_+)\big|_{u_s} + f_+^2(u_s,\hat{q},\hat{\omega}_+,\gamma)A_+(u,q,\hat{\omega}_+)\big|_{u_s}, \tag{2.1.91}$$

whereas for A_- we simply have according to equation (2.1.87)

$$\partial_u^2 A_-(u,\hat{q},\hat{\omega}_-)\big|_{u_s} + f_-(u_s,\hat{q},\hat{\omega}_-,\gamma)A_-(u,\hat{q},\hat{\omega}_-)\big|_{u_s} = 0, \tag{2.1.92}$$

with f_+^1, f_+^2 and f_- chosen appropriately. Using (2.1.86) gives

$$f_-(u_s,\hat{q},\hat{\omega}_-,\gamma)A_-(u,\hat{q},\hat{\omega}_-)\big|_{u_s} \to \left(1+\frac{265}{8}\gamma\right)\frac{\hat{\omega}_+^2-\hat{q}^2 f_m^2}{u f_m^2}A_+(u,\hat{q},\hat{\omega}_+)\big|_{u_s}, \tag{2.1.93}$$

[29] The equation (3.24) of [53] is not complete, which can be seen from a simple test: The quantity $\frac{c_{\text{out}}}{c_{\text{in}}}$, introduced in (2.1.103) has to vanish for $u_s \to 0$, since outgoing modes are forbidden, when the shell has reached its Schwarzschild horizon. With (3.24) of [53] this is not fulfilled. In this section we will rigorously derive the correct junction condition and test that the aforementioned property is fulfilled in our case. Regarding the final results in this section, there are however no qualitative differences to the off-equilibrium spectral density found in [53].

with $f_m = \sqrt{U(u_s)u_s}$. We now perform a coordinate transformation such that the EoM inside and outside of the shell are of the same shape. For this purpose we choose $\tilde{u}(u)$ such that

$$\frac{d^2\tilde{u}}{du^2} + \frac{d\tilde{u}}{du} f_+^1(\hat{\omega}_-, u, \gamma, q) = 0, \tag{2.1.94}$$

outside of the shell and $\tilde{u} = u$ inside of it. The EoM in this new coordinate reads outside of the shell

$$0 = \partial_{\tilde{u}}^2 A_+(u(\tilde{u}), q, \hat{\omega}_+, \gamma) + \tilde{f}_+(u(\tilde{u}), \hat{q}, \hat{\omega}_+, \gamma) A_+(u(\tilde{u}), q, \hat{\omega}_+, \gamma), \tag{2.1.95}$$

with

$$\tilde{f}_+(u(\tilde{u}), \hat{q}, \hat{\omega}_+, \gamma) := \Big(\frac{du}{d\tilde{u}}\Big)^2 f_+^2(u(\tilde{u}), \hat{q}, \hat{\omega}_+, \gamma). \tag{2.1.96}$$

We can read off the junction condition for $\partial_u A_\pm$, by considering

$$\partial_{\tilde{u}} A_- - \partial_{\tilde{u}} A_+ = \lim_{\epsilon \to 0} \int_{u_s - \epsilon}^{u_s + \epsilon} \partial_{\tilde{u}}^2 A. \tag{2.1.97}$$

The right hand side of this equation vanishes if we choose

$$\Big(\frac{d\tilde{u}}{du}\Big)\Big|_{u=u_s} = \sqrt{(u_s f_m^2)\frac{f_+^2(u_s, \hat{q}, \hat{\omega}_+, \gamma)}{\hat{\omega}_+^2 - \hat{q}^2 f_m^2}}\Big(1 - \frac{265}{16}\gamma\Big). \tag{2.1.98}$$

By an analogous computation as in (2.1.85) we obtain

$$\partial_u A_-(u, \hat{q}, \hat{\omega}_-)\Big|_{u_s} = f_m \sqrt{(u_s f_m^2)\frac{f_+^2(u_s, \hat{q}, \hat{\omega}_+, \gamma)}{\hat{\omega}_+^2 - \hat{q}^2 f_m^2}}\Big(1 - \frac{265}{16}\gamma\Big)\partial_u A_+(u, \hat{q}, \hat{\omega}_+)\Big|_{u_s}. \tag{2.1.99}$$

In the lightlike case $\omega = q$ this explicitly means

$$\begin{aligned}\sqrt{U(u_s)u_s}\Big(\sqrt{1-u_s^2} - \frac{1}{96}(u_s^2\sqrt{1-u_s^2}(53692 - 136807u_s^2 + 75735u_s^4 + 9216u_s\hat{w}^2 \\ - 9216u_s^3\hat{w}^2))\gamma\Big)\partial_u A_+(u, \hat{\omega}_+)\Big|_{u_s} = f_m^\gamma f_m \partial_u A_+(u, \hat{\omega}_+)\Big|_{u_s} = \partial_u A_-(u, \hat{\omega}_-)\Big|_{u_s},\end{aligned} \tag{2.1.100}$$

where we defined f_m^γ as

$$f_m^\gamma = \sqrt{1-u_s^2}\Big(1 - \frac{1}{96}(u_s^2(53692 - 136807u_s^2 + 75735u_s^4 + 9216u_s\hat{w}^2 - 9216u_s^3\hat{w}^2))\gamma\Big). \tag{2.1.101}$$

Outside of the shell we have both ingoing and outgoing wave solutions, since the geometry there has no singularities, so that we write

$$A_+(u, q = \omega) = c_{\text{in}} A_{\text{in}}(u, q = \omega) + c_{\text{out}} A_{\text{out}}(u, q = \omega), \tag{2.1.102}$$

whereas inside of the shell we only have ingoing modes. From the matching conditions deduced above one obtains the following relation

$$\frac{c_{\text{out}}}{c_{\text{in}}} = -\frac{f_m^\gamma A_- \partial_u A_{\text{in}} - A_{\text{in}} \partial_u A_-}{f_m^\gamma A_- \partial_u A_{\text{out}} - A_{\text{out}} \partial_u A_-}\bigg|_{u_s}. \tag{2.1.103}$$

At this point we can perform a non trivial check of our calculation. As explained in the footnote (29) the ratio $\frac{c_{\text{out}}}{c_{\text{in}}}$ has to vanish for $u_s \to 1$. To verify this we solve the equation of motion for A_- inside of the shell analytically. The solution inside of the shell for general virtuality, expressed by $w_+ =: \omega$ and Bessel functions J_1, Y_1 is

$$\begin{aligned} &A_-(u, \hat{q}, \hat{\omega}) = \\ &\sqrt{u}\Big(J_1\Big(2\hat{\omega}\Big(1 + \frac{265}{16}\gamma\Big)\sqrt{c(u_s, q/\omega)u}\Big) + iY_1\Big(2\hat{\omega}\Big(1 + \frac{265}{16}\gamma\Big)\sqrt{c(u_s, q/\omega)u}\Big)\Big), \end{aligned} \tag{2.1.104}$$

with

$$c(u_s, q/\omega) = \left(\frac{1}{U(u_s)u_s} - \frac{q^2}{\omega^2}\right). \tag{2.1.105}$$

Inserting the solution above into (2.1.103) and taking the limit $u_s \to 1$ actually gives $\frac{c_{\text{out}}}{c_{\text{in}}} \to 0$ both in order $\mathcal{O}(\gamma^0)$ and $\mathcal{O}(\gamma^1)$ as expected.

Again we make use of the relation (1.4.43) between the current-current correlator and the spectral density χ. There is, however, the subtlety that not only the gravitational propagator of A gets coupling corrections, but also the relation between said propagator and the boundary correlator could be modified in the finite λ case. Carefully inspecting the action for A and power counting in u shows that this is not the case here, such that we can proceed with relation (1.4.14), were the only additional γ-correction comes from the corrected temperature squared $T^2 = T_0^2(1 - 265/8\gamma)$. The coupling corrected off-equilibrium spectral density is thus given by

$$\chi(\hat{\omega}, u_s) = \frac{N^2 T^2}{2}(1 - \frac{265}{8}\gamma)\text{Im}\left(\frac{\partial_u A_+}{A_+}\right)\bigg|_{u=0}, \tag{2.1.106}$$

with

$$\text{Im}\left(\frac{A_+'}{A_+}\right)\bigg|_{u=0} = \text{Im}\left(\frac{\frac{c_{\text{out}}}{c_{\text{in}}}\partial_u A_{\text{out}} + \partial_u A_{\text{in}}}{\frac{c_{\text{out}}}{c_{\text{in}}} A_{\text{out}} + A_{\text{in}}}\right)\bigg|_{u=0}. \tag{2.1.107}$$

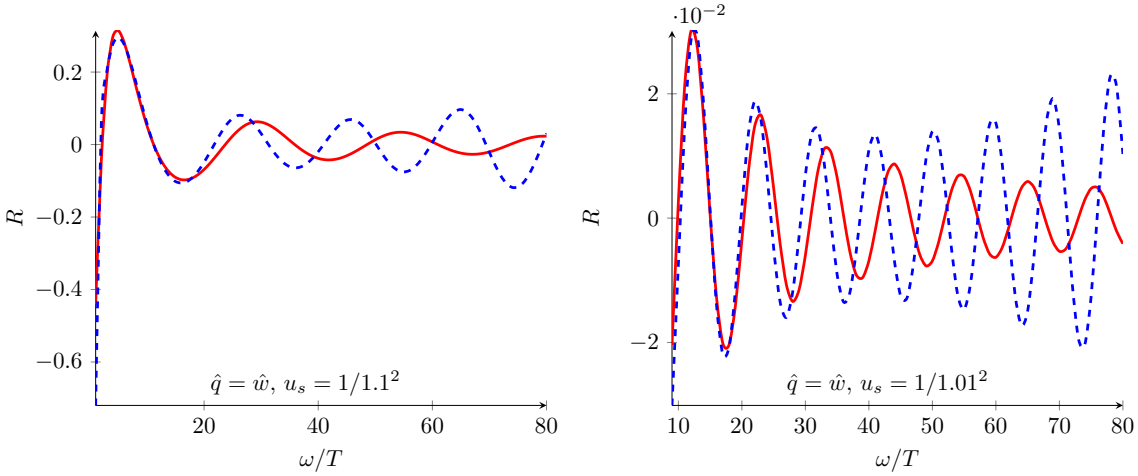

Figure 2.5: The function $R_\perp$ plotted for $r_h = 1.1$ on the left side and $r_h = 1.01$ on the right side. In both pictures the solid red line represents the $\lambda = \infty$ limit, whereas the dashed blue line shows the $\mathcal{O}(\gamma^1)$ corrected results at $\lambda = 300$.

We compare the cases $u_s = 1$ and $u_s = \frac{r_h^2}{r_s^2}$ with $r_s > r_h$ by calculating the quantity

$$R(\hat{\omega}, u_s) = \frac{\chi(\hat{\omega}, u_s) - \chi(\hat{\omega}, 1)}{\chi(\hat{\omega}, 1)}. \tag{2.1.108}$$

Figures 2.5 demonstrate that even with the new EoM for transverse gauge fluctuations including γ-corrections, the results of [53] regarding the behaviour of the off-equilibrium spectral densities didn't change significantly, after incorporating all error corrections. It is, however, questionable whether Fig. 2.5 demonstrates that top down thermalization is actually turned into a bottom up pattern in the coupling corrected case[30], as one might be drawn to speculate, considering that in the figures above the high frequency and high energy modes seem to be further away from equilibrium than those of intermediate energy. On the one hand the holographic dual of the collapsing shell model might be too far removed from the actual process of a equilibrating QGP. On the other hand it is unclear how much damage the assumption of a vanishing radial velocity of the shell actually causes to the applicability of the results. Finally, considering even higher order corrections in γ might change the picture drastically.

2.1.4 A surprising observation

In section 2.1.2 we derived the higher derivative correction to the EoM of gauge fields A_x. Everything followed strictly from the γ-corrected type IIb action. Now we will try a different approach, which is calculationally much easier but not mathematically

[30] As speculated in [53].

well justified without further insight [31]. Surprisingly, however, it gives identical results regarding the $\mathcal{O}(\gamma)$-corrections to the conductivity, the QNM, the photoemission rate, etc. It should be noted that the γ-correction to the off-equilibrium spectral density, see figure 2.5, differ from the actual results obtained in the previous section. This suggests that this prescription might only be valid for in-equilibrium quantities, which can be computed from the gravitational propagator (2.1.59). The motivation for the conjecture that the procedure we are going to present is equivalent to the strict calculation was to find an effective action, only for the metric, that does not require one to compute higher derivative corrections to the Ramond-Ramond five form directly.

The prescription how to obtain an effective action only for the geometry in order $\mathcal{O}(\alpha'^0)$ was given in the introduction (1.5.6) and the proof followed in the discussion below (1.5.7)-(1.5.10). However, there are good reasons to assume that this recipe is simply wrong in order $\mathcal{O}(\gamma^1)$: First of all the five form F_5 looses its self duality in order $\mathcal{O}(\gamma^1)$. The "doubling" of the contribution of the magnetic part in the action comes from exactly there. Second and even worse, we now have further highly non-trivial terms γW containing $(1+*)F_5$ and derivatives thereof. Therefore, it is not only highly doubtful whether the prescription regarding the five form, which we are used to in order $\mathcal{O}(\gamma^0)$, is still working. It is not even clear how exactly it should look like. Nonetheless, one intuitive ansatz, which we tried and worked well, is the following:

Take the solution of the magnetic part of the five form obtained in order $\mathcal{O}(\gamma^0)$ and only consider its dependence on the metric components $g^{\mu\nu}$ and A_μ. We will treat also those A_μ and their derivatives on which F_5 depends as free fields in the variation. Insert the α'-corrected background metric given in (1.5.16). Choose the $L(u)$-prefactor of the electric part of the five form in such a way that

$$dF_5^{mag} = d * F_5^{el} = \mathcal{O}(\gamma^2). \tag{2.1.109}$$

Explicitly this means

$$\begin{aligned}(F_5^{mag})^0 &= 4\sqrt{\det(g_{S_5})}dy_1 \wedge dy_2 \wedge dy_3 \wedge dy_4 \wedge dy_5 + \frac{4}{L(u)^5}\sqrt{|\det(g_{10})|}\sqrt{|\det(g_5)|} \\ &\Big(g_{10}^{tt}g_{10}^{uu}g_{10}^{yy}g_{10}^{xy_3}g_{10}^{zz}dy_1 \wedge dy_2 \wedge dx \wedge dy_4 \wedge dy_5 + g_{10}^{tt}g_{10}^{uu}g_{10}^{yy}g_{10}^{xy_4}g_{10}^{zz}dy_1 \wedge dy_2 \\ &\wedge dy_3 \wedge dx \wedge dy_5 + g_{10}^{tt}g_{10}^{uu}g_{10}^{yy}g_{10}^{xy_5}g_{10}^{zz}dy_1 \wedge dy_2 \wedge dy_3 \wedge dy_4 \wedge dx\Big).\end{aligned} \tag{2.1.110}$$

[31] We will give a proof of the validity of this procedure for a special case of a constant magnetic background field in the following chapter 2.2.2.

$$\frac{(F_5^{mag})^1_{ux}}{L(u)^4} = -\sqrt{\det(g_{S_5})}(\sin(y_1)\cos(y_1)g_{10}^{y_1y_1}g_{10}^{y_3y_3}du\wedge dx\wedge dy_2\wedge dy_5\wedge dy_4+$$
$$\cos(y_1)^2\sin(y_2)\cos(y_2)g_{10}^{y_2y_2}g_{10}^{y_4y_4}du\wedge dx\wedge dy_1\wedge dy_5\wedge dy_3-\sin(y_1)\times$$
$$\cos(y_1)\sin(y_2)^2g_{10}^{y_1y_1}g_{10}^{y_4y_4}du\wedge dx\wedge dy_2\wedge dy_3\wedge dy_5-\cos(y_1)\sin(y_1)\times$$
$$\cos(y_2)^2g_{10}^{y_1y_1}g_{10}^{y_5y_5}du\wedge dx\wedge dy_2\wedge dy_4\wedge dy_3-\cos(y_2)\sin(y_2)\cos(y_1)^2\times$$
$$g_{10}^{y_2y_2}g_{10}^{y_5y_5}du\wedge dx\wedge dy_1\wedge dy_3\wedge dy_4)(2\partial_u A_x(u,t,z))+\mathcal{O}(A_x(u,t,z)^2), \tag{2.1.111}$$

$$\frac{(F_5^{mag})^1_{tx}}{L(u)^4} = -\sqrt{\det(g_{S_5})}(\sin(y_1)\cos(y_1)g_{10}^{y_1y_1}g_{10}^{y_3y_3}dt\wedge dx\wedge dy_2\wedge dy_5\wedge dy_4+$$
$$\cos(y_1)^2\sin(y_2)\cos(y_2)g_{10}^{y_2y_2}g_{10}^{y_4y_4}dt\wedge dx\wedge dy_1\wedge dy_5\wedge dy_3-\sin(y_1)\times$$
$$\cos(y_1)\sin(y_2)^2g_{10}^{y_1y_1}g_{10}^{y_4y_4}dt\wedge dx\wedge dy_2\wedge dy_3\wedge dy_5-\cos(y_1)\sin(y_1)\times$$
$$\cos(y_2)^2g_{10}^{y_1y_1}g_{10}^{y_5y_5}dt\wedge dx\wedge dy_2\wedge dy_4\wedge dy_3-\cos(y_2)\sin(y_2)\cos(y_1)^2\times$$
$$g_{10}^{y_2y_2}g_{10}^{y_5y_5}dt\wedge dx\wedge dy_1\wedge dy_3\wedge dy_4)(2\partial_t A_x(u,t,z))+\mathcal{O}(A_x(u,t,z)^2), \tag{2.1.112}$$

$$\frac{(F_5^{mag})^1_{zx}}{L(u)^4} = -\sqrt{\det(g_{S_5})}(\sin(y_1)\cos(y_1)g_{10}^{y_1y_1}g_{10}^{y_3y_3}dz\wedge dx\wedge dy_2\wedge dy_5\wedge dy_4+$$
$$\cos(y_1)^2\sin(y_2)\cos(y_2)g_{10}^{y_2y_2}g_{10}^{y_4y_4}dz\wedge dx\wedge dy_1\wedge dy_5\wedge dy_3-\sin(y_1)\times$$
$$\cos(y_1)\sin(y_2)^2g_{10}^{y_1y_1}g_{10}^{y_4y_4}dz\wedge dx\wedge dy_2\wedge dy_3\wedge dy_5-\cos(y_1)\sin(y_1)\times$$
$$\cos(y_2)^2g_{10}^{y_1y_1}g_{10}^{y_5y_5}dz\wedge dx\wedge dy_2\wedge dy_4\wedge dy_3-\cos(y_2)\sin(y_2)\cos(y_1)^2\times$$
$$g_{10}^{y_2y_2}g_{10}^{y_5y_5}dz\wedge dx\wedge dy_1\wedge dy_3\wedge dy_4)(2\partial_z A_x(u,t,z))+\mathcal{O}(A_x(u,t,z)^2), \tag{2.1.113}$$

and

$$F^{mag} = (F_5^{mag})^0 + (F_5^{mag})^1_{tx} + (F_5^{mag})^1_{tx} + (F_5^{mag})^1_{ux}. \tag{2.1.114}$$

Here g_{S_5} denotes the metric of the five sphere, g_{10} the γ-corrected metric of the entire manifold (2.1.10) and g_5 the γ-corrected metric of the internal AdS space. Now replace the F_5^2-term in the action with two times $(F^{mag})^2$ and insert the $\mathcal{O}(\gamma^0)$-solution of F_5 into the higher derivative term γW of the type IIB SUGRA action. The result will be the new action for A_μ. Considering the prescription above we get together with

$$\frac{1}{2\times 5!}(F_5^{mag})^2 = \frac{8}{L(u)^{10}} + \frac{2}{3L(u)^6}F_{\mu\nu}F^{\mu\nu} \tag{2.1.115}$$

the following result for the part of the action depending on A_μ, which doesn't contain higher derivative terms

$$-\frac{1}{2\kappa_{10}}\int d^{10}x\sqrt{-g}\Big(\frac{L(u)^2}{3}+\frac{2}{3L(u)^6}\Big)F_{\mu\nu}F^{\mu\nu}. \tag{2.1.116}$$

The term $\frac{L(u)^2}{3}$ comes from the curvature scalar R_{10}. Again we only considered transverse fields A_x, respectively its Fourier transform $(A_x)_k$, with $k=(\omega,q)$. The result for the γW-part of the action given up to order $\mathcal{O}(A_x^2)$ is

$$\begin{aligned}\frac{\gamma}{8r_h^2}\int d^{10}x\sqrt{\det g_{10}}W &= \gamma\mathrm{vol}(S_5)\int\frac{d^4k}{(2\pi)^4}\Big(A_W(A_x)_k''(A_x)_{-k}+B_W(A_x)_k'(A_x)_{-k}'\\ &+C_W(A_x)_k'(A_x)_{-k}+D_W(A_x)_k(A_x)_{-k}+E_W(A_x)_k''(A_x)_{-k}''+F_W(A_x)_k''(A_x)_{-k}'\Big)\\ &+\mathcal{O}(\gamma^2)=:\gamma\mathrm{vol}(S_5)\int\frac{d^4k}{(2\pi)^4}\mathcal{L}^1_\gamma,\end{aligned} \tag{2.1.117}$$

where the primes $'$ stand for ∂_u and the functions $A_W, B_W, C_W, D_W, E_W, F_W$ are given by

$$A_W = \frac{4u^5}{9}\Big(41\hat{q}^2(1-u^2)-172\hat{\omega}^2\Big) \tag{2.1.118}$$

$$B_W = -\frac{2u^5}{9}\Big(-803u+1563u^3-216\hat{q}^2(1-u^2)-72\hat{\omega}^2\Big) \tag{2.1.119}$$

$$C_W = \frac{4u^4}{9(1-u^2)}\Big(\hat{q}^2(167-416u^2+249u^4)-59\hat{\omega}^2+511u^2\hat{\omega}^2\Big) \tag{2.1.120}$$

$$\begin{aligned}D_W =& \frac{2u^3}{9(1-u^2)^2}\Big(-90\hat{q}^4u(1-u^2)^2-\hat{\omega}^2(270-441u^2+99u^4+208u\hat{\omega}^2)+\hat{q}^2\\ &(1-u^2)(162-315u^2+153u^4-134u\hat{\omega}^2)\Big)\end{aligned} \tag{2.1.121}$$

$$E_W = -\frac{416}{9}u^6(1-u^2)^2 \tag{2.1.122}$$

$$F_W = -\frac{20u^5}{9}\Big(37-150u^2+113u^4\Big). \tag{2.1.123}$$

We already used the definitions $\hat{\omega}=\frac{\omega}{2\pi T}=\frac{\omega}{2r_h}+\mathcal{O}(\gamma)$ and $\hat{q}=\frac{q}{2\pi T}=\frac{q}{2r_h}+\mathcal{O}(\gamma)$ here. Together with (2.1.116) equations (2.1.118)-(2.1.123) explicitly give the $\mathcal{O}(\gamma)$-

Lagrangian for $(A_x)_k$ up to second order in $(A_x)_k$.

$$\begin{aligned}\mathcal{L} =&\frac{1}{2}\Big((A_x)_k(A_x)_{-k}\Big(\frac{\tilde{q}^2(1-u^2)-\tilde{\omega}^2}{u(1-u^2)}+\gamma\frac{5u}{8(1-u^2)}\Big(-10\tilde{q}^2u^2-197\tilde{q}^2u^4+207\tilde{q}^2u^6\\&-130\tilde{\omega}^2-120u^2\tilde{\omega}^2+274u^4\tilde{\omega}^2\Big)\Big)+(A_x)'_k(A_x)'_{-k}(1-u^2)\Big(1+\gamma\frac{5}{16}\Big(-260u^2-\\&235u^4+553u^6\Big)\Big)\Big)+\mathcal{L}^1_\gamma,\end{aligned}\tag{2.1.124}$$

with $\tilde{\omega}=\frac{\omega}{2r_h}$ and $\tilde{q}=\frac{q}{2r_h}$.

In the next step we derive the γ-corrected EoM for our gauge field $(A_x)_k$ by varying the action with respect to $(A_x)_k$. We do not want to focus on boundary terms here but merely on the resulting EoM for $(A_x)_k$. This simple exercise gives

$$2\left(u^2-1\right)(A_x)''_k+4u(A_x)'_k+\frac{2(A_x)_k\left(\tilde{q}^2\left(u^2-1\right)+\tilde{w}^2\right)}{u\left(u^2-1\right)}-\gamma H((A_x)_k)=\mathcal{O}(\gamma^2)\tag{2.1.125}$$

with

$$\begin{aligned}H((A_x)_k)=&\frac{u}{72(u^2-1)^2}\Big((u^2-1)^2\Big(u(A_x)''_k(-8576\hat{q}^2u^5+128u^3(67\hat{q}^2+208\hat{\omega}^2)\\&+1398243u^6-1740092u^4+459685u^2-11700)+4(A_x)'_k(-15008\hat{q}^2u^5\\&+160u^3(67\hat{q}^2+208\hat{\omega}^2)+401046u^6-373722u^4+60325u^2-5850)+\\&13312(u^2-1)u^4(u(u^2-1)(A_x)''''_k+4(5u^2-3)(A_x)'''_k)\Big)+2(A_x)_k(2880\\&\hat{q}^4u^3(u^2-1)^2+\hat{q}^2u^2(u^2-1)(21507u^4-31105u^2-4288uw^2+9598)+\\&2\hat{\omega}^2(30085u^6-75057u^4+3328u^3\hat{\omega}^2+55359u^2+2925))\Big).\end{aligned}\tag{2.1.126}$$

Exploiting that we have

$$(A_x)''_k+\frac{2u(A_x)'_k}{(u^2-1)}+\frac{(A_x)_k\left(\hat{q}^2\left(u^2-1\right)+\hat{w}^2\right)}{u\left(u^2-1\right)^2}=\mathcal{O}(\gamma)\tag{2.1.127}$$

reduces (2.1.126) to

$$\begin{aligned}\gamma H((A_x)_k)=&\frac{u\gamma}{72(1-u^2)}\Big((A_x)_k(-27648\hat{q}^4u^3(u^2-1)+\hat{q}^2(370501u^6-666170u^4+\\&307369u^2-11700)+9\hat{\omega}^2(5951u^4-9081u^2+2600))-10(u^2-1)^2\\&(-17600\hat{q}^2u^3+8493u^4-19450u^2+2340)(A_x)'_k\Big)+\mathcal{O}(\gamma^2).\end{aligned}\tag{2.1.128}$$

To simplify this further we define

$$\Sigma(u) = \frac{5\gamma\left(-7040q^2u^5 + 2831u^6 - 9725u^4 + 2340u^2\right)}{288\sqrt{1-u^2}} + \frac{1}{\sqrt{1-u^2}}, \tag{2.1.129}$$

so that with

$$\Psi = (A_x)_k/\Sigma(u) \tag{2.1.130}$$

we end up with the following EoM

$$\begin{aligned} 0 =& \Psi'' + \Psi\Bigg(\frac{u - \hat{q}^2(1-u^2) + \hat{\omega}^2}{u(1-u^2)^2} - \frac{\gamma}{144u(1-u^2)}\Bigg(- 27648\hat{q}^4u^5 + \hat{q}^2(-157499u^6 + \\ & 56331u^4 + 11700u^2 + 4770) + 297255u^7 - 698575u^5 + 53559u^4\hat{\omega}^2 + 326850u^3 \\ & - 28170u^2\hat{\omega}^2 - 11700u - 4770\hat{\omega}^2\Bigg)\Bigg), \end{aligned} \tag{2.1.131}$$

where we already used the γ corrected relation between the temperature and r_h

$$r_h = \pi T\Big(1 - \frac{265}{16}\gamma\Big). \tag{2.1.132}$$

From this differential equation one obtains identical γ-corrections for the conductivity, the photoemission rate and the QNM spectrum for all values of $\hat{q}$ considered. We want to highlight that this is quite likely not a coincidence. On the one hand this coupling corrected differential equation (2.1.131) should be taken with a grain of salt, since unlike (2.1.55) and (2.1.56) it doesn't follow mathematically, but by intuitively extending a calculational prescription into a regime, where it is not fully understood, why it should hold. On the other hand, since especially the coupling corrections to the QNM are identical in both our calculations, one could argue that it isn't a surprise that other quantities coincide with what we found previously. This is because the QNM govern huge parts of the behaviour of our system, especially when it is approaching thermal equilibrium.

2.1.5 Concluding Remarks

In this chapter we derived the finite coupling corrected EoM for gauge fields in AdS/CFT. It turned out that the finite λ corrections to several observables including QNM spectra, the conductivity, the photoemission rate and spectral functions in various settings are of the same order of magnitude as the analogous ones found in the spin 2 channel, which include shear QNMs and the shear viscosity (see table 2.1). The signs of the higher derivative correction terms to the photoemission rate in the limit of small and the limit of large frequency we found to fit to the expectations from weak coupling [23]. In addition we gave an alternative derivation of the coupling corrections to the aforementioned quantities presented in section 2.1.4. Interestingly we also found that

Quantity	$\mathcal{O}(\gamma^0)$	$\mathcal{O}(\gamma^1)$	Reference
$s\,(\frac{1}{2}\pi^2 N_c^2\,T^3)^{-1}$	1	$15\,\gamma$	[54]
$\eta\,(\frac{1}{8}\pi N_c^2\,T^3)^{-1}$	1	$135\,\gamma$	[52]
$4\pi\,\eta/s$	1	$120\,\gamma$	[52]
$\sigma\,(\frac{1}{4}\alpha_{\rm EM} N^2\,T)^{-1}$	1	$125\,\gamma$	This work
$\omega_2^{\rm shear}(q=0)\,(2\pi T)^{-1}$	$2.585 - 2.382\,i$	$(1.029 + 0.957\,i)\,10^4\,\gamma$	[17]
$\omega_2^{\rm EM}(q=0)\,(2\pi T)^{-1}$	$2 - 2\,i$	$(4.896 + 0.495\,i)\,10^3\,\gamma$	This work

Table 2.1: A collection of results for the zeroth and first order terms in the expansion of various thermal observables in powers of $\gamma = \frac{1}{8}\,\zeta(3)\lambda^{-3/2}$. Results are shown for the entropy density s, shear viscosity η, viscosity to entropy density ratio η/s, electrical conductivity σ and the second quasinormal mode frequencies, $\omega_2^{\rm EM}$ and $\omega_2^{\rm shear}$, at zero wave vector, for the electromagnetic current and shear channel of the stress-energy correlator, respectively.

the term in the EoM for coupling corrected gauge fields (2.1.55) governing the high energy behaviour (so the term proportional to $\hat{q}^4$), whose existence is crucial for the right behaviour of the photoemission rate in this limit is precisely the same as in the spin-2 channel, if we normalize the EoM there in an analogous way.

2.2 Higher derivative corrected magnetic black branes

In this chapter we are going to present a way to tackle the challenging task of computing higher derivative corrections to the magnetic black brane geometry and to tensor QNMs in a coupling corrected magnetic black brane background. The difficulty of this calculation is twofold: On the one hand there exists only a numerical solution to the $\mathcal{O}(\alpha'^0)$ metric for an AdS-black hole geometry with back reaction of a strong magnetic field. On the other hand the higher derivative correction terms (5.1.2) will now all contribute to the EoMs of the metric, the five form and fluctuations around the equilibrium solution, which we are going to consider afterwards. To our best knowledge, this is the first calculation, in which coupling corrections to a metric with back reaction of an additional field were determined.

Within a formalism that helps to describe QGPs far from equilibrium a natural aspect that can be analyzed is how and how fast such a system equilibrates. At late times this question breaks down to the analysis of QNM (see 1.4.2), fluctuations around the equilibrium state.

The aim of this calculation is to study how finite 't Hooft coupling corrections affect

the equilibration behaviour of a quark gluon plasma in a strong magnetic background field, as produced for a very short time during heavy ion collision. We achieve this by searching for QNM frequencies at finite 't Hooft coupling. The propagator of the modes h_{xy}, we are interested in, is dual to the two-point function of the xy component of the boundary stress energy tensor. The numerical analysis gave a well converging result for the lowest α'-corrected QNM frequency, which is the most interesting regarding the equilibration of a QGP in a strong background field.

On the other hand this analysis also has a more abstract application: So far, we don't have a satisfying dual theory, that describes QCD. The most prominent AdS/CFT duality allows us to non-perturbatively compute quantities in a conformal field theory, with $N \to \infty$ and $\lambda = g_{\mathrm{YM}}^2 N \to \infty$. Whereas QCD has a finite coupling, a finite $N = 3$ and is not conformally invariant. The calculation presented in this section is, as far as we know, the first of its kind, which simultaneously breaks conformal invariance and the infinite coupling limit of the dual field theory.

In the limit $\lambda \to \infty$ the holographic description of a QGP in a magnetic background field was realized in [13] by considering a Einstein-Maxwell-Chern-Simons theory. That this setting describes the physical properties of the real $SU(3)$ QGP in equilibrium at least qualitatively was shown in [21]. In this work we will convince ourselves that the ansatz chosen in [13] can be derived from a specific solution to SUGRA living in 10 dimensions. This allows us to determine α'^3-corrections first to the metric of a magnetic black brane, where the magnetic background field back-reacts on the geometry, and afterwards to QNM fluctuations around this specific solution. We are going to give a mathematical proof of a prescription, which was found in [18], to handle higher derivative corrections to the five form F_5 in the presence of gauge fields for the specific case of a constant background field. The higher derivative corrections to the QNM frequencies and the metric will be computed numerically using pseudo-spectral methods.

2.2.1 Reviewing magnetic black branes in the infinite coupling limit

Let us warm up with reviewing the calculations and results of the infinite coupling case. However, we are going to present the computations in a way that makes it more intuitive to extend them to finite λ. The action in five dimensions, which is the starting point of the $\lambda = \infty$ calculations here reads

$$S = \frac{1}{2\kappa} \int d^5x \sqrt{-g_5} \left[(R_5 - 2\Lambda) - F_{\mu\nu} F^{\mu\nu} \right], \tag{2.2.1}$$

where $\kappa = \frac{1}{8\pi G_N}$ with Newton constant G_N, $\Lambda = -6$, g_5 is the determinant of the 5-dimensional metric and $F_{\mu\nu} = \partial_\mu A_\nu - \partial_\nu A_\mu$ for a gauge field A_μ. The five sphere metric components depend on the radial coordinate of the AdS-space, if we consider α' corrections. This will stay true, when we include a strong magnetic background

field with back-reaction on the geometry. Therefore it is advisable to return to the 10-dimensional type IIB SUGRA action (1.2.11), from which (2.2.1) can be derived via a Kaluza-Klein reduction by integrating out the five sphere coordinates. The metric ansatz including a constant magnetic background field with field strength tensor $F_{xy} = br_h^2 = -F_{yx}$ has the familiar form

$$ds_{10}^2 = ds_{\text{AdS}}^2 + L(u)^2 \sum_{i=1}^{3} (d\mu_i^2 + \mu_i^2 (d\phi_i + \frac{2}{\sqrt{3}} A_\mu dx^\mu)^2), \tag{2.2.2}$$

$$ds_{AdS}^2 = -r_h^2 U(u) dt^2 + \tilde{U}(u) du^2 + r_h^2 e^{2V(u)} (dx^2 + dy^2) + r_h^2 e^{2W(u)} dz^2, \tag{2.2.3}$$

with $A_y = r_h^2 xb$, $A_\mu = 0$ for other directions and $u = \frac{r_h^2}{r^2}$. The five-sphere S_5 is described by the metric (1.5.15). The functions μ_i and angles ϕ_i are given in (1.5.13, 1.5.14). We have chosen the xy-direction of the field strength tensor to be $r_h^2 b$, such that b coincides with the corresponding magnetic field strength parameter chosen in [13]. As we are already used to by now, we are going to set $r_h = 1$, which again corresponds to a rescaling of the coordinates. Reintroducing r_h in the final differential equations for e.g. tensor modes by $\frac{\omega}{2} \to \hat{\omega} = \frac{\omega}{2r_h}$ and $\frac{q}{2} \to \hat{q} = \frac{q}{2r_h}$, where ω and q are the frequency and the momentum of the mode, corresponds to a rescaling to get the original form of the metric (2.2.3), (2.2.2). The relation between b and the physical magnetic field is given by

$$B = \frac{b}{v}, \tag{2.2.4}$$

where the constant v can be computed from the near boundary metric.

The self dual solution to the EoMs for the five form components (1.5.5) is

$$(F_5^0)^{el} = -\frac{4}{L(u)^5} \epsilon_{AdS}, \qquad (F_5^1)^{el} = \frac{1}{\sqrt{3} L(u)} \sum_{i=1}^{3} d(\mu_i^2) \wedge d\phi_i \wedge \bar{*} F_2, \tag{2.2.5}$$

$$F_5 = (1 + *)((F_5^0)^{el} + (F_5^1)^{el}), \tag{2.2.6}$$

with $F_2 = dA$ and $\bar{*}$ is the Hodge dual with respect to the internal AdS space. As before we call F_5^{el} the electric part of the five form and its Hodge dual $F_5^{mag} = *F_5^{el}$ the magnetic part.[32] In the $\lambda = \infty$ case the action (2.2.1) is the result of this setup in 10 dimensions with $L(u) = 1$. The factors $L(u^5)$ and $\frac{1}{L(u)}$ in front of the first and second term in (2.2.5) were not omitted, since later on we will need an expression for

[32] Admittedly this is a misleading notation, since both the electric part and the magnetic part of the five form depend on the magnetic background field. We use this nomenclature to be consistent with the literature.

F_5 for which

$$dF^{mag} = d * F^{el} = 0 \tag{2.2.7}$$

for arbitrary $L(u)$ and (2.2.5) does the job. The Einstein equations, or equivalently the differential equations obtained by varying the action, obtained from a Kaluza-Klein reduction with ansätze (2.2.2, 2.2.5, 2.2.6), with respect to U, $\tilde{U}$, W, L and V are given in the Appendix 5.4 where we already inserted (2.2.9) after the variation. The ansatz to solve these can be written as

$$U(u) = u_0 + u_1(1-u) + u_2(1-u)^2 + \dots \tag{2.2.8}$$

$$\tilde{U}(u) = \frac{1}{4u^3 U(u)} \tag{2.2.9}$$

$$V(u) = v_0 + v_1(1-u) + v_2(1-u)^2 + \dots \tag{2.2.10}$$

$$W(u) = w_0 + w_1(1-u) + w_2(1-u)^2 + \dots \tag{2.2.11}$$

$$L(u) = l_0 + l_1(1-u) + l_2(1-u)^2 + \dots . \tag{2.2.12}$$

As said above we have for $\lambda = \infty$ that $L(u) = 1$ is a solution to the Einstein equations, at which the form of the solution below (2.2.16) already hints. Furthermore we use the freedom to set $u_0 = 0$, in order to obtain a blackening factor and set $v_0 = w_0 = 0$, which can be achieved by rescaling. The constant u_1 is linked to the temperature of the system. In practical calculations we can set $u_1 = 2$ to give a Schwarzschild black hole for $b \to 0$, which together with our metric ansatz (2.2.3) links the temperature to the horizon radius r_h. Solving this system of differential equations near the horizon gives in the lowest order[33]

$$u_2 = -\frac{-b^2 l_0^{12} - 4b^2 l_0^4 - 9 l_0^{10} u_1 + 30 l_0^8 - 24}{12 l_0^{10}} \tag{2.2.13}$$

$$v_1 = -\frac{b^2 l_0^{12} + b^2 l_0^4 - 6}{6 l_0^{10} u_1} \tag{2.2.14}$$

$$w_1 = -\frac{-b^2 l_0^4 - 6}{6 l_0^{10} u_1} \tag{2.2.15}$$

$$l_1 = -\frac{-b^2 l_0^{12} + b^2 l_0^4 - 30 l_0^8 + 30}{30 l_0^9 u_1} \tag{2.2.16}$$

The next order term in this expansion is given in the Appendix 5.5.

Setting $l_0 = 1$ gives the same expansion as in [13], with $l_i = 0$ for all $i > 0$. What we are after is a solution in order $\mathcal{O}(\gamma^0)$ with minimal error on a sufficiently large u-interval $[l, k] \subset [0, 1]$. The solution for the geometry in order $\mathcal{O}(\gamma^0)$ is obtained by an expansion around the horizon to high order after a near-boundary expansion to low

[33] for U in the second order, since the first corresponds to the (rescaled) temperature.

order. After setting $b = \frac{5}{4}$, which corresponds to a physical strong background field of $\mathcal{B} = 34.4555T^2$ in the limit $\lambda \to \infty$ [34], and introducing the more convenient functions

$$U(u) = \frac{1 + u^2 U^0(u)}{u} \tag{2.2.17}$$

$$V(u) = \frac{1}{2}\log(\frac{V^0(u)}{u}) \tag{2.2.18}$$

$$W(u) = \frac{1}{2}\log(\frac{W^0(u)}{u}) \tag{2.2.19}$$

$$L(u) = 1 \tag{2.2.20}$$

$$\tilde{U}(u) = \frac{1}{4u^3 U^0(u)} \tag{2.2.21}$$

we expand $U^0(u)$, $V^0(u)$ and $W^0(u)$ in $(1-u)$ and solve the resulting equations order by order up to order[35] 260 in $(1-u)$.

2.2.2 A helpful prescription and its mathematical proof

In this section we claim and proof the validity of the prescription found in section 2.1.4 for the special case we are considering in this section. This will facilitate our calculation noticeably. Again the aim is to end up with an effective higher derivative corrected action only for the geometry. Explicitly the theorem states:

Solve the equation of motion for F_5 in the lowest order in α' for a strong background field, such that it depends on the metric components of the ansatz[36] made in (2.2.2, 2.2.3) and choose the $L(u)$-factor of the components of the electric part of the five form in such a way that

$$dF^{mag} = d * F^{el} = 0 + \mathcal{O}(\gamma^{4/3}) = dF^{el}. \tag{2.2.22}$$

Now replace the F_5^2 term in the action with 2 times $(F^{mag})^2$ and insert F_5 as given in (2.2.5, 2.2.6), which depends on metric components (that still have to be determined) into the higher derivative part of the action. The resulting action only depends on the absolute value of the z-component of the magnetic background field b and the metric, whose solution in order $\mathcal{O}(\gamma)$ will be determined by solving the system of differential equations obtained by varying this effective action with respect to $g^{\mu\nu}$.

[34] The relation between b and $\mathcal{B}$ deduced from the trace anomaly of the stress energy tensor might get finite coupling corrections, too. Since our focus is on how QNMs behave for large magnetic background fields, without the need to prioritize a precise value for $\mathcal{B}$, we will carry out the calculation including coupling corrections also with the choice $b = \frac{5}{4}$, while stressing that this only approximately corresponds to the $\lambda \to \infty$ result $\mathcal{B} \approx 34.5T^2$.

[35] There was no dire need to compute the geometry up to this order. However, since it is relatively easy to compute it in order $\mathcal{O}(\alpha'^0)$, we included as many orders as possible, to not waste precision unnecessarily.

[36] Those are general unkown functions at this point, which we later on (after solving their EoM) allow to be of order $\mathcal{O}(\gamma)$.

We justify this statement with the following proof, where we work with the metric ansatz given in (2.2.2), (2.2.3).

Lemma 2.2.1. *In order $\mathcal{O}(x^0)$ the magnetic parts of the five form don't get any γ-corrections, except for those coming from the finite λ correction to the metric. The non-trivial higher derivative corrections to the electric parts of F_5 (i.e. the finite λ terms, which are not caused by corrections to the metric, the $\mathcal{O}(\gamma^0)$ solution of F_5 depends on), are given by the respective directions of*

$$\frac{2\gamma}{\sqrt{-g}}\left(\frac{\delta\mathcal{W}}{\delta F_5}\right). \tag{2.2.23}$$

proof. Let us first focus on the $tuzy_3$-component of C_4. In order $\mathcal{O}(x^0)$ the diagram describing the system of differential equations, derived from (2.1.11), is given by

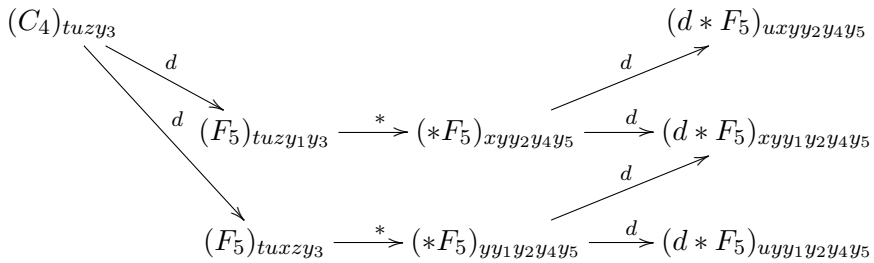

(2.2.24)

where the right hand side has to be equal to the corresponding directions of

$$d*\left(\frac{2\gamma}{\sqrt{-g}}\frac{\delta\mathcal{W}}{\delta F_5}\right). \tag{2.2.25}$$

In order $\mathcal{O}(x^0)$ there are no other contributions from C_4 to the right hand side of the diagram. From diagram (2.2.24) we can derive that up to terms, which are independent of u, the following equations hold

$$(F_5)_{tuzy_1y_3} = \frac{2\gamma}{\sqrt{-g}}\left(\frac{\delta\mathcal{W}}{\delta F_5}\right)_{tuzy_1y_3} + (\tilde{F}_5)_{tuzy_1y_3} + \mathcal{O}(x^1), \tag{2.2.26}$$

$$(F_5)_{tuxzy_3} = \frac{2\gamma}{\sqrt{-g}}\left(\frac{\delta\mathcal{W}}{\delta F_5}\right)_{tuxzy_3} + (\tilde{F}_5)_{tuxzy_3} + \mathcal{O}(x^1), \tag{2.2.27}$$

where $\tilde{F}_5$ describes the five form solution, depending on arbitrary metric components, shown in (2.2.5) and (2.2.6). Notice that we already used relation (2.2.22) (where $\tilde{F}_5$ corresponds to F_5 there) when deducing the solutions (2.2.5) and (2.2.6). The terms, which result into u-independent terms, when taking the Hodge dual and could be added to equation (2.2.26) and (2.2.27), if they don't corrupt the diagram dual to (2.1), can

be gauged away, since they have the same u, y_i-dependence as the F_5 in the lowest order in α' and thus correspond to different choices of b. Since we choose b to have no coupling corrections, these terms vanish. Very similar calculations provide analogous relations for the

$$tuzy_1y_4,\ tuzy_1y_5,\ tuzy_2y_4,\ tuzy_2y_5,\ tuxzy_3,\ tuxzy_4,\ tuxzy_5\ - \tag{2.2.28}$$

directions of the five form. Considering now equation (2.1.11) proves this lemma for those directions of the five form, which in the $\lambda = \infty$ limit are of order $\mathcal{O}(b^1)$ or higher. The analogous diagram for the $txyz$ direction of the four form C_4 is even easier and gives results analogous to (2.2.26), such that Lemma 2.2.1 follows by again applying relation (2.1.11). □

Lemma 2.2.2. *The magnetic parts of the five form components in (2.2.5, 2.2.6) with arbitrary $L(u)$, with lower indices and the electric parts of the five form components in (2.2.5, 2.2.6) with arbitrary $L(u)$, with upper indices times $\sqrt{-g}$ are independent of u.*

proof. This claim follows by carefully inspecting the magnetic part $F_5^{mag} = *F_5^{el}$ of F_5 given in (2.2.5, 2.2.6) and by using the self duality of this five form. □

comment 2.2.3. The magnetic parts of the five form components in (2.2.5, 2.2.6) with arbitrary $L(u)$, with lower indices and the electric parts of the five form components in (2.2.5, 2.2.6) with arbitrary $L(u)$, with upper indices times $\sqrt{-g}$ are actually independent of the AdS-part of the metric and independent of $L(u)$ if we choose the $L(u)$ factor of the magnetic part of the five form so that (2.2.22) holds.

Lemma 2.2.4. *For any five form, which doesn't depend on derivatives of a metric component $X \in \{g_{\mu\nu}\}_{\mu\nu\in\{1,\dots,10\}}$, we have*

$$\frac{\partial\partial_u(F_5)_{abcde}}{\partial\partial_u X} = \frac{\partial(F_5)_{abcde}}{\partial X} \tag{2.2.29}$$

for all directions abcde.

proof. Let $\{X_i\}_{i\in I}$ be equal to the set $\{g_{\mu\nu}\}_{\mu\nu\in\{1,\dots,10\}}$ and let $X_0 = X$. Then we have

$$\frac{\partial\partial_u(F_5)_{abcde}}{\partial\partial_u X} = \frac{\partial}{\partial\partial_u X}\frac{\partial(F_5)_{abcde}}{\partial X_i}\partial_u X_i = \frac{\partial}{\partial\partial_u X}\frac{\partial(F_5)_{abcde}}{\partial X_0}\partial_u X_0 = \frac{\partial(F_5)_{abcde}}{\partial X}, \tag{2.2.30}$$

where we made use of the sum convention. □

Lemma 2.2.5. *For any direction abcde of F_5 and any metric component X corresponding to the internal AdS_5-space or $L(u)$ we have that*

$$\frac{\partial \mathcal{W}}{\partial (F_5)_{abcde}} \frac{\partial (F_5)_{abcde}}{\partial X} + \frac{\partial \mathcal{W}}{\partial \partial_u (F_5)_{abcde}} \frac{\partial \partial_u (F_5)_{abcde}}{\partial X} - \frac{d}{du}\left(\frac{\partial \mathcal{W}}{\partial \partial_u (F_5)_{abcde}} \frac{\partial \partial_u (F_5)_{abcde}}{\partial \partial_u X} \right) \tag{2.2.31}$$

is equal to

$$\left(\frac{\partial \mathcal{W}}{\partial (F_5)_{abcde}} - \frac{d}{du} \frac{\partial \mathcal{W}}{\partial \partial_u (F_5)_{abcde}} \right) \frac{\partial (F_5)_{abcde}}{\partial X}. \tag{2.2.32}$$

proof. The claim follows immediately with Lemma 2.2.4. □

Theorem 2.2.6. *The prescription given in the introduction of this section is valid.*

proof. Due to Lemma 2.2.1 and due to the fact that the effective action for the metric is not allowed to depend on x, because of gauge invariance, the theorem 2.2.6 holds, if we can show that for any given direction *abcde*, for which the electric part of the five form F_5 is non-zero, the expression given by $-\gamma(2.2.31)|_{g\to\mathfrak{g}}$ is the same as

$$\left(\frac{\partial}{\partial X} \gamma \frac{\sqrt{-g}}{\sqrt{-\mathfrak{g}}} \left(\mathfrak{g}_{aa}\mathfrak{g}_{bb}\mathfrak{g}_{cc}\mathfrak{g}_{dd}\mathfrak{g}_{ee} \left(\frac{\partial \mathcal{W}}{\partial (F_5)_{abcde}} - \frac{d}{du} \frac{\partial \mathcal{W}}{\partial_u \partial (F_5)_{abcde}} \right) \Big|_{g\to\mathfrak{g}} \right) g^{aa} g^{bb} g^{cc} g^{dd} g^{ee} \right.$$
$$\left. ((F_5)_{abcde}|_{g\to\mathfrak{g}}) \right) \Big|_{g\to\mathfrak{g}} + \mathcal{O}(\gamma^2) \tag{2.2.33}$$

for $X \in \{g_{\mu\nu}\}_{\mu\nu\in\{1,\dots,10\}}$ and $\mathfrak{g}$ being the solution for the metric with back-reaction and without higher derivative corrections. The claim now follows immediately by applying Lemma 2.2.5 and Lemma 2.2.1, since comment 2.2.3 implies

$$(\partial_X \sqrt{-g} g^{aa} g^{bb} g^{cc} g^{dd} g^{ee})((F_5^{el})_{abcde})\Big|_{g\to\mathfrak{g}} = -(\sqrt{-g} g^{aa} g^{bb} g^{cc} g^{dd} g^{ee})((\partial_X F_5^{el})_{abcde})\Big|_{g\to\mathfrak{g}}. \tag{2.2.34}$$

□

We also can extend the prescription to include tensor fluctuations. Similar to the case $b = 0$ the tensor fluctuations h_{xy} of the back-reacted and coupling corrected geometry don't change the higher derivative corrected solutions of the five form in a non-trivial way. This means the only way the fluctuations h_{xy} perturb the five form is via the AdS-Hodge-dual $\bar{*}$ in (2.2.5, 2.2.6). We now show that the prescription given at the beginning of this section can be extended to also include metric fluctuations

$$ds_{10} + h_{xy} dx dy \tag{2.2.35}$$

and their treatment.

Lemma 2.2.7. *The magnetic part of (2.2.5, 2.2.6) with lower indices and the electric part with upper indices times $\sqrt{-g}$ don't depend on h_{xy}.*

proof. Since

$$\frac{\partial}{\partial h_{xy}}|g|(g^{xx}g^{yy}-(g^{xy})^2)=0 \tag{2.2.36}$$

the Lemma follows immediately. □

The proof of the validity of the extension of the prescription is now entirely analogous to the one presented for theorem 2.2.6.

2.2.3 An alternative method to compute higher derivative corrections to the AdS-Schwarzschild black hole geometry

In this chapter we present a way to compute higher derivative corrections to the AdS-Schwarzschild black hole solution, i.e. for $b = 0$. We start from the action (1.5.20) and the EoM for the metric derived from there. In contrast to section 1.5 we are going to determine the metric numerically and restrict ourselves to solutions on intervals $u = \frac{r^2}{r_h^2} \in [l,k] \subset [0,1]$, where l and k have to be chosen sufficiently close to 0 and 1. The motivation for the method, we discuss in this section, is that it can be rather easily generalized to the case of a non-vanishing background field with back-reaction on the geometry. In that case we cannot hope to be able to determine the higher derivative corrections to the metric analytically. Even a near boundary and a near horizon analysis of the higher derivative correction terms to the differential equations of the metric with back-reaction of a strong magnetic background field turns out to be extremely difficult. We justify the computational strategy we are going to apply to determine these corrections to the metric numerically by performing an analogous calculation in the case $b = 0$ and show that it gives the same results with small numerical errors as the analytic solutions first derived in [5].

Our metric ansatz is of the form (2.2.2), (2.2.3), with $V(u) = W(u)$. The differential equations are obtained by varying the action (1.2.11) plus (1.2.12) with respect to the functions $L(u)$, $V(u)$, $U(u)$ and $\tilde{U}(u)$.

Let now $\int \mathcal{L}_{10}$ be the action defined in (1.2.11) with $F_5^{el} = -\frac{4}{L(u)^5}\epsilon_{\text{AdS}}$. In addition we set

$$\mathcal{L}_{10}^W = \sqrt{|g_{10}|}\Big[C^4 + C^3\mathcal{T} + C^2\mathcal{T}^2 + C\mathcal{T}^3 + \mathcal{T}^4\Big], \tag{2.2.37}$$

where the contributions of the $\mathcal{T}$-tensors to the EoM vanish in the case of absent background fields $b = 0$. We have to solve the differential equations

$$\left(\frac{\partial}{\partial X(u)} - \frac{d}{du}\frac{\partial}{\partial X'(u)} + \frac{d^2}{du^2}\frac{\partial}{\partial X''(u)}\right)(\mathcal{L}_{10} + \gamma\mathcal{L}_{10}^W) = 0, \tag{2.2.38}$$

with $X(u) \in \{V(u) = W(u), U(u), \tilde{U}(u), L(u)\}$ and choose the ansätze

$$X(u) = X^0(u) + \gamma X^1(u). \tag{2.2.39}$$

Only the $X^0(u)$ parts are entering the terms

$$\gamma L_{10}^W(X) = \left(\frac{\partial}{\partial X(u)} - \frac{d}{du}\frac{\partial}{\partial X'(u)} + \frac{d^2}{du^2}\frac{\partial}{\partial X''(u)}\right)\gamma\mathcal{L}_{10}^W, \tag{2.2.40}$$

if we want to calculate the coupling corrections up to order $\mathcal{O}(\gamma)$. From the expansion around the horizon and up to order $\mathcal{O}(\gamma)$ of

$$L_{10}(X) := \left(\frac{\partial}{\partial X(u)} - \frac{d}{du}\frac{\partial}{\partial X'(u)} + \frac{d^2}{du^2}\frac{\partial}{\partial X''(u)}\right)\mathcal{L}_{10} \tag{2.2.41}$$

we can see that $L_{10}^W(X)$ is regular at the horizon for $X(u) \in \{\tilde{U}(u), V(u), L(u)\}$, whereas for $X(u) = U(u)$ it has a pole of first order at $u = 1$.[37] In the following our aim is to determine $L_{10}^W(X)$. We apply spectral methods. The strategy will be to determine

$$\frac{\partial}{\partial X(u)}\mathcal{L}_{10}^W, \qquad \frac{\partial}{\partial X'(u)}\mathcal{L}_{10}^W \quad \text{and} \quad \frac{\partial}{\partial X''(u)}\mathcal{L}_{10}^W \tag{2.2.42}$$

on the rescaled Gauss-Lobatto grid for the u-coordinate

$$\frac{l+k}{2} + \frac{l-k}{2}\cos\left(\frac{\pi n}{M}\right)_{n\in\{0,\ldots,M\}} \tag{2.2.43}$$

with $l = 0.1$ and $k = 0.99$, such that for $u \in [l, k]$ we have

$$-\frac{2u}{l-k} + \frac{l+k}{l-k} \in [-1, 1]. \tag{2.2.44}$$

This can be done without further ado both in the cases $b = 0$ and $b = \frac{5}{4}$, since we already determined the functions $U^0(u), \tilde{U}^0(u), V^0(u), W^0(u)$ numerically in section 2.2.1, in such a way, that the numerical error is negligible on the interval $[l, k]$ on which we have defined our Gauss-Lobatto grid (2.2.43). Since we consider the case $b = 0$ in this section we perform this calculation with $U^0(u), \tilde{U}^0(u), V^0(u), W^0(u)$ chosen such that (2.2.3) is the Schwarzschild black hole metric. The higher derivative corrections

[37] Finite coupling corrections don't cause additional poles in the metric.

will be determined by expanding the ansätze in the following way

$$U(u) = U^0(u) e^{\gamma u^{d_1}} \sum_{i=0}^{M} a_i^{U,M} c_i^M(xu-y) \tag{2.2.45}$$

$$\tilde{U}(u) = \tilde{U}^0(u) e^{\gamma u^{d_1}} \sum_{i=0}^{M} a_i^{\tilde{U},M} c_i^M(xu-y) \tag{2.2.46}$$

$$L(u) = L^0(u) e^{\gamma u^{d_2}} \sum_{i=0}^{M} a_i^{L,M} c_i^M(xu-y) \tag{2.2.47}$$

$$V(u) = W(u) = V^0(u), \tag{2.2.48}$$

$x = \frac{2}{k-l}$ and $y = \frac{l+k}{k-l}$ [38], c_i^M denotes the i-th cardinal function on the grid $\{-\cos(\frac{\pi n}{M})\}$ and $a_i^{\tilde{U},M}$, $a_i^{L,M}$, $a_i^{U,M}$ are the respective expansion coefficients. The determination of the constants d_1 and d_2 will be discussed below. The last equation (2.2.48) follows from the invariance of the metric ansatz under transformations of the form

$$u \to u(\tilde{u}) \tag{2.2.49}$$

to a new radial coordinate $\tilde{u}$, so that we set $a_i^{V,M} = 0$. Let P^γ be the projection on the first order expansion coefficient in γ of a function f, so $P^\gamma f = \frac{\partial}{\partial \gamma} f|_{\gamma \to 0}$, then we have

$$P^\gamma \left(L_{10}(\tilde{X}) + \gamma L_{10}^W(\tilde{X})\right)\Big|_{\{u \to \frac{y-\cos(\pi n/M)}{x}\}_{n\in\{0,\dots,M\}}} = 0 \tag{2.2.50}$$

for each $\tilde{X} \in \{V, U, L, \tilde{U}\}$. This can be written as a matrix equation of the form

$$A \cdot v = \chi, \tag{2.2.51}$$

where for $j \in \{0,1,2\}$, $m \in \{1,\dots,M+1\}$ and $(X_0, X_1, X_2) = (L, U, \tilde{U})$

$$A_{(M+1)j+m,n} = P^{v_n} P^\gamma \left(L_{10}(X_j)\right)\Big|_{\{u \to \frac{y-\cos(\pi(m-1)/M)}{x}\}} \tag{2.2.52}$$

is a real $3(M+1) \times 3(M+1)$-matrix. The vector v is given by

$$v_{j(M+1)+m} = a_{m-1}^{X_j,M} \tag{2.2.53}$$

and finally the $3(M+1)$-vector χ is

$$\chi_{j(M+1)+m} = -\left(L_{10}^W(X_j)|_{\{X(u)\to X^0(u)\}_{X\in\{W,V,L,U,\tilde{U}\}}}\right)\Big|_{\{u \to \frac{y-\cos(\pi(m-1)/M)}{x}\}}. \tag{2.2.54}$$

The resulting system of equations can be solved easily. We can perform a non trivial test of our calculation with the help of the observation that the equation obtained by inserting $\tilde{X} = V$ in (2.2.50) has to be fulfilled by the found solution of (2.2.52). Our calculation passed this test to quite good accuracy. The near boundary behaviour of

[38] Here x and y are simple parameters, not to be confused with spatial coordinates.

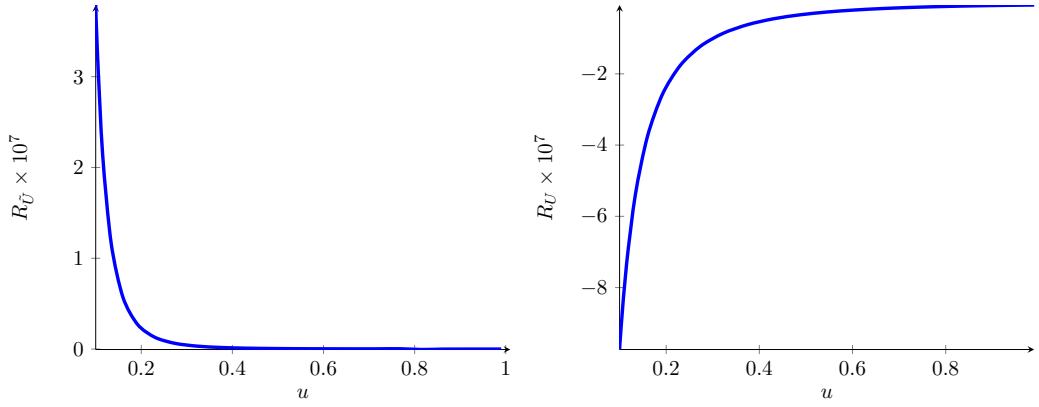

Figure 2.6: Relative error between the analytic solution and the numerical solution $R_{\tilde{U}}$ (left) and R_U (right) as defined in (2.2.55), obtained by calculating on a Gauss-Lobatto grid on the interval $[l, k]$, with the choice $d_1 = 1$, $d_2 = 0$, $l = 0.1$ and $k = 0.99$.

the higher derivative corrections to the metric in (2.2.45)-(2.2.48) is encoded in the still undetermined exponents d_1 and d_2. When solving these differential equations analytically we chose a specific expansion ansatz to obtain the higher derivative corrected EoM for the metric. One can show that the only undetermined expansion coefficient can be absorbed by a rescaling of the time coordinate.

By rescaling and by the requirement that the metric on the boundary should be conformally equivalent to the Minkowski metric, one can already reach $0 \leq d_2$ and $1 \leq d_1$. The explicit form of (2.2.45)-(2.2.48) with $d_2 = 4 = 2d_1$ follows from a near boundary analysis of the higher derivative corrected Einstein equations. However, we won't make use of this analysis and start the calculation naively with $d_2 = 0$, $d_1 = 1$, since this will also be the strategy in the case $b \neq 0$. Solving the system of equations for the expansion coefficients $\{a_i^{X,M}\}_{i\in\{0,\dots,M\},X\in\{\tilde{U},UL\}}$ on the Gauss-Lobatto grid on $[l, k]$ gives results, whose relative errors

$$R_X = \frac{X_\gamma^{\text{numerical}} - X_\gamma^{\text{analytical}}}{X_\gamma^{\text{analytical}}} \tag{2.2.55}$$

are displayed in Figure 2.6 for $M = 25$ and for the first order γ corrections to the functions U and $\tilde{U}$.

The error for U and $\tilde{U}$ are both of order 10^{-7}, the relative error for L has a maximal value of ≈ 0.00066. The solution to the problem of how to improve the numerical precision in a way that can be extended to the $b \neq 0$ case lies in the following observation:

If we choose the interval to be $[l, k]$, with $k = 0.99$ as before and l sufficiently large we have to reach a point, where the determinant of the system of equations for the expansion coefficients of the higher derivative corrections to the metric tends to

zero. This is because we thereby admit solutions, which are divergent at the boundary and whose suppression was achieved by choosing l sufficiently small. The same logic applies to the choice of d_1 and d_2 in (2.2.45)-(2.2.48). For a choice of d_1 and d_2, which is sufficiently far away from the actual near boundary behaviour, the determinant of A in (2.2.52) decreases. We can implicitly determine the near boundary behaviour by minimizing the function

$$\min\Big(\{((A^{-1})^{numerical}A - 1_{3M+3,3M+3})_{a,b}|a,b \in \{1,\dots,3M+3\}\}\Big) \tag{2.2.56}$$

where $(A^{-1})^{numerical}$ is the numerically determined inverse of the matrix in (2.2.52), keeping M, l, k fixed and only varying d_1 and d_2. This actually gives $d_1 = 2 = \frac{d_2}{2}$. The maximal absolute value of the relative error, which again appears for $R_X = R_L$, is now 7.3×10^{-9}.

2.2.4 Higher derivative corrections to the magnetic black brane metric

In this chapter we are going to apply techniques derived in section 2.2.3 to determine an approximation of higher derivative corrections to the metric computed in section 2.2.1. First of all we have to use the theorem derived in section 2.2.2. We apply the prescription from there to simplify our calculation. Following this theorem we define the five form F_5 in the following way: We start with the electric part of the five form, that does not depend on b, and its Hodge dual. For those we get

$$\begin{aligned}(F_5^{el})^0 &= -\frac{4}{L(u)^5}\sqrt{|\det(g_5)|}dt\wedge du\wedge dx\wedge dy\wedge dz\\ *\Big((F_5^{el})^0\Big) &= 4\sqrt{\det(g_{S_5})}dy_1\wedge dy_2\wedge dy_3\wedge dy_4\wedge dy_5 + \frac{4}{L(u)^5}\sqrt{|\det(g_{10})|}\sqrt{|\det(g_5)|}\\ &\quad\Big(g_{10}^{tt}g_{10}^{uu}g_{10}^{xx}g_{10}^{yy_3}g_{10}^{zz}dy_1\wedge dy_2\wedge dy\wedge dy_4\wedge dy_5 + g_{10}^{tt}g_{10}^{uu}g_{10}^{xx}g_{10}^{yy_4}g_{10}^{zz}dy_1\wedge dy_2\\ &\quad\wedge dy_3\wedge dy\wedge dy_5 + g_{10}^{tt}g_{10}^{uu}g_{10}^{xx}g_{10}^{yy_5}g_{10}^{zz}dy_1\wedge dy_2\wedge dy_3\wedge dy_4\wedge dy\Big).\end{aligned} \tag{2.2.57}$$

The electric components of the five form including the gauge field $A_y = bx$ is explicitly given by

$$\begin{aligned}(F_5^{el})^1 = \frac{2b}{\sqrt{3}L(u)}\sqrt{|\det(g_5)|}g_5^{xx}g_5^{yy}\big(&\sin(y_1)\cos(y_1)dt\wedge du\wedge dz\wedge dy_1\wedge dy_3 +\\ &\cos(y_1)^2\sin(y_2)\cos(y_2)dt\wedge du\wedge dz\wedge dy_2\wedge dy_4 - \cos(y_1)\sin(y_1)\sin(y_2)^2dt\\ &\wedge du\wedge dz\wedge dy_1\wedge dy_4 - \cos(y_1)\sin(y_1)\cos(y_2)^2dt\wedge du\wedge dz\wedge dy_1\wedge dy_5\\ &- \cos(y_2)\sin(y_2)\cos(y_1)^2dt\wedge du\wedge dz\wedge dy_2\wedge dy_5\big),\end{aligned} \tag{2.2.58}$$

while its Hodge dual simplifies to

$$
\begin{aligned}
*\Big((F_5^{el})^1\Big) = -\frac{2b}{\sqrt{3}} L(u)^4 \sqrt{\det(g_{S_5})}\big(& \sin(y_1)\cos(y_1) g_{10}^{y_1y_1}(g_{10}^{y_3y_3} - \sin(y_2)^2 g_{10}^{y_4y_3} - \\
& \cos(y_1)^2 g_{10}^{y_5y_3}) dx \wedge dy \wedge dy_2 \wedge dy_5 \wedge dy_4 + \cos(y_1)^2 \sin(y_2)\cos(y_2) \times \\
& g_{10}^{y_2y_2}(g_{10}^{y_4y_4} - g_{10}^{y_5y_4}) dx \wedge dy \wedge dy_1 \wedge dy_5 \wedge dy_3 - \sin(y_1)\cos(y_1) g_{10}^{y_1y_1} \\
& (\sin(y_2)^2 g_{10}^{y_4y_4} - g_{10}^{y_3y_4} + g_{10}^{y_5y_4}\cos(y_2)^2) dx \wedge dy \wedge dy_2 \wedge dy_3 \wedge dy_5 - \\
& \cos(y_1)\sin(y_1) g_{10}^{y_1y_1}(\cos(y_2)^2 g_{10}^{y_5y_5} - g_{10}^{y_3y_5} + g_{10}^{y_4y_5}\sin(y_2)^2) dx \wedge dy \wedge dy_2 \\
& \wedge dy_4 \wedge dy_3 - \cos(y_2)\sin(y_2) g_{10}^{y_2y_2}(g_{10}^{y_5y_5}\cos(y_1)^2 + \sin(y_1)^2 g_{10}^{y_4y_5}) dx \wedge dy \\
& \wedge dy_1 \wedge dy_3 \wedge dy_4 - \sin(y_2)\cos(y_2)\cos(y_1)^2 g_{10}^{y_2y_2}(g_{10}^{y_4y_3} - g_{10}^{y_5y_3}) dx \wedge dy \\
& \wedge dy_1 \wedge dy_5 \wedge dy_4\big).
\end{aligned} \tag{2.2.59}
$$

Here g_{10} stands for the general metric ansatz chosen in (2.2.2), (2.2.3), g_5 is the metric of the internal AdS space and g_{S_5} is the metric of the five sphere . The part of the five form entering

$$
-\frac{\sqrt{-g}(F^{mag})^2}{2 \times 5!} \tag{2.2.60}
$$

of the effective action for the metric components derived in Theorem 2.2.2 is $(F_5)^{mag} = *((F_5^{el})^0 + (F_5^{el})^1)$. The part of the 5-form F^+, which enters the $\mathcal{T}$-tensor in (1.2.15), is given by $F^+ = (1+*)((F_5^{el})^0 + (F_5^{el})^1)$. We define $\mathcal{L}_{10}^W$ as in (2.2.37). Since we consider a strong background field, it can therefore not be treated perturbatively. Each part of the higher derivative terms, given in (5.1.2), will contribute to the EoM for the metric components. Knowing the solution for the metric in order $\mathcal{O}(\gamma^0)$ and for $b = \frac{5}{4}$ on the interval $u \in [l, k]$ allows us to compute [39]

$$
\frac{\partial}{\partial X(u)}\mathcal{L}_{10}^W, \qquad \frac{\partial}{\partial X'(u)}\mathcal{L}_{10}^W \quad \text{and} \quad \frac{\partial}{\partial X''(u)}\mathcal{L}_{10}^W \tag{2.2.61}
$$

for $X \in \{U, \tilde{U}, W, V, L\}$ on said grid. This very tedious calculation can be abbreviated by the observation that the final result will only depend on y_1 and y_2 via the square root of the absolute value of the determinant of the metric.

We define $\mathcal{L}_{10}$ to be (1.2.11) with F_5^2 being replaced by

$$
2\big((F_5)^{mag}\big)^2 = 2\big(*(F_5)^{el}\big)^2 \tag{2.2.62}
$$

given in (2.2.57) and (2.2.59). As before we consider the system of differential equations (2.2.38). The ansatz for U, $\tilde{U}$, L, W and V is the same as in (2.2.45)-(2.2.48) with

[39] When we compute the variation, we are allowed to assume that the metric components abbreviated with $X \in \{L, U, \tilde{U}, W, V\}$ do not depend on x, since terms of the form $\frac{\partial}{\partial \partial_x X}\mathcal{L}_{10}^W$, $\frac{\partial}{\partial \partial_x^2 X}\mathcal{L}_{10}^W$ must vanish, exactly as in the case $\mathcal{O}(\gamma^0)$. Otherwise the EoM for the gauge field $A_y = bx$ would get mass terms. In addition $A_y = bx$ is also a solution to the higher derivative corrected EoM for gauge fields.

the difference that $V \neq W$, due to the symmetry breaking of the magnetic field in z-direction. The argument, why we could choose the higher derivative corrections to $W = V$ in the case $b = 0$ to vanish, can now be only applied to either W or V. Without loss of generality we set

$$X(u) = \tilde{X}^0(u) e^{\gamma u^{d_X}} \sum_{i=0}^{M} a_i^{X,M} c_i^M (xu-y) \tag{2.2.63}$$

for $X \in \{U, \tilde{U}, W, V, L\}$ and $a_i^{V,M} = 0$ henceforth. We again write (2.2.38) as a $(4M + 4) \times (4M + 4)$ matrix equation $A \cdot v = \chi$, where A, v and χ are defined analogously to section 2.2.3. We test our result by making sure that the EoM obtained by varying with respect to V is fulfilled by the solution to this system. Our calculation passed this test to very good accuracy.

The requirement that the metric induced on the boundary is the Minkowski metric gives $d_X > 0$ for $X \in \{U, \tilde{U}, W\}$. With an analogous procedure as in section 2.2.3 we obtain that $d_L > 1$. We determine the solution for several values of l, $M \in \{m_1, \ldots, m_2\}$ and for different values for k in the vicinity of 1[40] to ensure that the numerical error we make, due to the fact that we cannot choose the interval $[l, k]$ arbitrarily close to $[0, 1]$[41], doesn't cause unacceptably large errors in the following calculations. We apply the prescription for the temperature of the boundary field theory derived in the introduction and explicitly given in equation (1.4.28). For a background field parameter $b = \frac{5}{4}$ this leads to a correction factor of

$$T + \gamma T^\gamma = T\left(1 + \frac{\gamma}{2}\left(\frac{d}{d\gamma}(U(u) - \tilde{U}(u))|_{\gamma\to 0, u\to 1}\right)\right) \approx T(1 + \gamma\ 294.9). \tag{2.2.64}$$

In Figure 2.7 we computed the deviation from the average value of the α'^3-correction T^γ to the temperature

$$\Delta T^\gamma(l) = \frac{1}{m_2 - m_1 + 1} \sum_{M=m_1}^{m_2} \frac{|T^\gamma(M, l) - \bar{T}^\gamma|}{\bar{T}^\gamma}, \tag{2.2.65}$$

where $\bar{T}^\gamma$ is the average over all considered configurations $M \in \{m_1, \ldots, m_2\}$ and $l \in [1, 1.05, \ldots, 1.4]$, m_1 was chosen to be 10, m_2 was chosen to be 23, k was kept fixed at $k = 0.99$. The maximal relative difference between two results for the coupling corrected temperature corresponding to the various choices for M and l is

$$\delta T^{\max} := \frac{T^\gamma_{\max} - T^\gamma_{\min}}{\bar{T}^\gamma} = 0.00565, \tag{2.2.66}$$

[40] Divergences of several terms in the non-simplified version of (2.2.61), which cancel analytically, if we would expand them around the horizon, but not numerically due to finite machine precision, make it also impossible to choose $k = 1$.

[41] This would require an explicit, analytic near boundary analysis of (2.2.61), which is rather hopeless.

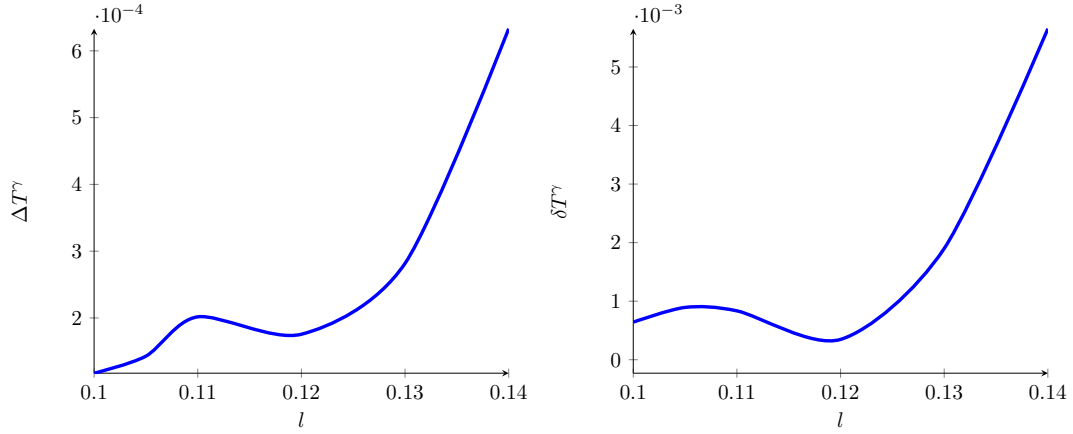

Figure 2.7: On the left the relative estimated error of the γ correction to the temperature averaged over M is plotted for different values of the interval boundary l. On the right hand side the function $\delta T^\gamma(l)$ defined in (2.2.67) is shown.

where both the minimal and the maximal value for T^γ are taken in the case $l = 0.14$, the maximal l-value of our analysis. Finally let us consider the function

$$\delta T(l) := \frac{T^\gamma_{\max}(l) - T^\gamma_{\min}(l)}{\bar{T}^\gamma}, \tag{2.2.67}$$

where $T^\gamma_{\max/\min}(l)$ is the maximal/minimal value for T^γ we obtained for a certain l. The results are displayed in Figure 2.7. Both plots in this figure suggest that the error regarding the higher derivative correction to the temperature computed in the case $l = 0.1$ and $k = 0.99$ is small[42]. This is also reflected more in Figure 2.8, where we display the results for the correction factor to the temperature obtained by calculations on intervals $[0.1, k]$, we extrapolated the resulting coupling corrections to the metric to $u = 1$.

[42]Roughly of order 10^{-3} for a correction term that is of order 10^3.

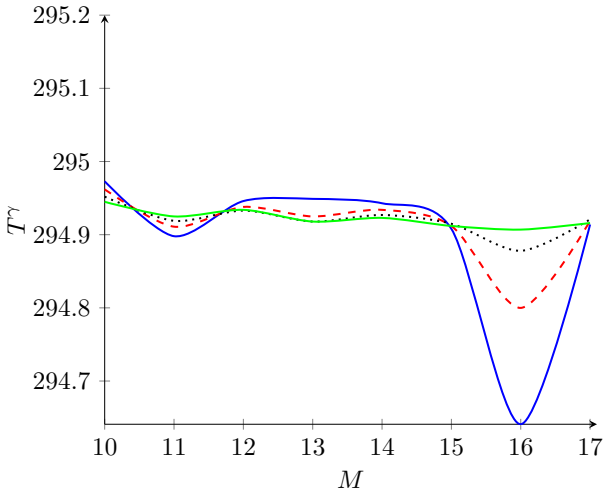

Figure 2.8: The higher derivative correction T^γ for to the temperature, computed on intervals $[0.1, k]$ for different values of M (shown in a smoothed plot). The solid blue line shows the results for $k = 0.975$, the dashed red line corresponds $k = 0.98$, the dotted black line corresponds to $k = 0.985$ and the solid green line corresponds to $k = 0.99$. The metric was extrapolated to $u = 1$.

2.2.5 Approximating higher derivative corrections to tensor QNMs of a Schwarzschild black hole

We prepare the following sections by first considering fluctuations of the metric of a coupling corrected AdS-Schwarzschild black hole. These fluctuation, introduced as quasinormal modes in section 1.4.2, are tiny perturbations of the geometry, that are dual to quasiparticles on the field theory side and encode the response of the system to excitations around the equilibrium. We will consider tensor, or spin-2-fluctuations h_{xy} with momentum in z direction. At first we are going to approximate higher derivative corrections to these tensor QNMs without considering background magnetic fields. In complete analogy to the previous two subsections, we present a method that can be easily extended to the case $b \neq 0$ and check that the results obtained for $b = 0$ coincide with those in the literature. We consider the linearized differential equations obtained by varying the higher derivative corrected action with respect to fluctuations $h_{xy}dxdy$ of the background geometry. These EoM were first derived in [25] and are given in the Appendix (5.6.1). The characteristic exponents of the differential equation (5.6.1) are given by $\pm\frac{i\hat{\omega}}{2}$, such that[43]

$$h = (1-u)^{-\frac{i\hat{\omega}}{2}}\phi(u) \tag{2.2.68}$$

where $\phi(u)$ is regular at the horizon and the exponent of $(1-u)^{-\frac{i\hat{\omega}}{2}}$ was chosen to correspond to infalling wave solutions. There is an ambiguity regarding the normalization

[43] We set $h_{xy} = h$ here and henceforth.

convention of QNM frequencies in the literature. Here $\hat{\omega}$ is defined as $\hat{\omega} = \frac{\omega}{2\pi T}$ to be consistent with the convention in [17]. In the case of $b = \frac{5}{4}$ we will use the convention $\hat{\omega} = \frac{\omega}{\pi T}$, $\tilde{\omega} = \frac{\omega}{r_h}$ to be consistent with [13], to allow for an easier comparison. Again we consider the Gauss-Lobatto grid (2.2.43). We define the discrete differentiation matrix $A(M)$ as

$$A(M)_{ij} = \frac{2}{k-l}\partial_u c_j|_{u\to u_i}, \tag{2.2.69}$$

where c_j is the j-th Chebyshev cardinal function $\frac{2u_j}{k-l} + \frac{l+k}{l-k}$. An equivalent, more elaborate but numerically more convenient definition of $A(M)$ is given in the Appendix 5.9, which builds on [28]. Expanding ϕ in Chebyshev cardinal functions $\tilde{c}$ corresponding to the grid (2.2.43) in the form

$$\phi(u) = \sum_{i=0}^{M} \tilde{c}_i(u) a_i \tag{2.2.70}$$

allows us to formulate (5.6.2) as a matrix equation for the zero momentum mode $q = 0$

$$O(M, \gamma, \hat{\omega})v = 0 \tag{2.2.71}$$

with $v = (a_i)_{i\in\{0,\dots,M\}}$ and

$$O(M,\gamma,\hat{\omega})_{ji} = \sum_{l=0}^{M} f_2(u_j)A(M)_{jl}A(M)_{li} + f_1(u_j,\gamma,\hat{\omega})A(M)_{ji} + f_0(u_j,\gamma,\hat{\omega})\delta_{ji}, \tag{2.2.72}$$

the function f_i for $q = 0$ are given in the Appendix 5.6. Analogously to the method presented in (2.1.72) and (2.1.73) we split up $O(M, \gamma, \hat{\omega})$ as

$$O(M,\gamma,\hat{\omega}) = O^0(M,\gamma) + \hat{\omega}O^1(M,\gamma) + \hat{\omega}^2 O^2(M,\gamma) \tag{2.2.73}$$

and write (2.2.71) as a generalized eigenvalue problem. We solve for $\hat{\omega}$ exactly in γ for different values

$$\gamma = \frac{\zeta(3)}{8} 1000^{-3/2} \frac{1 - \cos(\frac{\pi n}{\tilde{M}})}{2}. \tag{2.2.74}$$

We chose $n \in \{0, \dots, \tilde{M}\}$, $\tilde{M} = 80$. This Gauss-Lobatto grid corresponds to λ values between $\lambda = \infty$ and $\lambda = 1000$. The slopes at $\lambda = \infty$ of the curves of partially resummed coupling corrected results for $\hat{\omega}$ in the complex plane will give us the $\mathcal{O}(\gamma^1)$-corrections to the QNM frequency $\hat{\omega}$. The boundaries of the interval on which the Gauss-Lobatto grid (2.2.43) is defined are chosen to be $l = 0.1$ and $k = 0.99$. We depict the coupling corrections to the first QNM in Figure 2.9. The results are displayed for different values of the grid size M and show clear convergence towards the exact coupling corrections obtained in [17]. We plotted the first order coefficients of the γ-expansion of the first

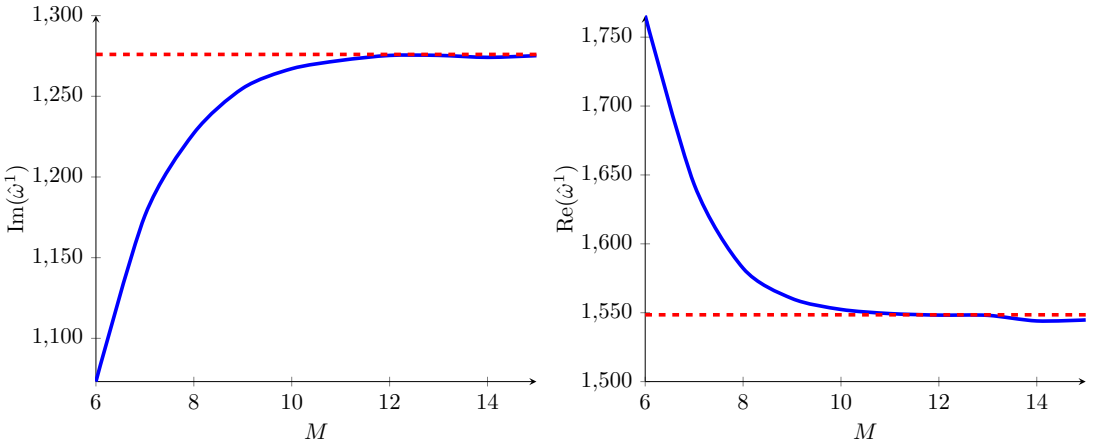

Figure 2.9: The first order correction $\hat{\omega}^1$ to the lowest tensor-QNM frequency for $b = 0$, $q = 0$, computed via spectral methods on a grid $u \in [0.1, 0.99]$ (solid blue line) compared with the exact result (red dashed line) for different values of M shown in a smoothed plot.

QNM frequency.

$$\hat{\omega}^1 := \partial_\gamma \hat{\omega}|_{\gamma=0}. \tag{2.2.75}$$

However, surprisingly, applying this method with $25 < M$ corrupts the numerical results noticeably. For $10 < M < 20$ we obtain good agreement with the already known results from [17, 19].

2.2.6 Approximating higher derivative corrections to the first tensor QNM in the finite-λ magnetic black brane geometry

With a magnetic background field in z direction the considered fluctuations $h_{x,y}$ decouple from other modes. Also the Chern-Simons term does not play a role in this case. This can be derived from the symmetries of the problem or from our general 10-dimensional ansatz (2.2.5), (2.2.6), (2.2.2), (2.2.3), which would have captured contributions to a Chern-Simons term after a Kaluza-Klein reduction, if it were relevant here.

As in the previous section we focus on the case $q = 0$. We already have found the metric, respectively the functions $\tilde{U}, U, V, W, L$ up to order $\mathcal{O}(\gamma)$ for the parameter $b = \frac{5}{4}$ in the previous sections. The following metric ansatz describes tensor fluctuations

in this geometry:

$$\begin{aligned} ds^2_{\text{fluc}} =& -U(u)dt^2 + \tilde{U}(u)du^2 + e^{2V(u)}(dx^2+dy^2) + e^{2W(u)}dz^2 + L(u)^2\frac{4b^2x^2}{3}dy^2 \\ &+ L(u)^2\frac{2bx}{\sqrt{3}}dy(dy_3\sin(y_1)^2 + dy_4\cos(y_1)^2\sin(y_2)^2 + dy_5\cos(y_1)^2\cos(y_2)^2) \\ & L(u)^2(dy_1^2 + \cos(y_1)^2dy_2^2 + \sin(y_1)^2dy_3^2 + \cos(y_1)^2\sin(y_2)^2dy_4 + \cos(y_1)^2 \\ & \cos(y_2)^2dy_5^2) + h_{x,y}(u,t)dxdy. \end{aligned} \tag{2.2.76}$$

Our strategy is very similar to the one of the previous chapters. We choose the same grids as before and evaluate the functions

$$\mathcal{J}(a,b) := \frac{\partial^2}{\partial(\partial_a h_{x,y})\partial(\partial_b h_{x,y})}\mathcal{L}_{10}^{W,\text{fluc}}\Big|_{h_{x,y}\to 0}, \tag{2.2.77}$$

on the respective grid points. Here we set

$$J(0,b) := \frac{\partial^2\mathcal{L}_{10}^{W,\text{fluc}}}{\partial(h_{x,y})\partial(\partial_b h_{x,y})}\Big|_{h_{x,y}\to 0}, \tag{2.2.78}$$

with $a,b \in \{t,z,u\}$ and

$$\mathcal{L}_{10}^{W,\text{fluc}} = \mathcal{L}_{10}^{W}\Big|_{ds^2_{10}\to ds^2_{\text{fluc}}}. \tag{2.2.79}$$

Together with the Fourier transformed version of $h_{x,y}$

$$h_{x,y}(u,t) = \int\frac{d\omega}{2\pi}\hat{h}(u,\omega)e^{i\omega t} =: \int\frac{d\omega}{2\pi}\hat{h}e^{i\omega t} \tag{2.2.80}$$

we can write

$$\begin{aligned} \int d^{10}x\mathcal{L}_{10}^{W,\text{fluc}} =& \text{vol}(S_5)\int\frac{d\omega}{2\pi}\int du\int dx^3\Big(\frac{1}{2}\mathcal{J}(0,0)\hat{h}^2 + \mathcal{J}(u,0)\hat{h}\partial_u\hat{h} + \frac{1}{2}\mathcal{J}(u,u) \\ & (\partial_u\hat{h})^2 + \mathcal{J}(uu,u)\partial_{uu}\hat{h}\partial_u\hat{h} + \frac{1}{2}\mathcal{J}(uu,uu)\partial_{uu}\hat{h}\partial_{uu}\hat{h} + \mathcal{J}(uu,0)\hat{h} \\ & \partial_{uu}\hat{h} + \frac{\omega^2}{2}\mathcal{J}(t,t)\hat{h}^2 + \frac{\omega^4}{2}\mathcal{J}(tt,tt)\hat{h}^2 - \omega^2\mathcal{J}(tt,0)\hat{h}^2 - \omega^2\mathcal{J}(tt,u) \\ & \partial_u\hat{h} + \omega^2\mathcal{J}(t,ut)\hat{h}\partial_u\hat{h} + \frac{\omega^2}{2}\mathcal{J}(ut,ut)(\partial_u\hat{h})^2 - \omega^2\mathcal{J}(tt,uu)\hat{h}\partial_{uu}\hat{h}\Big) \end{aligned} \tag{2.2.81}$$

plus higher orders in $\hat{h}$, which we ignore. A straightforward calculation shows that the rest of the action can be written as[44]

$$\int d^{10}x\sqrt{-g_{\text{fluc}}}\Big(R_{10}-\frac{8}{L(u)^5}-b^2(2e^{-4V(u)}+\frac{e^{-8V(u)}}{2}h_{x,y}(u,t)^2)(\frac{L(u)^2}{3}+\frac{2}{3L(u)^6})\Big). \tag{2.2.82}$$

We expand this action up to order $\mathcal{O}(\gamma)$ and up to order $\mathcal{O}(h_{xy}^2)$, which gives terms of the form $\mathcal{L}^{\gamma=0}(h_{xy},\partial_u h_{xy},\partial_t h_{xy},\partial_{uu}h_{xy},\partial_{tt}h_{xy},\partial_{ut}h_{xy},u)$ as well as $\gamma\mathcal{L}^{\gamma}(\dots)$, with the same arguments. With the Fourier representation of h_{xy} we write the terms above in the same way as $\mathcal{L}_{10}^{W,\text{fluc}}$ depending only on $\hat{h},\partial_u\hat{h},\partial_{uu}\hat{h},\omega,u$. Varying the total action

$$\int d^{10}x\Big(\mathcal{L}^{\gamma=0}+\gamma\mathcal{L}^{\gamma}+\gamma\mathcal{L}_{10}^{W\text{fluc}}\Big) \tag{2.2.83}$$

with respect to $\hat{h}$ provides the EoM for $\hat{h}$ depending on the functions $\mathcal{J}(a,b)$ and the order $\mathcal{O}(\gamma)$ parts of the metric as an expansion in cardinals functions. The coupling corrected relation between the horizon radius and the temperature, which is given in (2.2.64), shows that the characteristic exponents stay of the form $\pm\frac{i\hat{\omega}}{4}$. Here and in the following we will use the convention $\hat{\omega}=\frac{\omega}{\pi T}$ and $\tilde{\omega}=\frac{\omega}{r_h}$.

Considering solutions that are infalling at the horizon we set again

$$\hat{h}(u,\hat{\omega})=(1-u)^{-\frac{i\hat{\omega}}{2}}\phi(u,\hat{\omega}). \tag{2.2.84}$$

We consider Gauss-Lobatto grids on intervals $[l,k]\subset[0.1,0.99]$ of size M and approximate the function $\phi(u,\hat{\omega})$ by cardinal functions corresponding to these grids with expansion coefficients a_i^M. In analogy to the previous section the coupling corrected differential equation for ϕ in the presence of a strong magnetic background field is brought into the form (2.2.71). The coupling correction to the QNM is then again computed by considering this equation as a generalized eigenvalue problem in the same way as presented in (2.1.72) and (2.1.73). We performed this calculation for various intervals $[l,k]$ and various grid sizes M[45].

We define $\hat{\omega}^1(M,\tilde{l},\tilde{k})$ to be the $\mathcal{O}(\gamma^1)$ expansion coefficient of the lowest tensor QNM computed with spectral methods on a grid with size M defined on the interval $[0.1+\tilde{l},0.99-\tilde{k}]$. The aim is to study how the results, towards which $\hat{\omega}^1(M,\tilde{l},\tilde{k})$ converges for growing M, depend on the interval size. Figures 2.10 show the comparison between the M-dependent results for the real and imaginary part of $\hat{\omega}^1$ for different

[44] We omitted the prefactor $\frac{1}{2\kappa}$ in front of the action, since it will not be important for the following calculations.

[45] The higher derivative corrections to the metric were obtained by interpolations using cardinal functions on the interval $[0.1,0.99]$ and with $M=17$. We repeated the calculations displayed in figures (2.10,2.11) for metrics computed with various choices for M and the interval (while we extrapolated to the full size of the interval on which we computed the QNM, if necessary) and found negligible differences regarding the final results.

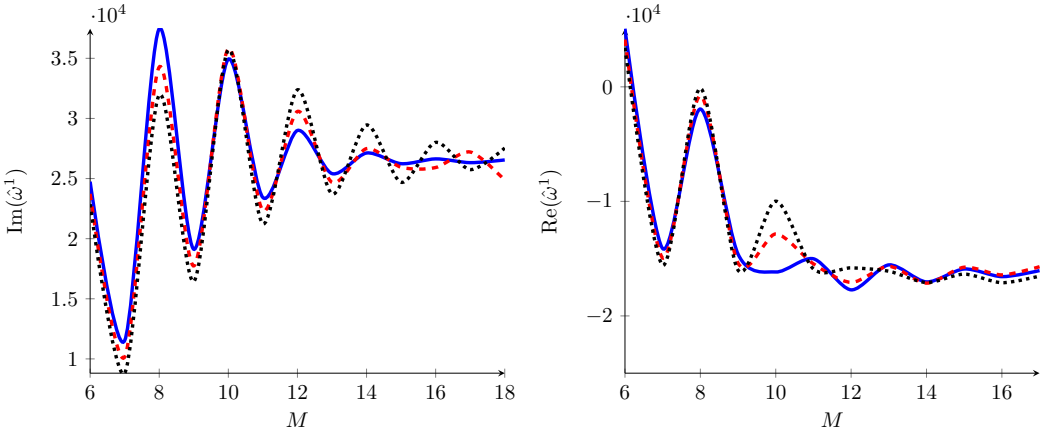

Figure 2.10: The convergence of the real and imaginary part of the correction $\hat{\omega}^1$ for $b = \frac{5}{4}$ of the first tensor QNM computed for various grid sizes M (shown in a smoothed plot) and for different interval sizes. The solid blue line corresponds to $[l, k] = [0.1, 0.99]$, the dashed red line corresponds to $[l, k] = [0.11, 0.98]$ and the dotted black line corresponds to $[l, k] = [0.12, 0.97]$.

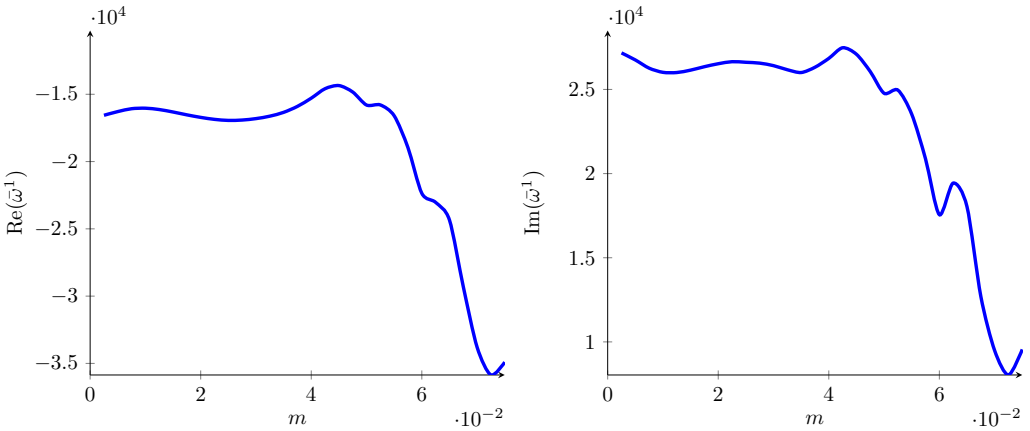

Figure 2.11: The convergence of $\bar{\omega}^1(m)$ for different interval sizes $[0.1 + m, 0.99 - m]$. The quantity $\bar{\omega}^1(m)$ is defined as the point of convergence of the M-dependent sequence $\hat{\omega}^1(M, m, m)$ with fixed m.

intervals $[l, k]$. The results for $\bar{\omega}^1(m)$, which is defined as the point of convergence with respect to M of $\hat{\omega}^1(M, \tilde{l}, \tilde{k})$ with $\tilde{l} = \tilde{k} = m$, are displayed in Figure 2.11. In general we observe reasonable convergence for relatively small values of M, similar to the case $b = 0$, such that we can give an approximation of the higher derivative correction to the first tensor QNM with $b = \frac{5}{4}$.[46] We obtain $\hat{\omega}^1 \approx (-1.6 + 2.7i)10^4$, such that

$$\frac{\omega}{\pi T} \approx (2.0 - 4.7i) + \gamma(-1.6 + 2.7i)10^4 + \mathcal{O}(\gamma^{4/3}). \tag{2.2.85}$$

[46]The numerical errors of the following α'-corrected QNMs were too large to give meaningful quantitative results. Regarding the size, as for the first QNM, their correction terms seemed to be one order of magnitude larger compared to the case of a vanishing background field.

The $\lambda \to \infty$ limit coincides with the known results in the literature [13]. The correction $\gamma(-1.6 + 2.7i)10^4$ to the lowest QNM in the case of very strong magnetic background field is, similar to the higher derivative correction to the temperature, one order of magnitude larger than in the case $b = 0$[47]. This raises the question, whether it makes sense, to evaluate this first order coupling corrected QNM at values for the 't Hooft coupling below a certain threshold at which the correction inevitably gets larger than the original $\lambda \to \infty$ result. For this specific correction term (2.2.85) this threshold is reached at $\lambda \approx 95$, which is far above the 't Hooft coupling value that would correspond to a more realistic QCD limit $\lambda \approx 11$, which is obtained by naively choosing

$$g^2_{\mathrm{YM}}/(4\pi) = \alpha_s|_{T \text{ large}} \approx 0.3 \tag{2.2.86}$$

and $N = 3$. We will discuss this problem in more detail in section 2.3. Unlike in the case $b = 0$ the sign of the real part of the first order correction term is negative. In section 2.3 we show that considering higher order corrections to the QNMs coming from the first order correction to the EoM of h_{xy} this behaviour is reversed already for small values of γ. For small values of λ the real part of the first (coupling correction resummed) QNM for $b = \frac{5}{4}$, determined in the following section, behaves similarly to the analogous quantity in the case $b = 0$.

2.2.7 Concluding Remarks

In the presence of a strong magnetic background field $B \approx 34.5T^2$ the corrections to the temperature T of a QGP and the lowest tensor QNM are about one order of magnitude larger than in the case $B = 0$. A strong influence of the magnetic field on these quantities at infinite coupling already suggested this trend. However, the size of the correction terms is nonetheless surprising.[48] The trend that a decreasing (but still large) 't Hooft coupling increases the equilibration time is strongly enforced by a magnetic background field. An interesting setting to study in future work would be to also include a chemical potential i.e. considering a non vanishing charge density in combination with a magnetic background field at finite t' Hooft coupling.

2.3 Resumming higher order corrections

To conclude this chapter we are going to discuss how to treat higher derivative corrected quantities at 'interesting' 't Hooft coupling values i.e. λ between 11 and 40 correspond-

[47] The background field we chose corresponds to a very strong magnetic background field, that already in the limit $\lambda \to \infty$ (see [13]) had a strong influence on observables.

[48] We chose our background field to coincide with the strongest field chosen by the authors of [13]. Already there in the case $\lambda \to \infty$ a field of this size showed a very strong influence on observables. The by far largest contributions to the coupling corrections come from terms in the higher derivative corrected action that involve $\mathcal{T}$-tensors. These terms simply vanish in the case $b = 0$.

ing to $\alpha_s \equiv g^2_{\mathrm{YM}}/(4\pi)$, $\alpha_s \in [0.3, 1]$. Considering table 2.1 or the result (2.2.85) makes it apparent that the first order correction is not enough to give reliable results in this regime. In [17] the author considered a first order corrected QNM spectrum in the spin 2 channel. There it was found that for $\lambda \approx 1000 - 500$ the curve connecting the discrete poles of the stress-energy correlator bends upwards towards the real axis, breaking the top down thermalization pattern at one point. A similar, however, weaker behaviour is suggested by our own results for the vector channel depicted in Figure 2.4. In this section we are going to introduce a partial resummation method with the motivation to prove that already the lambda values chosen in [17] and [53], which were at about $\lambda \approx 500$, are too small i.e. γ is to big to obtain reliable results from the first order correction. Not only are the partially resummed poles much closer to the $\lambda \to \infty$ limit, also the curve connecting the complex frequencies stays linear. In addition the 'resummed' results exhibit interesting patterns and properties, which we are going to discuss in the following.

The idea is to treat the truncated $\mathcal{O}(\gamma)$ differential equation for a specific field as its complete EoM and calculate exactly in γ henceforth. This is equivalent to computing all higher order corrections for certain quantities like QNM, which arise only from the $\mathcal{O}(\gamma)$-part of the underlying field's EoM and resum those contributions. The results obtained hereby should be interpreted carefully. In no way is it guaranteed that we get even close to the actual values at all orders in derivatives at very small λ, but since even higher derivative terms to the type IIb action are not explicitly known so far, this procedure gives the best results for small λ which are available at this point. In addition this procedure can be used to test how well behaved the first order corrections for certain λ values are:

If the truncated expansion $X_0 + \gamma X_1$ for the observable X is close to the actual quantity, which knows about all higher derivative corrections, for a given γ, then one can also expect the resummation to be close to the truncated expansion. If the resummed values differ noticeably from the first order corrected ones, meaning that the size of the partially resummed terms

$$\sum_{i=2}^{\infty} \gamma^i X_i, \tag{2.3.1}$$

obtained in the procedure explained above, is of the same order of magnitude as γX_1, then we cannot assume that the first order corrections are reliable at this γ-value.

2.3.1 A partial resummation of QNM frequencies

We follow a similar calculation as in 2.1.3.1. For a given value of $\hat{q}$ and γ using spectral methods we reduce (2.1.55) and (2.1.56) to a generalized eigenvalue problem for ω, as explained in (2.1.72)-(2.1.73), and repeat the calculation for points of a sufficiently

dense grid for γ. The endpoints of this curve are $\gamma = 0$ and $\gamma = \frac{\zeta(3)}{8}(11.3)^{-\frac{3}{2}}$, the latter of which corresponds to the value of λ naively obtained from the QCD-limit $\alpha_s = 0.3$ and $N = 3$.

For $\hat{q} = 1$ and $\hat{q} = 0$ these results are displayed in figure 2.12. Technically it is possible to go to very small values of λ ($\lambda \ll 1$). However, the exact size of the λ-interval in which the resummed poles still are reliable results is unclear, such that going to $\lambda = 11.3$ already is quite daring. Throwing all caution aboard and analyzing the resummed spectrum for values of $1 \gg \lambda$ makes the poles align near the real axis with very small but still negative imaginary part. The most interesting features of Figures 2.12 and 2.13 are that

- as the $\lambda \to \infty$ results, the resummed poles lie in a straight line, meaning the thermalization pattern stays unchanged here,
- the resummed results are noticeably closer to the $\lambda \to \infty$ QNM frequencies than the first order corrected ones as seen in picture 2.13. For small λ and for higher modes huge parts of the shift away from the zeroth order in γ, caused by the first order correction, seems to be canceled by the resummation of higher order terms,
- with the argument made in the discussion above, we conclude that the λ values chosen for the corrected poles in Figure 2.13 are too small for the first order correction to be reliable,
- the resummed poles stay in the lower half of the complex plane, even for very small values of λ, meaning that all modes have finite thermalization time, since every mode is damped over time,
- as Figure 2.12 shows, the resummed QNM frequency spectrum obtained at $\lambda \approx 11$, which corresponds to $\alpha_s = 0.3$, is not dramatically different from the infinite coupling results and still exhibits the same qualitative properties.

Apart from the QNM modes for gauge fields and their coupling corrections, we also have seen QNM spectra in the shear channel of the stress-energy correlator in the presence of a magnetic background field B in section 2.2.6 and without a background field in section 2.2.5. For the latter case the resummed results, obtained by truncating the differential equation given in the Appendix (5.6.1) and following the same steps as described above, are displayed in Figure 2.14. We find an analogous behaviour of the resummed poles in this channel, which are also positioned in a straight line, much closer to the infinite coupling results as the first order correction. The 't Hooft coupling λ is chosen to be 500 here.

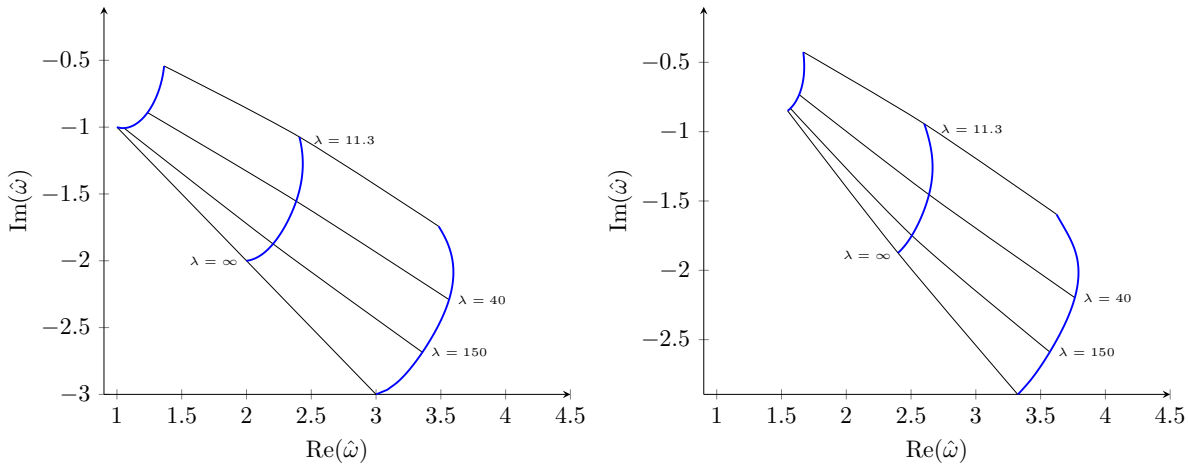

Figure 2.12: The flow of the first 3 EM-QNM frequencies, normalized by $2\pi T$, with the 't Hooft coupling between $\lambda = \infty$ and $\lambda = 11.3 \approx 4\pi\alpha_s N$, with $N = 3$ and $\alpha_s = 0.3$ computed in the resummation scheme [18, 19] with $\hat{q} = 0$ (left) and $\hat{q} = 1$ (right). The slopes of the curves at $\gamma = 0$ give the first order corrections 2.1.3.1.

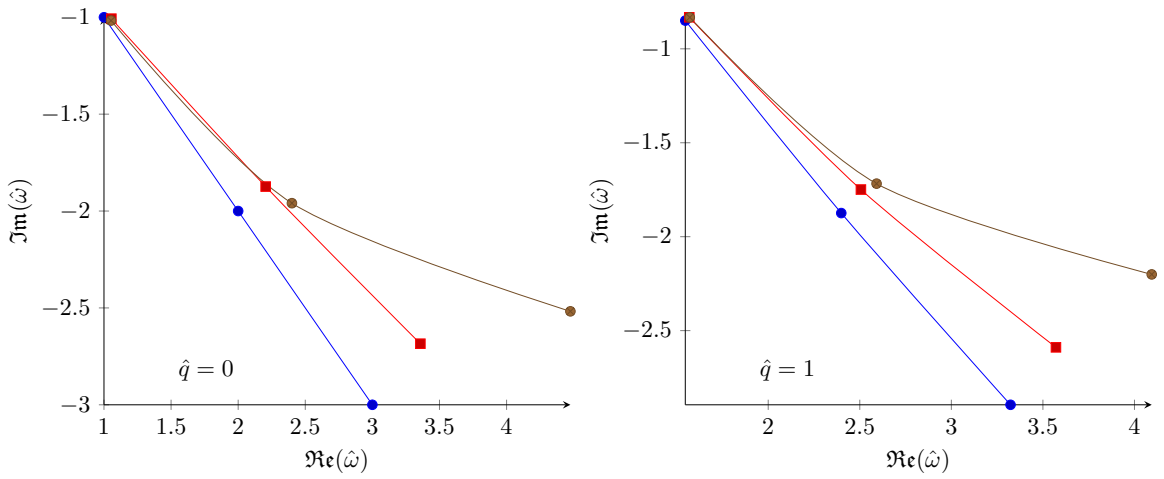

Figure 2.13: The first EM-QNM frequencies at $q = 2\pi T$ (right) and $q = 0$ (left) normalized by $2\pi T$ for $\lambda = \infty$ (blue) and their $\mathcal{O}(\gamma)$-corrections for $\lambda = 150$ (brown) and the resummed poles also taken at $\lambda = 150$ (red).

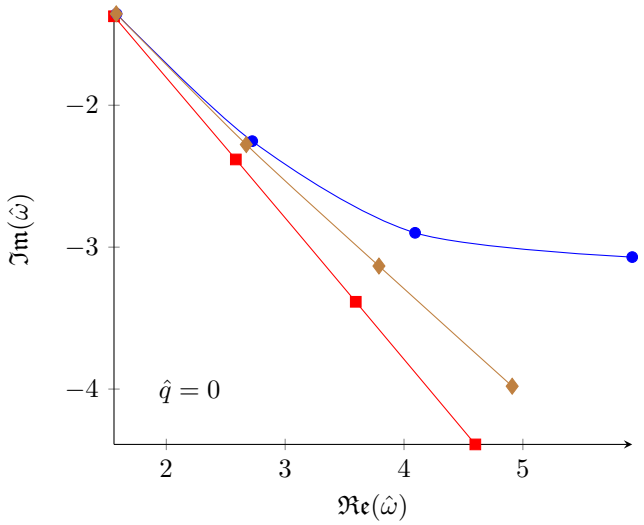

Figure 2.14: The first few QNM frequencies, divided by $2\pi T$, for the shear channel of the stress-energy correlator without background field, evaluated for $\hat{q} = 0$ and $\lambda = 500$. Results obtained by directly solving the QNM equation at this value of λ using spectral methods are shown as brown diamonds, while the red squares and blue circles show results truncated at zeroth and first order in γ, respectively. As before, lines merely serve to guide the eye.

In the case of a constant magnetic background field $B \approx 34.5T^2$ we found the first order correction of the lowest tensor QNM frequency to be one order of magnitude larger than in the case $B = 0$. Also the real part of the correction in the presence of a background field had a negative sign, unlike in the case $B = 0$. We now want to investigate how higher derivative resummations affect these trends. In analogy to the calculations above, we write the truncated EoM for h_{xy} as a generalized eigenvalue problem, which we solve for a set of γ values that correspond to $\lambda \in [11, \infty]$. The results are displayed in Figures 2.15-2.17. We find that the real part of the resummed pole starts decreasing with increasing γ, however, it quickly changes this behaviour and follows the same pattern as the $B = 0$ poles thereafter (compare left hand side of Fig. 2.15 with 2.16). The imaginary part of the resummed poles exhibits an interesting behaviour:

- For $B = 0$ it approaches zero with diverging γ, extremely small λ. This can be best seen in Figure 2.17. The absolute value of the imaginary part becomes extremely tiny as the 't Hooft coupling approaches 1, however, it stays non zero throughout the entire plotted interval.

- For a large background field $B \approx 34.5T^2$ the imaginary part also decreases monotonously, however converges towards -2.5, while λ is sent to 11. The point of convergence of the real part in this case is 2.5, which happens to be 2 times the magnetic field parameter $b = \frac{5}{4}$, we have chosen, such that the resummed QNM frequency converges to $2b(1 - i)$.

The interpretation of the first observation is rather clear: With a very small 't Hooft coupling and without any external fields there is nothing that drives equilibration. Thus, it is expected that the exact QNM frequency, that knows about all higher order terms, has a vanishing imaginary part for $\lambda \to 0$. Our resummed results reflect this expected trend.

The second observation is more surprising. As also reflected by the $\lambda \to \infty$ results, the magnetic background field decreases the equilibration time noticeably, meaning that it shifts the (negative) imaginary part to larger absolute values. However, the strong effect we are witnessing here is surprising. The explanation for this might lie in the γ-corrected relation between the magnetic field parameter b, which was held constant here, and the actual magnetic field, which could be obtained from a coupling corrected relation between the boundary geometry and the boundary stress energy tensor. It would not be bewildering, if this relation gives a divergent B for a divergent γ, meaning that the actual magnetic field we are dealing with at small λ is much larger than the $\lambda \to \infty$ estimate of $34.5T^2$. Another more physical interpretation of this is that a very strong magnetic background field forces the charged constituents of the QGP on

extremely small circles in the plane orthogonal to the field (which was chosen to be the z-direction). This, of course, damps x, y-oscillations of the QGP rather quickly, which is what we capture with considering the modes h_{xy}.

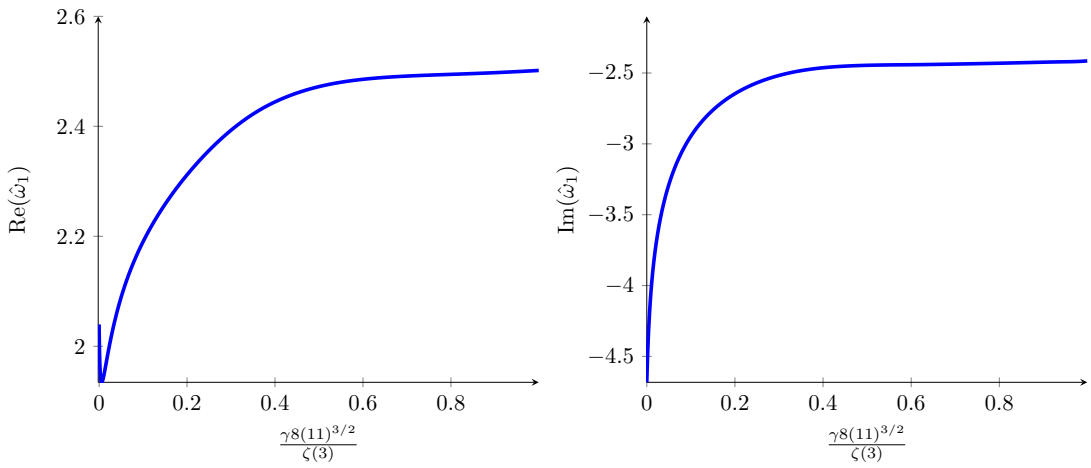

Figure 2.15: The coupling corrected and resummed imaginary and real part of the lowest QNM with $b = \frac{5}{4}$ and $q = 0$ averaged over different grid sizes and interval sizes. The maximal deviation from those suggest a negligible error for large λ, an error of $\approx 1\%$ for the imaginary part and $\approx 10\%$ for the real part for $\lambda \to 11$. Interestingly the average values as well as the curves for large M and large interval sizes $[l, k]$ converge for $\frac{\gamma 8(11)^{3/2}}{\zeta(3)} \to 1$, or $\lambda \to 11$ to $2b(1-i)$. The constant shape of the curve at small λ suggests that this is also the limit towards which the mode converges for $\lambda \ll 10$.

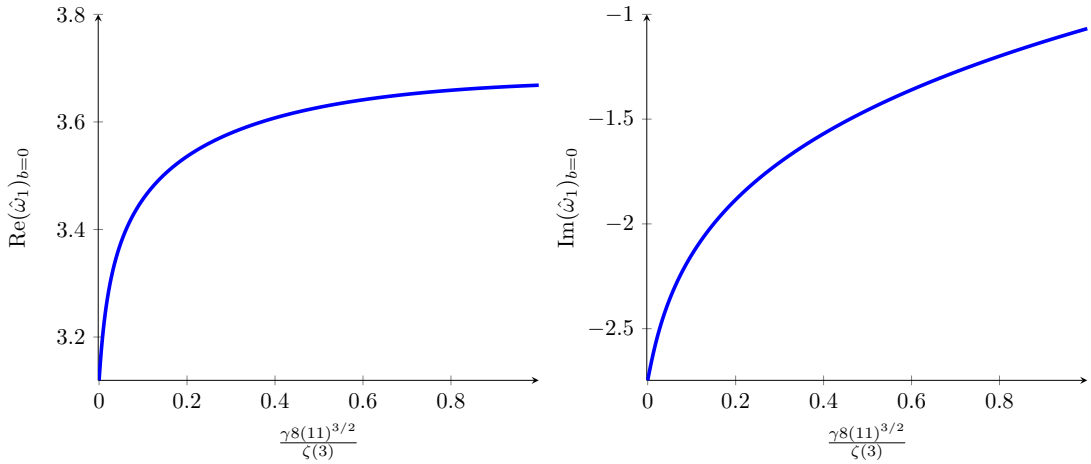

Figure 2.16: The coupling corrected and resummed imaginary and real part of the lowest QNM with $b = 0$ and $q = 0$ on the same γ-interval as the plots shown in figure (2.15). As in the $\lambda \to \infty$ limit [13] the magnetic background field decreases both the real part of the QNM frequencies and the equilibration time $\tau \propto -\frac{1}{\mathrm{Im}(\omega_1)}$.

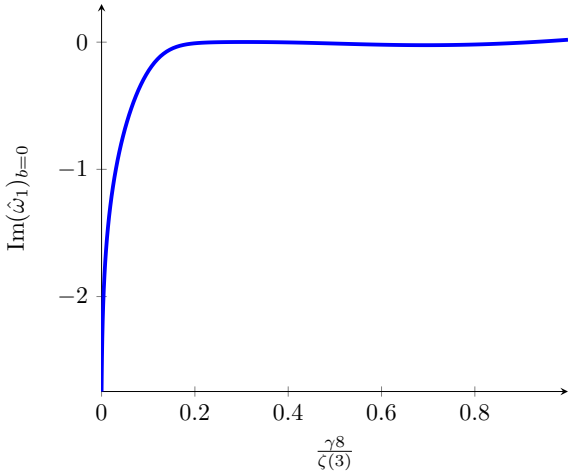

Figure 2.17: The imaginary part of the coupling correction resummed first QNM frequency for $b = 0$ on the γ-interval that corresponds to $\lambda \in [\infty, 1]$. Unlike in the case of $b = \frac{5}{4}$ the imaginary part becomes very small and approaches 0, reflecting that for weak interaction the equilibration time becomes extremely large.

2.3.2 The breakdown of the resummation technique and comparison with hot lattice QCD

Regarding the success of the resummation technique in decreasing the size of the corrections, it is interesting to quantify this improvement compared with the first order corrections. Therefore we consider and compare the λ values at which the correction to the infinite coupling results exceeds those. The results are displayed in Table 2.2 for the electromegnetic QNMs and in Table 2.3 for the shear QNMs.

	$\lambda_{\text{breakdown}}(\hat{q}=0)$		$\lambda_{\text{breakdown}}(\hat{q}=1)$	
k	$O(\gamma^1)$	resummed	$O(\gamma^1)$	resummed
1	139	≈ 22.5	57.1	< 5
2	382.2	≈ 21.7	195	≈ 8
3	767.5	≈ 21.3	437.2	≈ 14
4	1298	≈ 21.1	793.4	≈ 16

Table 2.2: Values of λ below which the deviation of the QNM frequency ω_k^{EM} from its $\lambda = \infty$ limit exceeds the $\lambda = \infty$ value. Respective columns show the results obtained using either the first order or resummed approximations for the QNM frequency.

	$\lambda_{\text{breakdown}}$	
k	$O(\gamma^1)$	resummed
1	27.6	< 2
2	71.2	< 3
3	135.5	< 4
4	220.6	< 4

Table 2.3: Values of λ below which the deviation of the QNM frequency ω_k^{shear} from its $\lambda = \infty$ limit exceeds the $\lambda = \infty$ value. Respective columns show the results obtained using either the first order or resummed approximations for the QNM frequency.

In addition we compare the coupling correction resummed conductivity, whose first order correction factor was determined to be $(1 + 125\gamma)$, with results from hot QCD lattice calculations[49]. For $\lambda = 11.3 \approx 4\pi N \alpha_s|_{N=3,\alpha_s=0.3}$ we obtain a resummed value of

$$\sigma = 0.29082 e^2 T. \tag{2.3.2}$$

This can be compared to results of hot QCD lattice calculations. For temperatures above T_c the authors of [56] found $\sigma \approx e^2 T(0.4 \pm 0.1)$. More recently this could be improved to $\sigma \approx e^2 T(0.31 \pm 0.05)$ for $T > 1.75 T_c$, see figure 10 in [57]. Without any coupling corrections the conductivity is given by

$$\sigma_\infty = \frac{9}{16\pi} e^2 T \approx 0.179 e^2 T. \tag{2.3.3}$$

In conclusion the coupling corrected and resummed result comes noticeably closer to hot-QCD lattice results.

[49] Caveat: The boundary field theory $\mathcal{N} = 4$ SYM plus the Maxwell action for $U(1)$ gauge fields at finite 't Hooft coupling, is not identical to QCD at high temperatures. Nonetheless it is worth investigating how far removed our boundary field theory from hot QCD really is.

Chapter 3

Numerical Simulations of dynamical processes in AdS/CFT

3.1 Simulating heavy ion collisions via (asymmetric) shockwave collisions in AdS_5

In this chapter we study asymmetric planar shockwave collisions in AdS_5 and the resulting hydrodynamic flow, which in the dual field theory gives collisions of planar shocks in a strongly coupled, maximally supersymmetric Yang-Mills theory. We will make extensive use of the introductory chapter 1.7, especially 1.7.1.

We aim at giving a didactic overview of how to build code to simulate gravitational shockwave collisions in AdS_5. In addition we are going to extend the work of [34–39] in particular the observation of "universal" flow with simple Gaussian rapidity dependence in the special case of symmetric collisions of planar shocks [33] to collisions involving asymmetric shockwidths.

Furthermore we are going to study the hydrodynamization time during asymmetric shockwave collisions and thereby address the question of how fast different sectors of the almond shaped QGP formed during a peripheral heavy ion collision reach a phase in which they can be described by relativistic hydrodynamics.

3.1.1 Motivation

The fluid 4-velocity u^μ of the QGP (as defined in (1.7.33)) during symmetric collisions of planar shockwaves turned out to be well described by boost invariant flow [33], meaning that

$$u^\tau = 1\,, \quad u^\xi = \boldsymbol{u}^\perp = 0\,, \tag{3.1.1}$$

on a hypersurface of constant proper time in the spacetime region, inside which hydrodynamics is applicable [50].

[50] With $ds^2 \equiv -d\tau^2 + \tau^2\, d\xi^2 + d\boldsymbol{x}_\perp^2$.

The rapidity distribution of the proper energy density inside this region was found to be well described by a Gaussian,

$$\epsilon(\xi, \tau_{\text{init}}) = \mu^4 \, A(\mu w) \, e^{-\frac{1}{2}\,\xi^2/\sigma(\mu w)^2} \,, \tag{3.1.2}$$

where ξ is the rapidity. The proper energy density ϵ is defined in (1.7.33) and as in section 1.7.2 we set

$$\widehat{T}^{\mu\nu} \equiv \frac{2\pi^2}{N_c^2} \, T^{\mu\nu} \,, \tag{3.1.3}$$

so that $\widehat{T}^{\mu\nu} \, u_\nu = -\epsilon \, u^\mu$. Introduced in (1.7.1), the energy scale μ is defined by the longitudinally integrated and rescaled energy density of one of the incoming shocks,

$$\mu^3 \equiv \int dz \, \widehat{T}^{00}(z \pm t)_{\text{incoming-shock}} , \tag{3.1.4}$$

which describes the energy per (transverse) unit area. It was found that both $\sigma(\mu w)$ and $A(\mu w)$ are given by simple, almost linear functions. One of our aims will be to generalize these results to the case of asymmetric collisions, where we choose to work in the center of momentum (CM) frame and find a model to describe the post collision flow for general collisions. Such a universal description would allow to approximate the proper energy density as a function of rapidity from a general formula of the incoming shock widths. Over a substantial range of incoming shock widths $\{w_+, w_-\}$ between $0.35/\mu$ to $0.075/\mu$, we find that the spacetime region in which hydrodynamics is applicable has little or no dependence on the shock widths, or their asymmetry, and only depends on the initial energy scale μ. Defining this region to be the largest connected subset of the forward lightcone, for which the hydrodynamic residual, defined in (3.1.61) is below 15%, we find that the boundary of the hydrodynamic region of validity remains at

$$\mu \, t_{\text{hydro}} \approx 2 \,, \tag{3.1.5}$$

even for highly asymmetric collisions.

Similarly, the fluid 4-velocity resulting from asymmetric collisions remains very close to ideal boost invariant flow (3.1.1), while the post-collision proper energy density ϵ remains well approximated by a Gaussian. It is important to note that the Gaussian fit of the proper energy density's rapidity distribution for asymmetric collisions is not as perfect as for symmetric ones. As a consequence we improved our model slightly, as discussed in section 3.1.5.2 in (3.1.69)- (3.1.72). However, up to small defects the simpler description (3.1.6)-(3.1.9) is a good approximation, as seen in Fig. 3.9.

The amplitude A, the shift of the maximum away from vanishing rapidity $\bar{\xi}$, and the width σ of the Gaussian rapidity dependence are now functions of both incoming

shock widths,

$$\epsilon(\xi, \tau_{\text{init}}) = \mu^4 \, A(\mu w_+, \mu w_-) \, e^{-\frac{1}{2}(\xi - \bar{\xi}(\mu w_+, \mu w_-))^2 / \sigma(\mu w_+, \mu w_-)^2} \, . \tag{3.1.6}$$

For asymmetric collisions, the outgoing energy density peaks at non-zero rapidity $\bar{\xi}$ which is well-described by

$$\bar{\xi}(\mu w_+, \mu w_-) \approx \Xi \, \frac{w_+ - w_-}{w_+ + w_-} \, , \tag{3.1.7}$$

where the coefficient Ξ is constant for $\tau > 2$ (as displayed below in Fig. 3.8) and has the value $\Xi \approx 7 \times 10^{-2}$. We find that the amplitude A is well-described by the geometric mean of the symmetric collision results

$$A(\mu w_+, \mu w_-) \approx \sqrt{A(\mu w_+) A(\mu w_-)} \, . \tag{3.1.8}$$

Shifting the symmetric proper energy density profiles by $\bar{\xi}$ shows that, in fact, the geometric mean of the shifted symmetric rapidity distributions themselves is a good approximation of the asymmetric profile within the shown ξ-interval. For the width this implies

$$\sigma(\mu w_+, \mu w_-) \approx \left[\tfrac{1}{2} \sigma(\mu w_+)^{-2} + \tfrac{1}{2} \sigma(\mu w_-)^{-2} \right]^{-1/2} \, . \tag{3.1.9}$$

As we will see in section 3.1.5 a more detailed universal description of the proper energy density distribution can be given. This even more accurate model involves the weighted geometric mean of the symmetric profiles. Given this extension to the previously found results for symmetric collisions, we now have the information needed for the starting conditions of the hydrodynamic flow resulting from collisions of projectiles with finite transverse extent, provided the transverse size of the incident projectiles is large compared to their (Lorentz contracted) longitudinal widths[51], so that spatial gradients in transverse directions are small compared to longitudinal gradients.

We consider the colliding system to be split up into subregions, which are independent on the time scale during which we study this highly relativistic collision, due to causal disconnection. In Fig. 3.1 we illustrate this process schematically. We assume each such "pixel" to have a size, which is small compared to the transverse extent of one of the Lorentz contracted heavy ions, but large compared to its longitudinal widths. For each pixel j we transform into its CM frame and evaluate its stress-energy tensor $T^{\mu\nu}(j)$ by using the result for the fluid velocity u^τ, $\mathbf{u}^\perp$ in (3.1.1) and our model describing the rapidity distribution of the proper energy density ϵ. Together with (1.7.34) this allows in future to reconstruct the entire stress energy tensor and thereby construct initial data for hydrodynamics for collision with non vanishing impact parameter, after

[51] Which is the case for highly Lorentz contracted nuclei.

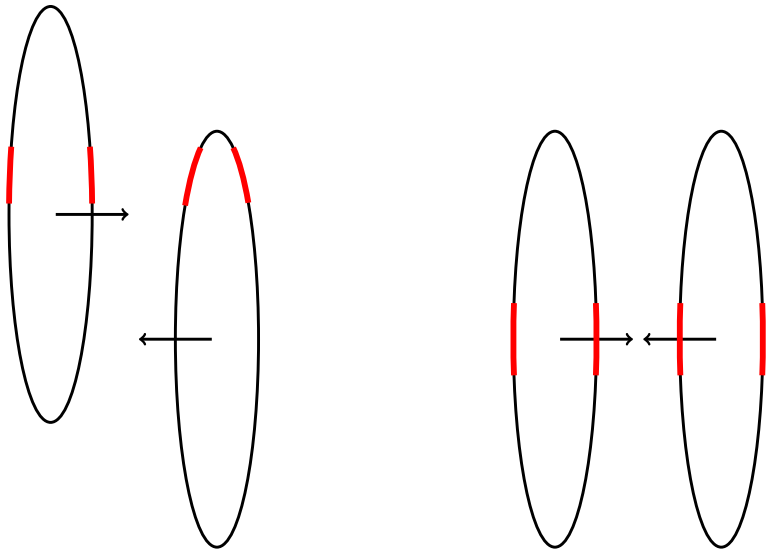

Figure 3.1: A simply graphic depiction of a heavy ion collision on the left with non vanishing impact parameter and on the right hand side with zero impact parameter. The red areas depict the "pixels" of causally disconnected subregions, in which we split the colliding system. The right hand side is covered by symmetric planar shock collisions [33]. Our formula describing the proper energy density distribution for general asymmetric collisions allows to also reconstruct the stress energy tensor $T^{\mu\nu}$ for the pixel displayed on the left, during a peripheral collision.

transforming back to the lab frame, without the need to perform 5D numerical relativity calculations, for each different setting. This procedure, based on planar shock results, should be viewed as the first term in an expansion in (small) transverse gradients. It would, of course, be interesting to derive, systematically, subsequent terms in this expansion.

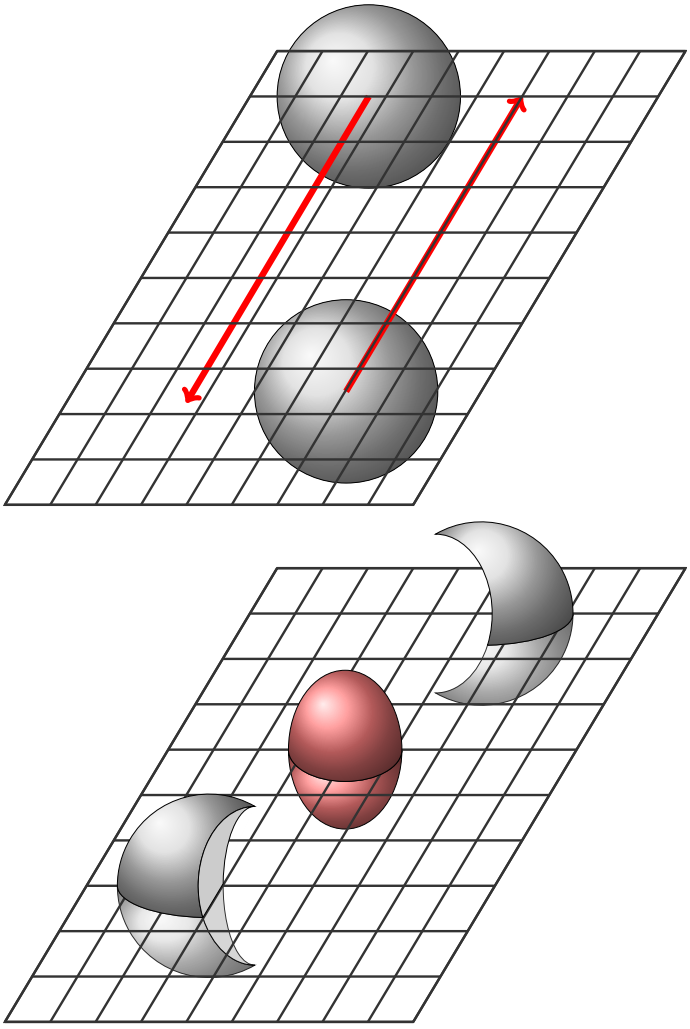

Figure 3.2: Sketch of a peripheral heavy ion collision. The almond shaped overlap region forms a quark-gluon plasma, not the spectator portions (shown in gray). The hydrodynamization time increases rapidly as one approaches the boundary of the overlap region, whose shape influences the value of the experimentally measured elliptic flow parameter v_2.

3.1.2 Computational strategy

In section 1.7.1 in particular in (1.7.10)-(1.7.16) we have derived the Einstein equations in Eddington-Finkelstein coordinates in their nested form. As discussed in 1.7 we can use the formula (1.6.20) to derive boundary conditions, that uniquely specify the bulk metric corresponding to a certain choice of the stress energy tensor in the boundary field theory in flat Minkowski space. Using the near boundary expansion of the metric components in EF-coordinates given in table 3.1 explicitly shows, where the boundary stress enters: $-a^{(4)}$, the forth order near boundary expansion coefficient of A is proportional to the energy density, $-f^{(4)}$ to the momentum density and $\hat{g}_{ij}^{(4)} - 1/2a^{(4)}$ to

field	asymptotic homogeneous solution(s)	boundary behaviour
Σ	r^1 and r^0	$\Sigma \sim r + \lambda$
F_i	r^2 and r^{-2}	$F_i \sim -\partial_i \lambda + f_i^{(4)} r^{-2}$
$d_+\Sigma$	r^{-2}	$d_+\Sigma \sim \frac{1}{2}(r+\lambda)^2 + a^{(4)} r^{-2}$
$d_+\hat{g}_{ij}$	$r^{-3/2}$	$d_+\hat{g}_{ij} \sim 0$
A	r^1 and r^0	$A \sim \frac{1}{2}(r+\lambda)^2 - \partial_t \lambda$

Table 3.1: Homogeneous solutions and asymptotic behaviour of the different fields.

the pressure. We have derived the precise relation in (1.7.22). We will use the relation (1.7.31) to determine the shift λ on each timeslice, which transforms the radial domain of integration into the interval [r =horizon, r =boundary]. For a single shock we already have a solution given by (1.7.2). The simple sum of two single shocks moving in opposite directions is not a solution to the Einstein equations. However, at a timeslice, on which they are sufficiently spatially separated, we can use their superposition as an almost perfect approximation to a solution inside our domain of integration. After a coordinate transformation to the EF metric (1.7.4), this gives $a^{(4)}$, $f^{(4)}$, $\hat{g}_{ij}$ and λ on a starting timeslice, on which we choose the left ($-$) and right ($+$) moving shockwaves sufficiently far separated such that $a_+^{(4)}, a_-^{(4)}$; $f_+^{(4)}, f_-^{(4)}$; $(\hat{g}_{ij})_+, (\hat{g}_{ij})_-$; λ_+, λ_- have minimal overlap[52]. Having determined the corresponding solution to (1.7.10)-(1.7.16) on this slice, we need an algorithm to update the boundary conditions, in order to solve these equations on the following ones. Knowing $\hat{g}_{ij}$, A and $d_+\hat{g}_{ij}$ allows us to update the spatial part of the metric via

$$\partial_t \hat{g}_{ij} = d_+ \hat{g}_{ij} - A \partial_r \hat{g}_{ij}. \tag{3.1.10}$$

The stationary horizon condition (1.7.32) provides the update for λ whereas the temporal derivatives of $a^{(4)}$ and $f^{(4)}$ can be derived from the conservation law of the stress energy tensor $\nabla^\mu \langle T_{\mu\nu} \rangle = 0$[53], it follows

$$\partial_t a^{(4)} = \frac{3}{2} \partial_i f_i^{(4)} \qquad \partial_t f_i^{(4)} = \frac{1}{2} \partial_i a^{(4)} - \partial_i \hat{g}_{ij}. \tag{3.1.11}$$

3.1.3 Planar shocks in Fefferman-Graham and Eddington Finkelstein coordinates

We have described how to sequentially solve Einstein's equations once we have transformed the FG-coordinate version (1.7.2) of the single shockwave metric to EF-coordinates.

[52] There is a subtlety regarding the superposition of λ_+ and λ_-, which we are going to discuss in detail in section 3.1.4.

[53] Which in turn follows from the Einstein equations.

The details of this transformation are addressed in section 3.1.4. Here we are discussing the needed ingredients of this transformation. It is so far not possible to write down a metric of shocks with arbitrary shape in EF form (1.7.4) analytically. On the other hand it is not possible to evolve a metric describing two colliding shocks forward in time in FG coordinates, which makes this tedious transformation necessary. In FG coordinates the metric for a generally formed shockwave can be written as

$$ds^2 = \tilde{\rho}^{-2}\left(-d\tilde{t}^2 + d\tilde{\mathbf{x}}_\perp^2 + d\tilde{z}^2 + d\tilde{\rho}^2 + h_\pm(\tilde{\mathbf{x}}_\perp, \tilde{x}_\mp, \tilde{\rho})d\tilde{x}_\pm^2\right) \tag{3.1.12}$$

with shock function $h_\pm$ describing left $(-)$ and right $(+)$ moving shocks. Since this metric has to satisfy the vacuum Einstein's equations we get the condition

$$\left(\partial_{\tilde{\rho}}^2 - \frac{3}{\tilde{\rho}}\partial_{\tilde{\rho}} + \nabla_\perp^2\right) h_\pm = 0 \quad . \tag{3.1.13}$$

Here we are going to consider planar shocks, which are infinitely extended in the $\mathbf{x}_\perp$ directions and do not depend on $\mathbf{x}_\perp$. With this assumption we can easily write down a solution to the differential equation (3.1.12) given by

$$h_\pm(\tilde{t}, \tilde{\mathbf{x}}, \tilde{\rho}) = \tilde{\rho}^4 h_\pm(\tilde{x_\pm}) \tag{3.1.14}$$

for any function $h_\pm$. To obtain equations for the coordinate transformation we first parameterize the FG coordinates for shocks moving in the $+z$ direction in a convenient way, given by

$$\begin{aligned} \tilde{t} &= t + u + \alpha(t-z,u) \quad , \quad \tilde{\mathbf{x}}_\perp = \mathbf{x}_\perp \quad , \\ \tilde{z} &= z - \gamma(t-z,u) \quad , \quad \tilde{\rho} = u + \beta(t-z,u) \end{aligned} \tag{3.1.15}$$

where u is the inverse radial coordinate, i.e. $u \equiv \frac{1}{r}$. Thus the boundary theory lives at $u = 0$. We solve for the functions α, β and γ by considering a congruence of infalling null geodesics in EF coordinates, and requiring that the image of this congruence fulfills the geodesic equation in FG coordinates. It is easy to see from (1.7.4) that the curve parametrized by (t_0, x_0^i, r) with affine parameter r and fixed t_0 and x_0^i is in fact a null geodesic in the (infalling) EF coordinates. Let us denote this curve by $X^\mu(r)$. The requirement that the same path in FG coordinates $\tilde{Y}(X(r))$ satisfies the geodesic equations as well reads

$$\frac{d^2\tilde{Y}^A}{dr^2} + \tilde{\Gamma}^A_{BC}\frac{d\tilde{Y}^B}{dr}\frac{d\tilde{Y}^C}{dr} = 0 \tag{3.1.16}$$

with the connection $\tilde{\Gamma}$ calculated with respect to the FG coordinates. We found it advantageous to work with the redefined functions α, β, γ now expressed by ζ, γ, δ as[54]

$$\alpha = -\gamma + \beta + \delta \quad , \quad \beta = -\frac{u^2\zeta}{1+u\zeta} \quad . \tag{3.1.17}$$

As can be seen from the derivation from [34] we obtain the following differential equations for the coordinate transformation

$$\begin{aligned} &\frac{1}{u^2}\frac{\partial}{\partial u}\left(u^2\frac{\partial\zeta}{\partial u}\right) + \frac{2uH}{(1+u\zeta)^5} = 0 \quad , \quad \frac{\partial\delta}{\partial u} - \frac{u^2}{(1+u\zeta)^2}\frac{\partial\zeta}{\partial u} = 0 \\ &\frac{\partial\gamma}{\partial_u} - \frac{u^2}{(1+u\zeta)^2}\frac{\partial\zeta}{\partial u} + \frac{u^4}{2(1+u\zeta)^2}\left(\frac{\partial\zeta}{\partial u}\right)^2 + \frac{u^4 H}{2(1+u\zeta)^6} = 0 \end{aligned} \tag{3.1.18}$$

with $H = h_+\left(t - z + u + \delta - u^2\zeta/(1+u\zeta)\right)$.
To apply the time evolution scheme described in the last sections we have to extract the initial values $\{\hat{g}_+, f^{(4)}_{z+}, a^{(4)}_+, \lambda_+\}$. First we parametrize the spatial metric $\hat{g}$ by [34]

$$\hat{g}_{ij} = \begin{pmatrix} e^B & 0 & 0 \\ 0 & e^B & 0 \\ 0 & 0 & e^{-2B} \end{pmatrix} \tag{3.1.19}$$

where we introduced the anisotropy function B which behaves as $B = u^4 b^{(4)} + \mathcal{O}\left(u^5\right)$ near the boundary (see table 3.1). From the required form of the EF metric (1.7.4) and the near boundary asymptotics (1.7.19) we then can extract the required data which are given by

$$a^{(4)}_+ = -\frac{2}{3}h_+ \quad , \quad f^{(4)}_{z+} = h_+ \quad , \quad \lambda_+ = -\frac{1}{2}\partial_u^2\beta\big|_{u=0} \quad . \tag{3.1.20}$$

From the requirement that the line elements in EF and FG coordinates coincide and the fact that

$$\left(\tilde{\rho}^2 h(\tilde{t}-\tilde{z}) - \frac{1}{\tilde{\rho}^2}\right)d\tilde{t}^2 \to \left(\frac{\partial\alpha}{\partial z}\right)^2\left((u+\beta)^2 H - \frac{1}{(u+\beta)^2}\right)dz^2 + \dots \tag{3.1.21}$$

$$\frac{1}{\tilde{\rho}^2}d\tilde{\rho}^2 \to \left(\frac{\partial\beta}{\partial z}\right)^2\frac{1}{(u+\beta)^2}dz^2 + \dots \tag{3.1.22}$$

[54] We checked our calculation by performing the coordinate transformation using α, β, γ as the functions to solve for as well.

$$\left(\tilde{\rho}^2 h(\tilde{t}-\tilde{z})+\frac{1}{\tilde{\rho}^2}\right)d\tilde{z}^2 \to \left(1-\frac{\partial\gamma}{\partial z}\right)^2\left((u+\beta)^2 H+\frac{1}{(u+\beta)^2}\right)dz^2+\dots \tag{3.1.23}$$

$$-2\tilde{\rho}^2 h(\tilde{t}-\tilde{z})d\tilde{z}d\tilde{t} \to -2(u+\beta)^2\left(\frac{\partial\alpha}{\partial z}\right)\left(-\frac{\partial\gamma}{\partial z}+1\right)H dz^2+\dots \tag{3.1.24}$$

we obtain

$$\left((u+\beta)^2(1-\partial_z\alpha-\partial_z\gamma)^2 H+\frac{-(\partial_z\alpha)^2+(\partial_z\beta)^2+(1-\partial_z\gamma)^2}{(u+\beta)^2}\right) \tag{3.1.25}$$

as the part of the line element of the metric in EF coordinates proportional to dz^2. Comparing this with

$$\frac{1}{\tilde{\rho}^2}d\tilde{x}^2,\ \frac{1}{\tilde{\rho}^2}d\tilde{y}^2 \to dx^2\frac{1}{(u+\beta)^2},\ dy^2\frac{1}{(u+\beta)^2}$$

results in

$$e^{-3B}=\Big((u+\beta)^4(1-\partial_z\alpha-\partial_z\gamma)^2 h_+(t-z+u+\gamma+\alpha)-(\partial_z\alpha)^2+(\partial_z\beta)^2+(1-\partial_z\gamma)^2\Big). \tag{3.1.26}$$

The anisotropy function can be read off to be

$$B_+=-\frac{1}{3}\log\left[-(\partial_t\alpha)^2+(\partial_t\beta)^2+(1+\partial_t\gamma)^2+(u+\beta)^4(1+\partial_t\alpha+\partial_t\gamma)^2 h_+\right]. \tag{3.1.27}$$

For numerical stability we will not use B_+ but $b_+\equiv\frac{B_+}{u^3}$ in the time evolution scheme. In the next section we will discuss technical details of how to actually implement this in the code.

3.1.4 Software construction

3.1.4.1 Transformation to infalling coordinates

As explained in [34] and the previous section, one can determine the coordinate transformation from FG-coordinates to EF-coordinates by solving for the congruence of infalling geodesics in FG-coordinates. Equivalently one can bring the equations of motions determining the coordinate transformation into the analytically simplified form (3.1.18). We implemented both sets of differential equations and found both of similar difficulty to handle numerically. Let us focus on (3.1.18) as the system of differential equations we wish to solve in the following.

We will perform the coordinate transformation only for right moving shocks and thus drop the index + in this chapter and define $b:=b_+$, $h:=h_+$, and so on. Since we

consider planar shocks, h only depends on $\tilde{t}-\tilde{z}$. Its general form is given by

$$h(x)=\mu^3\frac{1}{\sqrt{2\pi w^2}}e^{-\frac{x^2}{2w^2}}. \tag{3.1.28}$$

Using the ansatz given in (3.1.17) allows us to analyze the near boundary behaviour[55] of the functions α, β and γ. Defining $\beta=-u^2\tilde{\beta}$, $\alpha=u\tilde{\alpha}$, $\gamma=u^4\tilde{\gamma}$ and $\tilde{\beta}|_{u=0}=\tilde{\beta}_0$ we found for

$$\tilde{\beta}|_{\tilde{\beta}_0=0}=u^3\sum_{i=0}^{\infty}b_iu^i \quad , \quad \tilde{\alpha}|_{\tilde{\beta}_0=0}=u^4\sum_{i=0}^{\infty}a_iu^i \quad , \quad \tilde{\gamma}|_{\tilde{\beta}_0=0}=u\sum_{i=0}^{\infty}g_iu^i \tag{3.1.29}$$

the following expansions for arbitrary β_0

$$\tilde{\beta}=\sum_{i=1}^{\infty}(-u)^{i-1}\tilde{\beta}_0^i-u^3\sum_{i=0}^{\infty}b_iu^i\sum_{j=-1}^{\infty}\binom{5+j+i}{1+j}\tilde{\beta}_0^{1+j}(-u)^{1+j} \tag{3.1.30}$$

$$\tilde{\alpha}=\sum_{i=1}^{\infty}(-u)^{i}\tilde{\beta}_0^i-u^4\sum_{i=0}^{\infty}a_iu^i\sum_{j=-1}^{\infty}\binom{5+j+i}{1+j}\tilde{\beta}_0^{1+j}(-u)^{1+j} \tag{3.1.31}$$

$$\tilde{\gamma}=u\sum_{i=0}^{\infty}g_iu^i\sum_{j=-1}^{\infty}\binom{5+j+i}{1+j}\tilde{\beta}_0^{1+j}(-u)^{1+j}. \tag{3.1.32}$$

The coefficients $\{a_i\}_{i\in\{0,\dots,15\}}$, $\{b_i\}_{i\in\{0,\dots,15\}}$ and $\{g_i\}_{i\in\{0,\dots,15\}}$ are given in Appendix 5.7. Here the parameter $\tilde{\beta}_0$ corresponds to the radial shift $\delta\lambda$.

The idea is to solve the coordinate transformation using spectral methods, domain decomposition and a relaxation algorithm (e.g. Newton-Raphson) to determine α, β and γ, or respectively δ, α, ζ on a Fourier-grid in z-direction and a Gauss-Lobatto grid in u-direction. The integration depth $\rho_{\max}$ is determined by $\tilde{\beta}_0$ and the length of the u-grid. For a background energy density (BED) of 5-10% of the peak value (which can be simply added to $-a^{(4)}$) it is sufficient to choose $\tilde{\beta}_0=0$ and apply a numerical integrator with adaptive step-size to integrate into the bulk as deep as possible.

The regular singular point at the boundary forbids to solve the system (3.1.18) with the help of a numerical integrator starting at the boundary. In principle, we could solve (3.1.18) close to the boundary with the help of expansion (3.1.30)-(3.1.32) and hand the outcome at $u=\epsilon\ll 1$ to an adaptive Runge-Kutta algorithm (see Appendix 5.8) to determine α, β, γ deep in the bulk. For a higher numerical precision, we solved the metric using spectral functions on a starting interval (spanning from the boundary to a depth u_{max}) in the radial coordinate u and used a numerical integrator to determine the transformation functions deeper into the bulk.

We computed collisions of different widths with various BEDs (see table 3.2). Here

[55] We used Dirichlet boundary conditions here and chose the leading near boundary coefficients of the transformation functions to vanish.

we exemplarily describe two settings, one with a relatively large BED ϵ_0 of 10% and a small BED of 1% of the peak value. The latter is needed for the extrapolation to $\epsilon_0 = 0$ in order to be able to compare our results with hydrodynamics and test, whether the interesting features regarding the proper energy density found of [33] can be extended to the asymmetric case.

$$\text{In the case of } \begin{cases} \textbf{I.}\ 10\%\ \text{background energy density and } \tilde{\beta}_0 = 0 \text{ we define} \\ \delta = u^5 \sum_{i=0}^{2} d_i u^i + u^8 \tilde{\delta},\ \zeta = u^3 \sum_{i=0}^{2} z_i u^i + u^6 \tilde{\zeta},\ \gamma = u^5 \sum_{i=0}^{2} g_i u^i + u^8 \tilde{\gamma} \\ \\ \textbf{II.}\ 1\%\ \text{background energy density and } \tilde{\beta}_0 \neq 0 \text{ we define} \\ \delta = u^3 \tilde{\delta},\ \zeta = \tilde{\zeta},\ \gamma = u^3 \tilde{\gamma}, \end{cases} \tag{3.1.33}$$

where the coefficients $\{d_i\}$, $\{z_i\}$ and $\{g_i\}$ can be computed from those in Appendix 5.7. In principle the approach **II.** can also be applied to the case of a large BED, but it is difficult to apply approach **I.** to the small BED case.

The aim is to solve the resulting EoM equations for $\tilde{\delta}$, $\tilde{\zeta}$ and $\tilde{\gamma}$ in each case. Since we are dealing with a highly non-linear system of differential equations we will have to apply a root finding routine, if we want to make use of spectral methods. For this purpose we define $c_i(x)$ to be the i-th cardinal function corresponding to the Gauss-Lobatto grid

$$\left\{ -\cos\left(\frac{n\pi}{M}\right) \right\}_{n\in\{0,\dots,M\}}, \tag{3.1.34}$$

such that the function $c_i(2\frac{u}{u_{\max}} - 1)$ is well defined on the interval $u \in [0, u_{\max}]$. Assuming that $\tilde{\delta}$, $\tilde{\zeta}$, $\tilde{\gamma}$ live on this interval, we can approximate

$$X = \sum_{i=0}^{M} a_i^X c_i\left(2\frac{u}{u_{\max}} - 1\right) \tag{3.1.35}$$

for $X \in \{\tilde{\delta}, \tilde{\zeta}, \tilde{\gamma}\}$. Although a single grid isn't enough for thinner shocks, we will first discuss this easier case and generalize the following procedure to multi-domain-grids hereafter. The requirement that the first equation of (3.1.18) vanishes on all $M+1$ grid points gives $M+1$ equations for the $3M+3$ coefficients $\{a_i^X\}_{i\in\{0,\dots,M\}, X\in\{\tilde{\delta},\tilde{\zeta},\tilde{\gamma}\}}$, while derivatives are replaced by multiplications of the coefficient-vectors $(a_i^X)_{\text{ß}\in\{0,\dots,M\}}$ with the derivative matrix $-\frac{2}{u_{\max}} A(M+1)$ [56] defined in (5.9.13) for $M+1$ grid points. Together the differential equations (3.1.18) with the right boundary conditions lead to

[56] The minus sign arises due to the different conventions regarding the definition of the Gauss Lobatto grid. In literature the definition given in the Appendix is more common. For our purposes the definition given in (3.1.34) is more convenient.

a non linear system of $3M+3$ equations for the coefficients

$$\{a_i^X\}_{i\in\{0,\dots,M\},X\in\{\tilde{\delta},\tilde{\zeta},\tilde{\gamma}\}}, \tag{3.1.36}$$

of which the n-th line corresponds to the requirement that the $\lceil\frac{n}{M+1}\rceil$-th equation holds at the $(n-(M+1)\lfloor\frac{n}{M+1}\rfloor)$-th grid point. The boundary conditions in each case are given by

$$\begin{cases} \textbf{I. } \tilde{\zeta}|_{u=0}=z_3,\ \partial_u\tilde{\zeta}|_{u=0}=z_4,\ \tilde{\delta}|_{u=0}=d_3,\ \tilde{\gamma}|_{u=0}=g_3 \\ \textbf{II. } \tilde{\zeta}|_{u=u_{\max}}=0,\ \partial_u\tilde{\zeta}|_{u=0}=0,\ \tilde{\delta}|_{u=0}=0,\ \tilde{\gamma}|_{u=0}=0, \end{cases} \tag{3.1.37}$$

where **I** and **II** refer to the cases introduced in (3.1.33). Since the boundary is a regular singular point [34], we don't need more than those[57]. We implement them into our system of non-linear equations by deleting the respective line and replacing it with the equation enforcing the desired boundary condition. For instance in the case of $\tilde{\zeta}|_{u=0}=z_3$, we delete the first line of the block of equations in our system corresponding to the requirements that the first equation of (3.1.18) vanishes at each grid point and replace it with

$$a_0^{\tilde{\zeta}}=z_3. \tag{3.1.38}$$

Now we approximate our functions with cardinal functions on a multi-domain-grid containing s domains with $M+1$ grid points each

$$\left\{-\frac{u_{\max}}{2s}\cos\left(\pi n/(M)\right)+u_{\max}\frac{2k-1}{2s}\right\}_{n\in\{0,\dots,M\},k\in\{1,\dots,s\}} \tag{3.1.39}$$

stretching from $u=0$ to $u=u_{\max}$. We again obtain a system of $3s(M+1)$ equations, where four lines have to be replaced with the right boundary conditions corresponding to (3.1.37). The differentiation matrix becomes block-diagonal and we have to guarantee continuity of the functions $\tilde{\zeta}$, $\tilde{\gamma}$ and $\tilde{\delta}$ and their first derivatives at the domain walls. We do this by replacing the first and last line of the second to the last domain and the last line of the first domain with the right linear equation for each differential equation, which together enforce the continuity of our functions and their derivatives[58].

[57] Notice that the requirement that we can expand $\tilde{\zeta}$, $\tilde{\delta}$ and $\tilde{\gamma}$ in cardinal functions already decreases the size of the Hilbert space of solutions to the coordinate transformation.

[58] There was a subtlety involving the choice of which row to replace, if we would not require the continuity of derivatives: Relative to a given interior subdomain endpoint, one row approximates u derivatives using information on one side of the endpoint, while the other row approximates u derivatives using information on the other side. Since the behavior of the transformation functions is fixed, and known, at the $u=0$ boundary, one should regard the transformation equations as describing the propagation of information from the boundary into the bulk. Consequently, one should retain the row corresponding to the end of the domain closer to the boundary and replace the first grid point corresponing to the next domain deeper in the bulk.

We define our numerical collision experiment to happen in a finite spatial box stretching from $z \in [-z_0, z_0]$ and use a Fourier grid on this interval. The details of Fourier (cardinal) methods are explained in Appendix 5.9. We solve the system of equations z-slice for z-slice at $t = 0$ in order to obtain the single shock metric in EF-coordinates at this time slice on the Fourier-grid-points

$$\left\{ -z_0 + \frac{2z_0 k}{N} \right\}_{k\in\{0,\dots,N-1\}}, \tag{3.1.40}$$

for which the point z_0 is identified with $-z_0$. Again by using (pseudo-) spectral methods and approximating the solutions by their projections on a finite dimensional Hilbert space, tailored to the respective problem and spanned by the respective cardinal functions, we can approximate the exact derivatives of functions on this interval at the grid points with the discrete values obtained from the multiplication of the Fourier-grid-derivative-matrix $\frac{z_0}{\pi} A_f$ with the N-vector obtained by evaluating this function at the corresponding grid points. We justify the expansion in Fourier cardinals, which require periodicity of the expanded functions, by the observation that they are vanishing at z_0 and $-z_0$ for sufficiently large z_0 (and thus clearly periodic).

The system of equations for the expansion coefficients of the approximation of $\tilde{\zeta}$, $\tilde{\gamma}$, $\tilde{\delta}$ in Chebyshev cardinal functions on a given z-slice is then computed via a multi dimensional Newton-iteration.
Realistic parameters in the symmetric case are for **I.** e.g. $u_{\max} = 1.2$, $z_0 = 8$, $s = 14$, $N = 640$ and $M = 12$ for a shock width $w = 0.1$. In the case **II.** we used $u_{\max} = 2$, $z_0 = 8$, $s = 22$, $N = 960$ and $M = 12$ for a shock width of $w = 0.075$. If we would be satisfied with a background energy density of $\epsilon_0 \approx 20\%$ of the peak value, the depth $1.2 + \beta|_{u=1.2}$ would be sufficient to find the horizon within the region of the manifold, where we already solved the coordinate transformation. Since we want to reduce the BED as far as possible, we integrate further into the manifold applying a Runge-Kutta-double-step integrator as explained in Appendix 5.8. For simplicity we choose to integrate to a fixed u value not to a fixed $\tilde{\rho}$ value. This ties our hands regarding the maximal depth we can reach for the moment, but as it turns out this is sufficient for the settings we are interested in. Having obtained a solution to the coordinate transformation we now can use equations (3.1.20) and (3.1.26) to determine B, λ, $f^{(4)}$ and $a^{(4)}$ [59] on the $t = 0$ time slice. This gives us the a single shock solution in EF coordinates on a Fourier grid in spatial and a (multi-domain) Chebyshev grid in radial direction. The shock peaks (on the time slice $t = 0$) at the longitudinal coordinate $z = 0$ moving to the right (in positive z-direction) with the speed of light. The solution to a left moving shock at the same time and spatial coordinate would

[59] A finite ϵ_0 of x per cent of the peak value is achieved by shifting $a^{(4)}$ by $-\frac{3}{2}\frac{x}{100}\max(h(t-z))$.

simply correspond to

$$\{B(u,t-z),a^{(4)}(t-z),f^{(4)}(t-z),\lambda(t-z)\}\rightarrow\{B(u,t+z),a^{(4)}(t+z),-f^{(4)}(t+z),\lambda(t+z)\}. \tag{3.1.41}$$

We now want to set up the starting configuration of two shocks separated by a distance $\Delta z/2 = 2$ for broad, $\Delta z/2 = 1$ for thin and $\Delta z/2 = 1.5$ for asymmetric shocks at the time slice $t_0 = -\Delta z/2$ such that they have negligible overlap. As shown in [34] there will always be a region for which the superposition of a right moving and a left moving shock overlap inside the bulk no matter how far they are separated on the boundary. Inside this region a simple superposition of spatially separated shocks will not be a solution to the Einstein equations. However, one can show that this region lies inside the horizon for a sufficiently large spatial separation of the two shocks on the boundary. Being causally disconnected from the section of the manifold, where

$$B_{\text{total}}(u,t_0,z) = B(u,t_0-z)+B(u,t_0+z) \tag{3.1.42}$$

$$a^{(4)}_{\text{total}}(t_0,z) = a^{(4)}(t_0-z)+a^{(4)}(t_0+z) \tag{3.1.43}$$

$$f^{(4)}_{\text{total}}(t_0,z) = f^{(4)}(t_0-z)-f^{(4)}(t_0+z) \tag{3.1.44}$$

$$\lambda_{\text{total}}(t_0,z) = \lambda(t_0-z)+\lambda(t_0+z) \tag{3.1.45}$$

does not solve the Einstein equations, we are allowed to use this ansatz for the total functions corresponding to two shocks moving towards each other with the speed of light, separated by $\Delta z = -2t_0$ on the starting time slice t_0. One problem with this starting configuration remains to be fixed: The overlap of the shift functions $\lambda_\pm$ of the left and right moving shocks in the region close to $z = 0$ is significant. All other functions have negligible overlap. Since we choose the shocks on the first time slice well separated, we can assume that the geometry in between is pure AdS, which justifies to modify λ_{total} close to $z = 0$, without changing $B_{\text{total}}, a^{(4)}_{\text{total}}, f^{(4)}_{\text{total}}$. Thus, we set

$$\lambda_{\text{total}}(t_0,z) = \theta(-z)\lambda(t_0-z)+\theta(z)\lambda(t_0+z) \tag{3.1.46}$$

with

$$\theta(z) = \frac{1}{2}\left(1-\text{erf}\left(\frac{-z}{\sqrt{2}w}\right)\right). \tag{3.1.47}$$

For thin shockwave collisions of low BED we found it to be helpful to apply additional filtering techniques, which are explained in the second part of Appendix (5.11). The starting configuration $\{B, a^{(4)}, f^{(4)}, \lambda\}$ is filtered in z direction, while B is also filtered in u-direction using a method explained in (5.11). On each time slice of the evolution we additionally filter the final results in z-direction.

3.1.4.2 Finding the horizon

The final remaining task, before we can start the time evolution of the geometry, is to find the horizon on the first time slice and adjust λ accordingly, such that the shifted radial coordinate lies in the interval $u \in [\text{boundary}, \text{horizon}]$. As explained in section 1.7.1 and [34],[32], the horizon can be determined as the hypersurface on which the expansion rate $\nabla_\mu k^\mu$ of the congruence of outgoing geodesics vanishes (restricted to a specific time slice $t = const.$). In our specific case this means

$$0 = d_+\Sigma + \frac{e^{2B}}{6\Sigma^2}\left(3F^2\,\partial_r\Sigma + 2\Sigma\,\partial_z F + 4F\,\Sigma\,\partial_z B + 2F\,\partial_z\Sigma\right)\Big|_{r=r_h}. \tag{3.1.48}$$

Herewith we wish to determine the radial shift $\delta\lambda(t,z)$, such that for

$$u = \frac{\bar{u}}{1+\bar{u}\delta\lambda} \tag{3.1.49}$$

$u(\bar{u}_{\max})$ corresponds to the radial position of the horizon, while $\bar{u}$ lives on the interval $[0,\ldots,\bar{u}_{\max}]$. The value $\bar{u}_{\max}$ can be chosen to equal the fixed $u_{\max}$ from the coordinate transformation. Equation (3.1.48) is a highly non linear but ordinary differential equation for the shift function. Thus, (Fourier-) spectral methods with a root finding routine have to be applied once again. Linearizing equation (3.1.48) in $\delta\lambda$ allows us to apply a Newton iteration. In each iteration step the differential equations (5.10.2)-(5.10.4) have to be solved for a certain starting shift $\delta\lambda^m$ in order to obtain an improved guess for the shift function $\delta\lambda^{m+1}$. It turned out to be advantageous to choose $\delta\lambda^0 \in [0.1, 0.3]$ for our settings. It also turned out to be helpful to always start with a relatively large BED ϵ_0 of about 10% and tune it down slightly in each iteration step until the desired ϵ_0 is reached and the iteration converged.
During the time evolution we use the stationary requirement of the radial horizon position r_h, which results in a differential equation that can be used to update the total shift λ time-slice for time-slice. Using (5.10.2)-(5.10.8), together with the requirement that the time derivative of (3.1.48) vanishes gives equation (5.10.22). The more accurate horizon fixing by solving equations (3.1.48) for the shift function is then applied every $10-100$ time steps, depending on width and symmetry of the colliding shocks.[60]

[60] For asymmetric shock collisions with a small $\epsilon_0/\epsilon_{\max} \approx 0.01$ applying (3.1.48) too often turned out to spoil the higher derivatives of the shift function λ, which snowballed and caused the code to break down.

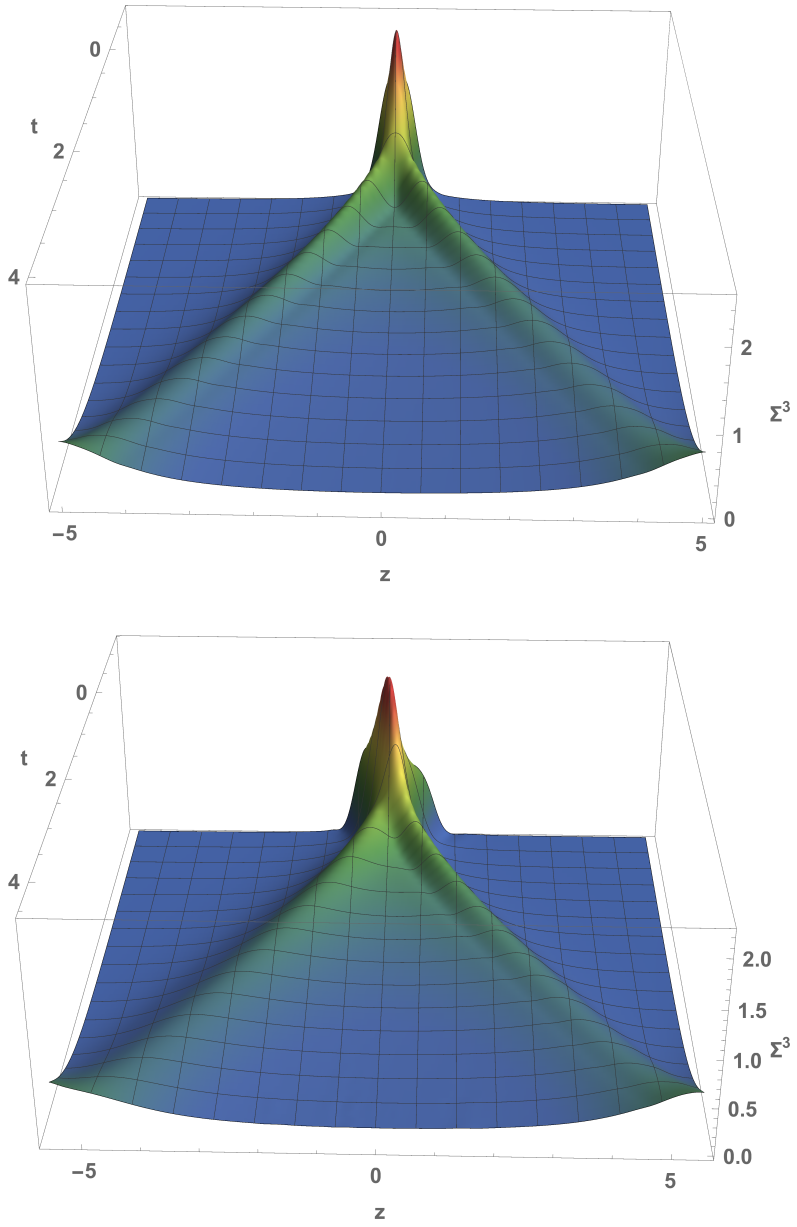

Figure 3.3: The volume element Σ^3 of the apparent horizon for a symmetric collision with shockwidth $w = 0.075$ (top) and an asymmetric collision with widths ($w_+ = 0.075, w_- = 0.35$) (bottom). All shocks have the same transverse energy density μ^3. In an equilibrated plasma the volume element Σ^3 is proportional to the entropy density s. Also for this interpretation the same caveat explained in more detail in the caption of Fig. 3.15 should be considered.

3.1.4.3 Time evolution

The differential equations (5.10.2)-(5.10.6) will be solved using multi-domain spectral methods. The details of parameter choices can be seen in table 3.2. In order to avoid instabilities due to inconvenient implementations of those differential equations we work with the following redefinitions of the functions $B, \Sigma, d_+\Sigma, d_+B$ and A, which can be extracted from the near boundary analysis of the EoM (5.10.2)-(5.10.6):

$$B(u,z,t) = \left(\frac{u}{1+u\lambda}\right)^3 b(u,z,t) \tag{3.1.50}$$

$$\Sigma(u,z,t) = \frac{1}{u} + \lambda + \left(\frac{u}{1+u\lambda}\right)^4 \sigma(u,z,t) \tag{3.1.51}$$

$$F(u,z,t) = -\partial_z\lambda + \left(\frac{u}{1+u\lambda}\right)^2 f(u,z,t) \tag{3.1.52}$$

$$d_+\Sigma(u,z,t) = \frac{1}{2}\left(\frac{1}{u}+\lambda\right)^2 + \left(\frac{u}{1+u\lambda}\right)^2 d_+\sigma(u,z,t) \tag{3.1.53}$$

$$d_+B(u,z,t) = \left(\frac{u}{1+u\lambda}\right)^2 d_+b(u,z,t) \tag{3.1.54}$$

$$A(u,z,t) = \frac{1}{2}\left(\frac{1}{u}+\lambda\right)^2 - \partial_t\lambda + \left(\frac{u}{1+u\lambda}\right)^2 a(u,z,t). \tag{3.1.55}$$

The EoM (5.10.2)-(5.10.6) shall be solved for the functions b, σ, f, $d_+\sigma$, d_+b, a on a given time slice. Handing them to the computer in a fashion, such that divergences at the boundary already are canceled out in the analytic expressions is essential. The differential equation (5.10.7) is not needed during the time evolution. Equation (5.10.8) can be obtained from the previous ones by Bianchi identity. The form of the conditions can be derived from the near boundary analysis

$$\sigma\big|_{u=0} = 0 \quad , \qquad \partial_u\sigma\big|_{u=0} = 0 \tag{3.1.56}$$

$$f\big|_{u=0} = f^{(4)} \quad , \qquad \partial_u f\big|_{u=0} = \frac{8b^{(4)}}{3} \tag{3.1.57}$$

$$d_+\sigma\big|_{u=0} = a^{(4)} \quad , \qquad \partial_u d_+\sigma\big|_{u=0} = \frac{\partial_z f^{(4)}}{3} \tag{3.1.58}$$

$$d_+b\big|_{u=0} = 0 \quad , \qquad \partial_u d_+b\big|_{u=0} = -2b^{(4)} \tag{3.1.59}$$

$$a\big|_{u=0} = 0 \quad . \tag{3.1.60}$$

At this point the only additional information in form of boundary conditions required to solve the Einstein equations on a given slice are the functions $a^{(4)}$ and $f^{(4)}$. However, we found it to be numerically advantageous to demand all of the conditions listed above to hold, even though the second row of the (double) list above follows from the first one.

The differential equations (5.10.2)-(5.10.6) are then solved in this order on the first time slice $t = t_0$ using spectral methods and applying the same Chebyshev grid as we used to determine $B|_{t_0}$. Finally we use the elliptic differential equation (5.10.22) to compute $\partial_t \lambda$. In order to update $\{B, f, a, \lambda\}$ to the next time slice, we need to know $\partial_t B|_{t_0}$, $\partial_t a|_{t_0}$, $\partial_t f|_{t_0}$ and $\partial_t \lambda|_{t_0}$. These can be obtained from equations (3.1.10) and (3.1.11).

We apply the fourth order Runge-Kutta method (RK4) to determine the needed starting conditions on the following slice. For broader shocks of $w > 0.3$ a Newton time stepper or third order Runge-Kutta would be sufficient. For shocks of width $w < 0.1$ we found it to be essential for the code to work without massive precision loss to use at least RK4. The size of the time step was chosen as $\delta t = 0.002$ in all settings. We filter the quadruple $\{B, f, a, \lambda\}$ only after each time step using a low pass filter in longitudinal direction, which is discussed in more detail in the Appendix section 5.11. We avoid numerically filtering any interim results during the calculations on each time slice. The filtering damps short wavelength numerical artefacts of the discretization.

3.1.5 Results

3.1.5.1 Collision parameters

In order to gather data for the extension of the model describing "universal" flow with Gaussian rapidity dependence found in [33] to the asymmetric case, where incomming shocks have different widths $w_+ \neq w_-$, we calculated several collisions at various shock-widths. The parameters of these computations and associated software are outlined in Table 3.2. All initial shocks had Gaussian profiles (3.1.28) and identical transverse energy densities proportional to μ^3. Thus we consider collisions in the center of momentum frame, which in the lab frame correspond to two shocks with energies μ_1 and μ_2, such that $\mu = \sqrt{\mu_1 \mu_2}$. For simplicity we rescaled our coordinates such that $\mu = 1$. Our shock widths ranged between 0.075 and 0.35. Due to the damping of numerical artifacts, as discussed above, an artificial background energy density was added whose size ranged from 5.5% down to 1.2% of the peak energy density of the narrower shock. Periodic boundary conditions with a period $L_z = [10, 11, 12]$ for [narrow, asymmetric, broad] collisions were applied in the longitudinal direction. The uniformly spaced (Fourier) grid in this direction had of up to $N_z = 720$ points. In the radial direction, domain decomposition with $M = 22$ subdomains of uniform size in the inverted radial coordinate $u = 1/r$ was used, with a Chebyshev-Gauss-Lobatto grid of up to $N_u = 13$ points within each subdomain. Time evolution used RK4 as explained in Appendix 5.8 with a fixed step size $\delta t = 0.002$ and total time durations ranging from $t = 4/\mu$ to $t = 20/\mu$ (which was used in figure 3.4).

Figure 3.4 shows the energy density $\widehat{T}^{00}(t, z)$, in units of μ^4, for two representative collisions. On the left is an asymmetric collision with $w_+ = 0.075/\mu$ and $w_- = 0.25/\mu$,

run	w_+	w_-	N_z	ϵ_0
1	0.35	0.35	720	{0.055, 0.066}
2	0.25	0.25	480	{0.039, 0.045}
3	0.1	0.25	660	{0.015, 0.017}
4	0.1	0.1	600	{0.015, 0.017}
5	0.075	0.35	660	{0.012, 0.015}
6	0.075	0.25	660	{0.012, 0.015}
7	0.075	0.075	600	{0.012, 0.015}

Table 3.2: Physical and computational parameters of specific computed collisions. Shown are the incoming shock widths $w_\pm$, number of longitudinal grid points N_z, and background energy densities ϵ_0. Shock widths $w_\pm$ are measured in units of μ^{-1}. The background energy density ϵ_0 is in units of the peak energy density of the narrower shock, or $\mu^3 w_+^{-1}/\sqrt{2\pi}$. Computed results at the two listed values of ϵ_0 were used to extrapolate to vanishing background energy density.

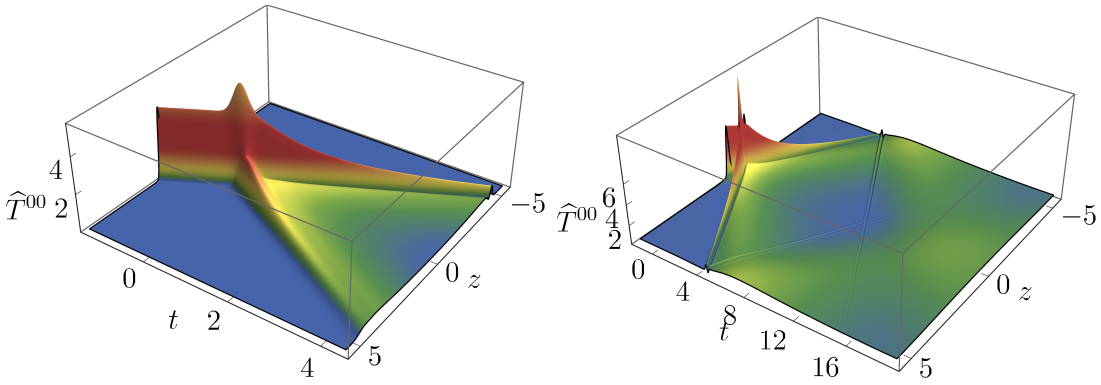

Figure 3.4: The energy density $\widehat{T}^{00}(t,z)$ plotted as a function of time t and longitudinal position z for an asymmetric collision (left) involving shocks of widths $w_- = 0.075/\mu$ and $w_+ = 0.25/\mu$ (Caveat: In this example the thin shock travels in negative z-direction. In most other examples shown and especially in table 3.2 the thin shocks travels in positive z-direction), and a symmetric collision (right) with shock width $w_\pm = 0.075/\mu$. All shocks have equal transverse energy density μ. In the symmetric collision (right) one sees unphysical wrap-around artifacts at $t \gtrsim 5/\mu$ due to the imposition of periodic boundary conditions in z. For smaller values of t this compactification does not affect the results.

while the right side plot shows a symmetric collision with $w_\pm = 0.075/\mu$. The time evolution in the latter case was run to late times where wrap-around artifacts from the periodic boundary conditions in z are clearly evident at $t \gtrsim 5/\mu$: The shocks collide again and again on the compactified z-interval here displayed as a finite box.

The maxima in the energy density on each timeslice are situated on the curve corresponding to the forward lightcone, as clearly seen in Fig. 3.2. These local maxima lie outside the hydrodynamic region as defined below in (3.1.61). As shown in Fig. 3.5,

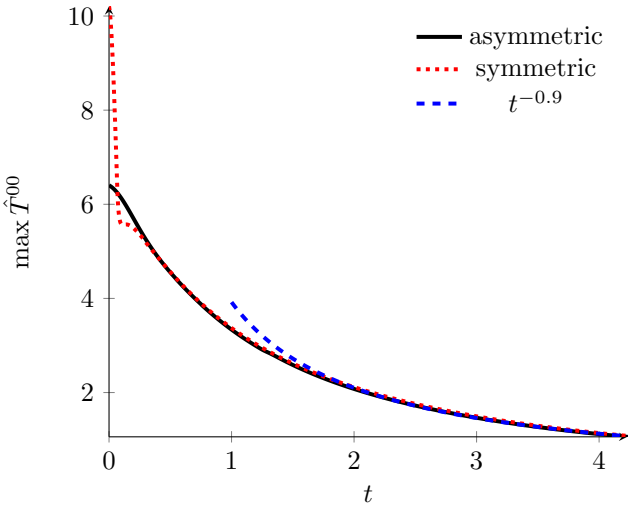

Figure 3.5: Comparison of time dependent amplitudes of the energy density maxima of the thinnest shock partner between a symmetric collision (solid red line) of two narrow shocks of width $w = 0.075$ and an asymmetric collision of shocks (dashed blue line) having widths $w = 0.075$ and $w = 0.25$, with all incoming shocks having the same transverse energy density. Also shown (long dashed black line) is a $t^{-0.9}$ asymptotic form. Except for short time transients ($t \lesssim 0.3$), the maxima in the symmetric and in the asymmetric case behave identically. For $t \gtrsim 1.5$ the amplitude decrease is well described as $t^{-0.9}$, as previously found in Ref. [34].

the amplitude of these local maxima decay with the same power-law time dependence as seen in symmetric collisions, in fact they decay with the exact same rate as the symmetric version of the thinner of both shockpartners.

3.1.5.2 Post-collision hydrodynamic flow and hydrodynamization time

Let us start this section with quantifying the proximity of our results to a hydrodynamics description by using the introductory section 1.7.2. As for the symmetric cases in Ref. [33], we define the spacetime region $\mathcal{R}$ in which hydrodynamics provides a good description as the largest connected region within the future lightcone in which the residual

$$\Delta \equiv \frac{1}{p}\sqrt{\delta T^{\mu\nu}\,\delta T_{\mu\nu}}\,, \qquad \delta T^{\mu\nu} \equiv T^{\mu\nu} - T^{\mu\nu}_{\rm hydro}, \tag{3.1.61}$$

measuring the difference between the holographically computed stress energy tensor and its hydrodynamic approximation (1.7.34), is smaller than 0.15.

For all the collisions we studied, both symmetric and asymmetric, with various combinations of incoming shock widths ranging from 0.35 down to 0.075, we found that the boundaries of the regions $\mathcal{R}$ differ negligibly from one another as displayed in Fig. 3.6 [61]. At $z = 0$ we find the same minimal time for which $\Delta < 0.15$ for asymmetric

[61] Only using a linear extrapolation to approximate a vanishing BED turned out to be insufficient

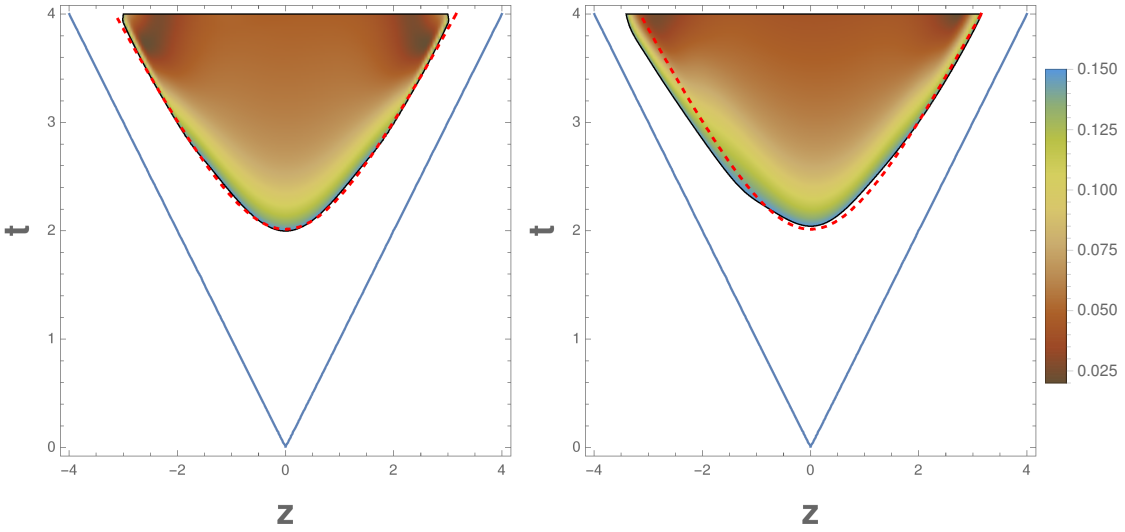

Figure 3.6: The largest connected spacetime region $\mathcal{R}$ in which $\Delta < 0.15$ (as defined in Eq. (3.1.61)) for a collision of narrow symmetric shocks ($w_+ = w_- = 0.075$) on the left, and asymmetric shocks ($w_+ = 0.1$, $w_- = 0.25$) on the right. The black dotted line shows the hyperbola $(t - 0.5)^2 - z^2 = \tau^2$, with $\tau = 1.5$. For both asymmetric and symmetric collisions the region $\mathcal{R}$ starts at $t_{\text{hydro}} \approx 2$. These plots were obtained by linearly extrapolating to vanishing BED. Another detail of this result that can be compared with experiments e.g. at ATLAS is the slight asymmetry regarding the onset of the hydro regime in the right figure. The time t at which the left moving (broader) blob of energy reaches the hydro regime is slightly smaller than the corresponding time for the right moving (thinner) one. In [83] it was found that for a proton (p) on lead (Pb) collision the hydrodynamization in Pb-direction happens slightly faster. This qualitative trait is reflected by our simulations.

and symmetric collisions given by

$$t_{\text{hydro}} \approx 2\,. \tag{3.1.62}$$

In the symmetric case this confirms results found previously in [33]. For the asymmetric case this implies that the hydrodynamization time in the center of momentum frame is the same as for symmetric ones. Figure 3.6 shows that the hydrodynamization time is (almost) a proper time lying on a hyperbolic curve with a small temporal shift $\delta t \approx 0.5$ for both symmetric and asymmetric collisions.[62] After scaling back to a dimensionful time and z-coordinate, we have $\mu t_{\text{hydro}} \approx 2$, where μ is frame dependent. This fits to the fact that during a peripheral collision of heavy ions, those parts of the

to give numerically reliable results for the region $\mathcal{R}$ plotted in 3.6 at late times $4 \ll t$. We restricted the plots to the spacetime region in which our $\mathcal{R}$ for symmetric collisions is identical with the findings in [33].

[62] Our setting of identical energy scales and asymmetric widths of the two colliding shocks implies that there is no frame, in which the asymmetric collision is fully symmetric.

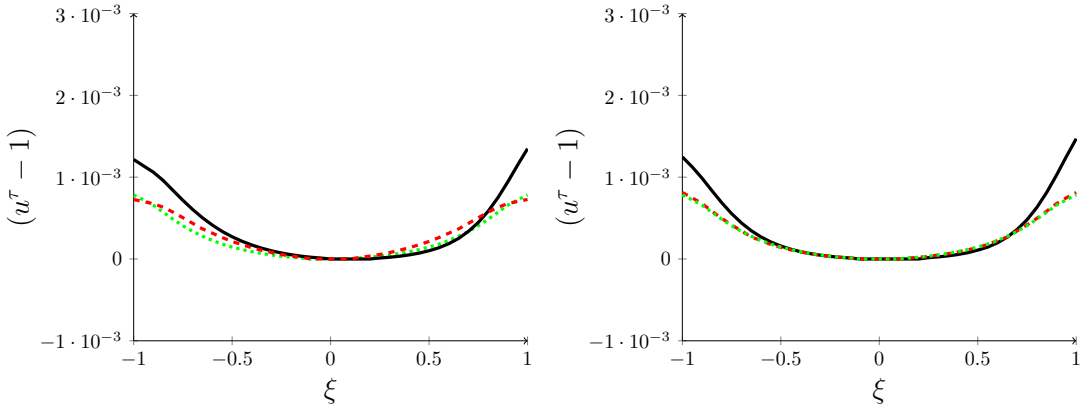

Figure 3.7: The difference of the proper time component of the fluid velocity from unity, $u^\tau - 1$, plotted as a function of rapidity at proper time $\tau = 3$ for the collisions $(w_+ = 0.075, w_- = 0.35)$ (black line), $(w_+ = 0.075, w_- = 0.075)$ (red dashed line) and $(w_+ = 0.35, w_- = 0.35)$ (green dotted line) on the left and $(w_+ = 0.075, w_- = 0.25)$ (black line), $(w_+ = 0.075, w_- = 0.075)$ (red dashed line) and $(w_+ = 0.25, w_- = 0.25)$ (green dotted line) on the right As in Ref. [33] we find that $u^\tau \approx 1$ with a deviation of a few parts in 10^{-3}, showing that the fluid velocity is quite well described by boost invariant flow.

ions, that do not collide with anything (shaded gray in Fig. 3.2), should take infinitely long to hydrodynamize.

By suitably adjusting the filtering to tackle artifacts coming from the discretization, as discussed in the Appendix 5.11, we could decrease the background energy density in our computations of asymmetric collisions to about 1% of the peak value of the energy density of the narrower shock. For asymmetric collisions it turned out to be quite challenging to achieve high precision and numerical stability with much smaller background energy densities. We extrapolate to 0 BED by repeating our calculations at slightly increased ϵ_0 and using a linear extrapolation.

Also for asymmetric collisions one obtains for the proper time component of the fluid velocity $u^\tau \approx 1$ as illustrated in Fig. 3.7, which implies boost invariant flow as in the symmetric case. The deviations from $u^\tau \approx 1$ are of order $\mathcal{O}(10^{-3})$ in the tested rapidity and proper time interval. Moreover, the rapidity distribution of the proper energy density on a surface of constant proper time $\tau \gtrsim \tau_{\rm hydro}$ continues to be well approximated by a Gaussian but now with a peak which is shifted away from vanishing rapidity:

$$\epsilon(\xi, \tau) = A(w_+, w_-; \tau)\, e^{-\frac{1}{2}\,(\xi - \bar{\xi}(w_+, w_-; \tau))^2/\sigma(w_+, w_-; \tau)^2}\,. \tag{3.1.63}$$

Our results for the rapidity shift $\bar{\xi}(w_+, w_-; \tau)$ are shown in Fig. (3.8) for three examples of asymmetric collisions. To a good approximation, the width dependence of the

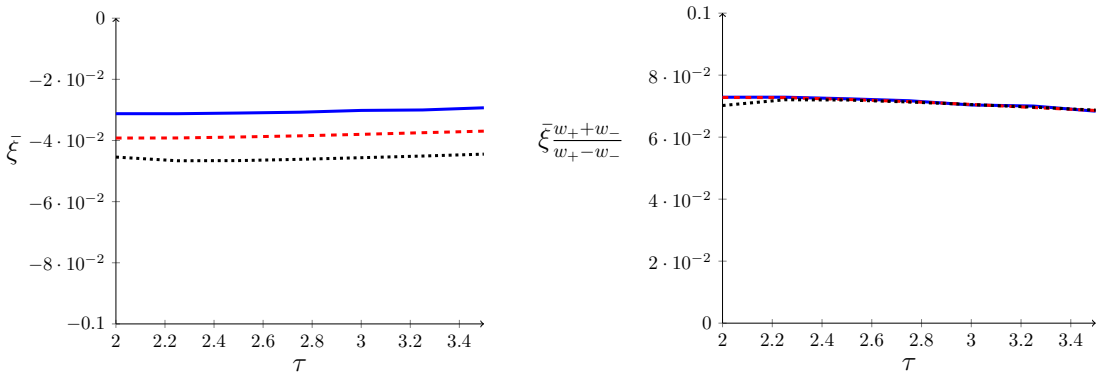

Figure 3.8: Left: the rapidity shift $\bar{\xi}(w_+, w_-; \tau)$ of the proper energy density distributions, as a function of proper time τ, for asymmetric collisions with shock widths $(w_+, w_-) = (0.075, 0.25)$ (dashed red line), $(w_+, w_-) = (0.1, 0.25)$ (solid blue line), and $(w_+, w_-) = (0.075, 0.35)$ (dotted black line). Right: The coefficient function $\Xi(\tau) \equiv \bar{\xi}(w_+, w_-; \tau)(\frac{w_+ + w_-}{w_- - w_+})$ for the same three cases.

rapidity shift has a simple factorized form for $\tau \gtrsim 2$,

$$\bar{\xi}(w_+, w_-; \tau) \approx \Xi(\tau) \, \frac{w_+ - w_-}{w_+ + w_-} \,, \tag{3.1.64}$$

with the coefficient $\Xi \approx 0.07$, that turned out to be constant for $\tau > 2$.

We find that the rapidity distribution of of the proper energy density for the asymmetric collisions is well approximated by the shifted geometric mean of the corresponding symmetric collision results, meaning that the widths of the asymmetric distributions can be approximated by the inverse quadratic mean of the respective quantities in the symmetric cases. We quantify the precision of this approximation regarding the widths of the distributions by computing the relative error

$$\delta[\sigma] = \frac{\bar{\sigma}(w_+, w_-) - \sigma(w_+, w_-)}{\sigma(w_+, w_-)}, \tag{3.1.65}$$

where $\sigma(w_+, w_-)$ corresponds to the asymmetric distribution, computed by solving for the widths for which the distribution reached $1/\sqrt{e}$ of its maximum. The quantity $\bar{\sigma}$ is the inverse quadratic mean of the widths in the respective symmetric cases

$$\bar{\sigma}(w_+, w_-) = \sqrt{\frac{2}{1/\sigma(w_+)^2 + 1/\sigma(w_-)^2}}. \tag{3.1.66}$$

We display this comparison in Fig. 3.12. The efficacy of these relations is illustrated in Fig. 3.9, which shows the proper energy density as a function of the rapidity ξ at proper times $\tau = 2$ (top) and 3 (bottom) for the case of $(w_+, w_-) = (0.075, 0.35)$ (left) and $(w_+, w_-) = (0.075, 0.25)$ (right). In each plot the solid blue line shows the result for

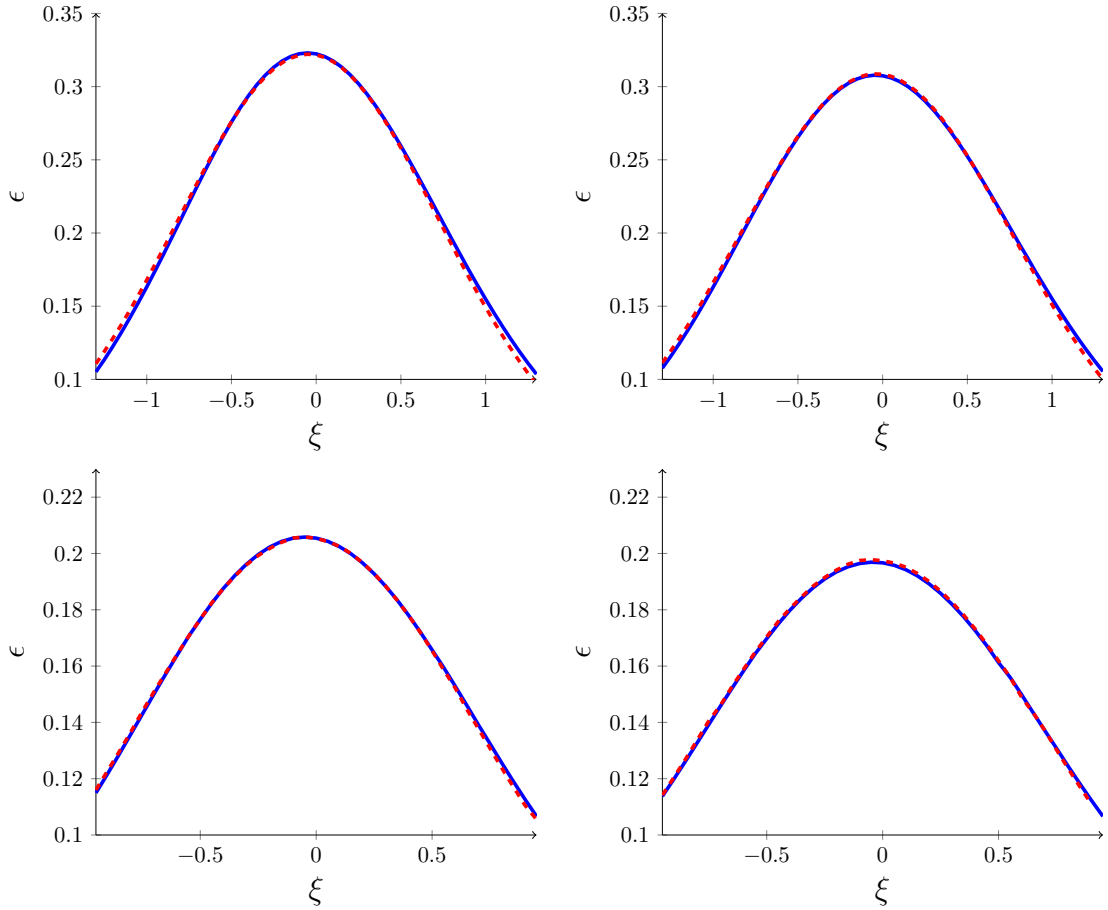

Figure 3.9: The proper energy density ϵ as a function of rapidity ξ at constant proper time $\tau_{\text{init}} = 2.0$ (first row) and $\tau = 3$ (second row) for asymmetric collisions ($w_+ = 0.075, w_- = 0.35$) (left) and ($w_+ = 0.075, w_- = 0.25$) (right) displayed by the solid blue curve. The red dashed curve shows the geometric mean of the corresponding symmetric distributions shifted by $\bar{\xi}$ given in (3.1.64). At $\xi > 1$ a small defect is visible.

the respective asymmetric collision. The red dashed curve shows the shifted geometric mean of the symmetric results. For $|\xi| < 1$ this model fits almost perfectly. For $|\xi| > 1$ tiny deviations from our simple description start to show.

To motivate the improved model, which handles these small imperfections, let

$$\langle X \rangle_p \equiv \left[\tfrac{1}{2} X(w_+)^p + \tfrac{1}{2} X(w_-)^p \right]^{1/p} \tag{3.1.67}$$

denote the generalized mean with power p of some quantity X, which is an observable in a symmetric collision of shocks with widths w_+ and w_-. We then define $p[X]$ as the power for which the generalized mean of symmetric collision results gives the result $X(w_+, w_-)$ of this observable in an asymmetric collision with shock widths (w_+, w_-).

Explicitly this means we solve the equation

$$\langle X \rangle_{p[X]} = X(w_+, w_-) \tag{3.1.68}$$

for $p[X]$, where the geometric mean equals the $p \to 0$ limit.

In Fig. 3.10 we display the resulting power $p[A(\tau)]$ for the amplitude A of the distributions in rapidity of the proper energy density, as a function of proper time τ, resulting from collisions with widths $(w_+, w_-) = (0.075, 0.35)$ on the left and $(w_+, w_-) = (0.1, 0.25)$ on the right.

Fig. 3.10 and 3.11 show that the improved model for asymmetric distributions has to fulfill that its maximum is given by the geometric mean of the maxima in the corresponding symmetric cases.

We modify our previously found model only slightly and consider

$$\epsilon(w_+, w_-; \zeta, \tau) \approx \sqrt{A(w_+;\tau)A(w_-;\tau)}\, g_+(\xi - \bar{\xi}, \tau)^{1-a(w_+,w_-;\xi-\bar{\xi},\tau)} g_-(\xi - \bar{\xi}, \tau)^{a(w_+,w_-;\xi-\bar{\xi},\tau)}, \tag{3.1.69}$$

where $A(w_\pm, \tau)$ is the amplitude of the distribution for the symmetric collisions of widths $w_\pm$, $\bar{\xi}$ is given in (3.1.64) and $g_\pm$ represents the normalized Gaussian

$$g_\pm = e^{-\frac{1}{2}\xi^2/\sigma(w_\pm;\tau)^2}. \tag{3.1.70}$$

Thus (3.1.69) describes the weighted geometric mean of the normalized and shifted Gaussian distributions in the corresponding symmetric cases with the amplitude that corresponds to the geometric mean of the respective ones in the symmetric cases.[63]. The simpler model, discussed above in (3.1.63) and the following paragraphs, is the special case

$$a(w_+, w_-; \xi, \tau) = \frac{1}{2}. \tag{3.1.71}$$

We find the function $a(w_+, w_-; \xi, \tau)$ to be remarkably insensitive to which configuration (w_+, w_-) is tested and constant for $\tau > 2$ with good accuracy. We solved equation (3.1.69) for the auxiliary function $\tilde{a}(\xi - \bar{\xi}) = a(\xi - \bar{\xi}) \times (\xi - \bar{\xi})$, since at the point $\xi = \bar{\xi}$, where, by construction, the shifted and normalized symmetric distributions intersect both with one another and with the normalized asymmetric one, the numerical solution for $a(\xi - \bar{\xi})$ would diverge. The results for $\tilde{a}$ in the cases $(w_+ = 0.075, w_- = 0.35)$, $(w_+ = 0.075, w_- = 0.25)$ and $(w_+ = 0.1, w_- = 0.25)$ are displayed in Fig. 3.13. As can be seen there, the weight functions $a(\xi)$ only differ negligibly from one another and can

[63] Which is equivalent to considering the weighted inverse quadratic mean of the widths $\sigma(\omega_\pm; \tau)$.

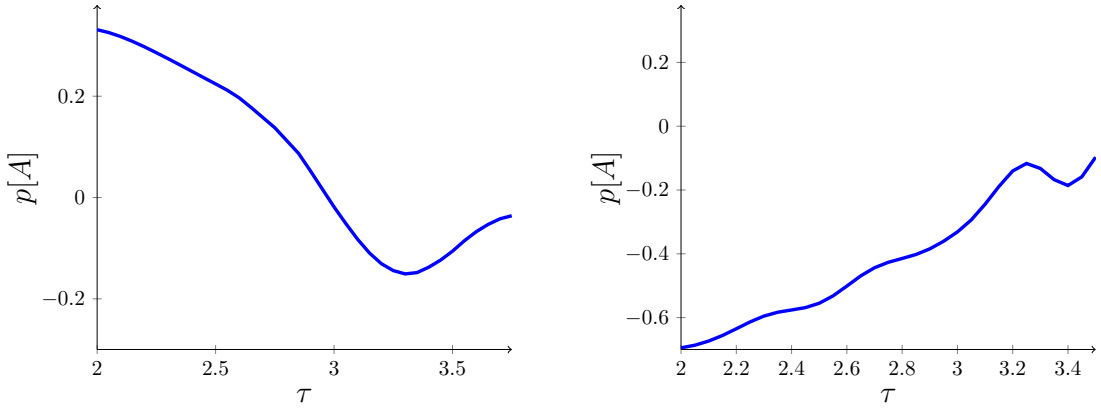

Figure 3.10: The exponents $p[A(\tau)]$ for the setting $(w_+ = 0.075, w_- = 0.35)$ (left) and $(w_+ = 0.1, w_- = 0.25)$ (right) defined as solutions to relation (3.1.67) for the amplitude A as a function of proper time τ.

be well fitted by the function[64]

$$a(w_+, w_-; \xi, \tau) \approx a(\xi) = \frac{1}{2}(1 - \frac{1}{2}\tanh(\xi)). \tag{3.1.72}$$

To show the efficacy of this model and the improvement compared with the former one, we again compared the asymmetric proper energy density profiles with the distributions obtained from the corresponding symmetric ones inserted in (3.1.69) and using (3.1.72). These results are displayed in Fig. 3.14.

[64] This corresponds to a weighted inverse quadratic mean for the widths of the symmetric distributions of the form

$$\left(\frac{2}{\frac{(1-1/2\tanh(\xi))}{\sigma(w_-,\tau)^2} + \frac{(1+1/2\tanh(\xi))}{\sigma(w_+,\tau)^2}} \right)^{1/2}.$$

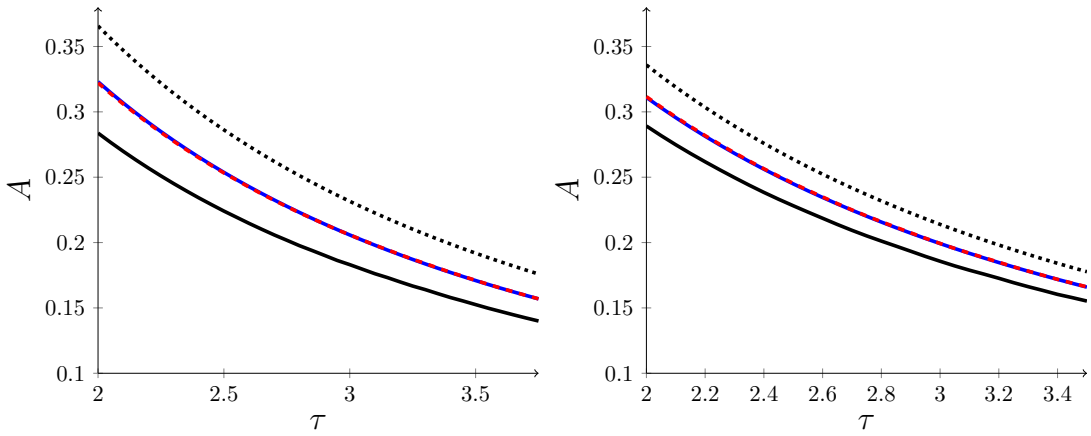

Figure 3.11: The comparison between the maxima of broad (black dashed line), thin (black line) and asymmetric (blue line) distributions for $(w_+ = 0.075, w_- = 0.35)$ (left) and $(w_+ = 0.1, w_- = 0.25)$ (right). The red dashed line is the geometric mean of the respective symmetric results.

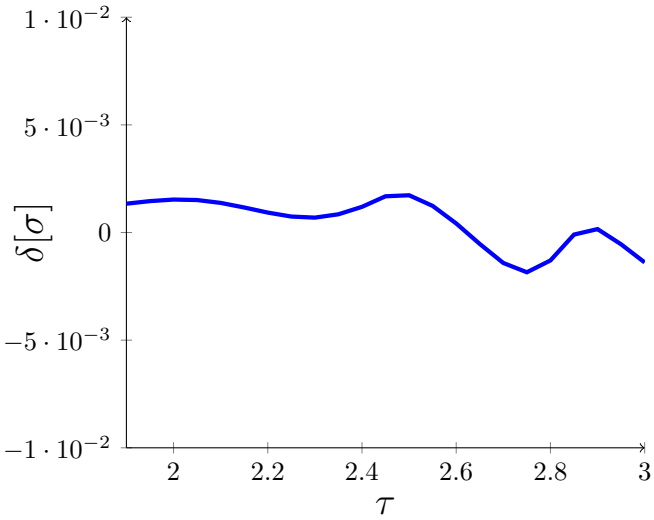

Figure 3.12: The relative error $\delta[\sigma]$ as introduced in (3.1.65) computed for the collision $(w_+ = 0.075, w_- = 0.25)$. This specific example was chosen, since the widths in the symmetric cases are sufficiently far apart over the plotted τ-range, such that it is the easiest to resolve, which mean of the widths in the symmetric cases corresponds to the asymmetric distribution. As shown, the relative error δ is only a fraction of a per cent.

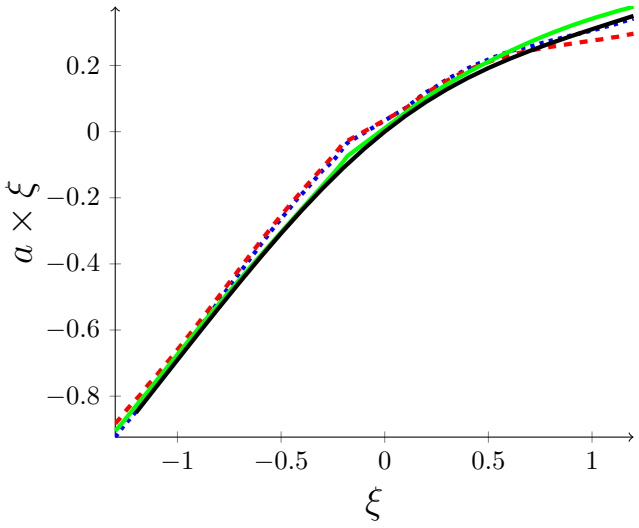

Figure 3.13: The auxiliary weight function $\tilde{a}(\xi) = a(\xi)\xi$ as a function of ξ for the cases $(w_+ = 0.075, w_- = 0.35)$ (green line), $(w_+ = 0.075, w_- = 0.25)$ (red dashed line), $(w_+ = 0.1, w_- = 0.25)$ (blue dotted line) evaluated at $\tau = 2$. Since a is not well defined at $\xi = 0$ we interpolated our results over this point. The black line corresponds to the fitting function $\frac{\xi}{2}(1 - \tanh(\xi)/2)$.

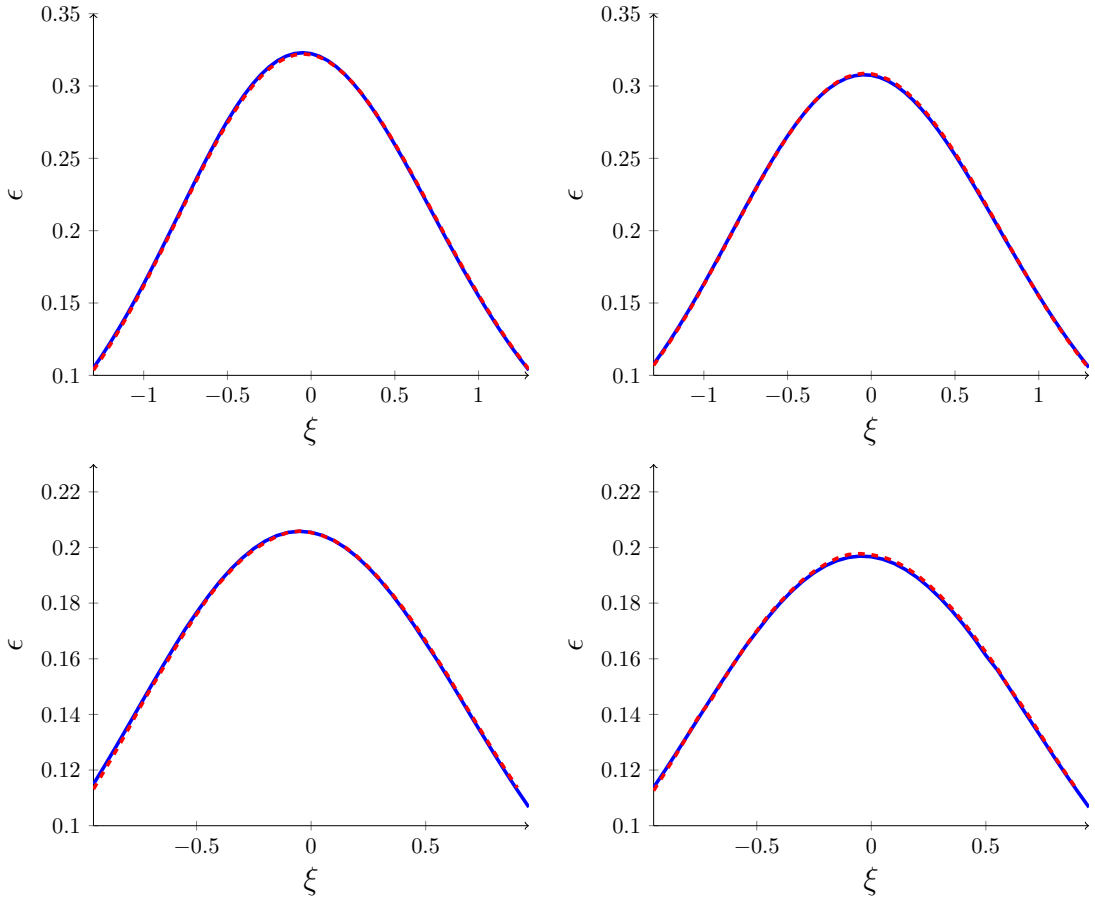

Figure 3.14: The proper energy density ϵ as a function of rapidity ξ at constant proper time $\tau_{\text{init}} = 2.0$ (first row) and $\tau = 3$ (second row) for asymmetric collisions $(w_+ = 0.075, w_- = 0.35)$ (left) and $(w_+ = 0.075, w_- = 0.25)$ (rigth) displayed by the solid blue curve. The red dashed curve shows the result obtained from (3.1.69) and the respective Gaussians distributions for the symmetric collisions. The function $a(w_+, w_-, \xi, \tau)$ was chosen as $a(w_+, w_-, \xi, \tau) = a(\xi) = \frac{1}{2}(1 - \frac{1}{2}\tanh(\xi))$ in all cases.

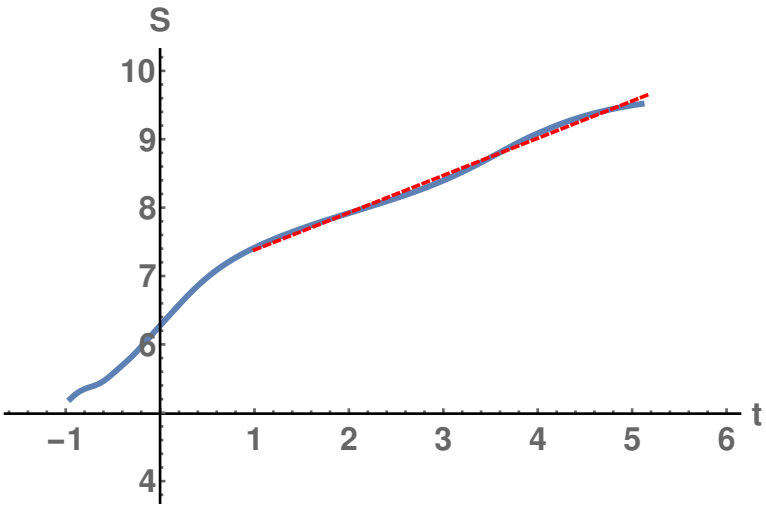

Figure 3.15: Entropy production during a symmetric collision of gravitational shockwaves of width $w = 0.075$. The gauge/gravity duality relates the entropy density s to the rescaled volume element $\pi\Sigma^3$ of the apparent horizon [14, 81, 82] (This comes with the caveat, that the size of the apparent horizon might be (time-)foliation dependent in some geometries, and thus the interpretation of its volume as a physical quantity comes with a grain of salt). To estimate the entropy production we integrate over the longitudinal coordinate. S is given in units of μ^2, where μ^3 is the transverse energy density of the shockfronts. For intermediate times $1 < t < 6$ we find an approximately linear behaviour (The linear fit, plotted as a red dashed line, is included to guide the eye). Ergodic systems such as classical Yang Mills theories are expected to eventually enter a regime of linear entropy growth governed by the Kolmogorov-Sinai entropy (before slowly approaching a saturation level). Although it is unclear, whether this also applies automatically to the corresponding quantum theories, it is still interesting to witness such a behaviour via holography. Turning the tables, one could even argue that this holographic calculation hints at the fact that the general behaviour of the entropy of classical chaotic theories survives their quantization.

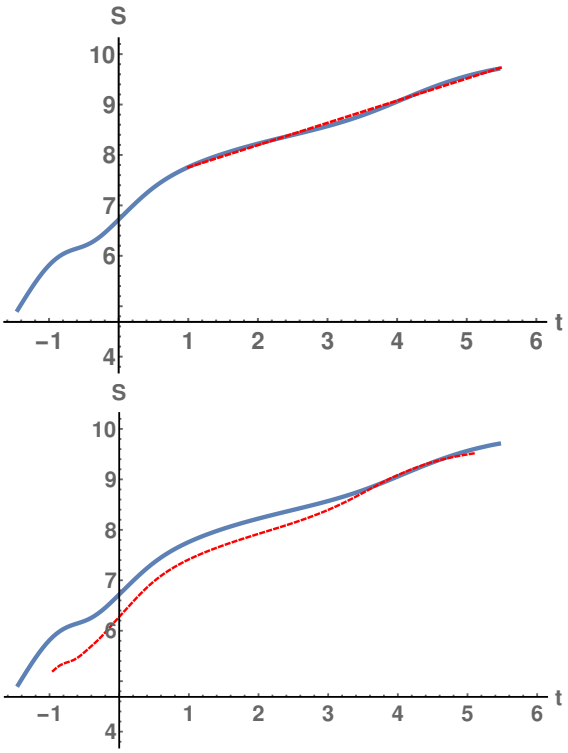

Figure 3.16: Same as in Fig. 3.15. The left plot shows the entropy production for an asymmetric collision ($w_+ = 0.075, w_- = 0.25$). The plot on the right shows the comparison between the entropy production of asymmetric and symmetric collisions. The observation made and described in the caption of Fig. 3.15 also applies to asymmetric collisions.

3.1.6 Concluding remarks

Our numerical simulations of asymmetric shockwave collisions provided several interesting and important results. On the one hand we could verify assumptions made by hydrodynamical models regarding the hydrodynamization time t_{hydro} of the almond shaped QGP formed after a heavy ion collision: We found that t_{hydro}, like in the symmetric case [33, 34], is generally insensitive to shockwidths and in addition also to the asymmetry of the incomming shocks. Only the transverse energy density scale μ^3 impacts the hydrodynamization time. Since in a lens shaped, highly relativistic heavy ion the transverse energy density only varies marginally with the transverse coordinates (except at the outer fringes of the projectiles) this implies that assuming a constant hydrodynamization time throughout most of the QGP is a good approximation also for peripheral collisions. On the other hand we found a general model describing the post collision flow during asymmetric collisions by simple means of the same during corresponding symmetric collisions. This extends the model found for special symmetric cases in [33] and allows to algorithmically construct the stress energy tensor and thus starting conditions for hydro evolutions without the need for simulating holographically localized peripheral shockwave collisions, granted that transverse gradients are suppressed due to highly relativistic effects. We gave a detailed and didactic description of the construction of our codes and concluded the discussion with an interesting observation regarding entropy production, that demands further inspection in future: After a certain amount of time $t \approx \frac{1}{\mu}$ the produced entropy enters an almost linear regime, both for symmetric and asymmetric collisions. This coincides with a behaviour that can be observed in classical ergodic systems that is also expected for QCD [86], which eventually enter a regime of linear entropy growth before slowly approaching a saturation limit in the far future.

3.2 Preparation of future work and supplementary material

3.2.1 Entanglement Entropy and non local observables in an asymmetric collision geometry

Studying non local observables, e.g. correlators or other n-point functions from a dynamical holographic setup is in general a challenging task. For the two point functions of an operator $\mathcal{O}$ with sufficiently large dimensional scaling Δ and the entanglement entropy (EE) relations (1.4.9) and (1.4.33) allow holographic computations of these quantities, by determining geodesics and minimal surfaces in a known (dynamical) AdS-geometry.

Our goal is to determine the entanglement entropy corresponding to stripe-shaped boundary regions during asymmetric shockwave collisions. To prepare this we start

with discussing how to compute correlators, following [61], where the authors considered this problem in a symmetric setup. For this one determines the geodesics between the boundary points $(t_0, 0, 0, 0, \pm\frac{l}{2})$, where the geometry is given by (1.7.4) together with our solutions for F_z, B, Σ and A corresponding to an asymmetric shockwave collision. We solve the geodesic equation

$$\frac{\partial^2 x^\mu}{\partial\sigma^2} + \Gamma^\mu_{\nu\rho}\frac{\partial x^\nu}{\partial\sigma}\frac{\partial x^\rho}{\partial\sigma} = -J\frac{\partial x^\mu}{\partial\sigma}, \tag{3.2.1}$$

with non zero Jacobian J. As pointed out in [61], working with a non affine parameter $\sigma \in [-1, 1]$ is numerically advantageous. This, of course, stays true for asymmetric collisions. Since we consider planar shocks and thus are dealing with a geometry that is invariant under translations into the x and y direction, we can reduce the dimensions of our problem to 3 and determine the solution of the geodesic equation (3.2.1) by considering the geometry

$$ds^2 = -2Adt^2 + 2dtdr - 2F_z dtdz + \Sigma^2 e^{-2B}dz^2, \tag{3.2.2}$$

and the points $(t, r, z) = (t_0, 0, \pm l/2)$. As explained in section 1.4.1 we need the vacuum solution to regularize the otherwise divergent geodesic length. In addition we can use this solution as a starting point of the relaxation algorithm, with which we solve (3.2.1) in the shockwave geometry. The analytic solution for the pure AdS-geometry obtained by setting

$$A = r^2/2,\ B = 0,\ F = 0,\ \Sigma = r \tag{3.2.3}$$

is given by

$$t(\sigma) = t_0 - \frac{1}{2}(\sigma\sqrt{2-\sigma^2}),\ r(\sigma) = \frac{2}{1-\sigma^2},\ z(\sigma) = \frac{1}{2}(\sigma\sqrt{2-\sigma^2}), \tag{3.2.4}$$

where we set $l = 1$ in this section. In practical calculation the geodesic length

$$L = \int d\sigma\Big(- 2A(\partial_\sigma t(\sigma))^2 + 2\partial_\sigma t(\sigma)\partial_\sigma r(\sigma) - 2F_z\partial_\sigma t(\sigma)\partial_\sigma z(\sigma) + \Sigma^2 e^{-2B}(\partial_\sigma z(\sigma))^2\Big)^{\frac{1}{2}} \tag{3.2.5}$$

is split up into two parts, one defined by choosing the integration interval $\sigma \in [\sigma_-, \sigma_+]$ such that $\sigma_\pm = (1 - 2/r_{cut})^{1/2}$, with $\epsilon = 1/r_{cut}$ being small. A near boundary analysis would allow to determine (3.2.5) in the remaining part of the full integration domain $\sigma \in [-1, 1]$ in terms of $\frac{1}{\epsilon}$. However, it is sufficient to repeat the numerical integration on $[\sigma_-, \sigma_+]$ for decreasing $1/r_{cut}$ until we observe convergence [61]. The difference between

L in (3.2.5) and the vacuum geodesic length L_0 defined by

$$L_0 = \int_{\sigma_+}^{\sigma_-} d\sigma \Big(-(\partial_\sigma t(\sigma))^2 + 2\partial_\sigma t(\sigma)\partial_\sigma r(\sigma) + (\partial_\sigma z(\sigma))^2 \Big)^{\frac{1}{2}} \tag{3.2.6}$$

delivers the regularized length $L^{reg} = L - L_0$. In addition we introduce the more convenient variable $u = \frac{1}{r}$, as we already did in section 3.1. One caveat to consider here is the shift parameter λ determined throughout the calculation in 3.1. The geodesic length itself is, of course, invariant under radial shifts, as the metric is covariant under them . However, the cut u_{cut} feels changes in λ, such that we first have to shift our shockwave geometry back to a

$$\bar{u} = \frac{u}{u + \lambda} \tag{3.2.7}$$

coordinate, for which $\lambda = 0$, before we can compare and subtract the geodesic lengths computed from the shockwave metric and the vacuum AdS-solution.

As shown in [61, 62] the computation of the entanglement entropy corresponding to a stripe-shaped boundary region is equivalent to determining correlators in an auxiliary spacetime. In the following we will explain this in greater detail and apply this algorithm to an asymmetric shockwave collision geometry:

The entanglement entropy corresponding to a boundary region A can be computed from the minimal surface Σ_A, extending into the bulk, that spans A (see introductory section 3.2.1, equation (1.4.33)). If A is a 3-surface with finite extent in longitudinal direction z and infinite extent in direction x and y we can make use of an auxiliary spacetime. The quantity we have to minimize is given by

$$\int d^3\sigma \sqrt{\det \frac{\partial X^\mu}{\partial \sigma^i} \frac{\partial X^\nu}{\partial \sigma^j} g_{\mu\nu}}, \tag{3.2.8}$$

where $X^\mu(\sigma^i)$ is the embedding of Σ_A into the (asymmetric) shockwave geometry, whose metric we call $g_{\mu\nu}$ here. The boundary conditions on X^μ are that $\partial\Sigma_A = \partial A$. In the aforementioned case of a stripe-shaped boundary region A the problem of finding a minimizer of (3.2.8) reduces to finding a geodesic in the conformally equivalent auxiliary geometry, given by $\Sigma^4 e^{2B} g_{\mu\nu}$. This is because (3.2.8) can be written in this case as

$$\int dx \int dy \int d\sigma \sqrt{\Sigma^4 e^{2B} g_{\mu\nu} \frac{\partial X^\mu}{\partial \sigma} \frac{\partial X^\nu}{\partial \sigma}}, \tag{3.2.9}$$

where $\sigma^1 = X^1 = x$ and $\sigma^2 = X^2 = y$. The factor $\Sigma^4 e^{2B} g_{\mu\nu}$ comes from the xx and yy component of the colliding-shockwave-metric. In order to track the evolution of the entanglement entropy corresponding to different boundary regions, parametrized

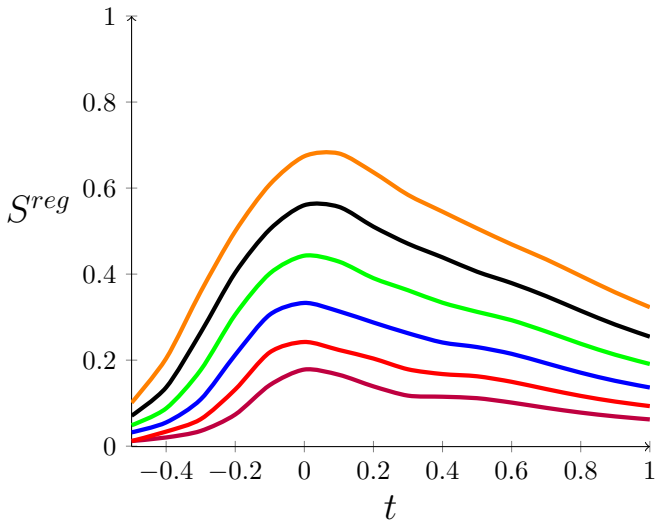

Figure 3.17: The renormalized entanglement entropy per transverse volume in units of μ^3, the transverse energy density, for an aysmmetric collision of shockwaves with widths $w_+ = 0.1$, $w_- = 0.25$. The lowest (purple) curve corresponds to a stripe-shaped boundary region A, with longitudinal extent $l = 0.2$ (given in units of $1/\mu$). The higher lying red, blue, green, black and orange curves correspond to $l = 0.3$, $l = 0.4$, $l = 0.5$, $l = 0.6$ and $l = 0.7$ in this order. In [61] the authors found an interesting pattern regarding the evolution of entanglement entropy of stripe-shaped boundary regions for symmetric collisions: The entanglement entropy observed during collisions of thin shocks ($w \approx 0.1$) exhibited a second smaller but clear peak, after the collision took place. Intermediate ($w \approx 0.25$) and broad shocks ($w \approx 0.5$) lacked this feature. Thus, it was argued that the entanglement entropy serves as an order parameter to distinguish transparency (thin) and full stopping (broad) scenarios for collisions. Colliding thin $w_+ = 0.1$ and intermediate $w_- = 0.25$ shocks, as shown above, revealed that the pattern of the evolution of the entanglement entropy is dominated by the broader shockwave.

by their longitudinal length l, during an asymmetric shockwave collision, we consider[65] the regularized entanglement entropy per transverse volume $V = \int dx \int dy$ in units of $4G_5$

$$S_{reg} = L - L_0, \tag{3.2.10}$$

where L and L_0 correspond to the lengths of the geodesics in the auxiliary spacetime and its pure AdS-version, spanning between the endpoints of A's longitudinal size l. We proceed in complete analogy to the calculation of correlation functions in the beginning of this small section. Our results are collected and analyzed in Fig. 3.17 and its caption.

[65] As the authors of [61] did for symmetric collisions.

3.2.2 Preparation for higher dimensional Codes

Collisions of localized shockwaves have manifold applications. On the one hand they allow us to test the robustness of our general model for the post-collision flow (section 3.1.5.2 in combination with [33]), in addition they can be used to study collisions with non negligible transverse dynamics, and in future, collisions of rotating (boosted) Kerr-black holes, simulating spin. Here we only consider starting conditions obtained from boosted non rotating black holes. The geometry in Fefferman-Graham coordinates, including transverse dynamics is given by[66]

$$ds^2 = \frac{1}{s^2}(-dt^2 + dx_\perp^2 + dz^2 + ds^2 + h_\pm(x_\perp, z_\pm, s)dz_\pm^2), \tag{3.2.11}$$

with $z_\pm = z \pm t$. In order to fulfill the Einstein equations, the function $h_\pm$ has to fulfill equation (3.1.13). In addition, we want the boundary stress energy tensor, whose 00, zz and ± 1 times its $0z$-component is proportional to $H_\pm$ with[67]

$$h_\pm(\vec{x}_\perp, z_\pm, s) = \int \frac{d^2k_\perp}{4\pi^2} e^{i\vec{k}_\perp \vec{x}_\perp} \tilde{H}_\pm(\vec{k}_\perp, z_\pm) 8 \frac{s^2}{k_\perp^2} I_2(|\vec{k}_\perp| s) \tag{3.2.12}$$

to be a decent model of a heavy ion. Thus, following [40], we set

$$H_\pm(\vec{x}_\perp, z_\pm) = \frac{A}{\sqrt{2\pi w^2}} \exp\left(-\frac{z_\pm^2}{2w^2}\right) \exp\left(-\frac{(\vec{x}_\perp \pm \vec{b}/2)^2}{R^2}\right) \tag{3.2.13}$$

where w is width of the longitudinal extent of the lens shaped (since Lorentz-contracted) energy density distribution, $\vec{b}$ is the impact parameter, with components in the transverse direction xy, and R measures the transverse size of the localized shock. Our goal here is to solve the integral (3.2.12) analytically[68]. This will substantially facilitate the (numerically performed) coordinate transformation, as it means, that we do not have to solve a rather involved integral numerically on each xyz-gridpoint of the discretized spatial coordinates. Thus, this preparation work will make it very cheap to compute starting conditions for localized shockwave collisions.[69]

[66] Here we use the nomenclature of [40].

[67] Here I_2 denotes the Besselfunction of second kind.

[68] Or at least find an almost perfect analytical approximation, we will make more precise what is meant by this in the curse of this section.

[69] In practical calculations, the coordinate transformation with this improvement only took a few hours on a 16-core desktop machine.

For this purpose we set

$$f_{\pm}(z) = \frac{1}{w}\exp\Big(-\frac{z_{\pm}^2}{2w^2}\Big) \tag{3.2.14}$$

$$g_{\pm}(\vec{x}_{\perp}) = \frac{A}{\sqrt{2\pi}}\exp\Big(-\frac{(\vec{x}_{\perp}\pm\vec{b}/2)^2}{2R^2}\Big) \tag{3.2.15}$$

we consider a shift $\vec{b} = b\hat{y}$ and focus on the integral

$$wh_{\pm}(\vec{x}_{\perp},0,s) = \int \frac{d|\vec{k}_{\perp}|d\phi_k}{4\pi^2}|\vec{k}_{\perp}|\tilde{g}_{\pm}(\vec{k}_{\perp})e^{i\vec{k}_{\perp}\vec{x}_{\perp}}8\frac{s^2}{k_{\perp}^2}I_2(|\vec{k}_{\perp}|s) \tag{3.2.16}$$

with

$$\tilde{g}_{\pm}(\vec{k}_{\perp}) = \frac{A}{\sqrt{2\pi}}\exp\Big(-\frac{\vec{k}_{\perp}^2R^2}{2} - ibk_y\Big)R^2. \tag{3.2.17}$$

The ϕ_k dependent parts of the integral (3.2.21) are give by

$$\ldots\exp\big(-ib|\vec{k}_{\perp}|\sin(\phi_k) + i|\vec{k}_{\perp}||\vec{x}_{\perp}|\cos(\phi_{\angle})\big), \tag{3.2.18}$$

while $\phi_{\angle} = \phi_k - \arctan\left(\frac{y_{\perp}}{x_{\perp}}\right) =: \phi_k - \delta$. One gets for (3.2.18)

$$\exp\big(i(\sin(\delta)-b)|\vec{k}_{\perp}|\sin(\phi_k) + i|\vec{k}_{\perp}||\vec{x}_{\perp}|\cos(\delta)\cos(\phi_k)\big). \tag{3.2.19}$$

Integrating this over ϕ_k from 0 to 2π gives

$$2\pi J_0(|\vec{k}_{\perp}|\sqrt{\cos(\delta)^2|\vec{x}_{\perp}|^2 + (|\vec{x}_{\perp}|\sin(\delta)-b)^2}) = 2\pi J_0(|\vec{k}_{\perp}|\sqrt{x^2+(y-b)^2}). \tag{3.2.20}$$

Such that one obtains

$$wh_{\pm}(\vec{x}_{\perp},0,s) = \int \frac{d|\vec{k}_{\perp}|}{4\pi^2}L(|\vec{k}_{\perp}|,s,x,y) \tag{3.2.21}$$

$$L(|\vec{k}_{\perp}|,s,x,y) = \sqrt{2\pi}J_0(|\vec{k}_{\perp}|\sqrt{x^2+(y-b)^2})8\frac{s^2}{|\vec{k}_{\perp}|}I_2(|\vec{k}_{\perp}|s). \tag{3.2.22}$$

This expression is now expanded in s. Every expansion term can be integrated in (3.2.21) analytically. Together the result for (3.2.12) takes the form

$$\frac{A}{\sqrt{2\pi^3w^2}}e^{-\frac{z_{\pm}^2}{w^2}}e^{-\frac{x^2+(y-b)^2}{2R^2}}\sum_{k=0,k\in2\mathbb{Z}}^{\infty}\sum_{l=0}^{k/2}\frac{(-1)^l}{(l!)^2}\frac{(\frac{k}{2})!(\frac{k}{2}+2)!}{(k/2-l)!}\Big(\frac{R}{\sqrt{2}}\Big)^{k-2l}\Big(\frac{x^2+(y-b)^2}{4}\Big)^l\frac{s^{k+4}}{R^{2k}}. \tag{3.2.23}$$

Although exact, this expression is still useless for numerical calculations due to the sum to infinity. However the structure of this result allows the following observation:

If $x^2 + (y-b)^2$ is large, then the Gaussian forces this term to be negligible and if $x^2 + (y-b)^2$ is small the faculties in the sum together with $1/R^{2k}$ cause the terms of order $\mathcal{O}(s^{o(\text{interval})})$ or higher to be negligible. The order $o(\text{interval}) \in 2\mathbb{Z}$ depends on the size of the interval in which we consider s. For $s \in [0,5]$, $R = 4$ terms of order $s^{40<}$ are smaller then 10^{-20} for all x and y. In this case the complicated function $h_\pm(\vec{x}_\perp, z_\pm, s)$ can be perfectly approximated by a polynomial times two simple Gaussians

$$\frac{A}{\sqrt{2\pi^3 w^2}} e^{-\frac{z_\pm^2}{w^2}} e^{-\frac{x^2+(y-b)^2}{2R^2}} \sum_{k=0, k\in 2\mathbb{Z}}^{40} \sum_{l=0}^{k/2} \frac{(-1)^l}{(l!)^2} \frac{(\frac{k}{2})!(\frac{k}{2}+2)!}{(k/2-l)!} \left(\frac{R}{\sqrt{2}}\right)^{k-2l} \left(\frac{x^2+(y-b)^2}{4}\right)^l \frac{s^{k+4}}{R^{2k}}. \tag{3.2.24}$$

When we want to determine the metric of a single shock, then we can forget about b and t and set both to 0 in the formula above. Obviously (3.2.23) then only depends on $\vec{x}_\perp^2$, which further decreases computation time.

Chapter 4

Conclusion

4.1 Summary and discussion

In this thesis we discussed several projects, which are linked by the endeavour to bring AdS/CFT closer to QCD and heavy ion physics. Errors in the literature [10–12] regarding the deduction and final form of the higher derivative corrected EoMs of gauge fields within AdS/CFT where found and rectified. We showed that this drastically changes previously obtained results regarding the 't Hooft coupling corrections to the photoemission rate, quasinormal mode spectra, the conductivity and spectral functions [10–12, 19, 53]. The actual 't Hooft coupling corrections turned out to be one order of magnitude smaller than previously thought. For the large frequency limit of the photoemission rate we could resolve a conflict between predictions from weak coupling regarding the sign of the correction factor.

We found a prescription to treat the higher derivative corrected Ramond-Ramond five form and proved it for the case of a constant magnetic background field. We then proceeded to determine the metric solution corresponding to α'^3-corrected magnetic black branes and studied tensor quasinormal modes in this geometry. The dual field theoretic setting describes a quark gluon plasma in a strong magnetic field, which also forms during actual heavy ion collisions. It was found that the magnetic background field had a strong influence on the equilibration time of a quark gluon plasma especially, if we include α'^3-corrections. For large background fields equilibration times were consistently shorter then without.

Finishing the discussion of higher derivative corrections to the AdS/CFT correspondence, we presented a resummation technique, that allows us to estimate the range of applicability of α'^3-corrections and exhibits interesting properties itself:
The resummed corrections were substantially smaller and more well behaved than the third order in α' corrections. Resummed quasinormal mode spectra stayed within the lower complex plane for all tested 't Hooft coupling values and maintained a pattern

that corresponds to top-down thermalization.

The second focal point of this thesis is the construction of software to simulate heavy ion collisions by colliding gravitational shockwaves in AdS_5, pioneered by P. Chesler and L. G. Yaffe [34, 35]. On the one hand we gave a didactical overview of how to build shockwave collision code from scratch. On the other hand we went beyond the models so far and studied the collision of shockwaves of asymmetric widths, whereby we simulate pixels of peripheral collisions. We showed that the observations regarding boost invariant and universal flow also hold in the asymmetric case. We were able to give a formula describing the post collision proper energy density distributions only depending on the asymmetric widths, rapidity ξ and proper time τ. With the help of the hydrodynamic approximation, this allows to construct the stress energy tensor of highly relativistic peripheral collisions (where we assume transverse gradients to be negligible compared to the projectiles' speed) without the necessity to perform 5-dimensional shockwave collisions.

4.2 Outlook

There are several ways, in which this research can be extended in the future. Here we collected the most important and promising projects, building on this work.

- *Finite 't Hooft coupling corrections to shockwave collisions*: Considering the success of AdS/CFT in dynamically modeling heavy ion collisions in the $\lambda \to \infty$ limit, it is of special interest to determine finite 't Hooft coupling corrections to this process, allowing to study it in a substantially more realistic setting of finite coupling. The first hurdle to overcome here is the difficult task to determine $\mathcal{O}(\alpha')$ corrections to the relation between the near boundary geometry of the AdS space and the boundary stress energy tensor.

- *Study (asymmetric) localized shock collisions*: Localized shock collisions are notoriously difficult to simulate. However, there are several burning questions that can be answered with this. On the one hand we could test how robust the model found in this thesis regarding the post collision flow during peripheral heavy ion collisions really is. On the other hand we can use such a higher dimensional code to investigate the influence the rotating fireball has on the experimentally measured polarization of emitted particles, by studying vorticity. Also simulating asymmetric (so e.g. $p+Pb$) heavy ion collisions with localized shocks can provide interesting insights regarding qualitative comparison with experimental data.

- *Magnetic black branes + chemical potential at finite 't Hooft coupling*: Regarding the computation of higher derivative corrections to the black brane geometry presented in this work, it is an attractive next question to study finite 't Hooft

coupling corrected magnetic black branes at non zero chemical potential and investigate anomaly driven effects at finite λ.

- *Simulating shockwave collisions with phase transition*: Another interesting setting to explore is the model obtained from the formulation of shockwave collisions, describing heavy ions in the boundary field theory, in theories obtained from other sectors of string theory. Especially the Witten model, which is dual to the low energy limit of type IIa super string theory, would be a promising candidate. Since via this duality one can gravitationally model phase transitions, there is hope, that the confinement/deconfinement phase transition can be at least approximated in dynamical simulations.

- *Simulating heavy ion collisions with spin*: This challenging task can only be achieved via computing localized shockwave collisions as described in the second bullet. In addition it comes with the substantial complication that now the starting conditions would have to be derived from boosted Kerr-black holes, not Schwarzschild black holes. Nonetheless, this should be feasible with sufficient computational resources.

- *Computing shockwave collisions with constant magnetic background field*: This interesting project would allow to investigate the influence the strong magnetic field, that forms for very short times during heavy ion collisions, has on, among others, the post collision flow, the hydrodynamization time and entropy production.

Acknowledgements

First of all I would like to thank my supervisor Andreas Schäfer on the one hand for hiring me as a PhD student and on the other hand for countless useful discussions going back many years to the first QFT lectures I listened to, when I was writing my physics Bachelor thesis under his supervision. His instinct for very interesting projects was the initiative of a huge part of the research presented in this thesis. His lectures in QCD and String Theory together with Vladimir Braun's QED and QFT lectures sparked my interest in theoretical particle physics. Regarding the work on this thesis I also greatly profited from Meinulf Göckeler's differential geometry lecture, Tilo Wettig's group theory lecture, Felix Finster's lectures on functional analysis and PDEs and John Schliemann's lecture on GR. Although the content of her algebraic topology lectures did not play a huge role in this thesis, I still want to thank Clara Löh, the supervisor of my Master thesis in mathematics. Her impressively well structured way of approaching scientific problems strongly impacted my research (at least I hope so).

I especially thank the Elite Network of Bavaria, which accompanied me throughout my PhD study, for the generous financial support in form of a (2+1 year) research scholarship and the broad range of program offers.

My work on numerical simulations of asymmetric shockwave collisions in AdS_5 would not have been possible without the help and advise in form of many Skype sessions with Larry Yaffe, who together with Paul Chesler pioneered the use of characteristic formulation of the bulk field equations in the context of gravitational collisions in Anti-de Sitter space. His exceptional expertise, in this case especially regarding gravity and subtleties of the numerics, was essential for the from-scratch-building of the asymmetric shockwave collision code that was constructed and used in this work. Especially this project and my first paper [19] also greatly profited from two several month long research stays of Larry in Regensburg. Regarding the project on shockwave collisions I thank Larry, Andreas Schäfer and Andreas Rabenstein for a great collaboration.

I would also like to especially thank Aleksi Vuorinen on the one hand for his sup-

port, great collaboration and hospitality during my work on my first publication on higher derivative corrections on the other hand for discussions (also with his research group) and again his hospitality during my work on the second publication on the list of papers this thesis is built on. In this context I also want to thank Christian Ecker and Martin Schvellinger for several discussions.

I also thank the University of Helsinki, the Technical University of Wien and the University of Washington for their hospitality during shorter stays.

Furthermore several projects presented in this thesis profited from useful comments from and discussions with Anton Rebhan and his research group, Johanna Erdmenger and her research group, Kostas Skenderis, Martin Ammon, Norbert Bodendorfer, Michal Heller and Matthias Kaminski.

Finally and most importantly I would like to thank my entire family for their strong support during my PhD studies.

Chapter 5

Appendix

5.1 Explicit higher derivative correction terms to IIb SUGRA

In the introductory chapter 1.2 we discussed higher derivative corrections to the type IIb SUGRA action. The explicit terms, schematically collected in (1.2.12) and the parameters n_i in (1.2.13) are explicitly given by

$$\begin{aligned}(n_i)_{i=1,\dots,20} =&(-43008, 86016, 129024, 30240, 7392, -4032, -4032, -118272,\\ &-26880, 112896, -96768, 1344, -12096, -48384, 24192, 2386,\\ &-3669, -1296, 10368, 2688)\end{aligned} \tag{5.1.1}$$

as well as

$$\begin{aligned}(M_i)_{i=1,\dots,20} =&(C_{abcd}C^{abef}C^{c}{}_{egh}C^{dg}{}_{f}{}^{h}, C_{abcd}C^{aecf}C^{bg}{}_{eh}C^{d}{}_{gf}{}^{h},\\ &C_{abcd}C^{a}{}_{e}{}^{f}{}_{g}C^{b}{}_{fhi}\mathcal{T}^{cdeghi}, C_{abc}{}^{d}C^{abc}{}_{e}\mathcal{T}_{dfghij}\mathcal{T}^{efhgij},\\ &C_{a}{}^{bcd}C^{a}{}_{bef}\mathcal{T}_{cdghij}\mathcal{T}^{efghij}, C_{a}{}^{bc}{}_{d}C^{ae}{}_{cf}\mathcal{T}_{beghij}\mathcal{T}^{dfghij}\\ &C_{a}{}^{bcd}C^{a}{}_{ecf}\mathcal{T}_{bghdij}\mathcal{T}^{eghfij}, C_{a}{}^{bc}{}_{d}C^{ae}{}_{fg}\mathcal{T}_{bcehij}\mathcal{T}^{dfhgij},\\ &C_{a}{}^{bc}{}_{d}C^{ae}{}_{fg}\mathcal{T}_{bcehij}\mathcal{T}^{dhifgj}, C_{a}{}^{bc}{}_{d}C^{a}{}_{e}{}^{f}{}_{g}\mathcal{T}_{bcfhij}\mathcal{T}^{dehgij},\\ &C_{a}{}^{bc}{}_{d}C^{ae}{}_{fg}\mathcal{T}_{bcheij}\mathcal{T}^{dfhgij}, C^{abcd}\mathcal{T}_{abefgh}\mathcal{T}_{cd}{}^{eijk}\mathcal{T}^{fgh}{}_{ijk},\\ &C^{abcd}\mathcal{T}_{abefgh}\mathcal{T}_{cd}{}^{fijk}\mathcal{T}^{egh}{}_{ijk}, C^{abcd}\mathcal{T}_{abefgh}\mathcal{T}_{cd}{}^{fijk}\mathcal{T}^{eg}{}_{i}{}^{h}{}_{jk},\\ &C^{abcd}\mathcal{T}_{abefgh}\mathcal{T}_{c}{}^{efijk}\mathcal{T}_{d}{}^{gh}{}_{ijk}, \mathcal{T}_{abcdef}\mathcal{T}^{abcdgh}\mathcal{T}^{e}{}_{gijkl}\mathcal{T}^{fij}{}_{h}{}^{kl},\\ &\mathcal{T}_{abcdef}\mathcal{T}^{abcghi}\mathcal{T}^{de}{}_{jg}{}^{kl}\mathcal{T}^{f}{}_{hki}{}^{j}{}_{l}, \mathcal{T}_{abcdef}\mathcal{T}^{abcghi}\mathcal{T}^{d}{}_{gj}{}^{ekl}\mathcal{T}^{f}{}_{h}{}^{j}{}_{ikl}\\ &\mathcal{T}_{abcdef}\mathcal{T}^{abcghi}\mathcal{T}^{d}{}_{gj}{}^{ekl}\mathcal{T}^{f}{}_{hki}{}^{j}{}_{l}, \mathcal{T}_{abcdef}\mathcal{T}^{aghdij}\mathcal{T}^{b}{}_{gk}{}^{e}{}_{il}\mathcal{T}^{c}{}_{h}{}^{kf}{}_{j}{}^{l}).\end{aligned} \tag{5.1.2}$$

5.2 Explicit components of five form solution

In section 2.1.2 we used the magnetic and electric part of the Ramond-Ramond five form F_5 in the presence of a (transversely polarized) gauge field A_x in order $\mathcal{O}(\alpha'^0)$.

Here we display the explicite forms:
We start with the gauge field free electric part and its Hodge dual and get

$$
\begin{aligned}
(F_5^{el})^0 &= -4\sqrt{|\det(g_5)|}dt\wedge du\wedge dx\wedge dy\wedge dz\\
*(F_5^{el})^0 &= 4\sqrt{\det(g_{S_5})}dy_1\wedge dy_2\wedge dy_3\wedge dy_4\wedge dy_5+4\sqrt{|\det(g_{10})|}\sqrt{|\det(g_5)|}\\
&\Big(g_{10}^{tt}g_{10}^{uu}g_{10}^{yy}g_{10}^{xy_3}g_{10}^{zz}dy_1\wedge dy_2\wedge dx\wedge dy_4\wedge dy_5+g_{10}^{tt}g_{10}^{uu}g_{10}^{yy}g_{10}^{xy_4}g_{10}^{zz}dy_1\wedge dy_2\\
&\wedge dy_3\wedge dx\wedge dy_5+g_{10}^{tt}g_{10}^{uu}g_{10}^{yy}g_{10}^{xy_5}g_{10}^{zz}dy_1\wedge dy_2\wedge dy_3\wedge dy_4\wedge dx\Big)=:(F_5^{mag})^0,
\end{aligned}
\tag{5.2.1}
$$

where g_{10} is the metric of the 10 dimensional manifold corresponding to an AdS-Schwarzschild black hole times S_5, g_5 is the metric corresponding to the internal AdS space and g_{S_5} is the metric of the five sphere. The nomenclature $(F_5^{mag})^0$ shouldn't distract from the fact that it nevertheless depends on A_μ via $g_{10}^{xy_5}$, $g_{10}^{xy_4}$ and $g_{10}^{xy_3}$. The electric components of the five form including the gauge field $A_x(u,t,z)$ are explicitly given by

$$
(F_5^{el})^1=(F_5^{el})^1_{ux}+(F_5^{el})^1_{tx}+(F_5^{el})^1_{zx} \tag{5.2.2}
$$

with

$$
\begin{aligned}
(F_5^{el})^1_{ux} &= \frac{2\partial_u A_x(u,t,z)}{\sqrt{3}}\sqrt{|\det(g_5)|}g_5^{xx}g_5^{uu}\big(\sin(y_1)\cos(y_1)dt\wedge dy\wedge dz\wedge dy_1\wedge dy_3+\\
&\cos(y_1)^2\sin(y_2)\cos(y_2)dt\wedge dy\wedge dz\wedge dy_2\wedge dy_4-\cos(y_1)\sin(y_1)\sin(y_2)^2dt\\
&\wedge dy\wedge dz\wedge dy_1\wedge dy_4-\cos(y_1)\sin(y_1)\cos(y_2)^2dt\wedge dy\wedge dz\wedge dy_1\wedge dy_5\\
&-\cos(y_2)\sin(y_2)\cos(y_1)^2dt\wedge dy\wedge dz\wedge dy_2\wedge dy_5\big),
\end{aligned}
\tag{5.2.3}
$$

$$
\begin{aligned}
(F_5^{el})^1_{tx} &= -\frac{2\partial_t A_x(u,t,z)}{\sqrt{3}}\sqrt{|\det(g_5)|}g_5^{xx}g_5^{tt}\big(\sin(y_1)\cos(y_1)du\wedge dy\wedge dz\wedge dy_1\wedge dy_3+\\
&\cos(y_1)^2\sin(y_2)\cos(y_2)du\wedge dy\wedge dz\wedge dy_2\wedge dy_4-\cos(y_1)\sin(y_1)\sin(y_2)^2du\\
&\wedge dy\wedge dz\wedge dy_1\wedge dy_4-\cos(y_1)\sin(y_1)\cos(y_2)^2du\wedge dy\wedge dz\wedge dy_1\wedge dy_5\\
&-\cos(y_2)\sin(y_2)\cos(y_1)^2du\wedge dy\wedge dz\wedge dy_2\wedge dy_5\big),
\end{aligned}
\tag{5.2.4}
$$

$$
\begin{aligned}
(F_5^{el})^1_{zx} &= -\frac{2\partial_z A_x(u,t,z)}{\sqrt{3}}\sqrt{|\det(g_5)|}g_5^{xx}g_5^{zz}\big(\sin(y_1)\cos(y_1)dt\wedge dy\wedge du\wedge dy_1\wedge dy_3+\\
&\cos(y_1)^2\sin(y_2)\cos(y_2)dt\wedge dy\wedge du\wedge dy_2\wedge dy_4-\cos(y_1)\sin(y_1)\sin(y_2)^2dt\\
&\wedge dy\wedge du\wedge dy_1\wedge dy_4-\cos(y_1)\sin(y_1)\cos(y_2)^2dt\wedge dy\wedge du\wedge dy_1\wedge dy_5\\
&-\cos(y_2)\sin(y_2)\cos(y_1)^2dt\wedge dy\wedge du\wedge dy_2\wedge dy_5\big).
\end{aligned}
\tag{5.2.5}
$$

Analogously we write the magnetic part as

$$(F_5^{mag})^1 = (F_5^{mag})^1_{ux} + (F_5^{mag})^1_{tx} + (F_5^{mag})^1_{zx} \tag{5.2.6}$$

with

$$\begin{aligned}(F_5^{mag})^1_{ux} = &-\sqrt{\det(g_{S_5})}\big(\sin(y_1)\cos(y_1)g_{10}^{y_1y_1}g_{10}^{y_3y_3}du\wedge dx\wedge dy_2\wedge dy_5\wedge dy_4+\\ &\cos(y_1)^2\sin(y_2)\cos(y_2)g_{10}^{y_2y_2}g_{10}^{y_4y_4}du\wedge dx\wedge dy_1\wedge dy_5\wedge dy_3-\sin(y_1)\times\\ &\cos(y_1)\sin(y_2)^2g_{10}^{y_1y_1}g_{10}^{y_4y_4}du\wedge dx\wedge dy_2\wedge dy_3\wedge dy_5-\cos(y_1)\sin(y_1)\times\\ &\cos(y_2)^2g_{10}^{y_1y_1}g_{10}^{y_5y_5}du\wedge dx\wedge dy_2\wedge dy_4\wedge dy_3-\cos(y_2)\sin(y_2)\cos(y_1)^2\times\\ &g_{10}^{y_2y_2}g_{10}^{y_5y_5}du\wedge dx\wedge dy_1\wedge dy_3\wedge dy_4)\frac{2\partial_u A_x(u,t,z)}{\sqrt{3}}+\mathcal{O}(A_x(u,t,z)^2),\end{aligned} \tag{5.2.7}$$

$$\begin{aligned}(F_5^{mag})^1_{tx} = &-\sqrt{\det(g_{S_5})}\big(\sin(y_1)\cos(y_1)g_{10}^{y_1y_1}g_{10}^{y_3y_3}dt\wedge dx\wedge dy_2\wedge dy_5\wedge dy_4+\\ &\cos(y_1)^2\sin(y_2)\cos(y_2)g_{10}^{y_2y_2}g_{10}^{y_4y_4}dt\wedge dx\wedge dy_1\wedge dy_5\wedge dy_3-\sin(y_1)\times\\ &\cos(y_1)\sin(y_2)^2g_{10}^{y_1y_1}g_{10}^{y_4y_4}dt\wedge dx\wedge dy_2\wedge dy_3\wedge dy_5-\cos(y_1)\sin(y_1)\times\\ &\cos(y_2)^2g_{10}^{y_1y_1}g_{10}^{y_5y_5}dt\wedge dx\wedge dy_2\wedge dy_4\wedge dy_3-\cos(y_2)\sin(y_2)\cos(y_1)^2\times\\ &g_{10}^{y_2y_2}g_{10}^{y_5y_5}dt\wedge dx\wedge dy_1\wedge dy_3\wedge dy_4)\frac{2\partial_t A_x(u,t,z)}{\sqrt{3}}+\mathcal{O}(A_x(u,t,z)^2),\end{aligned} \tag{5.2.8}$$

$$\begin{aligned}(F_5^{mag})^1_{zx} = &-\sqrt{\det(g_{S_5})}\big(\sin(y_1)\cos(y_1)g_{10}^{y_1y_1}g_{10}^{y_3y_3}dz\wedge dx\wedge dy_2\wedge dy_5\wedge dy_4+\\ &\cos(y_1)^2\sin(y_2)\cos(y_2)g_{10}^{y_2y_2}g_{10}^{y_4y_4}dz\wedge dx\wedge dy_1\wedge dy_5\wedge dy_3-\sin(y_1)\times\\ &\cos(y_1)\sin(y_2)^2g_{10}^{y_1y_1}g_{10}^{y_4y_4}dz\wedge dx\wedge dy_2\wedge dy_3\wedge dy_5-\cos(y_1)\sin(y_1)\times\\ &\cos(y_2)^2g_{10}^{y_1y_1}g_{10}^{y_5y_5}dz\wedge dx\wedge dy_2\wedge dy_4\wedge dy_3-\cos(y_2)\sin(y_2)\cos(y_1)^2\times\\ &g_{10}^{y_2y_2}g_{10}^{y_5y_5}dz\wedge dx\wedge dy_1\wedge dy_3\wedge dy_4)\frac{2\partial_z A_x(u,t,z)}{\sqrt{3}}+\mathcal{O}(A_x(u,t,z)^2).\end{aligned} \tag{5.2.9}$$

5.3 Important components of $\frac{\delta\mathcal{W}}{\delta F_5}$

In section 2.1.2 we determined the higher derivative correction terms $\frac{\delta\mathcal{W}}{\delta F_5}$ to the EoM of the Ramond-Ramond five form. The most important components of the form $\frac{\delta\mathcal{W}}{\delta F_5}$ are given in below:

$$\begin{aligned}\left(\frac{\delta\mathcal{W}}{\delta F_5}\right)_{xy_1y_2y_4y_5} =&\gamma\frac{\cos(y_1)^3\sin(y_1)\sin(y_2)\cos(y_2)}{6\sqrt{3}}\big((-117\frac{u^5}{(1-u^2)}\partial_t^2A_x+(468u^6-\\ &468u^8)\partial_u^2A_x+83u^5\partial_z^2A_x+(4312u^5-5248u^7)\partial_uA_x)\big)+\mathcal{O}(A_x^2)\end{aligned} \tag{5.3.1}$$

$$\left(\frac{\delta\mathcal{W}}{\delta F_5}\right)_{xzy_2y_4y_5} = -\gamma\frac{(\cos(y_1)^4\sin(y_2)\cos(y_2))}{6\sqrt{3}}((415u^6-415u^8)\partial_u^2\partial_z A_x + \frac{415u^5}{4(-1+u^2)}$$
$$\partial_z\partial_t^2 A_x - \frac{261u^5}{4}\partial_z^3 A_x + (3220u^5-4050u^7)\partial_u\partial_z A_x +$$
$$(2181u^4-3216u^6)\partial_z A_x) + \mathcal{O}(A_x^2) \tag{5.3.2}$$

$$\left(\frac{\delta\mathcal{W}}{\delta F_5}\right)_{uxy_2y_4y_5} = \gamma\frac{(\cos(y_1)^4\sin(y_2)\cos(y_2))}{6\sqrt{3}}((-733u^6+733u^8)\partial_u^3 A_x + \frac{733u^5}{4(1-u^2)}$$
$$\partial_u\partial_t^2 A_x - \frac{257u^5}{4}\partial_z^2\partial_u A_x + (-4398u^5+7330u^7)\partial_u^2 A_x +$$
$$\frac{3117u^4-1651u^6}{4(1-u^2)^2}\partial_t^2 A_x - 1145u^4\partial_z^2 A_x + (-2056u^4+12162u^6)\partial_u A_x)$$
$$+\mathcal{O}(A_x^2) \tag{5.3.3}$$

$$\left(\frac{\delta\mathcal{W}}{\delta F_5}\right)_{txy_2y_4y_5} = -\gamma\frac{(\cos(y_1)^4\sin(y_2)\cos(y_2))}{6\sqrt{3}}((733u^6-733u^8)\partial_u^2\partial_t A_x + \frac{257u^5}{4}\partial_z^2\partial_t A_x$$
$$+\frac{733u^5}{4(-1+u^2)}\partial_t^3 A_x + (548u^5-2014u^7)\partial_u\partial_t A_x + (u^4(-609+912u^2))$$
$$\partial_t A_x) + \mathcal{O}(A_x^2) \tag{5.3.4}$$

5.4 EoM for metric with backreaction of a strong magnetic field in the infinite coupling case

In section 2.2.1 we determined the Einstein(-Maxwell) equations derived from the Kaluza-Klein reduced type IIb action with ansatz (2.2.2), (2.2.3), (2.2.5) and (2.2.6) in order $\mathcal{O}(\alpha'^0)$. These EoM are explicitly given by:

$$0 = b^2L(u)^{12} + 2b^2L(u)^4 + 30L(u)^8e^{4V(u)}(4u^3U(u)L'(u)^2-1) + 30u^2L(u)^9e^{4V(u)}$$
$$(uL'(u)U'(u) + U(u)(2uL''(u) + L'(u)(4uV'(u) + 2uW'(u) + 3))) + 6u^2L(u)^{10}$$
$$e^{4V(u)}(uU'(u)(2V'(u)+W'(u)) + U(u)(4uV''(u) + V'(u)(4uW'(u)+6)$$
$$+6uV'(u)^2 + 2uW''(u) + 2uW'(u)^2 + 3W'(u))) + 12e^{4V(u)} \tag{5.4.1}$$

$$0 = b^2L(u)^{12} + 2b^2L(u)^4 + 30u^3L(u)^9e^{4V(u)}L'(u)(U'(u) + 2U(u)(2V'(u)+W'(u)))$$
$$+30L(u)^8e^{4V(u)}(4u^3U(u)L'(u)^2-1) + 6u^3L(u)^{10}e^{4V(u)}(U'(u)(2V'(u)+$$
$$W'(u)) + 2U(u)V'(u)(V'(u)+2W'(u))) + 12e^{4V(u)} \tag{5.4.2}$$

$$
\begin{aligned}
0 =& 7b^2L(u)^{12} - 2b^2L(u)^4 + 90L(u)^8e^{4V(u)}(4u^3U(u)L'(u)^2 - 1) + 120u^2L(u)^9e^{4V(u)} \\
& (2uL'(u)U'(u) + U(u)(2uL''(u) + L'(u)(4uV'(u) + 2uW'(u) + 3))) + 15u^2 \\
& L(u)^{10}e^{4V(u)}(2(uU''(u) + U(u)(4uV''(u) + V'(u)(4uW'(u) + 6) + 6uV'(u)^2 \\
& + 2uW''(u) + 2uW'(u)^2 + 3W'(u))) + U'(u)(8uV'(u) + 4uW'(u) + 3)) \\
& - 60e^{4V(u)}
\end{aligned} \tag{5.4.3}
$$

$$
\begin{aligned}
0 =& b^2L(u)^{12} + 2b^2L(u)^4 - 30L(u)^8e^{4V(u)}(4u^3U(u)L'(u)^2 - 1) - 30u^2L(u)^9e^{4V(u)} \\
& (2uL'(u)U'(u) + U(u)(2uL''(u) + L'(u)(2uV'(u) + 2uW'(u) + 3))) - 3u^2 \\
& L(u)^{10}e^{4V(u)}(2uU''(u) + U'(u)(4uV'(u) + 4uW'(u) + 3) + U(u)(4u(V''(u) \\
& + W''(u)) + V'(u)(4uW'(u) + 6) + 4uV'(u)^2 + 4uW'(u)^2 + 6W'(u))) \\
& - 12e^{4V(u)}
\end{aligned} \tag{5.4.4}
$$

$$
\begin{aligned}
0 =& b^2L(u)^{12} + 2b^2L(u)^4 + 30L(u)^8e^{4V(u)}(4u^3U(u)L'(u)^2 - 1) + 30u^2L(u)^9e^{4V(u)} \\
& (2uL'(u)U'(u) + U(u)(2uL''(u) + L'(u)(4uV'(u) + 3))) + 3u^2L(u)^{10}e^{4V(u)} \\
& (2(uU''(u) + U(u)(4uV''(u) + 6uV'(u)^2 + 6V'(u))) + U'(u)(8uV'(u) + 3)) \\
& + 12e^{4V(u)},
\end{aligned} \tag{5.4.5}
$$

Consistently the function $L(u)$ is solved by 1 in this order of α'.

5.5 Second expansion coefficients of the megnetic black brane geometry

In section 2.2.1 we derived the magnetic black brane geometry as expansion in the shifted radial coordinate $(1-u)$ (i.e. an expansion around the horizon). We give the next order coefficients as an example of the near horizon expansion of the magnetic black brane geometry so far without higher derivative corrections

$$
\begin{aligned}
u_3 =& -\frac{1}{1080l_0^{20}u_1}\Big(- 16b^4l_0^{24} - 76b^4l_0^{16} - 108b^4l_0^8 - 135b^2l_0^{22}u_1 - 540b^2l_0^{14} \\
& u_1 + 240b^2l_0^{20} + 1440b^2l_0^{12} - 720b^2l_0^4 - 675l_0^{20}u_1^2 + 4050l_0^{18}u_1 - 3240l_0^{10}u_1 \\
& - 5400l_0^{16} + 10800l_0^8 - 6480\Big)
\end{aligned} \tag{5.5.1}
$$

$$v_2 = -\frac{1}{360 l_0^{20} u_1^2}\Big(11b^4 l_0^{24} + 11b^4 l_0^{16} + 8b^4 l_0^8 + 45b^2 l_0^{22} u_1 + 45b^2 l_0^{14} u_1 + 30b^2 l_0^{20} - 180b^2 l_0^{12} - 270 l_0^{10} u_1 + 900 l_0^8 - 720\Big) \tag{5.5.2}$$

$$w_3 = -\frac{1}{360 l_0^{20} u_1^2}\Big(-7b^4 l_0^{16} - 8b^4 l_0^8 - 45b^2 l_0^{14} u_1 + 120b^2 l_0^{12} - 270 l_0^{10} u_1 + 900 l_0^8 - 720\Big) \tag{5.5.3}$$

$$l_2 = -\frac{1}{1800 l_0^{19} \mathrm{u1}^2}\Big(-12b^4 l_0^{24} + 5b^4 l_0^{16} + 7b^4 l_0^8 - 45b^2 l_0^{22} u_1 + 45b^2 l_0^{14} u_1 - 60b^2 l_0^{20} + 120b^2 l_0^{12} - 60b^2 l_0^4 - 1350 l_0^{18} u_1 + 1350 l_0^{10} u_1 - 2700 l_0^8 + 2700\Big). \tag{5.5.4}$$

5.6 Equation of motion of tensor fluctuations for $b = 0$

In section 2.2.5 we made use of the higher derivative corrected EoM of tensor fluctuations in the (coupling corrected) AdS-Schwarzschild black hole geometry without a magnetic background field. We define the function $h := h_x^y$, such that one obtains [25]

$$h''(u) - \frac{u^2+1}{u(1-u^2)}h'(u) + (\hat{\omega}^2 - \hat{q}^2\frac{1-u^2}{u(1-u^2)^2}h(u) + \frac{\gamma}{4}\Big((3171u^4 + 3840\hat{q}^2u^3 + 2306u^2 - 600)uh'(u) + \frac{u}{(1-u^2)^2}\Big(600\omega^2 - 300\hat{q}^2 + 50u + (3456\hat{q}^2 - 2856\hat{\omega}^2)u^2 + 768u^3\hat{q}^4 + (2136\hat{\omega}^2 - 6560\hat{q}^2)u^4 - (768\hat{q}^4 + 275)u^5 + 3404\hat{q}^2u^6 + 225u^7\Big)h(u) + 120\frac{\hat{\omega}^2 - \hat{q}^2(1-u^2)}{u(1-u^2)^2}h(u)\Big) = 0 \tag{5.6.1}$$

from varying the higher derivative corrected action with respect to h_{xy}. This differential equation simplifies to

$$f_2(u)\phi''(u) + f_1(u,\gamma,\hat{\omega})\phi'(u) + f_0(u,\gamma,\hat{\omega})\phi''(u) = 0 \tag{5.6.2}$$

defining $h(u) = (1-u)^{-\frac{i\omega}{2}}\phi(u)$, where we set $q = 0$. The coefficients f_0, f_1, f_2 are given by

$$f_0(u,\gamma,\hat{\omega}) = ((-2\hat{\omega}(-2i + 4\hat{\omega} + u^2\hat{\omega} + u(-2i + 3\hat{\omega})) + \gamma(1+u)(u^5(-100 - 2306i\hat{\omega}) + u^7(450 - 3171i\hat{\omega}) - 3171iu^6\hat{\omega} - 240\hat{\omega}^2 + 100iu^3(i + 6\hat{\omega}) - 120u^2\hat{\omega}(-5i + 12\hat{\omega}) + 2u^4\hat{\omega}(-1153i + 2136\hat{\omega}))) \tag{5.6.3}$$

$$f_1(u,\gamma,\hat{\omega}) = 2(1+u)(4-2906\gamma u^4-865\gamma u^6+3171\gamma u^8+u^2(4+600\gamma-4i\hat{\omega})-4iu\hat{\omega}) \quad (5.6.4)$$

$$f_2(u) = 8u(1+u)^2(-1+u). \quad (5.6.5)$$

5.7 Near boundary expansions of coordinate transformation

In section 3.1.4 we gave explicit formulas to determine the transformation functions[70] $\tilde{\alpha}$, $\tilde{\beta}$ and $\tilde{\gamma}$ as expansions in the radial coordinate u. The coefficients $\{a_i\}_i$ of the near boundary expansion (3.1.31) of $\tilde{\alpha}$ are given by

$$a_0 = \frac{2\sqrt{\frac{2}{\pi}}e^{-\frac{z^2}{2w^2}}}{15w} \quad (5.7.1)$$

$$a_1 = \frac{11ze^{-\frac{z^2}{2w^2}}}{60\sqrt{2\pi}w^3} \quad (5.7.2)$$

$$a_2 = \frac{37ze^{-\frac{z^2}{2w^2}}(z^2-3w^2)}{2016\sqrt{2\pi}w^7} \quad (5.7.3)$$

$$a_3 = \frac{e^{-\frac{z^2}{w^2}}(768w^7+23\sqrt{2\pi}e^{\frac{z^2}{2w^2}}(3w^4-6w^2z^2+z^4))}{12096\pi w^9} \quad (5.7.4)$$

$$a_4 = \frac{ze^{-\frac{z^2}{w^2}}(1896w^7+7\sqrt{2\pi}e^{\frac{z^2}{2w^2}}(15w^4-10w^2z^2+z^4))}{21600\pi w^{11}} \quad (5.7.5)$$

$$a_5 = \frac{e^{-\frac{z^2}{w^2}}(-48456w^9+89736w^7z^2-67\sqrt{2\pi}e^{\frac{z^2}{2w^2}}(15w^6-45w^4z^2+15w^2z^4-z^6))}{1425600\pi w^{13}} \quad (5.7.6)$$

[70] Describing the transformation of a single shock geometry in FG coordinates to EF coordinates.

The coefficients $\{b_i\}_i$ of the near boundary expansion (3.1.30) of $\tilde{\beta}$ are given by

$$b_0 = -\frac{e^{-\frac{z^2}{2w^2}}}{6\sqrt{2\pi}w} \tag{5.7.7}$$

$$b_1 = -\frac{ze^{-\frac{z^2}{2w^2}}}{10\sqrt{2\pi}w^3} \tag{5.7.8}$$

$$b_2 = \frac{e^{-\frac{z^2}{2w^2}}(w^2 - z^2)}{30\sqrt{2\pi}w^5} \tag{5.7.9}$$

$$b_3 = \frac{ze^{-\frac{z^2}{2w^2}}(3w^2 - z^2)}{126\sqrt{2\pi}w^7} \tag{5.7.10}$$

$$b_4 = \frac{e^{-\frac{z^2}{w^2}}(-116w^7 - 3\sqrt{2\pi}e^{\frac{z^2}{2w^2}}(3w^4 - 6w^2z^2 + z^4))}{4032\pi w^9} \tag{5.7.11}$$

$$b_5 = -\frac{ze^{-\frac{z^2}{w^2}}(312w^7 + \sqrt{2\pi}e^{\frac{z^2}{2w^2}}(15w^4 - 10w^2z^2 + z^4))}{8640\pi w^{11}} \tag{5.7.12}$$

The coefficients $\{g_i\}_i$ of the near boundary expansion (3.1.32) of $\tilde{\gamma}$ are given by

$$g_0 = -\frac{e^{-\frac{z^2}{2w^2}}}{5\sqrt{2\pi}w} \tag{5.7.13}$$

$$g_1 = -\frac{3ze^{-\frac{z^2}{2w^2}}}{20\sqrt{2\pi}w^3} \tag{5.7.14}$$

$$g_2 = \frac{5e^{-\frac{z^2}{2w^2}}(w^2 - z^2)}{84\sqrt{2\pi}w^5} \tag{5.7.15}$$

$$g_3 = -\frac{11ze^{-\frac{z^2}{2w^2}}(z^2 - 3w^2)}{672\sqrt{2\pi}w^7} \tag{5.7.16}$$

$$g_4 = \frac{e^{-\frac{z^2}{w^2}}(-32w^7 - \sqrt{2\pi}e^{\frac{z^2}{2w^2}}(3w^4 - 6w^2z^2 + z^4))}{576\pi w^9} \tag{5.7.17}$$

$$g_5 = -\frac{ze^{-\frac{z^2}{w^2}}(3408w^7 + 13\sqrt{2\pi}e^{\frac{z^2}{2w^2}}(15w^4 - 10w^2z^2 + z^4))}{43200\pi w^{11}} \tag{5.7.18}$$

Thus, equation (3.1.26) implies for the near boundary expansion of the anisotropy function B, where we set $B = \sum_i B_i u^i$:

$$B_i = 0 \quad \text{for } i \in \{0, 3\}\,, \tag{5.7.19}$$

$$B_4 = -\frac{e^{-\frac{z^2}{2w^2}}}{3\sqrt{2\pi}w} \tag{5.7.20}$$

$$B_5 = \frac{e^{-\frac{z^2}{2w^2}}\left(20\lambda w^2 - 3z\right)}{15\sqrt{2\pi}w^3} \tag{5.7.21}$$

$$B_6 = \frac{e^{-\frac{z^2}{2w^2}}\left(-50\lambda^2 w^4 + w^2(15\lambda z + 1) - z^2\right)}{15\sqrt{2\pi}w^5} \tag{5.7.22}$$

$$B_7 = \frac{e^{-\frac{z^2}{2w^2}}\left(2100\lambda^3 w^6 - 63\lambda w^4(15\lambda z + 2) + 3w^2 z(42\lambda z + 5) - 5z^3\right)}{315\sqrt{2\pi}w^7} \tag{5.7.23}$$

$$\begin{aligned} B_8 = \frac{e^{-\frac{z^2}{w^2}}}{10080\pi w^9}\Big(&\sqrt{2\pi}e^{\frac{z^2}{2w^2}}(-58800\lambda^4 w^8 + 7056\lambda^2 w^6(5\lambda z + 1) - 3w^4(2352\lambda^2 z^2 \\ &+ 560\lambda z + 15) + 10w^2 z^2(56\lambda z + 9) - 15z^4) - 280w^7\Big) \end{aligned} \tag{5.7.24}$$

$$\begin{aligned} B_9 = \frac{e^{-\frac{z^2}{w^2}}}{30240\pi w^{11}}\Big(&1120(6\lambda w^9 - w^7 z) + \sqrt{2\pi}e^{\frac{z^2}{2w^2}}(282240\lambda^5 w^{10} - 14112\lambda^3 w^8(15\lambda z \\ &+ 4) + 72\lambda w^6(784\lambda^2 z^2 + 280\lambda z + 15) - 15w^4 z(448\lambda^2 z^2 + 144\lambda z + 7) \\ &+ 10w^2 z^3(36\lambda z + 7) - 7z^5)\Big) \end{aligned} \tag{5.7.25}$$

$$\begin{aligned} B_{10} = \frac{e^{-\frac{z^2}{w^2}}}{453600\pi w^{13}}\Big(&\sqrt{2\pi}e^{\frac{z^2}{2w^2}}(-6350400\lambda^6 w^{12} + 1905120\lambda^4 w^{10}(3\lambda z + 1) - 1620\lambda^2 \\ &w^8(1176\lambda^2 z^2 + 560\lambda z + 45) + 15w^6(20160\lambda^3 z^3 + 9720\lambda^2 z^2 + 945\lambda z + 14) \\ &- 90w^4 z^2(270\lambda^2 z^2 + 105\lambda z + 7) + 105w^2 z^4(9\lambda z + 2) - 14z^6) - 84w^7(5400\lambda^2 w^4 \\ &- 4w^2(450\lambda z + 19) + 137z^2)\Big) \end{aligned} \tag{5.7.26}$$

5.8 Runge-Kutta methods with and without adaptive stepsize

In section 3.1.4 we made use of Runge-Kutta methods twice for two different kinds of problems that require two slightly different versions of this algorithm. We start with presenting the standard 4-th order Runge-Kutta method (RK4) and proceed with an adaptive step size integrator. Given a differential equation for a $\mathbb{R}^k$ valued field $\Phi(t)$ of the form

$$\partial_t \Phi(t) = F(t, \Phi(t)), \quad \Phi(t_0) = \Phi_0 \tag{5.8.1}$$

we can sequentially approximate its solution at the point $t_{n+1} = t_n + \delta t$ from $\Phi(t_n)$ by computing

$$\Phi(t_{n+1}) \approx \Phi(t_n) + \delta t \sum_{i=1}^{4} b_i k_i, \tag{5.8.2}$$

where the k_i are given by

$$k_j = F(t + \alpha_j \delta t, \Phi(t_n) + \delta t\, \alpha_j k_{j-1}), \tag{5.8.3}$$

with the two vectors [71]

$$\alpha = \left\{0, \frac{1}{2}, \frac{1}{2}, 1\right\} \quad b = \left\{\frac{1}{6}, \frac{1}{3}, \frac{1}{3}, \frac{1}{6}\right\}. \tag{5.8.4}$$

This algorithm was used for the time evolution discussed in 3.1.4 with

$$\Phi = \{\lambda, B, a^{(4)}, f^{(4)}\}. \tag{5.8.5}$$

In order to extend this method to one with an adaptive stepsize, we need a local error estimation, i.e. we want to know how large the expected error at a given slice t_n[72] is, in order to adapt the step size accordingly. The easiest way to achieve this is to split the t-stepping in half. After each iteration (5.8.1)-(5.8.4) with step size δt_n we repeat the calculation for $\delta t_n/2$ two times to end up at slice t_{n+1} as well. The calculation with the double step suffers, of course, from a much smaller numerical error, such that we can think of it as the "exact" solution, with which we compare the numerical one. Let us call the double step solution $\tilde{\Phi}_n$ and the single step solution Φ_n both on t_n. Let

$$\text{err} = \max(|\Phi_n - \tilde{\Phi}_n|), \tag{5.8.6}$$

where the maximum is taken over all components of Φ. If we allow our solution to have a numerical error of approximately 10^{-a}, we update the time stepping on the n-th slice as

$$\delta t_{n+1} = \delta t_n \left(\frac{10^{-a}}{\text{err}}\right)^{1/4}. \tag{5.8.7}$$

The "learning rate" of this adaptive algorithm is governed by the exponent $\frac{1}{4}$ in (5.8.7). The justification for the specific choice of the exponent is this: Since we work with 4th order RK method, the numerical error Δ_n is of the size δt_n^4, for a step of size δt_n.

[71] The general Runge-Kutta method works with a Butcher-tableaux instead of vectors.

[72] We keep the same notation as in the beginning of this Appendix chapter for consistency, even though the adaptive integrator was applied to solve an initial value problem for the radial coordinate u not t.

Thus the error Δ_{n+1} corresponding to a stepping δt_{n+1} can be estimated via

$$\delta t_n \Delta_{n+1}^{1/4} \approx \delta t_n \delta t_{n+1} \approx \delta t_{n+1} \Delta_n^{1/4}. \tag{5.8.8}$$

5.9 Pseudospectral Methods

In this appendix we will explain the basics of (pseudo)-spectral methods which we used throughout the entire thesis, in chapter 3.1.5, in chapter 2.2, in chapter 2.3 and extensively in chapter 3.1. Spectral methods allow us to transform linear differential equations of the form

$$Lu = f \tag{5.9.1}$$

with L being a differential linear operator, to linear algebra problems, that are easy to handle numerically and whose precision increases rapidly, with increasing the size of the linear system. The idea is to project a solution of (5.9.1) onto a finite dimensional functions space with a (weighted) scalar product, spanned by orthogonal basis functions ϕ_i:

$$u \approx u_N = \sum_{i=0}^{N} u_i \phi_i. \tag{5.9.2}$$

Requiring that (5.9.2) is a good approximation of the solution u is equivalent to demanding that the residual R defined by

$$R = Lu_N - f = L \sum_{i=0}^{N} u_i \phi_i - f \tag{5.9.3}$$

is small[73]. Not all systems of orthogonal functions have the desired properties that allow us to construct good approximations. Also which system is the best can depend on the differential operator L and the boundary conditions to (5.9.1). However, in most cases the following rule of thumb delivers the best results:

'Always use Chebyshev polynomials or (Chebyshev) cardinal functions (further explained below in 5.9.1), unless the boundary conditions are periodic. Then use Fourier (cardinal-) functions'.
In most cases we used the corresponding cardinal functions c_m, which fulfill

$$c_m(x_n) = \delta_{mn} \tag{5.9.4}$$

[73]The term 'small' is to be understood with respect to the norm induced by the scalar product of the infinite dimensional Hilbert space obtained by taking the $N \to \infty$ limit in (5.9.2), i.e. the closed hull of $\{\phi_n\}_{n\in[0,\infty]}$.

for a discrete grid x_n also in the non periodic cases, since it turned out to be advantageous for implementing boundary conditions. Let w be the weight function of the weighted scalar product. For instance for Chebyshev polynomials w is given by $\frac{1}{\sqrt{1-x^2}}$. By construction the residual vanishes on the finite dimensional Hilbert space, spanned by c_m. This means for (5.9.1) generally given by

$$L = \sum_{p=0}^{M} p_p(x) \frac{d^p}{dx^p} \quad . \tag{5.9.5}$$

the following relation

$$\sum_{p=0}^{M} \sum_{n=0}^{N} \int_{-1}^{1} dx p_p(x) u_n \Big(\frac{d^p}{dx^p} c_n(x) \Big) c_m(x) \omega(x) = \int_{-1}^{1} dx f(x) c_m(x) \omega(x), \tag{5.9.6}$$

where the cardinal functions are defined on the interval $[-1, 1]$. Approximating a function $\tilde{u}$ living on a general interval $[a, b]$ is easily obtained by considering

$$\tilde{u}\Big(\frac{a+b}{2} + \frac{b-a}{2} x \Big). \tag{5.9.7}$$

In the case of a Gauss-Lobatto grid x_m and Chebyshev cardinal functions c_m, that fulfill relation (5.9.4) this leads to

$$\sum_{p=0}^{M} \sum_{n=0}^{N} \sum_{l=0}^{N} u_n p_p(x_l) \frac{d^p c_n}{dx^p}|_{x=x_l} \delta_{ml} = \sum_{l=0}^{N} f(x_l) \delta_{ml}. \tag{5.9.8}$$

The matrix by applying the Chebyshev-Gauss-Lobatto quadrature. Summing out the Kronecker deltas the above equation yields the linear system

$$\sum_{p=0}^{M} \sum_{n=0}^{N} u_n p_p(x_m) \frac{d^p C_n}{dx^p}|_{x=x_m} = f(x_m). \tag{5.9.9}$$

5.9.1 Explicit expressions

If the cardinal functions corresponding to a certain discrete grid x_m are constructed from polynomials, as in the case of Chebyshev cardinal functions, we can write them as

$$c_n = \prod_{k=0}^{n-1} \frac{x - x_k}{x_n - x_k} \prod_{k=n+1}^{N} \frac{x - x_k}{x_n - x_k}. \tag{5.9.10}$$

Thus, the differentiation matrix found in (5.9.9) can be easily computed. Here the Gauss-Lobatto grid is given by [74]

$$x_i = \cos\left(\frac{i\pi}{N}\right) \quad i = 0, \ldots, N \quad . \tag{5.9.11}$$

The Chebyshev cardinal functions can also be obtained directly from the N-th Chebyshev polynomial T_N in the following way

$$C_j(x) = (-1)^{j+1} \frac{(1-x^2)}{c_j N^2 (x - x_j)} \frac{dT_N(x)}{dx} \quad . \tag{5.9.12}$$

with $c_0 = c_N = 2$ and $c_i = 1 \; \forall \; i = 1, \ldots, N-1$.
Either from this equation or from (5.9.10) the differential matrices can be calculated to give [28]

$$\left.\frac{dC_j}{dx}\right|_{x=x_i} = \begin{cases} (1+2N^2)/6 & i = j = 0 \\ -(1+2N^2)/6 & i = j = N \\ -x_j / \left[2(1-x_j^2)\right] & i = j; 0 < j < N \\ (-1)^{i+j} c_i / \left[c_j (x_i - x_j)\right] & i \neq j \end{cases} \quad . \tag{5.9.13}$$

Higher derivatives can be obtained by taken powers of this matrix.
For Fourier polynomials the endpoint grid is given by [28]

$$x_i = \frac{\pi i}{N} \quad i = 0, \ldots, 2N-1 \tag{5.9.14}$$

The corresponding cardinal functions are given by

$$C_j(x) = \frac{1}{2N} \sin\left[N(x - x_j)\right] \cot\left[\frac{1}{2}(x - x_j)\right] \tag{5.9.15}$$

and the differentiation matrices take the form

$$\left.\frac{dC_j}{dx}\right|_{x=x_i} = \begin{cases} 0 & i = j \\ \frac{1}{2}(-1)^{i+j} \cot\left[\frac{1}{2}(x_i - x_j)\right] & i \neq j \end{cases} \tag{5.9.16}$$

$$\left.\frac{d^2C_j}{dx^2}\right|_{x=x_i} = \begin{cases} -(1+2N^2)/6 & i = j \\ \frac{1}{2}(-1)^{i+j+1} / \sin^2\left[\frac{1}{2}(x_i - x_j)\right] & i \neq j \end{cases} \quad . \tag{5.9.17}$$

[74] Throughout the calculations using spectral methods we used a different sign convention, such that x_0 corresponds to -1. We use this convention to be consistent with the source [28].

5.10 Einstein Equations for planar shocks

In this appendix we give explicit forms for the Einstein equations (1.7.10)-(1.7.16) of planar shocks. We follow the same notation as [34]. Since we do not have transverse gradients and assume isotropy in the transverse direction $\{x, y\}$ we can parametrize the spatial metric $\hat{g}$ with

$$\hat{g} = \begin{pmatrix} e^B & 0 & 0 \\ 0 & e^B & 0 \\ 0 & 0 & e^{-2B} \end{pmatrix} \tag{5.10.1}$$

with an anisotropy function $B(u, t, z)$. Here we set $u = \frac{1}{r}$. With the same argument as given for the form of (5.10.1) also the functions F_x and F_y can be set to zero. From now on we name the F_z component F for brevity. With this simplifications the Einstein's equations in Eddington-Finkelstein (EF) coordinates read

$$\left(\partial_r^2 + Q_\Sigma[B]\right)\Sigma = 0 \quad , \tag{5.10.2}$$

$$\left(\partial_r^2 + P_F[B,\Sigma]\partial_r + Q_F[B,\Sigma]\right)F = S_F[B,\Sigma] \quad , \tag{5.10.3}$$

$$\left(\partial_r + Q_{d_+\Sigma}[\Sigma]\right)d_+\Sigma = S_{d_+\Sigma}[B,\Sigma,F] \quad , \tag{5.10.4}$$

$$\left(\partial_r + Q_{d_+B}[B,\Sigma]\right)d_+B = S_{d_+B}[B,\Sigma,F,d_+\Sigma] \quad , \tag{5.10.5}$$

$$\partial_r^2 A = S_A[B,\Sigma,F,d_+\Sigma,d_+B] \quad , \tag{5.10.6}$$

$$\left(\partial_r + Q_{d_+F}[B,\Sigma]\right)d_+F = S_{d_+F}[B,\Sigma,F,d_+\Sigma,d_+B,A] \quad , \tag{5.10.7}$$

$$d_+\left(d_+\Sigma\right) = S_{d_+^2\Sigma}[B,\Sigma,F,d_+\Sigma,d_+B,A] \quad . \tag{5.10.8}$$

The source terms on the right hand side of (5.10.2)-(5.10.8) are given by

$$Q_\Sigma = \tfrac{1}{2}B'^2 \,, \tag{5.10.9}$$

$$P_F = 2B' + \Sigma'\,\Sigma^{-1} \,, \tag{5.10.10}$$

$$Q_F = 2B'' + \left(6B'\,\Sigma' + 4\Sigma''\right)\Sigma^{-1} + 3B'^2 - 4\Sigma'^2\,\Sigma^{-2} \,, \tag{5.10.11}$$

$$S_F = 2B'_{,z} + \left(4\Sigma'_{,z} + 6B'\,\Sigma_{,z}\right)\Sigma^{-1} + 3B_{,z}\,B' - 4\Sigma'\,\Sigma_{,z}\,\Sigma^{-2} \,, \tag{5.10.12}$$

$$Q_{d_+\Sigma} = 2\Sigma'\,\Sigma^{-1} \,, \tag{5.10.13}$$

$$\begin{aligned} S_{d_+\Sigma} = -2\Sigma + \frac{e^{2B}}{12\Sigma^3}\Big\{ & 8\Sigma\big[F\left(2\Sigma'_{,z} + F'\,\Sigma'\right) + F^2\,\Sigma'' + F_{,z}\,\Sigma' + \Sigma_{,zz}\big] \\ & + 2\Sigma\left(F\,\Sigma' + \Sigma_{,z}\right)\left(8(F\,B' + B_{,z}) + F'\right) - 4\left(F\Sigma' + \Sigma_{,z}\right)^2 \\ & + \Sigma^2\Big[2F\left(4B'_{,z} + B'\left(7B_{,z} + 4F'\right) + F''\right) + 2F'_{,z} + 4B'F_{,z} \\ & \quad + F^2\left(4B'' + 7B'^2\right) + 4B_{,z}F' + 7B_{,z}^2 + 4B_{,zz} + F'^2\Big]\Big\} \,, \end{aligned} \tag{5.10.14}$$

$$Q_{d_+B} = \tfrac{3}{2}\Sigma'\,\Sigma^{-1}\,, \tag{5.10.15}$$

$$\begin{aligned} S_{d_+B} = {}& \tfrac{3}{2}B'\,d_+\Sigma\,\Sigma^{-1} - \frac{e^{2B}}{6\Sigma^4}\Big\{\Sigma^2\big(2F'_{,z} + B'F_{,z} + B_{,z}F' + B_{,z}^2 + B_{,zz} + F'^2\big) \\ & + F\Big[\Sigma(4\Sigma'_{,z} + B'\,\Sigma_{,z} + B_{,z}\,\Sigma' - 2F'\,\Sigma') + 2\Sigma^2\big(B'_{,z} + B'(B_{,z} + F') + F''\big) \\ & - 8\Sigma'\Sigma_{,z}\Big] + F^2\Big[\Sigma\big(B'\Sigma' + 2\Sigma''\big) + \Sigma^2\big(B'' + B'^2\big) - 4\Sigma'^2\Big] \\ & + \Sigma(B_z\Sigma_{,z} - 4F'\Sigma_{,z} + 2F_{,z}\Sigma' + 2\Sigma_{,zz}) - 4\Sigma_{,z}^2\Big\}\,, \end{aligned} \tag{5.10.16}$$

$$\begin{aligned} S_A = {}& \tfrac{3}{2}d_+B\,B' - 6d_+\Sigma\,\Sigma'\,\Sigma^{-2} + 2 + \frac{e^{2B}}{4\Sigma^4}\Big\{ - 8\Sigma\Big[F(\Sigma'_{,z} + F'\,\Sigma' + F\Sigma'') \\ & + F\Sigma'_{,z} + F_{,z}\,\Sigma' + \Sigma_{,zz} + 2(F\,B' + B_{,z})(F\,\Sigma' + \Sigma_{,z})\Big] + 4\big(F\Sigma' + \Sigma_z\big)^2 \\ & + \Sigma^2\Big[- 7(F\,B' + B_{,z})^2 + F'^2 - 4\big(F\big(2B'_{,z} + B'\,F'\big) + F^2\,B'' + B'\,F_{,z} + B_{,zz}\big)\Big]\Big\}\,, \end{aligned} \tag{5.10.17}$$

$$Q_{d_+F} = 2B' - 2\Sigma'\,\Sigma^{-1}\,, \tag{5.10.18}$$

$$\begin{aligned} S_{d_+F} = {}& -2(A'_{,z} + F\,A'' + A'\,F') - 2(B' - \Sigma'\,\Sigma^{-1})(FA' + A_{,z}) + A'F' \\ & - 3d_+B\Big[F\,B' + B_{,z} + 2(F\Sigma' + \Sigma_{,z})\,\Sigma^{-1}\Big] - 2\big(F\,(d_+B)' + (d_+B)_{,z}\big) \\ & + d_+\Sigma\,\big(3\Sigma F' + 4(F\Sigma' + \Sigma_{,z})\big)\,\Sigma^{-2} - 4\big(F\,(d_+\Sigma)' + (d_+\Sigma)_{,z}\big)\,\Sigma^{-1}\,, \end{aligned} \tag{5.10.19}$$

$$\begin{aligned} S_{d_+^2\Sigma} = {}& -\frac{e^{2B}}{3\Sigma^2}\Big\{\Sigma\Big[FA'_{,z} + F\big(A'_{,z} + FA'' + A'F'\big) + 2(FA' + A_{,z})(FB' + B_{,z}) \\ & + A'\,F_{,z} + A_{,zz} - 2d_+F\,(F\,B' + B_{,z}) - (d_+F)_{,z} - F(d_+F)'\Big] \\ & + (F\Sigma' + \Sigma_{,z})(FA' + A_{,z} - d_+F)\Big\} - A'\,d_+\Sigma + \tfrac{1}{2}\Sigma\,d_+B^2\,. \end{aligned} \tag{5.10.20}$$

Above we used the subscript z for derivatives in the z direction and prime $'$ to denote derivatives in the radial r direction. The conditions for the horizon at a fixed radial position (1.7.31) explicitly reads

$$0 = d_+\Sigma + \frac{e^{2B}}{6\Sigma^2}\left(3F^2\,\partial_r\Sigma + 2\Sigma\,\partial_zF + 4F\,\Sigma\,\partial_zB + 2F\,\partial_z\Sigma\right)\Big|_{r=r_h}\,. \tag{5.10.21}$$

The stationary horizon equation derived from (1.7.32) can be written as

$$\begin{aligned} 0 = {}& \frac{e^{2B}\,(\Sigma B' + 2\Sigma')^2\,F^4}{4\Sigma^4} + \frac{e^{2B}\,(\Sigma B' + 2\Sigma')\,(\Sigma\,(2F' + B_z) + 2\Sigma_z)\,F^3}{2\Sigma^4} \\ & + \frac{3d_+\Sigma'F^2}{2\Sigma} + \left(\frac{e^{2B}{\Sigma_z}^2}{\Sigma^4} + \frac{e^{2B}(2F' + B_z)\Sigma_z}{\Sigma^3} + \frac{e^{2B}(F'^2 + 4B_zF' + {B_z}^2)}{4\Sigma^2} - 6\right)F^2 \\ & - \frac{3d_+\Sigma_zF}{\Sigma} - \frac{3}{2}e^{-2B}\Sigma^2d_+B^2 + A_z\Big(- F' + F\Big(\frac{2\Sigma'}{\Sigma} - 2B'\Big) + 2B_z + \frac{\Sigma_z}{\Sigma}\Big) \end{aligned}$$

$$
\begin{aligned}
&+ A_{zz} + \Big(-\frac{3}{2}B'F^2 + \Big(B_z - \frac{4\Sigma_z}{\Sigma}\Big)F + 2F_z\Big)d_+B \\
&+ \frac{(3(\Sigma B' + \Sigma')F^2 + (\Sigma(3F' - 2B_z) + 2\Sigma_z)F - \Sigma F_z)d_+\Sigma}{\Sigma^2} \\
&+ \frac{1}{4}A\Big(-24e^{-2B}\Sigma^2 + F^2B'^2 + F'^2 + 7{B_z}^2 - 4F'B_z - 4B'F_z \\
&+ 4F(B'(F' - 2B_z) - B'_z) - 2F'_z + 4B_{zz} + 24e^{-2B}\Sigma' d_+\Sigma \\
&- \frac{1}{\Sigma}\Big((8B'\Sigma' + 6\Sigma'')F^2 + (4F'\Sigma' - 24B_z\Sigma' + 4B'\Sigma_z - 4\Sigma'_z)F - 12\Sigma'F_z \\
&+ 2F'\Sigma_z - 16B_z\Sigma_z - 8\Sigma_{zz}\Big) + \frac{16F^2\Sigma'^2 + 8F\Sigma_z\Sigma' - 4{\Sigma_z}^2}{\Sigma^2}\Big)
\end{aligned}
\tag{5.10.22}
$$

Which is obtained by exploiting the Einstein equations (5.10.2)-(5.10.8). This elliptic differential equation can be solved using (Fourier-) spectral methods.

5.11 Filtering

For the calculation presented in chapter 3.1 filtering our functions turned out to be very useful for computations with low background energy density. The filters have to be applied carefully. Applying them in the course of the calculation on one time slice could cause precision loss. We only filter $\{B, a, f, \lambda\}$ at the end of the calculations of each time slice. During the time evolution we only filter in z-direction. The technique explained in the second subsection can only be applied to $B|_{t_0}$ for single shock solutions, before they are added together.

5.11.1 Fourier filter

There are several ways to introduce filtering of expansions in Fourier cardinals functions $\{c^{\mathrm{F}}(z,i)\}_{i\in\{0,\dots,N-1\}}$. Here we consider the manipulation of the discrete Fourier

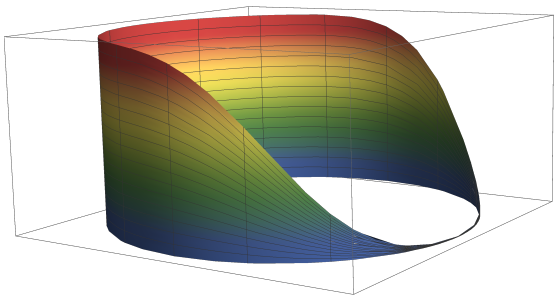

Figure 5.1: Visualization of the cut off for periodic functions. Low frequency modes with index k such that $|\pi - 2\pi k/N| > \frac{\pi}{3}$ are not modified. The parameter w_0 is chosen to be 0.5 in this example.

transformation of the set $\{\phi_n\}_{n\in\{0,\dots,N-1\}}$, where

$$f(z) = \sum_{i=0}^{N-1} \phi_i c^{\mathrm{F}}(z,i) \tag{5.11.1}$$

is the function we wish to filter. Periodicity is ensured by identifying $\phi_N := \phi_0$. For this set of points one defines

$$\tilde{\phi}_k = \frac{1}{N} \sum_{n=0}^{N-1} \phi_n e^{-\frac{2\pi i k n}{N}}, \tag{5.11.2}$$

such that $\{\tilde{\phi}_k\}_{k\in\{0,\dots,N-1\}}$ is the discrete Fourier transformation of $\{\phi_n\}_{n\in\{0,\dots,N-1\}}$. Imagining the points $\{\phi_n\}_{n\in\{0,\dots,N-1\}}$ as a discrete map

$$2\pi k/N \to \phi_k \tag{5.11.3}$$

we can think of $\tilde{\phi_k}$ with k close to $\frac{N}{2}$ as high frequencies coefficients of a Fourier transformation. As explained in [34], due to the discretization of non linear PDEs high frequency modes grow throughout the time evolution and cause precision loss up to the entire breakdown. Filtering these modes turns out to be essential for the computation of thin shock collisions. Thus we define

$$f(k) = \frac{1}{2}\Big(1 - \mathrm{erf}\Big(2\pi\frac{k-k_0}{Nw_0}\Big)\Big) + \frac{1}{2}\Big(1 - \mathrm{erf}\Big(2\pi\frac{k-N+k_0}{Nw_0}\Big)\Big) \tag{5.11.4}$$

if we want to cut off frequencies $\tilde{\phi_k}$ with $|N/2-k| < |N/2-k_0|$. The parameter w_0 is responsible for the smoothness of the cutoff. The new grid

$$\tilde{\iota}_k = f(k)\tilde{\phi}_k \tag{5.11.5}$$

is transformed back to

$$\iota_n = \sum_{i=0}^{N-1} \tilde{\iota}_k e^{\frac{2\pi i k n}{N}}. \tag{5.11.6}$$

We continue to calculate with the filtered function

$$f_{\mathrm{filtered}}(z) = \sum_{i=0}^{N-1} \iota_i c^{\mathrm{F}}(z,i). \tag{5.11.7}$$

In the implementation of the code it is convenient to write this manipulation as a matrix multiplication for the vector $(\phi_k)_k$. This matrix can be straightforwardly obtained by computing the outcome of the filtering of Fourier cardinal basis functions in terms of Fourier cardinal functions.

5.11.2 Near boundary filter

From the coordinate transformation explained in the paper we obtain a function $B|_{t_0}$ for a single shock moving in $+z$ direction. Plotting the function $\partial_u^3 \partial_z^3 b|_{t_0}$, with

$$B|_{t_0} = u^3 b|_{t_0} \tag{5.11.8}$$

close to the boundary shows non-physical noise even after filtering in z-direction. We are tackled with the problem of getting rid of these oscillations in higher derivatives close to the boundary, while at the same time avoiding any information loss.

This can be achieved by using the expansions (3.1.30)-(3.1.32) and equation (3.1.26). We expand b around the horizon up to n-th order. This analytic approximation for b close to the boundary will be called $\tilde{b}$. It only depends on w, z, u and $\tilde{\beta}_0$. The function $\tilde{\beta}_0$ was determined in the coordinate transformation. We define a function $\Delta(u, z)$, which is zero for all values of u, that are bigger then the n-th Chebyshev grid point. On our discrete grids this means, that $\Delta(u, z)$ is described by $n \times N$ real numbers, where N is the size of the Fourier grid in z-direction. We demand Δ to fulfill

$$\partial_u^m \tilde{b}|_{u=0,t_0} = \partial_u^m b|_{u=0,t_0} + \partial_u^m \Delta|_{u=0,t_0} \tag{5.11.9}$$

for all values in z and for $m \leq n$. This gives us $n \times N$ equations, which uniquely define Δ on the discrete grid. Choosing $n = 7$ or higher actually kills all noisy oscillations in the vicinity of the boundary up to almost arbitrary high derivatives in u and z direction. The new function, with which we proceed our calculations is $b|_{t_0} + \Delta|_{t_0}$. In contrast to standard filters in u-direction, which rely on transforming forth and back onto a smaller Chebyshev grid, this technique is, of course, restricted to the vicinity of the boundary. However, there is no information or precision loss, if anything we brought the function $b|_{t_0}$ closer to the exact solution of the coordinate transformation.

Bibliography

[1] J. M. Maldacena, *The Large N limit of superconformal field theories and supergravity,* Int. J. Theor. Phys. **38** (1999) 1113 [Adv. Theor. Math. Phys. **2** (1998) 231] doi:10.1023/A:1026654312961, 10.4310/ATMP.1998.v2.n2.a1 arXiv:9711200 [hep-th].

[2] E. Witten *Anti-de Sitter space and holography , Adv. Theor. Math. Phys. 2 (1998) 253–291*,arXiv:hep-th/9802150

[3] A. M. Polyakov *Quantum geometry of bosonic strings*, *Physics Letters B* **103**, 1981, p.207

[4] M. F. Paulos, *Higher derivative terms including the Ramond-Ramond five-form J. High Energy Phys.* **0810** (2008) 047, arXiv:0804.0763

[5] J. Pawelczyk, S. Theisen $AdS_5 x S^5$ *Black Hole Metric at* $\mathcal{O}(\alpha'^3)$ arXiv:hep-th/9808126 [hep-th], *J. High Energy Phys.* **9809** (1998) 010.

[6] S. de Haro, K. Skenderis, S. N. Solodukhin *Holographic Reconstrcution of Spacetime and Renormalization in the AdS/DFT Correspondence* arXiv:hep-th/0002230

[7] A. Buchel, J. T. Liu, A. O. Starinets, *Coupling constant dependence of the shear viscosity in N=4 supersymmetric Yang-Mills theory* arXiv:hep-th/0406264 [hep-th], Nucl. Phys. B **707**, 56-68 (2005).

[8] P. Benincasa, A. Buchel, *Transport properties of N=4 supersymmetric Yang-Mills theory at finite coupling, J. High Energy Phys.* **0601** (2006) 103, arXiv:hep-th/0510041

[9] P. K. Kovtun, A. O. Starinets, *Quasinormal modes and holography* Phys. Rev. D **72**, 086009 (2005), arXiv:hep-th/0506184.

[10] B. Hassanain and M. Schvellinger, *Plasma conductivity at finite coupling, J. High Energy Phys.* **1201** (2012) 114, arXiv:1108.6306.

[11] B. Hassanain and M. Schvellinger, *Plasma photoemission from string theory, J. High Energy Phys.* **1212** (2012) 095, arXiv:1209.0427 [hep-th].

[12] B. Hassanain and M. Schvellinger, *Diagnostics of plasma photoemission at strong coupling, Phys. Rev.* **D 85** (2012) 086007, arXiv:1110.0526 [hep-th].

[13] S. Janiszewski, M. Kaminski, *Quasinormal modes of magnetic and electric black branes versus far from equilibrium anisotropic fluids,* arXiv:1508.06993 [hep-th], doi:10.1103/PhysRevD.93.025006

[14] S. Grozdanov, W. van der Schee *Coupling constant corrections in a holographic model of heavy ion collisions* arXiv:1610.08976 [hep-th]

[15] V. Balasubramanian, P. Kraus, *A Stress Tensor For Anti-de Sitter Gravtiy* arXiv:hep-th/9902121

[16] P. Kraus, F. Larsen, R. Siebelink *The Gravitational Action in Asymptotically AdS and Flat Sapcetimes* arXiv:hep-th/9906127

[17] S. Stricker, *Holographic thermalization in $N = 4$ Super Yang-Mills theory at finite coupling* arXiv:1307.2736

[18] S. Waeber and A. Schäfer, *Studying a charged quark gluon plasma via holography and higher derivative corrections, J. High Energy Phys.* **1807** (2018) 069, arXiv:1804.01912 [hep-th].

[19] S. Waeber, A. Schaefer, A. Vuorinen, L. G. Yaffe *Finite coupling corrections to holographic predictions for hot QCD, J. High Energy Phys.* **1511** (2015) 087, arXiv:1509.02983 [hep-th].

[20] M. Ammon, M. Kaminski, R. Koirala, J. Leiber, J. Wu, *Quasinormal modes of charged magnetic black branes & chiral magnetic transport J. High Energy Phys.* **1704** (2017) 067, arXiv:1701.05565.

[21] G. Endrodi, M. Kaminski, A. Schäfer, J. Wu, L. Yaffe *Universal magnetoresponse in QCD and $\mathcal{N} = 4$ SYM J. High Energy Phys.* **1809** (2018) 070, arXiv:1806.09632 [hep-th]

[22] M. Panero *Thermodynamics of the QCD plasma and the large-N limit*, Phys. Rev. Lett **103** (2009) 232001, arXiv:0907.3719

[23] S. Caron-Huot, P. Kovtun, G. D. Moore, A. Starinets and L. G. Yaffe, *Photon and dilepton production in supersymmetric Yang-Mills plasma, J. High Energy Phys.* **0612** (2006) 015, hep-th/0607237.

[24] K. Peeters, A. Westerberg *The Ramond-Ramond sector of string theory beyond leading order* doi:10.1088/0264-9381/21/6/022, arXiv:hep-th/0307298

[25] A. Buchel, M. Paulos *Relaxation time of a CFT plasma at finite coupling* arXiv:0806.0788

[26] A. O. Starinets *Quasinormal Modes of Near Extremal Black Branes* arXiv:hep-th/0207133 [hep-th]

[27] A. Chamblin, R. Emparan, C. V. Johnson, R. C. Myers *Charged AdS Black Holes and Catastrophic Holography* Phys. Rev. D **60**, 064018 (1999), arXiv:hep-th/9902170

[28] J. P. Boyd, *Chebyshev and Fourier Spectral Methods (Revised)*,2001, http://depts.washington.edu/ph506/Boyd.pdf

[29] A. Buchel *Sensitivity of holographic $\mathcal{N} = 4$ SYM plasma hydrodynamics to finite coupling corrections* arXiv:1807.05457 [hep-th]

[30] R. A. Janik, R. Peschanski *Asymptotic perfect fluid dynamics as a consequence of AdS/CFT* arXiv:hep-th/0512162, Phys.Rev.D73:045013,2006

[31] M. Le Bellac, *Thermal Field Theory*, Cambridge, 1996

[32] E. Poisson, *An advanced course in general relativity*, 2002

[33] P. M. Chesler, N. Kilbertus and W. van der Schee, *Universal hydrodynamic flow in holographic planar shock collisions,* J. High Energy Phys. **1511** (2015) 135, arXiv:1507.02548 [hep-th].

[34] P. M. Chesler and L. G. Yaffe, *Numerical solution of gravitational dynamics in asymptotically anti-de Sitter spacetimes,* J. High Energy Phys. **1407** (2014) 086 arXiv:1309.1439

[35] P. M. Chesler, L. G. Yaffe, *Holography and colliding gravitational shock waves in asymptotically AdS_5 spacetime,* DOI: 10.1103/PhysRevLett.106.021601 arXiv:1011.3562 [hep-th]

[36] M. P. Heller, D. Mateos, W. van der Schee and D. Trancanelli, *Strong Coupling Isotropization of Non-Abelian Plasmas Simplified,* Phys. Rev. Lett. **108** (2012) 191601, arXiv:1202.098 [hep-th].

[37] M. P. Heller, R. A. Janik and P. Witaszczyk, *A numerical relativity approach to the initial value problem in asymptotically Anti-de Sitter spacetime for plasma thermalization - an ADM formulation,* Phys. Rev. D **85** (2012) 126002, arXiv:1203.0755 [hep-th].

[38] J. Casalderrey-Solana, M. P. Heller, D. Mateos and W. van der Schee, *From full stopping to transparency in a holographic model of heavy ion collisions,* Phys. Rev. Lett. **111** (2013) 181601, arXiv:1305.4919 [hep-th].

[39] A. Buchel, M. P. Heller and R. C. Myers, *Equilibration rates in a strongly coupled nonconformal quark-gluon plasma,* Phys. Rev. Lett. **114** (2015) no.25, 251601, arXiv:1503.07114 [hep-th].

[40] P. M. Chesler and L. G. Yaffe, *Holography and off-center collisions of localized shock waves,* J. High Energy Phys. **1510** (2015) 070 arXiv:1501.04644

[41] J. F. Fuini and L. G. Yaffe, *Far-from-equilibrium dynamics of a strongly coupled non-Abelian plasma with non-zero charge density or external magnetic field,* J. High Energy Phys. **1507** (2015) 116, arXiv:1503.07148 [hep-th].

[42] A. Buchel, J. T. Liu and A. O. Starinets, *Coupling constant dependence of the shear viscosity in N=4 supersymmetric Yang-Mills theory,* Nucl. Phys. B **707** (2005) 56, arXiv:0406264 [hep-th].

[43] L. Adamczyk *et al.* [STAR Collaboration], *Global Λ hyperon polarization in nuclear collisions: evidence for the most vortical fluid,* Nature **548** (2017) 62 doi:10.1038/nature23004, arXiv:1701.06657 [nucl-ex].

[44] T. Lappi and R. Venugopalan, *Universality of the saturation scale and the initial eccentricity in heavy ion collisions,* Phys. Rev. C **74** (2006) 054905, arXiv:0609021 [nucl-th].

[45] V. Balasubramanian *et al.*, *Thermalization of Strongly Coupled Field Theories,* Phys. Rev. Lett. **106** (2011) 191601, arXiv:1012.4753 [nucl-th].

[46] W. van der Schee , *Gravitational collisions and the quark-gluon plasma,* arXiv:1407.1849 [hep-th].

[47] V. Balasubramanian *et al.*, *Holographic Thermalization,* Phys. Rev. D **84** (2011) 026010, arXiv:1103.2683 [hep-th].

[48] H. Bondi, *Gravitational Waves in General Relativity,* Nature **186** (1960) no.4724, 535. doi:10.1038/186535a0

[49] R. K. Sachs, *Gravitational waves in general relativity. 8. Waves in asymptotically flat space-times,* Proc. Roy. Soc. Lond. A **270** (1962) 103. doi:10.1098/rspa.1962.0206

[50] E. Poisson, *An advanced course in general relativity,* 2002, https://www.physics.uoguelph.ca/poisson/research/agr.pdf

[51] D. T. Son, A. O. Starinets, *Minkowski-space correlators in AdS/CFT correspondence: recipe and applications, J. High Energy Phys.* **0209** (2002) 042, hep-th/0205051.

[52] A. Buchel, *Resolving disagreement for η/s in a CFT plasma at finite coupling, Nucl. Phys.* **B 803** (2008) 166, arXiv:0805.2683 [hep-th].

[53] D. Steineder, S. A. Stricker, A. Vuorinen, *Probing the pattern of holographic thermalization with photons, J. High Energy Phys.* **1307** (2013) 014, arXiv:1304.3404.

[54] S. S. Gubser, I. R. Klebanov, A. A. Tseytlin *Coupling Constant Dependence in the Thermodynamics of $\mathcal{N} = 4$ Supersymmetric Yang-Mills Theory* arXiv:9805156 [hep-th].

[55] D. J. Gross and E. Witten, *Superstring modifications of Einstein's equations Nucl. Phys.* **B 277** (1986) 1

[56] G. Aarts, C. Allton, J. Foley, S. Hands, S. Kim, *Spectral functions at small energies and the electrical conductivity in hot, quenched lattice QCD* arXiv:0703008 [hep-th].

[57] G. Aarts, C. Allton, A. Amato, P. Giudice, S. Hands, J. Skullerud, *Electrical conductivity and charge diffusion in thermal QCD from the lattice* arXiv:1412.6411 [hep-th].

[58] S. de Haro, A. Sinkovics, K. Skenderis, *On alpha'-corrections to D-brane solutions* arXiv:hep-th/0302136.

[59] M. Ammon, J. Erdmenger *Gauge/Gravity Duality, Foundations and Applications*, Cambridge University Press, 2015

[60] A. V. Ramallo *Introduction to the AdS/CFT correspondence* arXiv:1310.4319 [hep-th].

[61] C. Ecker, D. Grumiller, P. Stanzer, S. A. Stricker, W. van der Schee *Exploring nonlocal observables in shock wave collisions J. High Energy Phys.* **1611** (2016) 054, arXiv:1609.03676 [hep-th]

[62] C. Ecker, D. Grumiller, S. A. Stricker *Evolution of holographic entanglement entropy in an anisotropic system*, *J. High Energy Phys.* **1507** (2015) 146, arXiv:1506.02658 [hep-th]

[63] Y. Brihaye, E. Radu *Five-dimensional rotating black holes in Einstein-Gauss-Bonnet theory* arXiv:0801.1021 [hep-th]

[64] J. Casalderrey-Solana, D. Mateos, W. van der Schee, M. Triana *Holographic heavy ion collisions with baryon charge*, *J. High Energy Phys.* **1609** (2016) 108, arXiv:1607.05273

[65] V. Balasubramanian, S. F. Ross *Holographic Particle Detection*, *Phys.Rev.* **D61** (1999) 044007, arXiv:hep-th/9906226

[66] G. Festuccia, H. Liu *Excursions beyond the horizon: Black hole singularities in Yang-Mills theories (I)* *J. High Energy Phys.* **0604** (2006) 044, arXiv:hep-th/0506202v2

[67] P. Romatschke *Do nuclear collisions create a locally equilibrated quark-gluon plasma?*, DOI: 10.1140/epjc/s10052-016-4567-x, arXiv:1609.02820 [hep-th]

[68] P. M. Chesler, L .G. Yaffe *Holography and colliding gravitational shock waves in asymptotically AdS_5 spacetime* DOI: 10.1103/PhysRevLett.106.021601, arXiv:1011.3562 [hep-th]

[69] S. Waeber *Quasinormal modes of magnetic black branes at finite 't Hooft coupling*, *J. High Energy Phys.* **1908** (2019) 006, arXiv:1811.04040 [hep-th]

[70] S. Waeber, A. Rabenstein, A. Schäfer, L. G. Yaffe *Asymmetric shockwave collisions in AdS_5* *J. High Energy Phys.* **1908** (2019) 005, arXiv:1906.05086 [hep-th]

[71] P. Kovtun, D. T. Son, A. O. Starinets *Viscosity in Strongly Interacting Quantum Field Theories from Black Hole Physics*, Phys.Rev.Lett. 94 (2005) 111601, arXiv:hep-th/0405231

[72] R. M. Wald *General relativity*, Chicago Univ. Pr. (1984)

[73] J. Polchinski *String Theory, An Introduction to the Bosonic String*, Cambridge University Press, 1998

[74] W. van der Schee *Gravitational collisions and the quark-gluon plasma* arXiv:1407.1849 [hep-th]

[75] C. Ecker *Entanglement Entropy from Numerical Holography* arXiv:1809.05529 [hep-th]

[76] P. M. Chesler, L. G. Yaffe *Boost invariant flow, black hole formation, and far-from-equilibrium dynamics in $N = 4$ supersymmetric Yang-Mills theory* arXiv:0906.4426 [hep-th], *Phys.Rev.* **D82** (2010) 026006

[77] P. M. Chesler, L. G. Yaffe *Horizon formation and far-from-equilibrium isotropization in supersymmetric Yang-Mills plasma* arXiv:0812.2053 [hep-th], DOI: 10.1103/PhysRevLett.102.211601

[78] R. A. Janik, R. Peschanski *Asymptotic perfect fluid dynamics as a consequence of AdS/CFT*, doi: 10.1103/PhysRevD.73.045013, arXiv:hep-th/0512162

[79] J. Casalderrey-Solana, M. P. Heller, D. Mateos, W. van der Schee, *Longitudinal Coherence in a Holographic Model of Asymmetric Collisions*, Phys. Rev. Lett **112** (2014) 221602, arXiv:1312.2956

[80] W. Israel *Singular hypersurfaces and thin shells in general relativity*, Nuovo Cim. B **44S10** (1966) 1

[81] N. Engelhardt, A. C. Wall *Coarse Graining Holographic Black Holes*, *J. High Energy Phys.* **1905** (2019) 160, arXiv:1806.01281 [hep-th]

[82] N. Engelhardt, A. C. Wall *Decoding the Apparent Horizon: A Coarse-Grained Holographic Entropy*, Phys. Rev. Lett **121** (2018) 211301, arXiv:1706.02038 [hep-th]

[83] A. Milov on behalf of the ATLAS Collaboration *Particle production and long-range correlations in p+Pb collisions with the ATLAS detector*, Report Number: ATL-PHYS-PROC-2014-017, arXiv:1403.5738 [nucl-ex]

[84] T. Sakai, S. Sugimoto *Low energy hadron physics in holographic QCD*, arXiv:hep-th/0412141

[85] A. Rebhan, *The Witten-Sakai-Sugimoto model: A brief review and some recent results,* arXiv:1410.8858 [hep-th].

[86] B. Müller, A. Schäfer *Entropy Creation in Relativistic Heavy Ion Collisions*, DOI: 10.1142/S0218301311020459, arXiv:1110.2378 [hep-th]

[87] S. Ryu, T. Takayanagi *Holographic derivation of entanglement entropy from AdS/CFT*,Phys. Rev. Lett. **96** (2006), arXiv:hep-th/0603001

[88] J. Sonner, M. Vielma *Eigenstate thermalization in the Sachdev-Ye-Kitaev model*, *J. High Energy Phys.* **1711** (2017) 149, arXiv:1707.08013 [hep-th]

[89] M. Luzum, P. Romatschke *Conformal Relativistic Viscous Hydrodynamics: Applications to RHIC results at* $\sqrt{(}s_N N) = 200GeV$, Phys. Rev. **C78** 034915 (2008), arXiv:0804.4015 [hep-th]

[90] H. Bantilan, T. Ishii and P. Romatschke, *Holographic Heavy-Ion Collisions: Analytic Solutions with Longitudinal Flow, Elliptic Flow and Vorticity,* arXiv:1803.10774 [nucl-th]

Ort, Datum	Sebastian Waeber